Investigating the genetic component of Parkinson's disease through the use of human induced pluripotent stem cells and gene editing

Carles Calatayud Aristoy

UNIVERSITAT DE BARCELONA

Investigating the genetic component of Parkinson's disease through the use of human induced pluripotent stem cells and gene editing

Memòria presentada per **Carles Calatayud Aristoy** per optar al títol de
Doctor per la Universitat de Barcelona
Programa de **Doctorat de Biomedicina**
Línea de Recerca de **Neurociències**

Realitzada sota la direcció de la **Dra. Antonella Consiglio** a
L'Institut de Biomedicina de la Universidad de Barcelona (IBUB)

Directora de la tesi:
Dra. Antonella Consiglio

Codirector de la tesi:
Dr. Ángel Raya Chamorro

Tutor de la tesi:
Dr. José Antonio del Río Fernández

Autor de la tesi:
Carles Calatayud Aristoy

Barcelona, 2017

Agraïments

Supose que fer una tesi doctoral pot ser dur, molt dur o duríssim. He transitat per tots tres graus d'intensitat però afortunadament sempre he comptat amb les persones adients per tal de continuar. És difícil fer justícia a l'hora d'escriure uns agraïments. Almenys en el meu cas no ho he trobat fàcil. El que sempre havia tingut clar és que la primera persona que hi havia de figurar és ma mare. Fa un parell d'anys recorde que em digué una frase que contenia una metàfora molt ben triada: "Hijo, nunca cortarás el cordón umbilical". Doncs ara em reafirme, és així i ho dic amb orgull. Amb el temps, una segona persona començà a compartir la tasca d'aguantar-me, la meua parella, Carla. En acabar la jornada vaig passar de trucar a ma mare per lamentar-me dels problemes diaris, a després fer-ho en persona amb Carla, a no necessitar fer-ho en absolut. Pareix que és una evolució positiva. Sense el suport emocional de totes dues haguera sigut impossible dur a terme aquest treball.

També voldria recordar al meu pare, Félix i a les meues germanes Emma i Cristina, així com la nostra gossa Calle i la meua iaia que tristament va faltar durant l'etapa final de la tesi. Els caps de setmana en família a Benicàssim o a València, de vegades fugaços, han tingut un caire terapèutic i m'han ajudat molt a fer front al que em venia per davant. Sempre m'he sentit recolzat i amb les esquenes ben cobertes. També voldria recordar-me dels amics en general i en particular d'aquells que han estat amb mi a Barcelona en els darrers anys: Ricardo, Miguel i Bonjo, Santi i Mar, els meus ex-companys de pis Javi i Carlos...

L'ambient al laboratori també ha sigut excepcional. He pogut gaudir de molts bons companys, tot i que seria més just utilitzar companyes ja que sempre hem estat en minoria. Des dels inicis amb Roger i Irene fins als actuals, Giulia, Armida, Angie, Monika, Marco, Isabel i Alba. També vull recordar-me dels que han estat com Francesca, Ana, Sara... Tanmateix, dos persones, Irene i Armida, han participat molt activament en aquest projecte fins al punt que la feina és tant meua com seua. De la mateixa manera que Senda i Yvonne. La seua col·laboració i els seus consells han estat essencials. També els dels nostres col·laboradors Nino, Mario i Rubén que ens han introduït en el món de la genètica i de Toni i Claudio per ensenyar-me les tècniques d'edició gènica tan imprescindibles en el desenvolupament de la tesi.

També hem tingut la sort de comptar amb la gent de l'IBEC i del CMRB. Sigué una època molt bonica quan estàvem tots junts al Parc Científic amb Claudi, Isil, Juan, Isaac, Senda, Yvonne, Juanlu, Sergio... També amb els companys del CMRB, especialment Julián que ha esdevingut un molt bon amic durant la nostra estada allà.

Finalment també volia agrair a la primera doctora del laboratori, Adriana. Ella començà amb l'actual model de malaltia de Parkinson que ens ha permès a mi, i també a Roger, introduir-nos en el món de la recerca amb uns projectes molt encisadors. I amb ella també agrair a Ángel i Antonella per haver-me donat la seua confiança i haver-me possibilitat formar part d'un projecte molt motivador que m'han permès que adquirirà unes tècniques i unes habilitats que estan a

l'avantguarda de la recerca biomèdica actual. No m'havia imaginat mai durant la carrera que faria el doctorat treballant amb hiPSC i *gene editing.*

Tampoc no vull estendre'm massa ni acabar fent uns agraïments lacrimògens, espere que el lector trobe el present projecte tant interessant com jo l'he trobat i que d'alguna manera aquesta feina haja pogut contribuir a esclarir les encara obscures causes del Parkinson.

Resumen

La enfermedad de Parkinson (EP) es la segunda enfermedad neurodegenerativa más común tras la enfermedad de Alzheimer afectando a alrededor del 1% de la población mayor de 60 años. Causa una incapacidad progresiva en los pacientes con una importante afectación de las funciones motoras y en la mayoría de los casos desemboca otras disfunciones no motoras como depresión, ansiedad, trastornos de la función autonómica y demencia. Dos son los rasgos distintivos de la enfermedad: la muerte de las neuronas dopaminérgicas de la parte compacta de la sustancia negra, lo que precipita el cuadro motor y el diagnostico, y la formación de acúmulos proteicos en los cuerpos y las neuritas de las neuronas supervivientes. Estos acúmulos, que reciben el nombre de cuerpos de Lewy, están compuestos principalmente por la proteína alfa-sinucleína.

Pese a los hallazgos genéticos de las últimas décadas, la mayoría de los casos son clasificados como idiopáticos. Sin embargo, cerca del 15% de los casos presentan una historia familiar y en cerca del 30% de los mismos se conoce la mutación que segrega con la enfermedad (Kumar K. R. et al., 2011). Entre los genes relacionados con la EP familiar, destaca LRRK2. El conjunto de mutaciones patogénicas en este gen representan el 10% de los casos de los cuales la mitad son atribuibles a su mutación más común, la sustitución Gly2019Ser (G2019S). Inesperadamente, esta mutación también se encuentra en el 1-2% de los casos esporádicos y está asociada a un parkinsonismo clínicamente indistinguible del de los casos idiopáticos (Bardien S. et al., 2011). La mutación presenta una penetrancia incompleta que varía entre poblaciones y que está sujeta a la presencia de otros factores, genéticos y/o ambientales que la modulan (Hentati F. et al., 2014; Trinh J. et al., 2016). Otra característica interesante de la sustitución G2019S es que en familias con historia de EP hay una frecuencia aumentada de fenocopias, esto es, miembros afectados no portadores de la mutación (Latourelle J. C. et al., 2008). Finalmente, la relación entre LRRK2 y la EP esporádica no sólo se limita a la mutación -rara- G2019S. Estudios de asociación a escala genómica han implicado también a polimorfismos frecuentes situados en el locus de LRRK2 en la enfermedad esporádica (Nalls M. A. et al., 2014).

Por todo ello, la determinación de los mecanismos protectores frente a la acción patogénica de LRRK2 son de gran interés desde el punto de vista terapéutico, ya que pueden ayudar a combatir no sólo los casos de EP asociados a mutaciones en LRRK2 sino también los casos idiopáticos. Para ello, en el contexto de este proyecto hemos analizado la penetrancia de la mutación G2019S en nuestro modelo *in vitro* de la EP, confirmando que la protección *in vivo* de los individuos portadores asintomáticos se reproduce *in vitro* e iniciando una aproximación para determinar los factores genéticos responsables de dicha protección.

Abstract

Despite the advances in the identification of genes and proteins involved in Parkinson's disease (PD), there are still appreciable gaps in our understanding of the mechanisms underlying the chronic neurodegenerative process in PD. In the lab, it has been demonstrated that iPSC technology can be used to observe phenotypes relevant to neurodegeneration in PD, and also provided first proof-of-principle evidence that neurons with the genome of a sporadic PD patient exhibited similar phenotypes as seen in iPSC derived from patients with monogenic LRRK2 (G2019S) PD. In the present study we generated a complementary set of iPSC lines from asymptomatic individuals carrying pathogenic LRRK2 mutations, whose gene pool may have a prevailing protective effect. We then corrected the LRRK2 mutation by using TALEN-mediated genetic engineering in the symptomatic LRRK2-iPSC lines, as well as well as introduced it in our already established control-iPSC lines. Dopaminergic neurons differentiated in parallel from this subset of iPSC lines have been cultured over a long time span and monitored for the appearance of neurodegeneration phenotypes (including reduced numbers of neurites and neurite arborization and α-synuclein accumulation) after 75 days in culture. Interestingly we found that while PD iPSC-derived DA neurons showed altered morphology and shorter/fewer neurites, DAn derived from NMC show mature morphology and long neurites with complex arborization, similar to those differentiated from Ctrl-iPSC. We have also identified mutation-linked phenotypes such as α-synuclein accumulation whose appearance was delayed in NMC neurons compared to LRRK2-PD neurons. Complementarily, we have sequenced the exome of our cohort in order to identify the genetic modifiers of LRRK2 mutation penetrance. Importantly, the availability of a refined set of PD patient-specific iPSC lines representing symptomatic and asymptomatic cases of familial PD sharing the same pathogenic mutation in LRRK2, as well as isogenic iPSC lines in which the mutation has been edited out, will open a new window for the early diagnosis and individualized treatment of the prodromic period of the disease.

List of acronyms employed in the present thesis

AADC: aromatic amino decarboxylase
AAO; age at onset
AAV: adeno-associated virus
chESC: conditioned human embryonic stem cell (medium)
CNV: copy number variant
CV-CD: common variant – common disease
CRISPR: Clustered Regularly Interspaced Short Palindromic Repeats
DA: dopamine/dopaminergic
DBS: deep brain stimulation
EB: embryoid body
eQTL: expression quantitative trait locus
ER: endoplasmic reticulum
GAD: glutamic acid decarboxylase
GD: Gaucher's disease
GPe: glubus pallidus external segment
GPi: glubus pallidus internal lsegment
GRS: genetic risk score
GTEx: genotype-tissue expression
GWAS: genome-wide association study
hESC: human embryonic stem cell
hiPSC: human induced pluripotent stem cell
hPSC: human pluripotent stem cell
L2-NMC: non-manifesting carrier of the LRRK2 G2019S mutation
L2-PD: PD patient carrying the LRRK2 G2019S mutation
MPTP: 1-methyl-4-phenyl-1,2,3,6-tetrahydropyridine
MPPP: 1-methyl-4-phenyl-4-propionoxypiperidine
MSN: medium spiny neurons
OR: odds ratio
PD: Parkinson's disease
PIGD: postural instability and gait difficulty
RBD: REM sleep behavior disorder
REM: Rapid eye movement
REMC: Roadmap Epigenomics Consortium
RNAi: RNA interference
RVD: repeat variable di-residue
SNP: single nucleotide polymorphism
SNpc: substantia nigra pars compacta
SSN: site-specific nuclease
STN: subthalamic nucleus
TALEN: transcription activator-like effector nucleases
TF: transcription factor
TH: tyrosine hydroxylase
TGN: trans-golgi network
WES: whole exome sequencing

Index of Contents

Introduction 15

Parkinson's Disease 17

A growing public health problem 17

Clinical features 17

The basal ganglia and the loss of nigral neurons 18

Non-motor symptoms. Before the onset of the motor symptoms and after 20

Treatment 21

Etiology 23

Environmental risk factors 24

Genetic factors 24

Familial (Mendelian) PD genes 25

Particular features of LRRK2: insights into genetics and function 28

Susceptibility genes 31

Genes modulating age at disease onset 35

Mechanishms leading to neurodegeneration 35

Mitochondrial pathology 36

Proteostatic stress and the prion theory 37

Defects in vesicle-related processes: from protein sorting, to autophagy-lysosome system and synapses 38

PD models 40

Animal models 42

Toxin-based animal models 42

Genetic animal models 43

In vitro cell models 45

The generation of induced pluripotent stem cells (iPSC) and its application to 45

human disease modeling

A model describing spontaneous neurodegeneration phenotypes in patient-specific Ipsc 48

Gene editing tools in iPSC-based modeling. The importance of genetically-matched controls 52

Generating lineage-specific reporter lines by gene editing 54

Objectives 59

Materials and methods 63

Results 71

Part I: Investigating the genetic component of Parkinson's disease through the use of human induced pluripotent stem cells and gene editing 73

Recruitment of candidate protected LRRK2 G2019S carriers and hiPSC generation 73

Generation of isogenic controls differing in the presence or absence of the G2019S mutation 76

Long-term culture of L2-NMC-iPSC derived DA neurons does not result in DA cell loss as with L2-PD-iPSC derived DA neurons 80

L2-NMC-iPSC derived DA neurons present a variable degree of morphological abnormalities 83

LRRK2 G2019S is a major driver of the accumulation of alpha-synuclein 84

Exome interrogation provides clues regarding the increased protection of L2-NMC against LRRK2-related pathogenic effects 87

Part II: Generation of a Tyrosine Hydroxylase reporter hiPSC line 92

Generation of control and L2-PD TH reporter hiPSC lines 92

Purified mOrange+ cells survive after FAC sorting and restart neuritogenesis. 94

mOrange+ DA neurons present less number and slower mitochondria compared to Synapsin-EGFP+ neurons. 96

Discussion 99

Patient-specific iPSC for familial PD modeling and the importance of generating genetically matched controls 101

An experimental platform for modeling the reduced penetrance of LRRK2 G2019S using non-manifesting carrier-specific hiPSC 101

Identification of variants associated with AAO in LRRK2 G2019S non-manifesting carriers 102

Generation of a genetic reporter of the TH gene to circumvent iPSC-inherent variability 105

Future directions 106

Conclusions 109

References 113

Annexes 137

Annex I: Review article 139

Annex II: Research article 151

Annex III: Research article 209

INTRODUCTION

Parkinson's Disease

A growing public health problem

First clinical definition of Parkinson's disease dates from 1817 when James Parkinson described whose major recognizable features were the involuntary tremulous motion and the bent posture when walking (Parkinson 2002). Strikingly, one of the reasons that led James Parkinson to write his *Essay on the shaking palsy* was to convince the medical community he was describing an as yet unreported disease. Nowadays it may seem odd that a disease such as PD had gone unnoticed at that time, however, the incidence of PD rises with age and the life expectancy in the beginning of the 19th century did not exceed 40 years in the UK (Zijdeman & Ribeira da Silva 2015). Since then, there has been a trend towards increasing life expectancy and in western countries, it is currently surpassing the 8th decade of life. Accordingly, progressive aging of the population is increasing the incidence of age-associated pathological conditions such as PD (Dorsey et al. 2007). The disease is known to affect more than 1% of the population older than 60. In 2013, in the Spanish population, more than 160,000 people had a PD diagnosis (Peñas Domingo et al. 2015). Nowadays, more than 38% of the Spanish population is older than 50, and demographic forecasts increase that figure to nearly 50% in 2,029 (INE 2014). Altogether, these facts emphasize the urgency for finding disease modifying or preventing therapies that may help to reduce the personal and economic burden associated to this severe disorder.

Clinical features

Parkinson disease is a debilitating neurodegenerative disorder that dramatically reduces the quality of life of the affected individuals and of their relatives. In terms of pathophysiology, the two major hallmarks of the disease are: i) the loss of dopaminergic neurons from the substantia nigra pars compacta and ii) the presence of protein aggregates mainly composed by the protein alpha-synuclein. It is evident that the first hallmark is the responsible for the defects in motor coordination, however there is a profound debate about the implications of the latter. PD is not the only clinical entity related to alpha-synuclein pathology. The more general term synucleinopathy, which encompasses PD, dementia with Lewy bodies, multiple system atrophy or pure autonomic failure among others, is used to refer to all these neurodegenerative disorders that are associated with alpha-synuclein accumulation. However each of them displays a different clinical picture. Delving deeper into the clinical manifestation, PD presents with bradykinesia, rest tremor, rigidity, gait disturbance and postural instability. These motor deficits are collectively termed as parkinsonism. Diagnosis is mainly motivated by bradykinesia; nonetheless there are certain cases whose first sign is rest tremor. In this regard, two major different motor subtypes can be identified. An earlier-onset tremor dominant form with slow progression and a later-onset form presenting postural instability and gait difficulty (PIGD) with rapid progression (Jankovic et al. 1990). The

underlying cause of PD is currently unknown. However, there are a small percentage of cases that present family history and very likely attributable to the presence of certain genetic conditions.

The basal ganglia and the loss of nigral neurons

In order to understand how the loss of SNpc DA neurons leads to the motor (and some non-motor) symptoms of PD we should first understand what are the basal ganglia and how do they control movement execution. The basal ganglia are a group of subcortical brain nuclei that include the striatum (Str), the internal and external globus pallidus (GPi and GPe), the subthalamic nucleus (STN) and the substantia nigra pars compacta (SNpc) and pars reticulata (SNpr). These different brain regions are interconnected and connected with the motor cortex through separated but parallel loops. These circuits comprise motor, associative (cognitive) and limbic (emotional) domains. The functioning of the motor circuit implicates direct and indirect pathways that are mainly responsible for global motor activation or inhibition. The balance between both pathways is crucial for proper motor execution and the misbalance is behind motor disorders such as PD and Huntington's disease. The striatum can be considered as the hub that integrates both pathways. It integrates both excitatory (cortex and SNpc) and inhibitory (SNpc) inputs. Two different dopamine receptors are responsible for the opposite effects of dopamine in striatal neurons. D1 dopamine receptors are present in a population of striatal medium spiny neurons (MSNs) that initiate the direct pathway. These neurons are activated by nigral dopamine and extend their inhibitory projections to the GPi. Inhibition of the GPi reduces its inhibitory signaling in the thalamus consequently activating the motor cortex. The indirect pathway has an opposite effect over the thalamocortical motor center. It is initiated by the inhibitory activity of the nigral dopamine on MSN bearing D2 dopamine receptors. These D2-type MSNs activate the GPi through a polysynaptic pathway that implicates the GPe and the STN. Activation of the GPi overinhibits the thalamus therefore inhibiting the motor cortex. In Parkinson's disease, the motor symptoms arise when there is a loss of nigrostriatal terminals in the striatum that causes an 80% drop in dopamine. In this situation, the direct pathway is hypoactive whereas the indirect is hyperactive therefore resulting in the akinetic-rigid syndrome (Figure 1 and check Obeso, Rodriguez-Oroz, Stamelou, Bhatia, & Burn, 2014 for a detailed review).

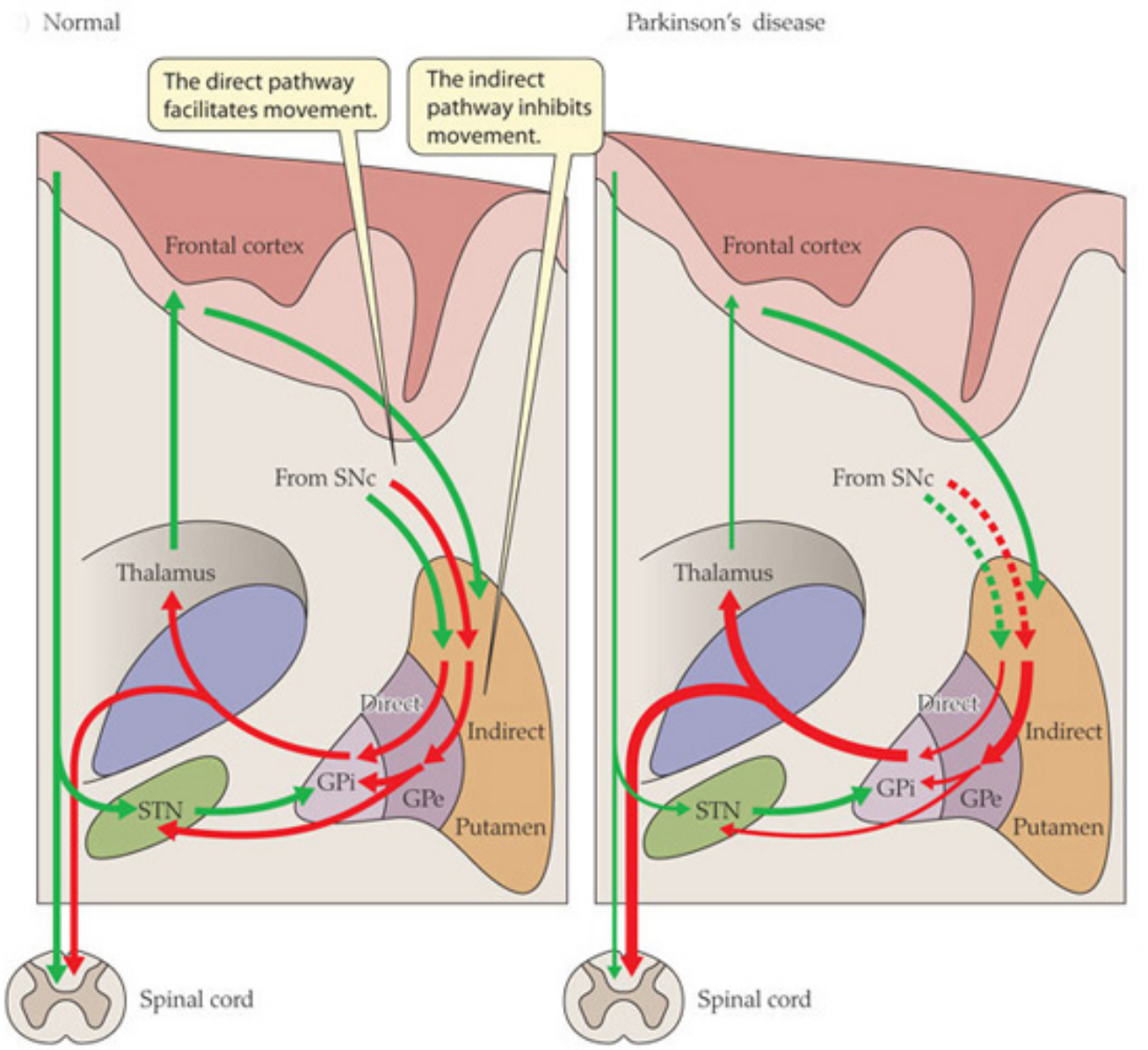

Figure 1: Basal ganglia circuitry in normal and parkinsonian brains
Red arrows indicate inhibitory (mainly GABA-ergic projections), green arrows represent excitatory (mainly glutamatergic) projections. In the normal state (A), the putamen receives cortical excitatory input and projects to output neurons in the GPi through a direct pathway, and by a polysynaptic indirect pathway via the GPe and the STN. Dopamine is thought to inhibit neuronal activity in the indirect pathway and to excite neurons in the direct pathway. In the parkinsonian state (B), when neuronal degeneration in the SNpc and dopamine striatal depletion falls below 50% and 80%, respectively, striatal physiology is disrupted. Dopamine D1 receptor-expressing striatal neurons in the direct pathway become hypoactive, whereas dopamine D2 receptor-bearing striatal neurons in the indirect pathway become hyperactive. The latter response leads to increased inhibition of the GPe, and disinhibition of the STN. Overactivity in STN neurons and reduced inhibition in the direct pathway provokes excessive excitation of neurons in the GPi and overinhibition of thalamocortical and brainstem motor centers, resulting in parkinsonism. From (Hill et al. 2012)

Non-motor symptoms. Before the onset of the motor symptoms and after

The motor disorder is the most recognizable aspect of PD but it is neither the first nor the only symptom associated to the disease. During the course of the disease other non-motor symptoms occur both before and after the onset of the nigral degeneration. The period between the onset of the neurodegenerative process and the manifestation of the motor symptoms is termed the prodrome. The duration of the prodrome is uncertain and it may vary between different patients and PD subtypes but it probably takes more than a decade. There are some prodromal signs that antedate the advent of clinical PD and could serve as biomarkers to identify individuals at risk. These comprise hyposmia, REM sleep behavior disorder (RBD) and dysautonomia (constipation, urinary incontinence and erectile dysfunction). All of these prodromal signs fit into the Braak's staging system of the disease. Braak's hypothesis asserts that the disease process is dictated by the chronological and regional deposition of alpha-synuclein (Braak et al. 2003). It should be noted some cases are discordant with this staging system, probably reflecting certain PD subtypes (Burke et al. 2008). Prodromal symptoms mentioned before correlate well with the regions where alpha-synuclein pathology is first observed. These are the anterior olfactory nucleus, the dorsal motor nucleus of the vagus and the peripheral nervous system.

Each prodromal sign has a different predictive value for detecting an underlying synucleinopathy. For instance, one study indicated that in idiopathic RBD patients at least 94% of them had an underlying synucleinopathy (Boeve et al. 2013). Nowadays, RBD is considered the best predictor for prodromal PD along with imaging techniques such as DaT-SPECT (Iranzo et al. 2010; Jennings, D., et al. 2015) or transcranial sonography (Berg et al. 2011). The International Parkinson Disease and Movement Disorders Society (MDS) Prodromal Parkinson Criteria is establishing predictive models that integrate information from several prodromal features plus sex and age with the aim to identify individuals at risk for developing PD. Good predictive tools are crucial for investigating preventive approaches (Berg et al. 2015). However, it should be noted that when patients are stratified into PD subtypes, not all prodromal criteria are equally applicable. In the case of familial PD linked to the LRRK2 G2019S mutation, hyposmia and RBD have a lower predictive value compared to idiopathic PD, however, DaT-SPECT and SN hyperechogenicity keep on being the most reliable prodromal markers (Sierra et al. 2013; Saunders-Pullman et al. 2015).

Among the non-motor features that arise or consolidate in later stages of the disease we can cite depression, anxiety and dementia. The advent of dementia has been very well studied since it is considered the major cause of disability in the long-term. Contrary to the motor symptoms which are associated to the nigrostriatal pathway, a study in a mouse model suggests that the onset of dementia correlates with the emergence of Lewy bodies in mesocorticolimbic dopaminergic and septohippocampal cholinergic pathways (Hall et al. 2014). Dementia affects to approximately 80% of PD cases (Hely et al. 2008). However its emergence is highly dependent on the PD subtype. Those patients whose disease starts in the elderly (>70 years) have a faster progression with dementia appearing earlier. In contrast, those patients diagnosed around the age of 55 years show

a slower progression with dementia occurring at very late stages of the disease (Obeso et al. 2010).

Treatment

Up to date, there is no definitive cure for PD. However, pharmacological and surgical management of PD have been proved to be efficient in managing the associated symptomatology. There is a broad collection of drugs targeting both motor and non-motor symptoms and their use has to be smartly managed through the progressive course of the disease.

The gold standard for managing the motor symptoms is based on the treatment with levodopa (L-DOPA). The rationale for the use of L-DOPA is to increase the levels of dopamine in the striatum. L-DOPA is a precursor of dopamine (and other catecholamines), and the conversion ia catalysed by the enzyme L-amino acid decarboxylase (AADC). It is amenable to oral administration since contrary to dopamine, L-DOPA is able to cross the blood brain barrier. Along with L-DOPA, several other drugs are co-administered to boost the conversion to dopamine (pyridoxine) or to prevent it in peripheral tissues (carbidopa or benserazide). Inhibitors of the catechol-*O*-methyltransferase (COMT), one of the enzymes responsible for catecholamine degradation, help to maintain dopamine levels therefore prolonging its effect. L-DOPA administration has to be tightly controlled by the clinician and kept the doses low as long as possible. Indeed, during the initial phases of the disease in which the motor impairment is rather mild, other dopamine agonist or monoamine oxidase-B (MAO-B) inhibitors are used instead.
Unfortunately, the “honeymoon” of L-DOPA efficacy expires in the long term. Complications emerge in these patients. Motor complications, termed dyskinesias, and fluctuating responses to L-DOPA with phases with good (“on” state) or no response (“off” state).

Surgical approaches are often indicated for the medication-resistant late stages. Two different interventions can be applied to relieve otherwise intractable motor symptoms: deep brain stimulation (DBS) and lesional approaches. Both strategies are aimed to compensate for the unbalanced neuronal activity of the motor circuit of the basal ganglia. DBS consists in the implantation of a *neurostimulator* that excites certain brain nuclei involved in the motor circuit of the basal ganglia. Lesional approaches commonly target the globus pallidus (pallidotomy), which results in the suppression of dyskinesias. There interventions are reserved for those patients that do not respond to the medication or that have become insensitive.

There are several lines of research for the development of therapies aimed to prevent, to slow down or to restore the neuronal loss. Transplantation of dopamine producing cells has been attempted since the late 80s with some controversial reports describing the autologous transplantation of chromaffin cells in the striatum (Backlund et al. 1985; Madrazo et al. 1987).
Almost contemporarily, open label trials consisting in the grafting of VM cell preparations from

miscarriaged foetus were carried out in Lund (Sweden) (Lindvall et al. 1990; Lindvall et al. 1989) reporting significant neurochemical and functional improvement. They were followed by similar studies in the USA, Canada and Europe. Most of the patients receiving foetal VM grafts showed variable but general improvement in their UPDRS scores. Some patients even withdrew anti-PD pharmacological treatment. The aforementioned success in the open-label trials plus the advent of the Clinton administration opened the funding for trials using foetal tissue. This legal shift motivated the start up of two sham-surgery controlled transplantation procedures in the USA. The results of those trials were published in 2001 and 2003 and mainly reported bad results(Freed et al. 2001; Olanow et al. 2003). Grafted patients did not experience neither subjective nor objective improvement and a fraction of them developed severe graft-induced dyskinesias (GIDs). Retrospective studies have shed light on the reasons behind those negative results. Two theories were raised to explain GIDs. The first of them claimed that these were induced by uneven distribution of the graft-derived innervation, therefore creating DA hotspots (Ma et al. 2002). The other hypothesis attributed the GIDs to excessive serotonergic innervation arising from the grafts. This latter theory prevails nowadays and avoiding serotonergic contamination in VM preparations is a factor to be taken into account for future trials. The issue of the absence of improvement was analyzed in detail during the years that followed. After stratifying the patients by age and by disease stage, authors found out that those patients showing (the highest) improvement were the ones in which the disease was least advanced on baseline. With the preservation of the ventral striatal innervation being a crucial factor (Piccini et al. 2005). All the lessons learnt from these experiences are being integrated in a new European network (TRANSEURO) for promoting standardized procedures for fetal VM transplantations in PD patients (http://www.transeuro.org.uk/).

However, the availability of aborted fetal ventral midbrain tissue is low and it is accompanied by ethical concerns. A limitless source of VM DA neurons is needed. In this regard, pluripotent stem cells (PSCs) represent the ideal source for such neurons. PSCs are cells with limitless self-renewal capability and with the ability to give rise to virtually any cell type from the adult body (Evans & Kaufman 1981). Two types of PSCs have been proposed: hESC and hiPSC. The first one is derived from the early embryo, so it shares to some extent the same ethical issues as the fetal VM tissue. The second are derived from adult somatic cells therefore avoiding using embryonic tissue and allowing the generation of autologous PSC (Takahashi et al. 2006). Currently, bona-fide VM A9 DA neurons can be generated from PSC using defined procedures (Kirkeby, Grealish, Wolf, Nelander, Wood, et al. 2012; Kriks et al. 2011) and their pre-clinical efficacy and has been corroborated and compared to that of the fetal counterparts (Hallett et al. 2015; Morizane et al. 2013; Grealish et al. 2014; Kirkeby et al. 2017). With further refinement of current techniques, the introduction of PSC in the PD clinical field will probably be a reality in the next decade (Barker et al. 2015). However, fully restorative therapy for PD would need complementary treatments since disease progresses outside the nigra in grafted patients (Politis et al. 2012)

Finally ongoing clinical trials are evaluating the safety and efficacy of gene delivery into the basal ganglia using viral vectors. The most utilized vectors are adeno-associated viruses (AAV) due to

their lack of genomic integration, low immunogenicity and the ability to transduce quiescent cells. These are based on two different principles: those based on the overexpression of trophic factors and those based on the improvement of dopamine metabolism. The glial family of ligands, neurturin and GDNF, have demonstrated pre-clinical efficacy in animal models (reviewed in (Kordower & Bjorklund 2013). Unfortunately the two clinical trials performed with neurturin have failed in providing improvement of the motor deficits (Marks et al. 2010; Bartus et al. 2015). Another clinical trial using GDNF is ongoing but researchers have pointed out that primary efficacy endpoint has not been met (unpublished information). The advanced nigrostriatal degeneration in those patients enrolled in the trial has been postulated to be behind the negative results (Kordower et al. 2013). On the other hand, viral gene delivery of aromatic amino decarboxylase (AADC) or AADC plus tyrosine hydroxylase (TH) and GTP cyclohydrolase (hence reconstituting the DA synthesis pathway) have provided positive results in terms of motor improvement (Palfi et al. 2014; Mittermeyer et al. 2012). Finally, gene therapy based on glutamic acid decarboxylase

Further refinement of the aforementioned techniques is likely to revolutionize PD clinical management. There is also an urgent need to detect those patients at risk to develop PD since they represent the ideal target to explore preventive treatments (Noyce et al. 2017).

Etiology

As in many other late-onset neurodegenerative diseases, the strongest risk factor for PD is the age. The prevalence of PD rises steeply with age. It is difficult to provide a worldwide estimate, given that there are many confounding variables related to diagnosis criteria or reduced life expectancy in different countries. It is commonly accepted that PD affects to 1% of the population over the age of 60 (Guttmacher et al. 2003). Ethnicity and gender are also considered to affect the prevalence with Asian and black people and women being less affected respectively (de Lau et al. 2006). Although some of these findings are still disputed (Morens et al. 1996).

Most PD cases are classified as idiopathic, meaning that the underlying causes are unknown. The traditional view supported the idea that the etiology was mainly environmental. This hypothesis was reinforced by the notion of some environmental toxins such as pesticides, metals and some chemicals causing parkinsonism (http://www.pdf.org/environment_parkinsons_tanner). The pictured changed 20 years ago when a point mutation in the gene encoding for alpha-synuclein (*SNCA*) was found to cause PD. That same year, alpha-synuclein was identified as one of the most abundant components of Lewy Bodies (Spillantini et al. 1997). This finding represented a paradigm shift since not only some PD cases could be classified as genetic but also they were pathophysiologically linked to the sporadic disease. Since then, more than a dozen genes have been associated with familial PD and the list keeps growing. In the case of the more common sporadic PD, its causes are way more complex. In this case, the picture that emerges is that of the

environment exerting its effect over a particular genetic makeup. In this section the current knowledge regarding the aetiology of PD will be discussed.

Environmental risk factors

There is a limited and well-defined list of environmental toxins that cause parkinsonism. MPTP, An incidental by-product that appears during the synthesis of the opioid drug MPPP has been reported to induced neuronal death specifically in the substantia nigra (Langston et al. 1983). Occupational exposures such as those associated to farming or well water drinking are also related to increased PD risk (Pezzoli & Cereda 2013). In particular the pesticide rotenone and the herbicide paraquat, which are inhibitors of the complex-I of the mitochondrial respiratory chain, have shown to selectively deplete nigral neurons in animal models (Greenamyre et al. 2000a). Welding and exposure to heavy metals have also been associated to increased PD risk. Iron deposition in brains from PD patients is a common finding in PD patients' brains (Dexter et al. 1987) and and it is a hallmark of certain familial mutations.

However, there is a series of habits that confer higher risk for most of the diseases that in the case of PD, they are associated to a reduced risk. These are tobacco smoking and coffee drinking. A meta-analysis pooling a large number of case-control and cohort studies of tobacco and coffee yielded relative risks estimates ranging from 0.80 (past) to 0.39 (current) for smokers and 0.60 for coffee drinkers (Hernán et al. 2002).

Genetic factors

Initial studies in twins performed during the 90s precluded that the genetic influence was low. However this conclusion was questioned (Johnson et al. 1990) and a separate study found a 100% concordance between monozygotic twins when the age at onset was less than 50 years (Tanner et al. 1999). This fact together with the finding of kindreds in which the heritability of PD followed a Mendelian pattern led researchers to start considering the study of the genetic component of the disease. Several strategies have been pursued to tackle the genetic contribution and they mainly differ in the amount of risk associated to each particular genetic variant and the molecular nature of such variant. On the other hand, the progress in PD genetics has has grown thanks to the introduction of new techniques for whole-genome interrogation as well as the recruitment of large cohorts of patients to increase statistical power to draw reliable conclusions.

Familial (Mendelian) PD genes

The observation of some families showing aggregation of PD (Lazzarini et al. 1994) coupled with the existence of families in which the transmission of the disease was consistent with the segregation of one gene motivated the launch of genetic studies. These initial studies consisted in the identification of genomic portions that specifically co-segregated with the disease in affected families. To do so, geneticists sequentially pursue identifiable genetic variants or polymorphisms that are increasingly more proximal to the causal variant. After having narrowed down to a region small enough to be sequenced, the disease causing polymorphism can be eventually identified. Through this approach, the first PD-causing mutation was ascertained in one Italian and three independent Greek families with an autosomal dominant inheritance. It was a nonsynonymous substitution in the fourth exon of the *SNCA* gene causing the Ala53Thr substitution in the protein. Clinically, associated PD was atypical with an early onset (30-50 years of age) and rapid progression with Lewy body disease. Many attempts to reproduce this finding in PD families from other countries were mostly unsuccessful, suggesting that the Ala53Thr mutation was a rare cause of PD (Scott et al. 1997; Muñoz et al. 1997; Vaughan et al. 1998). In the years that followed, many other alpha-synuclein mutations (Krüger et al. 1998; Zarranz et al. 2004) and locus multiplications (Ibáñez et al. 1998; Chartier-Harlin et al. 2001; Singleton et al. 2003) as well as other genomic loci were linked to familial PD. Besides alpha-synuclein, mutations in Parkin (PARK2) (Kitada et al. 1998), PINK1 (PARK6) (Bonifati et al. 2005) and DJ-1 (PARK7) (Valente et al. 2004) were also found in early onset familial PD cases. Interestingly, though not fully penetrant, heterozygous CNVs and point mutations in Parkin and point mutations in PINK1 are relatively common and important risk factors for developing PD (Klein, Lohmann-Hedrich, Rogaeva, Schlossmacher, & Lang, 2007; Huttenlocher et al., 2015;Puschmann et al., 2017)

However, these mutations kept on representing a very small fraction of the even reduced proportion of familial cases. Furthermore, their associated disease is clinically different from the idiopathic cases. In 2004, the gene responsible for the association of autosomal dominant PD with the locus PARK8 was identified. Several coding mutations were found to segregate with the disease in 3 Basque and 1 English families (Paisán-Ruíz et al. 2004) and 1 German-Canadian and 1 western Nebraskan families (Zimprich et al. 2004). One year after, three simultaneous publications reported the discovery of the most common LRRK2 mutation, the G2019S substitution. Di Fondo A. and coworkers found the mutation in 4 out of 61 families, 2 from Italy and the other 2 from France and Brasil (Di Fonzo et al. 2005). Nichols W. *et al*. found the G2019S mutation in 20 out of 358 families and interestingly 1 individual presented the mutation in homozygosis with no obvious enhancement of the pathogenicity (Nichols et al. 2004). The third study, investigated the occurrence of the mutation in idiopathic PD cases. Gilks W. P. *et al.* found that 1.6% of the cases were carriers of LRRK2 G2019S mutation. This particular feature of the G2019S mutation in LRRK2 was confirmed by independent studies (Bardien et al. 2011; Healy et al. 2008).

Nowadays the number of genes responsible for familial cases of the disease exceeds the dozen (Table 1). A graphical representation of the different forms of genetic PD and their clinical particularities and epidemiological features is depicted in figure 2 The incorporation of new sequencing technologies such as whole genome (WGS) or whole exome (WES) sequencing alone or in combination with genome wide association analysis (GWAS) are speeding up the discovery of new variants. An example of this is the recent discovery of novel genes mutated in familial PD: *VPS35* (Vilariño-Güell et al. 2011; Zimprich et al. 2011), *TNR* and *TNK2* (Farlow et al. 2016), *CHCHD2* (Funayama et al. 2015), *TREM230* (Deng et al. 2016) and *DNAJC13* (Vilariño-Güell et al. 2014). Despite the implication of the last two is still disputed because both were initially found in the same affected kindred. In all of these cases, exome sequencing alone or in combination with linkage analysis has allowed to interrogate the whole coding genome and subsequently find pathogenic variants that closely correlated with the disease in the affected individuals.

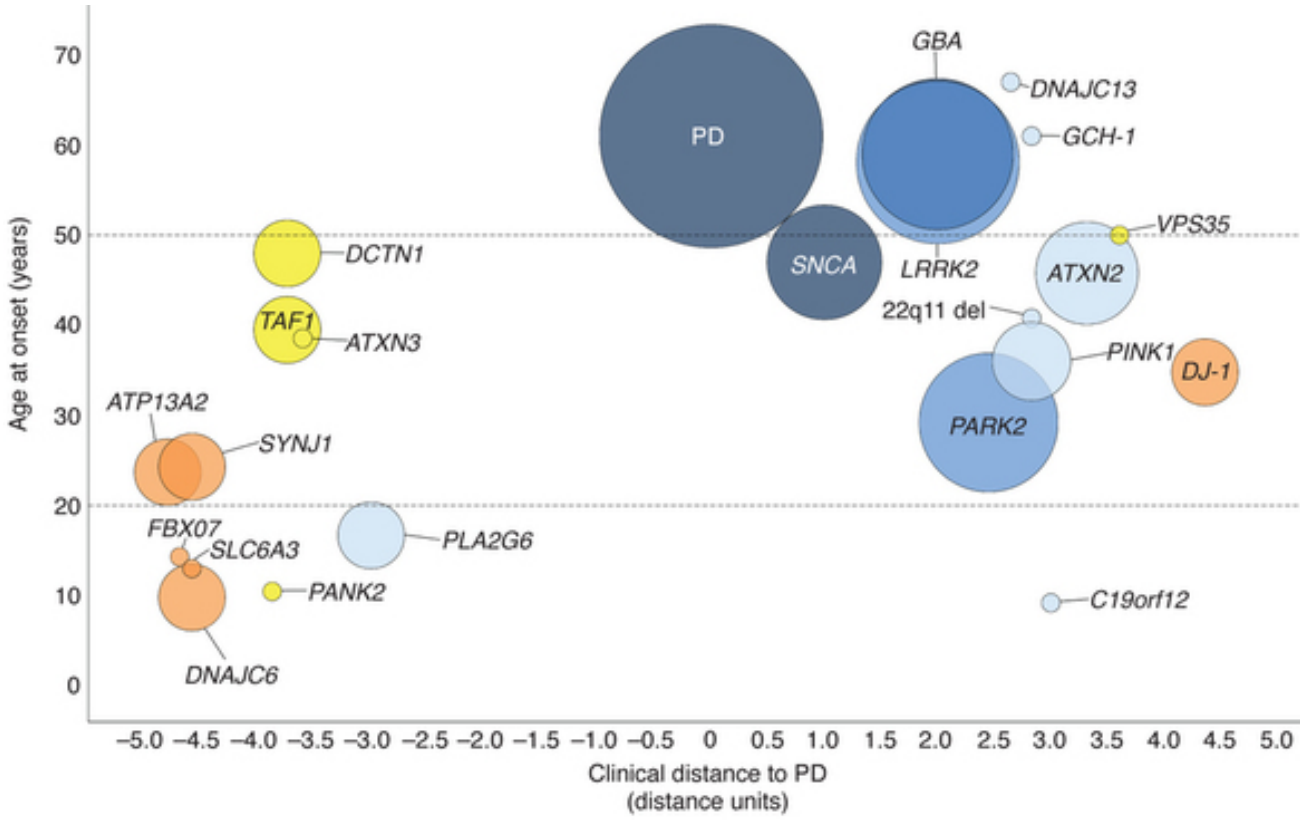

Figure 2: correlation between different forms of genetic Parkinsonism and sporadic PD with age at onset. To more readily the relationship between various forms of parkinsonism and sporadic Parkinson's disease, we used the information of diverse nature (genetics, clinical assessments and neuropathology) to calculate the Euclidean distance of the clinical manifestations of the gene, mutation or condition listed relative to sporadic Parkinson's disease (x axis). The y axis represents the age of onset of disease, and the size of each bubble represents the relative prevalence. The bubble labeled “PD” refers to idiopathic PD whose genetic component is uncertain. Color shades were used to reflect this as follows: dark blue indicates Lewy body pathology in all cases; medium blue indicates variable findings with the majority of cases showing Lewy body pathology; light blue indicates Lewy body pathology in only a few cases; yellow indicates that Lewy body pathology was not found but the data are sparse or incomplete; orange indicates no data were available.From (Langston et al. 2015).

Table 1: Genes involved in Mendelian forms of the disease

PARK CODE	Gene name	Chr. location	Inheritance	Onset	Histopathology	Proposed pathway
PARK1, PARK4	*SNCA*	4q22.1	AD	EOPD	LB+	Multiple
PARK2	*PRKN*	6q26	AR	EOPD	Absence of LB in most of the cases	Mitochondrial
* PARK5	*UCHL1*	4q13	AD	LOPD	N/R	Proteostasis
PARK6	*PINK1*	1p36.12	AR	EOPD	LB+ in a few cases	Mitochondrial
PARK7	*DJ-1*	1p36.23	AR	EOPD	N/R	Redox
PARK8	*LRRK2*	12q12	AD	LOPD	Mutation-dependent LB+, tauopathy in few G2019S cases	Vesicle trafficking, lysosome
PARK9	*ATP13A2*	1p36.13	AR	JPD	LB N/R, iron deposition	Lysosome
*PARK11	*GIGYF2*	2q37.1	AD	LOPD	N/R	Translation control
*PARK13	*HTRA2*	2p13.1	AD	LOPD	N/R	Mitochondrial?
PARK14	*PLA2G6*	22q13-1	AR	JPD	Iron deposition in some of the cases	Lipid metabolism
PARK15	*FBXO7*	22q12.3	AR	JPD	N/R	Mitochondrial
PARK17	*VPS35*	16q11.2	AD	LOPD	LB-	Vesicle trafficking
*PARK18	*EIF4G1*	3q27.1	AD	LOPD	LB+	Translation control
PARK19A/B	*DNAJC6*	1p31.3	AR	JPD (A), EOPD	N/R	Vesicle trafficking
PARK20	*SYNJ1*	21q22.2	AR	EOPD	N/R	Vesicle trafficking
**PARK21	*DNAJC13*	3q22.1	AD	LOPD	LB+	Vesicle trafficking
**PARK21	*TMEM230*	20p12	AD	LOPD	LB+	Vesicle trafficking
*PARK22	*CHCHD2*	7p11.2	AD	LOPD	N/R	Mitochondrial
PARK23	*VPS13C*	15q22.2	AR	EOPD	LB+	Mitochondrial, vesicle trafficking
-	***TNR*	1q25.1	AD	LOPD	N/R	Neurite growth, cell adhesion and Na channel functioning
-	***TNK2*	3q29	AD	LOPD	N/R	Survival pathways

* These associations are controversial; some of them have not being confirmed in separate replication studies. However reduced penetrance could account for the discordances in most cases.

** These associations are conflicting since they were found in the same large multiplex kindred. Further studies are advised.

*** Authors reporting these genes do not explicit they are Mendelian but suggest they have intermediate penetrance (such as LRRK2 G2019S).

Particular features of LRRK2: insights into genetics and function

Normal physiological function of LRRK2 within the cells is largely unknown. Its multi-domain nature suggests it may be related to multiple cellular functions. It contains several domains, some of them having enzymatic activity such as the ROC-COR domains and its GTPase activity and the kinase domain as well as other domains with mainly protein-protein interaction functions. Most PD pathogenic mutations map to the enzymatic domains (see Fig. 3)

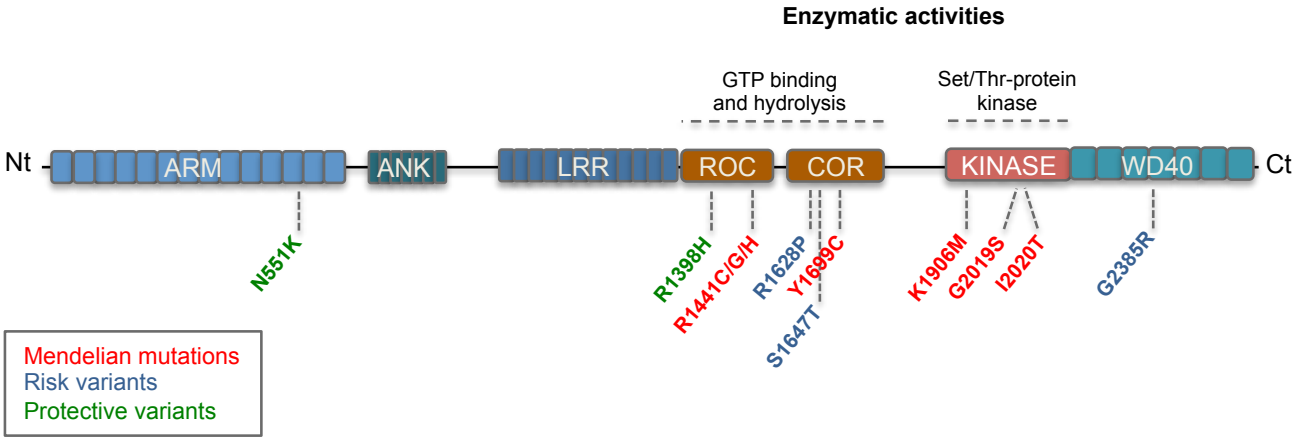

Figure 3: LRRK2 protein structure
LRRK2 is a large multidomain protein (2527 aa) with two catalytic domains (ROC-COR and KINASE) and several protein-protein interaction domains. It acts as an homodimer . Disease-causing mutations cluster in the enzymatic core (indicated in red). However, several mutations modulating PD risk are found both inside and outside the catalytic domains. Risk-conferring variants are indicated in blue and protective variants in green.

In this regard, there are several approaches that can provide an approximate idea of what could be the biological processes related to LRRK2. Regarding subcellular localization, LRRK2 has been shown to co-purify with vesicular structures after subcellular fractionation (Biskup et al. 2006). However, co-localization with tubular structures immunoreactive for tubulin is observed upon inhibition of the kinase domain or in the case of ROC-COR domains mutants (Dzamko et al. 2010; Blanca Ramírez et al. 2017). The association of LRRK2 with vesicle-related process is reinforced by the identification of both interaction partners and phosphotargets. Beilina A. and colleagues performed an unbiased proteomic identification major LRRK2 interacting proteins using a protein-protein array and confirmed in brain lysates. They drew a protein network comprising Bag5, GAK and Rab7L1 (a.k.a. Rab29). The latter two belong to loci previously related to the disease in GWAS studies that will be discussed in the following section. In order to assess their effect on LRRK2-related phenotypic effects, they transfected these genes in primary neuronal cultures. Similar to LRRK2 G2019S overexpression, forced expression of Bag5, GAK and Rab7L1 reduced total neurite length. Given that Rab7L1 and GAK localized to the trans-Golgi network (TGN) and that Rab7L1 forced LRRK2 re-localization to the Golgi, they analyzed the organelle structural appearance. Experiments performed in primary neurons and in HEK293 showed an increased autophagic clearance of the Golgi apparatus upon overexpression of each interactor. Intriguingly, most LRRK2 pathogenic mutations exacerbated this affect as it did co-expression of Rab7L1.

Another interesting observation was that the effect of each protein was abrogated when one of the interactors were knocked-down by small interfering RNA (siRNA) (Beilina et al. 2014). However, this was not the first report linking LRRK2 to Rab7L1 and vesicle sorting. MacLeod D. A. followed an interesting approach that consisted in finding a SNP that impacted the brain transcriptome of healthy subjects in a similar fashion as the LRRK2 GWAS hit (rs11176052). The GWAS hit that presented a higher degree of overlap in terms of global transcriptome impact was rs823114 located in PARK16, the locus that contains Rab7L1. Additionally, a strong epistatic interaction was detected between both variants after analyzing the odds ratios (ORs) of different allelic combinations. Then, the authors performed experiments in primary neurons to determine the mechanistic nature of such genetic interaction. They observed that either LRRK2 G2019S mutation or reduced Rab7L1 expression impaired protein sorting from the Golgi due to a defective retromer complex function. The retromer complex is responsible recycling membrane proteins that have ended up in the endosome back to the Golgi. An example of such membrane proteins is the cation independent mannose 6-phosphate receptor (CI-M6PR) whose main function is to target lysosomal enzymes from the Golgi to the lysosome. Therefore, defective retromer complex function could lead to lysosomal dysfunction. Conversely, when the neurons overexpressed the PD- and retromer-related *VPS35* gene proper protein sorting was resumed. These experiments reinforce the idea of *LRRK2*, along with other PD genes, playing a role in vesicle management.

Another interesting feature of the most common LRRK2 G2019S mutation is its reported variable penetrance. It is commonly accepted that penetrance estimates are affected by several biases. The most important might be the fact that the penetrance of mutations causing autosomal dominant disorders is mostly ascertained studying affected families. As aforementioned, there exist a considerable proportion of LRRK2 G2019S PD cases of sporadic origin. The lack of family history could have several explanations ranging from an incomplete clinical record of the family to early decease of other family carriers, de novo mutations (never reported) or to reduced penetrance in certain families. This raises the possibility of the existence of certain families in which the carriers remain asymptomatic throughout their lives. The variability of LRRK2 G2019S associated penetrance has also been observed among different populations or ethnic groups. As idiopathic PD, LRRK2-related PD is also progressive and age-dependent. First penetrance figure reported was 85% at age 70 years in families from the USA and Europe (J Kachergus et al. 2005). Other reports in relatively small and genetically uniform populations point to reduced penetrance estimates such as 26% at age 70 years in Cantabria (Northern Spain) (Sierra et al. 2011) or 24% at age 80 years among Ashkenazim (Marder et al. 2015). A recent publication has compared the age dependent penetrance of both idiopathic and LRRK2 G2019S-related PD in Arab-Berber from Tunisia and in the ethnic Norwegian population. Interestingly, while the incidence and the penetrance of idiopathic PD did not differ between both groups, the LRRK2 G2019S mutation had a much lower penetrance in Norwegian when compared to the Tunisian Arab-Berber population (43% *versus* 86% at age 70 years) (Hentati et al. 2014). On the other hand, LRRK2 G2019S carrier families also present an increased number of phenocopies compared to what it would be expected by chance. Phenocopies are affected individuals in one family who do not carry the

mutation (Gaig et al. 2006; Nichols et al. 2004). Suggesting that there might an increased burden of disease-fostering variants in those families in which higher penetrance of the mutation. In line with this finding, Lubbe and colleagues analyzed the frequency of rare variants in Mendelian PD genes and GBA in patients *versus* controls. They found that in general, those PD patients whose disease was attributable to the presence of a Mendelian mutation, the frequency of bearing additional rare variants in Mendelian genes doubled those of the controls or of idiopathic PD cases and there was a trend towards lower AAO. In the case of LRRK2 G2019S carriers, almost half of those additional variants lied in the ATP13A2 gene. This suggests oligogenic inheritance of rare mutations in specific cellular pathways contribute to disease in Mendelian cases. Altogether, these facts point to the existence of modifiers, either genetic or environmental, of the penetrance and AAO of LRRK2 G2019S-related PD.

In this regard, several research groups have been sought out genetic modifiers of LRRK2 penetrance, both targetedly and genome-wide. Besides Macleod A. et al., other investigators have studied the interaction of PARK16 and LRRK2. Philstrøm L. and colleagues found some haplotypes defined by three SNPs spanning the transcription start site of Rab7L1 that were significantly less frequent in PD cases compared to controls. Using these haplotypes, they also replicated the epistatic interaction between LRRK2 GWAS hit and PARK16 (Pihlstrøm et al. 2015). However, the association of the different variants in PARK16 with the disease and also with LRRK2 seems to be very population dependent (Trinh et al. 2015). For example, in the Ashkenazi Jewish population, the haplotype with the highest and lowest attributable risk was defined by other alleles in two of the positions and a different SNP (Gan-Or et al. 2012). These findings emphasize the importance of finding alternative alleles that reduce the PD risk below the population average risk since they indicate path to take for eventual protective treatments (Gan-Or et al. 2015). There is a couple of genome-wide attempting to find determinants of reduced AAO of LRRK2 PD mutations. The first of them performed a GWAS with AAO in a cohort of 113 familial LRRK2 PD mutations carriers. They found association in two linkage peaks located in 1q32.1 and 16q12.1 respectively. However no SNPs in those regions were found that reached the criteria for genome-wide significance (Latourelle et al. 2011). A follow-up of that study was performed in a more homogeneous experimental setting. They narrowed down to both a single LRRK2 mutation –G2019S– and a genetically uniform population –Arab-Berber from Tunisia–. In this case, a linkage peak was found between 1q23.3 to 1q24.3. After association mapping with SNPs lying in that region, one SNP (rs2421947) showed genome-wide significance and was tagging a haplotype covering the *DNM3* gene. The AAO was extended by a median of 12.5 years in the Arab-Berber cohort when the C allele was carried in homozygosis. The association with the AAO was replicated in other populations though its effect was less pronounced. Brain expression data suggested that rs2421947 was an eQTL of DNM3 and *in vitro* approaches confirmed the interaction between LRRK2 and DNM3 (Trinh et al. 2017). This finding strengthens the connection between LRRK2 and the vesicle biology since dynamin proteins are responsible for the final excision of newly formed vesicles from their original membranes (Ferguson & De Camilli 2012).

Parkinson's disease is not the only clinical entity associated to LRRK2 mutations. Mutations in LRRK2 are a risk factor for Chron's disease (Barrett et al. 2008), leprosy (Zhang et al. 2009) and certain types of cancer (Agalliu et al. 2015). This fact suggests that LRRK2 might have several and probably interconnected functions. On the other hand, LRRK2 is expressed everywhere within the brain, in kidney, lung, as well as in immune cells in high levels. Indeed, when querying in gene expression databases for experiments in which LRRK2 shows a differential gene expression, most of the entries are related to immune system functions such as response to IFN-γ, LPS or infection. Knockout studies in mouse and rat or chemical inhibition in non-human primates have provided interesting clues about LRRK2 biology. The tissues mostly affect by the absence of LRRK2 are precisely the kidney, lungs and the immune system (Baptista et al. 2013; Fuji et al. 2015; Herzig et al. 2011; Tong et al. 2010) and to a lesser extent some behavioral features (Hinkle et al. 2012). In kidney and lung, vesicular structures are found accumulated in these tissues, reinforcing the idea of LRRK2 coordinating vesicle-related processes. Therefore the participation of other tissues rather than the brain should be taken into account when studying the disease pathophysiology.

Susceptibility genes

We have to be aware that mutations in the genes summarized in Table 1 account for a relatively small portion of familial PD cases. In fact, less than 10% of the familial cases are linked to monogenic mutations (Trinh & Farrer 2013). There is still a large extent of heritability that has not been ascribed to any genetic defect. In this respect, the application of the genome-wide genotyping technologies has allowed to explore the contribution of common variants with a small associated risk. The common variant common disease (CV-CD) states that polymorphisms that are commonly found in the general population can contribute with a small portion of the total risk of manifesting a certain disease. This type of approach requires large cohorts of cases and controls and genome-wide interrogation tools such as single nucleotide polymorphism (SNP) array. The differential presence of a given variant in either the control or the diseased group is indicative of its association to the disease or the non-affected condition. The magnitude of the differential association to any of those conditions is represented by the *odds ratio* (OR) value. When OR>1 it means that the effect allele (typically the alternative allele) is more frequent within affected individuals and therefore associated to the disease. And the other way round, when OR<1, it suggests that the effect allele protects against the disease. In any case, it should be noted that the associations found only point to genomic loci related to the disease. Nor the exact variant nor its disease-related effect is cleared out through this approach. Further experiments are required to unveil the actual mechanistic link.

Middle way between the very rare and highly penetrant PD mutations and common, low-risk variants, there is another gene that deserves special attention: *GBA*. Homozygous or compound heterozygous mutations of the gene encoding for the GCase cause Gaucher's Disease (GD).

Initially, the fact that Parkinsonism was frequently observed in GD patients was controversial given that type 2 and type 3 GD are neuronopathic. However, it was also noted that non-neuronopathic GD type 1 patients (McKeran et al. 1985) and heterozygous carriers of *GBA* mutations also showed increased incidence of Parkinsonism (Goker-Alpan et al. 2004). Several studies were conducted to investigate the incidence of *GBA* mutations among PD patients. A meta-analysis published in 2009 reported a strong association between *GBA* mutations and PD with ORs of 9.68 and 3.30 for GD-related L444P and N370S in non-Ashkenazi subjects respectively (Sidransky et al. 2009). This same study pointed to the convenience of not limiting the screening to GD-related mutations given that the OR for all *GBA* mutations was 6.51. An indirect confirmation of this last figure was the detection of the GBA locus in the study by Nalls et al., (2014) with its associated SNP showing an OR of 1.824. Nowadays, *GBA* is considered the strongest genetic risk factor for developing PD with lifetime risk estimates lying somewhere in between 15% and 30% (McNeill et al. 2012; Anheim et al. 2012)

In the case of PD, several GWAS studies have been published to date. Through these studies the CV-CD hypothesis was confirmed with several loci showing significant genome-wide significance. Simón-Sánchez J. and coworkers found association in genomic regions that contained: genes previously linked to PD (*SNCA*, *LRRK2*), genes previously associated to other diseases such as *MAPT* and a new locus that was termed *PARK16*. This loci contained three genes in a linkage disequilibrium block: *NUCKS1*, *RAB7L1*, and *SLC41A1* (Simón-Sánchez et al. 2009; Satake et al. 2009). Studies to unveil the contribution of this locus to the disease will be discussed in a separate section. By using this same approach, but in familial PD, similar results were obtained with *SNCA* and *MAPT* as well as SNPs located in the locus containing *GAK/TMEM175/DGKQ* (Pankratz N. et al., 2009). Some other GWAS were carried out noticing new variants, however the big step forward was given in 2014 when the results of an extensive meta-analysis were published. In this study, a total of 24 risk loci were identified, 6 of those reported for the first time (Table 2). Interestingly, 8 of those loci contained a second independent risk allele and 4 out of them remained significant in the replication phase totaling to 28 independent risk variants (Nalls M.A. et al., 2014). Despite the small risk associated to the different susceptibility variants, combinatorial models can be elaborated to calculate or infer the risk associated to carrying more than one risk allele. In the particular case of the aforementioned meta-analysis, risk profiles were computed utilizing the 28 SNPs that met the significance criteria. When comparing the distribution of the genetic risk, the difference between the first and the fifth quintiles of genetic risk score the OR was 3.31. That figure is comparable to the risk of bearing GD-related GBA mutations.

Table 2: List of 26 loci presenting genome-wide significant in Nalls et al. (2014) meta-analysis

Polymorphism	Location (hg19)	Gene	Ethnicity	# Samples	# Studies	Allele contrast	1000G CEU	1000G CHB+JPT	Meta OR (95%CI)	I2 (95%CI)	Meta P-value
rs356182	chr4:90626111	SNCA [-19139bp]	All: C	120,238	21	G vs. A	0.417 (G)	0.375 (A)	1.34 (1.30-1.38)	50 (17-70)	1.85e-82
rs17649553	chr17:43994648	MAPT	All: C	114,483	20	T vs. C	0.217 (T)	-	0.77 (0.75-0.80)	0 (0-37)	6.11e-49
rs34311866	chr4:951947	TMEM175	All: C	120,238	21	C vs. T	0.15 (C)	0.075 (C)	1.26 (1.22-1.31)	52 (21-71)	6.00e-41
rs71628662	chr1:155359992	ASH1L	All: C	110,323	18	T vs. C	-	-	0.52 (0.46-0.58)	0 (-)	6.86e-28
rs12637471	chr3:182762437	MCCC1	All: C	120,238	21	A vs. G	0.242 (A)	0.417 (G)	0.84 (0.81-0.87)	35 (0-62)	5.38e-22
rs1955337	chr2:169129145	STK39 [+24494bp]	All: C	120,238	21	T vs. G	0.083 (T)	0.317 (T)	1.21 (1.16-1.26)	17 (0-51)	1.67e-20
rs6430538	chr2:135539967	intergenic	All: C	120,238	21	T vs. C	0.408 (T)	0.025 (C)	0.88 (0.85-0.90)	0 (0-45)	3.35e-19
rs11724635	chr4:15737101	BST1	All: C	120,238	21	C vs. A	0.433 (C)	0.458 (A)	0.89 (0.87-0.91)	8 (0-42)	4.26e-17
rs823118	chr1:205723572	NUCKS1 [+4168bp]	All: C	120,238	21	C vs. T	0.45 (C)	0.417 (T)	0.89 (0.87-0.92)	41 (0-65)	1.96e-16
rs1555399	chr14:67984370	TMEM229B	All: C	108,99	15	T vs. A	0.475 (T)	0.45 (T)	1.15 (1.11-1.19)	97 (96-98)	5.70e-16
rs76904798	chr12:40614434	LRRK2	All: C	120,238	21	T vs. C	0.158 (T)	-	1.16 (1.11-1.20)	0 (0-47)	4.86e-14
rs199347	chr7:23293746	GPNMB	All: C	120,238	21	G vs. A	0.392 (G)	0.325 (G)	0.90 (0.87-0.92)	11 (0-46)	5.62e-14
rs9275326	chr6:32666660	HLA-DQB1 [+30500bp]	All: C	99,286	13	T vs. C	0.175 (T)	0.083 (T)	0.80 (0.75-0.85)	2 (0-58)	5.81e-13
rs2414739	chr15:61994134	intergenic	All: C	120,238	21	G vs. A	0.283 (G)	0.183 (G)	0.90 (0.87-0.92)	19 (0-52)	3.59e-12
rs14235	chr16:31121793	BCKDK	All: C	120,238	21	A vs. G	0.45 (A)	0.092 (G)	1.10 (1.07-1.14)	31 (0-59)	3.63e-12
rs329648	chr11:133765367	MIR4697 [-3032bp]	All: C	120,238	21	T vs. C	0.333 (T)	0.267 (T)	1.11 (1.07-1.14)	0 (0-47)	8.05e-12
rs117896735	chr10:121536327	INPP5F	All: C	104,595	13	A vs. G	0.017 (A)	-	1.77 (1.50-2.08)	15 (0-54)	1.21e-11
rs6812193	chr4:77198986	FAM47E	All: C	120,238	21	T vs. C	0.392 (T)	0.092 (T)	0.91 (0.88-0.93)	36 (0-62)	1.85e-11
rs12456492	chr18:40673380	RIT2	All: C	120,238	21	G vs. A	0.375 (G)	0.4 (G)	1.10 (1.07-1.14)	17 (0-51)	2.15e-11
rs11060180	chr12:123303586	CCDC62	All: C	105,818	17	G vs. A	0.483 (G)	0.208 (G)	0.91 (0.88-0.93)	21 (0-56)	3.08e-11
rs7155501	chr14:55347827	GCH1	All: C	108,99	15	A vs. G	-	-	1.12 (1.08-1.15)	9 (0-46)	1.25e-10
rs10797576	chr1:232664611	SIPA1L2	All: C	120,238	21	T vs. C	0.092 (T)	0.092 (T)	1.13 (1.09-1.18)	0 (0-41)	1.76e-10
rs55785911	chr20:3153503	UBOX5 [+12661bp]	All: C	120,238	21	A vs. G	0.417 (A)	0.392 (G)	0.91 (0.88-0.94)	29 (0-58)	3.30e-10
rs62120679	chr19:2363319	TMPRSS9 [-26450bp]	All: C	99,286	13	T vs. C	0.292 (T)	0.3 (C)	1.14 (1.09-1.19)	47 (0-72)	2.52e-09
rs3793947	chr11:83544472	DLG2	All: C	108,99	15	A vs. G	0.375 (A)	0.442 (A)	0.91 (0.88-0.94)	0 (0-19)	2.59e-08
rs591323	chr8:16697091	intergenic	All: C	120,238	21	A vs. G	0.325 (A)	0.383 (A)	0.91 (0.89-0.94)	0 (0-43)	3.17e-08

Bioinformatic analyses have been conducted in order to investigate the mechanism by which these variants confer increased PD risk. GWAS hits only indicate genomic regions in which there exists genetic variability that influences the risk of suffering the disease. Most probably they are a proxy SNP (SNP in close linkage disequilibrium) of the actual variants. Two main mechanisms can be considered: i) the hit is linked to coding variation in nearby genes or ii) the hit is linked to variation in regulatory regions such as CpG islands, copy number variations (CNV), transcription factor (TF) binding sites (Soldner et al. 2016; Coetzee et al. 2016) or binding sites for regulators of chromatin architecture (Coetzee et al. 2016; Lupiáñez et al. 2015). In the latter case, those variants are termed expression quantitative trait loci (eQTL) since each allele is associated to increased or reduced expression of nearby genes. Two studies have tried to find out which are the mechanisms through which GWAS hits lying in the non-coding regions modify PD risk. To this end, Vermunt M. V. *et al.* elaborated a detailed catalogue of distal enhancers that are active in different brain regions. Crossing this information with the GWAS hits in the *SNCA* gene and PARK16 locus shed interesting information. The hit in *SNCA,* was in tight linkage disequilibrium with two other SNPs located in a putative enhancer in intron 4. This enhancer was shown to interact physically not only with *SNCA* promoter but also with nearby genes. Using a murine reporter system for enhancer activity, they ascertained that the enhancer was active in the brain from E11.5 on. The posterior hindbrain-midbrain boundary and the dorsal root ganglia were the regions with the highest activation, two regions in which the synucleinopathy becomes evident during the first stages of the disease (Sumikura et al. 2015; Seidel et al. 2015). The functional effect of variation at this enhancer has been also studied in detail using an elegant *in vitro* human model that will be discussed in a separate section (Soldner et al. 2016). PARK16 hit was itself placed in an enhancer that presented increased activity in the cerebellum in the human data and in the midbrain and neural tube in the murine reporter. Coetzee S. G. and colleagues applied a similar but slightly divergent approach. Instead of restricting their analysis to brain-specific enhancers, they crossed the collection of GWAS hits with the Roadmap Epigenomics Mapping Consortium (REMC) database (Bernstein et al. 2010). The objective of this consortium is to gather epigenetic information from a total of 77 cell types of diverse tissue and lineage origin. They found that a significant number of GWAS hits or SNPs in close linkage disequilibrium were located in enhancers that were active in different tissues other than the brain such as the liver, fat or blood cells. Some of them were also shown to modulate the expression of nearby genes (Coetzee et al. 2016). Besides those variants analyzed in GWAS, it is becoming quite evident that other sorts of genetic variation such as indels (Mok et al. 2016; Butcher et al. 2013) and rare variants (Spataro et al. 2015; Lubbe et al. 2016) should be explored as well.

Despite the vast collection of variants and genome regions related to the disease, there is still a gap between the evidence of their association and their particular phenotypic effect. In this regard, genetically controlled and genuinely human models are necessary to be able to ascribe particular phenotypic effects to genetic findings in PD.

Genes modulating age at disease onset

The genetic information derived from GWAS is very valuable since it can be adapted to the study of alternative clinical parameters other than disease status. Similar to what was previously discussed with LRRK2, the existence of genetic modifiers of AAO or motor progression in idiopathic PD has been investigated. Before high-density genotyping platforms were available, some genome-wide linkage analysis started to provide evidence of the association of certain genomic loci to the AAO. In particular, the locus containing PARK3, a genomic region previously associated to autosomal dominant PD, was associated to reduced age at onset (DeStefano et al. 2002). Some years later, a locus in the chromosome 11 and a SNP close to PARK3 were related to AAO. The latter association was detected with a SNP located in the *AAK1* gene, a molecular interactor of GAK (Latourelle et al. 2009). Data acquired through GWAS designed for identifying susceptibility variants can be used to generate models to compute genetic risk scores (GRS). These GRS are inferred from the differential distribution of risk variants between cases and controls (OR). This way, a distribution of genetic risk can be generated and plotted against AAO. Nalls M. A. and colleagues correlated calculated genetic risk scores with age at onset of the participants of the meta-analysis. They found a trend to higher genetic risk scores being associated with earlier age at onset (Nalls et al. 2015). However no single variant was associated with an important reduction in AAO except the SNP in *GAK/TMEM175/DGKQ*. Another group genotyped 23 out of the 28 top SNPs from Nalls M. A. *et al*. (2015) in a cohort of 1,572 Danish PD patients and correlated each SNP and combinations of SNPs through GRS to age at onset. They did observe a larger correlation between GRS and AAO than the previous study (a reduction of 294 *versus* 37 days per single standard deviation in genetic risk score). Interestingly this effect was mainly driven by the SNPs in *GBA* and again in *GAK/TMEM175/DGKQ* (Lill et al. 2015). These results suggest that risk genes have a modest effect on AAO except for *GBA* and *GAK/TMEM175/DGKQ* and that GWAS specifically set for this purpose are required to unveil further genetic determinants of AAO.

Mechanisms leading to neurodegeneration

The neuropathological features of PD have been largely defined during the last 5 decades. Patient examination during all the phases of the disease (pre-diagnostic, post-diagnostic and post-mortem) has lead to the definition of the two major PD hallmarks: the loss of the DA neurons from the SNpc and the presence of Lewy bodies inside the surviving neurons of the nigra and in other brain regions. The detailed examination of the prodrome and post-mortem autopsies in early PD has lead clinicians to establish a chronology of events prior to the nigral cell loss (Heiko Braak et al. 2003). However, there are many gaps in our understanding regarding the mechanisms that initiate the disease process. Those gaps have evolved into several generic questions that are shared by the PD research community. Why are nigral DA neurons especially vulnerable? What are the pathological processes that lead to the neuronal death? Is alpha-synuclein central to the

disease process? What is the trigger of alpha-synuclein pathological aggregation? Is alpha-synuclein a prion? What do Lewy bodies imply in the disease process? To which extent do the familial and idiopathic forms of the disease overlap mechanistically? Is neurodegeneration a neuronal cell-autonomous mechanism?

Mitochondrial pathology

During several decades, most of the information regarding the pathophysiology of the disease was derived from post-mortem studies and from accidental toxin-induced parkinsonism. However, post-mortem studies describe very late-onset stages of the disease in which the original disease mechanisms are largely masked. On the other hand, toxin-induced parkinsonism has provided valuable clues about the mechanisms of the motor impairment but its mechanistic overlap with the most common idiopathic form is minimal to none. However, they pointed to impaired bioenergetics as weak point of SNpc DA neurons. The first genetic findings implying alpha-synuclein in the etiology of some familial cases together with the ascertainment of this protein as a major component of Lewy bodies started to provide some mechanistic clues about the disease process. With the discovery of mutations in the mitochondria-related genes *Parkin*, *PINK1* and *DJ-1*, a disease pathway including mitochondria, mitochondrial quality control and oxidative stress (Greene et al. 2003; Clark et al. 2006; Park et al. 2006; Shendelman et al. 2004). Indeed PINK1 and Parkin participate in the same pathway with PINK1 acting upstream of Parkin for targeting damaged mitochondria for degradation through autophagy or mitophagy (Narendra et al. 2010; Vives-Bauza et al. 2010). Other mitophagy-related genes have also related to both idiopathic and familial PD. Mutations in the mitophagy-related *FBXO7* gene have been associated to an autosomal recessive atypical parkinsonian syndrome (Shojaee et al. 2008; Fonzo et al. 2009). A similar case is the one of *VPS13C*, related to autosomal recessive Lewy body PD. Authors proposed a mechanism related to cargo recognition during mitophagy initiated by Parkin/PINK1 (Lesage et al. 2016). Common variation has also related *SREBF1* to idiopathic PD. *SREBF1* is a TF that regulates the transcription of genes involved in lipid and cholesterol metabolism. This gene has also been implicated in the autophagy pathway through a genome-wide RNAi screen (Ivatt et al. 2014). The implication of defective mitochondrial quality control has been related to the increased susceptibility of A9 DA neurons since these have particularly high energetic demands. It has been described that A9 DA neurons have higher basal oxidative phosphorylation (OXPHOS) rates, a smaller reserve capacity, a higher density of axonal mitochondria, more basal oxidative stress and increased axonal arborisation in comparison with their less affected neighbours A10 VTA DA neurons (Pacelli et al. 2015).

Proteostatic stress and the prion theory

Another disease mechanism that has drawn much attention since almost a decade ago is the prion-like behaviour of misfolded alpha-synuclein. In 2008, two teams analyzed post-mortem brains of two PD patients who received fetal nigral grafts more than a decade ago and found lewy bodies in grafted neurons (Kordower et al. 2008; Li et al. 2008). This fact was interpreted as a host-to-graft transmission of misfolded alpha-synuclein. Despite this finding, the grafts continued providing symptomatic relief to recipient patients suggesting that the synucleinopathy was insufficient to cause functional impairment or it was in its initial stages (Mendez et al. 2008; Li et al. 2008; Cooper et al. 2009). In any case, it lead to some researchers to postulate that the disease may result from an infective form of alpha-synuclein that induces misfolding of healthy, native alpha synuclein (Brundin et al. 2008; Olanow & Prusiner 2009). However the studies of Braak and collaborators published 5 years before implicitly suggested such possibility (Heiko Braak et al. 2003; H. Braak et al. 2003).
Since then, many research groups have been testing this hypothesis experimentally. Lewy body preparations from PD brains or just synthesized in the test tube have been injected into mice and monkeys brains and have shown to induce neurodegeneration and spread (Luk et al. 2012; Recasens et al. 2014). And this phenomenon has been demonstrated to be dependent on endogenous alpha-synuclein since *SNCA*-KO mice failed to propagate the initial inoculum (Recasens et al. 2014). Similar experiments were conducted but injecting alpha-synuclein in the periphery or in the olfactory bulb in order to corroborate the progression of the synucleinopathy proposed by Braak (Rey et al. 2016; Sacino et al. 2014). Finally, recent reports have provided interesting information about alpha-synuclein aggregation and spread. Studies in mice have shown that aggregates found in MSA behave like prions whereas the PD ones not (Prusiner et al. 2015). Therefore suggesting important etiological differences. On the other hand, (Fares et al. 2016) have reported that important inter-species differences in synuclein proteins explain the absence of fibrillization in experimental mice models. In this line, triple-KO of alpha-, beta-, and gamma-synuclein, and expression of human alpha-synuclein is able to recapitulate fibrillization (Fares et al. 2016).

Currently, the prion theory for alpha-synuclein remains controversial. The findings by Kordower and Li are very powerful sound arguments supporting the prion behavior. Other aged grafts did not show LB pathology (Mendez et al. 2008) but that could be explained by either different treatment parameters (immunosuppressive treatments, patients ascertainment, etc.) (Braak & Del Tredici 2008) or to a different underlying pathophysiology. Supportive of this latter idea is the fact that not all the familial PD cases present Lewy bodies at autopsy. This is the case for LRRK2 G2019S cases. LRRK2 G2019S is a common cause for both familial and sporadic PD and it is clinically indistinguishable from the tremor-dominant subtype of the latter. Lewy bodies are only shown in a fraction of patients carrying the mutation (Zimprich et al. 2004; Gaig et al. 2006; Kalia et al. 2015). Therefore it remains to be clarified whether Lewy bodies arise as a result of a cellular homeostatic defect or these are the origin of the cellular impairment. There is also the possibility of

different etiological entities leading to a fairly similar clinical picture: PD. Further studies in appropriate models will shed more light in this unsolved question.

Defects in vesicle-related processes: from protein sorting, to the autophagy-lysosome system and synapses.

Genetic findings also point to another group of genes involved in vesicle trafficking and other aspects of vesicle biology (Abeliovich & Gitler 2016). Many tissue-specific functions such as neurotransmitter storage and release, endocytosis, membrane receptor internationalization, autophagy-lysosome pathway, secretion of hormones or digestive enzymes; are dependent on the proper performance of vesicle formation and trafficking. Despite the apparent diversity of such processes, the underlying molecular machinery is largely coincident.

Starting from the first familial PD gene, *SNCA*, the protein acts as a soluble N-ethylmaleimide-sensitive factor attachment protein receptor (SNARE)-complex co-chaperone by binding to one of its components, synaptobrevin-2/VAMP2 (Burré et al. 2010). SNARE proteins are responsible for fusing two independent membranes or lipid bilayers, such as those of the synaptic vesicles and the plasma membrane, those of the ER-derived vesicles and the Golgi apparatus or those that mediate autophagosome and lysosome fusion. Physiological alpha-synuclein function has been related to synaptic and secretory functions (Burré et al. 2010; Burré et al. 2014; Logan et al. 2017). Nonetheless, when alpha-synuclein is over-expressed, other vesicle-related transport processes such as ER-to-Golgi become affected because of impaired vesicle fusion to the cis-Golgi surface. Interestingly, Rab proteins RAB1 (ER-Golgi), RAB3A (synapsis-related) and RAB8A (post-Golgi) reversed this trafficking defect (Cooper et al. 2006; Gitler et al. 2008).

Rab proteins are major regulators of vesicle trafficking processes and are strongly related to the pathophysiology of PD. Indeed, *RAB39B* is associated with X-linked familial PD and both PINK1 and LRRK2 have been shown to phosphorylate specific subsets of Rab proteins involved in diverse cellular functions (Lai et al. 2015; Steger et al. 2016).

As extensively commented in the genetics section, most cellular functions attributed to LRRK2 are related to vesicle-related processes in concert with other PD genes such as *RAB7L1, VPS35* and *GAK*. The latter (a.k.a. *DNAJC26* or *auxilin-2*) is an ubiquitous mediator of clathrin disassembly from recently invaginated vesicles both in the brain and in other tissues (Greener et al. 2000; Park et al. 2015). Mutations in the neural-specific *GAK* homologue *auxilin/DNAJC6* and in *DNAJC13* have been shown to cause early onset recessive and dominant familial PD respectively (Edvardson et al. 2012; Vilariño-Güell et al. 2014). Intriguingly, mutations in either gene are suspected to cause PD in an opposite fashion. While *DNAJC6* mutations are loss of function and cause autosomal recessive PD, *DNAJC13* ones represent gain of function and cause autosomal dominant disease. It is still uncertain how common variation in *GAK* is related to PD risk, however the work by Beilina A. and colleagues suggests that *GAK* expression is inversely correlated to the

pathology (Beilina et al. 2014). Hence, it seems that overall deregulation of vesicle biogenesis is a common pathway for PD more than upregulation or dowregulation alone.

Two other players of clathrin-mediated vesiculation have also been related to LRRK2 both genetically –*DNM3*- and molecularly –EndoA1-. Endophilin-A1 (a.k.a. SH3GL2) is a protein that induces the membrane curvature needed for vesicle protrusion from lipid bilayers at synaptic termini. It works by inserting alpha-helices into the membranes and forcing curvature mechanically. LRRK2 has been shown to phosphorylate two residues in those alpha-helices thermodynamically impeding EndoA1 membrane insertion (Matta et al. 2012; Arranz et al. 2015). Synaptojanin-1 (SYNJ1) mutations are also responsible for early-onset autosomal recessive parkinsonism with generalized seizures (Quadri et al. 2013; Krebs et al. 2013). SYNJ1 participates in the last steps of clathrin-mediated endocytosis by dephosphorylating specific hydroxyl groups of phosphatidylinositides, necessary for the shedding of endocytic factors from membranes. *SYNJ1* PD mutation causes the accumulation of clathrin-coated intermediates (Cao et al. 2017). It is worth noting that the vesicles generated at the presynaptic termini could serve either as synaptic vesicles or as docking membranes for autophagosome mediators such as Atg3 or Atg18a (Soukup et al. 2016; Vanhauwaert et al. 2017).

The lysosome is another convergent point in PD genetics. In fact, one of the first pathological effects described for LRRK2 G2019S mutation was neurite shortening produced by excessive autophagy (Plowey et al. 2008). Mutant forms of LRRK2, along with alpha-synuclein, have also been shown to interfere with chaperone-mediated autophagy (CMA) (Cuervo et al. 2004). CMA differs from macroautophagy in the way the cargoes are internalized into the lysosome. It occurs through a sequential process. The first step is the recognition of the peptapetide motif KFERQ in the target proteins by the cytosolic chaperone Hsc70. The next step is the unfolding of the cargo protein and its approximation to the lysosomal surface where the lyosomal receptor multimerizes forming a translocation complex. Finally the unfolded cargo is internalized and degraded by lysosomal hydrolases (Cuervo 2011). The inhibitory effect in CMA is not directly related to LRRK2 function but to a mere blockade in its internalization into the lyosome. The retention of mutant LRRK2 in the cytosolic facade of the lysosome hinders the lysosomal uptake of other CMA targets such as alpha-synuclein (Orenstein et al. 2013).

Improper functioning of the retromer complex due to a PD-related mutation in *VPS35* results in autophagy defects too. Mutant VPS35 fails to recruit WASH complex to the endosome. One of the functions of the WASH complex is to promote the assembly of actin patches in the wall of the endosome. These patches induce tubulation and fission of endosomal pieces that will be subsequently redirected to their target organelle (Reviewed in Seaman, Gautreau, & Billadeau, 2013). Authors explain the defective execution of autophagy owing to an abnormal trafficking of the autophagy-related protein Atg9 (Zavodszky et al. 2014).

Genes coding for lysosomal enzymes or integral membrane proteins are also a target of PD mutations. ATP13A2 is an integral lysosomal membrane protein that transports inorganic cations into the lysosome. Mutations in this gene cause a rare autosomal recessive form of PD with brain iron accumulation (Ramirez et al. 2006; Brüggemann et al. 2010). Regarding lysosomal enzymes,

mutations in the *GBA* gene have been revealed as the major genetic risk factor for PD. Other genes coding for lysosomal enzymes also present a higher frequency of rare coding mutation among idiopathic PD patients (Robak et al. 2017). In the case of the susceptibility genes, common variation in the *SCARB2* gene, encoding for the lysosomal integral membrane protein-2 (LIMP-2), has been linked to a reduced risk of PD (Nalls et al. 2014b; Do et al. 2011). It should be noted that LIMP-2 is responsible for the targeting of GCase from the Golgi to the lysosome (Zunke et al. 2016). Mutations in this gene have also been shown to cause action myoclonus renal failure (AMRF) syndrome –a disease affecting the kindeys with neurological involvement-, Gaucher's disease and myoclonic epilepsy.

PD models

As for any other disease whose pathophysiology is largely unknown the development of faithful experimental models is instrumental in the study of the disease process. Observations made through careful examination of epidemiological data and the histological and biochemical analysis of post-mortem brains lead to the generation of interesting hypotheses that require faithful experimental models in which to be tested. Indeed the major disadvantage of post-mortem patients brains is that they often represent end-stages of the disease in which the original pathogenic mechanisms is very likely masked (Hartmann 2004).

Every type of disease model offers a balance between biological complexity and ease of experimental manipulation. The selection of a certain type of disease model depends on the level of complexity associated to the particular disease trait to be studied. In this section the different PD models will be discussed with a special emphasis in their advantages and drawbacks.

Finally, the development of reliable disease models is also crucial for the development of therapies aimed to prevent, slow down or stop disease progression.

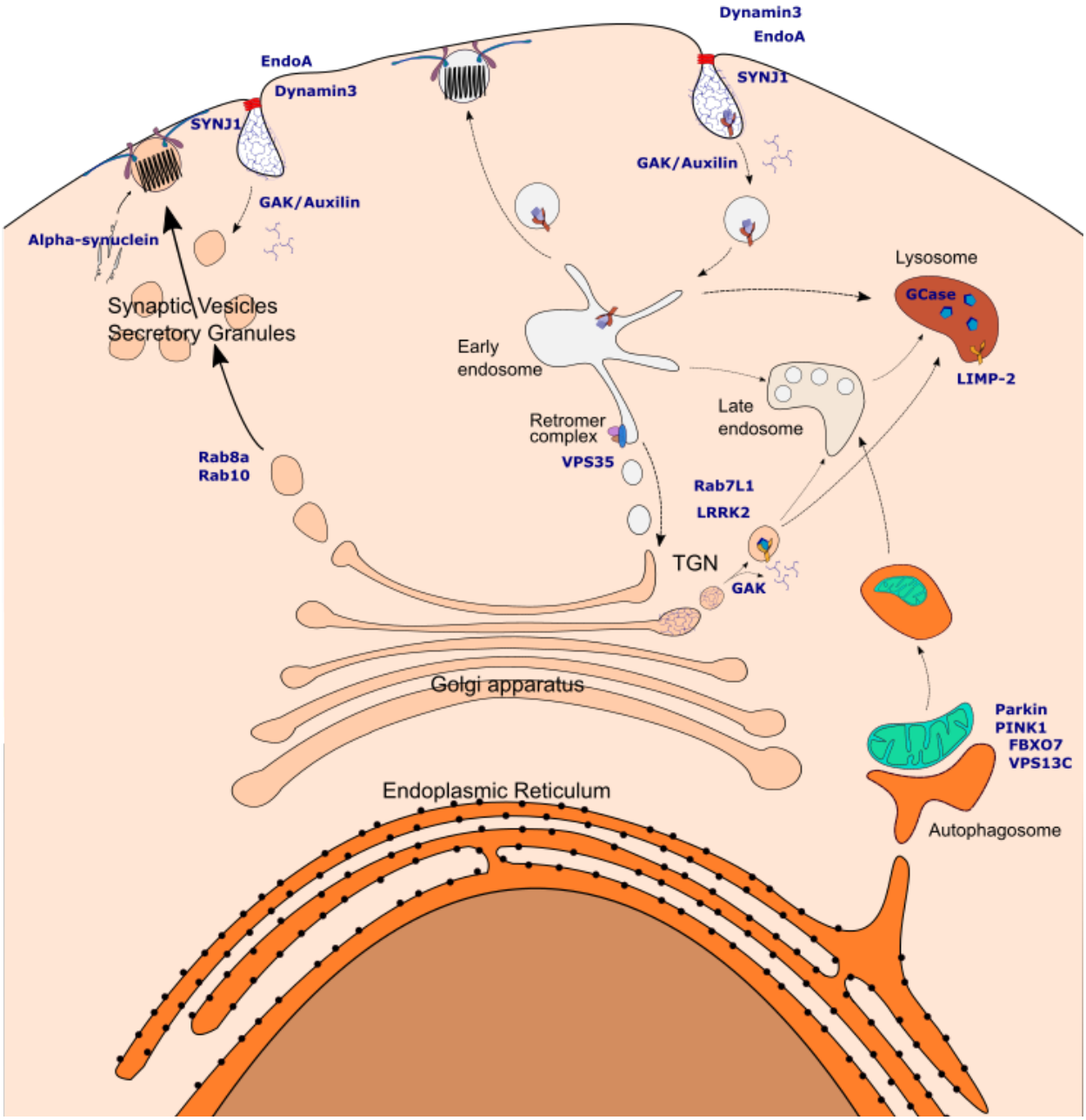

Figure 4: Vesicle related cellular processes.
The scheme depicts the different cellular processes in which vesicles play a central role. The participation of PD-related proteins and LRRK2 interactors (Rab8a, Rab10, EndoA, Dynamin3, GAK and Rab7L1) is indicated in blue.

Animal models

Animal models have represented the golden standard in PD modeling to date. These models have approached the pathophysiology of PD through two main strategies: i) inducing the disruption of the nigrostriatal pathway or ii) forcing the expression (or the ablation) of PD-related genes. The former strategy has obvious applications in the testing dopamine replacement therapies such as the administration of dopamine agonist or dopamine cell grafting. Instead, the latter has more mechanistic implications. The choice of the animal species is closely linked to the previous disjunction. While invertebrate models, such as *Drosophila melanogaster* or *Caernohabditis elegans,* are more amenable to rapid and straightforward genetic manipulation, their dopaminergic systems are anatomically and functionally different from the human ones. On the other side, mammalian disease models such as the mouse, rat or non-human primates show an increasing anatomical and physiological analogy in their nigrostriatal system. Nevertheless, they have longer generation times (from 10 weeks –mice- to several years –non-human primates-) and transgenic approaches are time-consuming except those based on viral transduction.

Toxin-based animal models

The first animal models were based on the first rationale, the disruption of the nigrostriatal bundle. To achieve this, there is a collection of neurotoxins of diverse nature and mechanism of action that target specifically ventral midbrain dopaminergic neurons. These compounds include MPTP, 6-OHDA, Rotenone, Paraquat among others (Blesa & Przedborski 2014). MPTP has been widely employed in both mice and monkeys to induce parkinsonism while rats are more resistant to this toxin (likely because of metabolic differences (Johannessen et al. 1985)). The effects in mice and monkeys brain parallel those observed in humans (Langston et al. 1983). Furthermore, there is another anatomical coincidence between experimental and clinical MPTP-induced parkinsonism: the SNpc neurons are more affected than VTA ones (Seniuk et al. 1990) and the putamen more denervated than the caudate nucleus (Moratalla et al. 1992). In the case of rats, the neurotoxin of choice is 6-OHDA (Ungerstedt 1968). Target specificity does not differ from the MPTP one and likewise neither toxin produces Lewy body pathology (Shimoji et al. 2005; Halliday et al. 2009). Long-term follow-up of MPTP-injected monkeys revealed increased levels of alpha-synuclein but not Lewy bodies. Therefore suggesting that either the damage induced by MPTP is either insufficient or non-specific to form Lewy Body or it is human-specific feature (Halliday et al. 2009).
In this regard, two other toxins fill the gap left by MPTP and 6-OHDA. Rotenone and Paraquat, in addition to recapitulating the specific toxicity towards SNpc dopaminergic neurons, form protein aggregates positive for alpha-synuclein and ubiquitin (Greenamyre et al. 2000b; Manning-Bog et al. 2002). Despite this superior modeling feature, rotenone and Paraquat are much less employed due to the difficulty in performing reproducible lessions and the high mortality associated (Miller 2007).

Despite the widespread use of toxins to reproduce some PD pathological features, there are two major drawbacks associated. None of them induces slow and progressive nigral degeneration neither the formation of Lewy bodies, at least in the case of the most employed ones (MPTP and 6-OHDA). Hence these models are not well suited to investigate the mechanisms behind the pathogenesis in PD. Instead, these models have proven very valuable in assaying cell replacement therapies for PD. Indeed they are commonly used to test the efficacy of dopamine producing cells derived from many different sources (Kriks et al. 2011; Grealish et al. 2014; Kirkeby, Grealish, Wolf, Nelander, Porzio, et al. 2012; Dunnett et al. 1981; Espejo et al. 1998; Hallett et al. 2015). Successful grafting of dopamine cells in these animal models has become a prerequisite for further progress into the human clinical application.

Genetic animal models

The increasing awareness regarding the existence of a genetic predisposition to suffer PD has lead to the development of genetically modified animals with familial PD mutations. The expression of PD related genes has been carried out using different strategies differing in the promoter used (strong or physiological; ubiquitous or cell type-specific), the form of the gene being overexpressed (mutated or *wild type*; human or murine) or the transgenic approach (targeted insertion, BAC transgenesis, gene knockout, lentiviral overexpression…).

The gene that has been more extensively investigated using genetic animal models is alpha-synuclein. This is due for two main reasons. It was the first PD-causing gene discovered and it is unequivocally linked to the most common sporadic disease. First transgenic animals expressed either human A53T mutant alpha-synuclein or the wild type human form from very strong promoters such as the murine Prion protein (PrP) promoter (Giasson et al. 2002), the Thy1 promoter (van der Putten et al. 2000) or the human platelet-derived growth factor-β (hPDGF-β) promoter (Masliah et al. 2000). All these transgenic animals showed deposits mainly composed by alpha-synuclein but no cell loss in the SNpc. Indeed Thy-1 promoter failed to induce expression in DA neurons from the SNpc. Only the hPDGF-β:hα-Syn mice displayed DA terminal loss in the basal ganglia (Masliah et al. 2000). Despite lack of DA neurons loss, human alpha-synuclein transgenic mice showed motor deficits and other behavioral abnormalities.
Other groups attempted to induce damage in the nigra by using midbrain DA-specific promoters such as the rat *tyrosine hydroxylase* (TH) or the *PITX3* genes promoters. A 4.8-kb version of the former failed to induce DA-specific cell death or alpha-synuclein deposition in the transgenic mice (Matsuoka et al. 2001). It was necessary to extend the recombinant promoter to 9-kb and to use a double mutant A53T/A30P human alpha-synuclein to observe nigral pathology in the absence of alpha-synuclein accumulation (Thiruchelvam et al. 2004). The other approach consisted in the employment of a binary tetracycline-dependent inducible gene expression in which the reverse tetracycline transactivator (rtTA) was expressed under the *PITX3* promoter. Therefore, dietary

administration of doxycycline induced strong A53T alpha-synuclein expression in midbrain DA neurons. These mice displayed robust midbrain DA neuron degeneration accompanied by Golgi apparatus fragmentation, impairment of autophagy and a reduction of the midbrain DA-specific transcription factor Nurr1 expression and function (Lin et al. 2012).
These transgenic mice underscore the need of very high midbrain DA neuron-specific expression of alpha-synuclein expression to observe nigral DA neurons loss and a certain alpha-synuclein accumulation during mice lives. Stereotaxic injection of viral vectors encoding for alpha-synuclein gathers both requirements. Both lentiviral (LV) and adeno-associated (AAV) vectors have been employed successfully in rats to target midbrain DA neurons (Lo Bianco et al. 2002; Kirik et al. 2002; M. Decressac et al. 2012). AAV-mediated overexpression of alpha-synuclein (both in the striatum and in the nigra) has been used to disentangle a complicated pathogenic loop in which alpha-synuclein overexpression induces Nurr1 depletion and consequently reduced expression of proteins required for transducing DA neuron-specific survival cues such as GDNF (Volakakis et al. 2015; Mickael Decressac et al. 2012; Decressac et al. 2011).
Finally, there is a third class of animal models suited for the study of alpha-synuclein pathological effects. Those described extensively in a separate section consisting in the inoculation of pre-formed alpha-synuclein fibrils in mice.

In the case of LRRK2 the phenotype of transgenic animal models has been more disappointing in terms of overt neurodegeneration or the presentation of other PD-related phenotypes. Knockout mice and rats are viable and have an intact dopaminergic system. Instead, the phenotypic defects associated with the lack of LRRK2 are observed in kidney and lungs (Tong et al. 2010; Herzig et al. 2011). Conversely, overexpression of the most common G2019S mutation results in slow and specific as well as limited (≈20%) loss of midbrain DA neurons. Even so, the loss of the nigral DA neurons was not reflected in the reduction of striatal DA nor any motor alteration (Ramonet et al. 2011; Chen et al. 2012). Lin and colleagues observed an exacerbation of alpha-synuclein pathology in the A53T transgenic mice in the presence of G2019S LRRK2. Conversely, genetic ablation of murine Lrrk2 abrogated alpha-synuclein accumulation and its associated pathological effects (Lin et al. 2009). Increased expression of mutated versions of human LRRK2 via BAC or viral (Lee et al. 2010; Tsika et al. 2015; Dusonchet et al. 2011) transgenesis did not provide substantial novel insights into the pathogenesis of the human mutations. More recently, the effect of LRRK2 knockout or LRRK2 mutations has been examined in non-nigral compartment such as the striatum. LRRK2 was shown to modulate synaptogenesis and transmission in striatal projecting neurons through its interaction with PKA. Lrrk2 deficiency or mutations affecting its ROC-COR domain (R1441C) increased PKA synaptic translocation and deregulation of the aforementioned processes (Parisiadou et al. 2014). Negative effects on striatal synaptogenesis and transmission were also observed with the G2019S mutation (Matikainen-Ankney et al. 2016; Tsika et al. 2015).
Finally, animal models have also been employed to investigate the contribution of LRRK2 to inflammatory bowel disease such as Chron's. In Paneth cells (resident immune system) LRRK2, along with Rab2a and Nod2 and in concert with commensal bacteria orchestrate the secretion of lysozyme from dense core granules in order to maintain the intestinal homeostasis. Lack of any of

these proteins results in failure to control proper symbiosis with the microbiota and in enhanced susceptibility to microbial infection (Zhang et al. 2015). The proposed role of LRRK2 in coordinating lysozyme secretion is in line with previous reports linking LRRK2 with vesicle management and with several members of the Rab family of proteins. Indeed, Steger and collaborators suggested one year later that the role of LRRK2 and the specific subset of Rab proteins that it regulates might vary in every different tissue (Steger et al. 2016).
In summary, insight gained from animal models points to LRRK2 mutations inflicting a subtle and cumulative pathogenic effect that would likely manifest in the elderly.

Many other genetic animal models have been generated harboring other PD Mendelian mutations. However their connection to the present thesis is loose and to avoid digression they will not be discussed here.

In vitro cell models

Initial cellular models of PD were conceived to gain understanding regarding the function and dysfunction of PD-related genes and proteins. The classical approach relied in the overexpression or the silencing/ablation of these genes in order to exacerbate the phenotypic outcome. The cells in which these experiments were carried out ranged from immortalized cell lines from diverse origins to primary neuronal cultures from mice or rats. The simplicity of such systems offers the opportunity to test multiple hypotheses in a very short time. Nonetheless, the conclusions drawn should be taken with caution since the overexpression of any gene may lead to spurious observation that would not be confirmed by independent experimental approaches.
Despite that, many authors have fine-tuned their experimental designs in an attempt to minimize the occurrence of artifacts (Beilina et al. 2014; Steger et al. 2016). In this regard, the careful selection of controls, the implementation of unbiased approaches and the reproduction of the results obtained in different models are providing very interesting clues about the mechanism of action of PD mutations.

The generation of induced pluripotent stem cells (iPSC) and its application to human disease modeling.

In this context the groundbreaking technique described by Kazutoshi Takahashi and Shinya Yamanaka in 2006, whereby a somatic cell can be reverted back to the pluripotent status typical of the first cells of the embryo has revolutionized many aspects of medicine and biology (Takahashi & Yamanaka 2006). In that germinal work, the two researches elaborated a curated list of transcription factors implicated in different aspects of stem cell biology and forced their expression in mouse fibroblasts. They observed the activation of an embryonic gene which was maintained

after reducing the gene number to four: Oct3/4, Sox2, Myc and Klf4. These cells were demonstrated to be largely indistinguishable from embryo-derived stem cells –ES cells- (Evans & Kaufman 1981). Properly selected iPSC clones (Okita et al. 2007) fulfilled the stringent criteria for pluripotency established in the field, such as ES cell-specific marker expression or ability to give rise to derivatives of the three germ layers. Additionally, other molecular test were generalized such as the independence from the exogenous reprogramming factors and the reactivation of the endogenous pluripotency gene network (Takahashi & Yamanaka 2006). Furthermore, they were also demonstrated to be able to pass the most challenging pluripotency test: the tetraploid complementation assay (Zhao et al. 2009). This test consists in checking whether PSCs injected into a tetraploidized embryo could resume embryonic development. The discovery of induced reprogramming was claimed to have broad implications in regenerative medicine, developmental studies, disease modeling, and drug testing/discovery.
The next year, two independent groups managed to obtain iPSC from human fibroblast (hiPSC) by either the same (Takahashi et al. 2007) or a slightly different combination of genes (Yu et al. 2007). From that moment, the field exploded and the rate of publications dealing with iPSC rose steeply.

The generation of hiPSC from adult somatic cells opened the door to the generation of patient-specific iPSCs, which offered an unprecedented opportunity to study disease in a genuinely human setting. This approach offered three major advantages over other modeling alternatives. The first of them is that they are of human origin. There are genetic animal models that do not recapitulate the features of the human disease even in the case of severe Mendelian childhood diseases. Secondly, they allowed the generation of the cell type specifically affected by the disease. This is an urgent need in PD since neurodegeneration and synucleinopathy only affect certain brain nuclei and cell loss is mostly observed in the nigra. Finally, they recapitulate the genetic particularities of the donor subject and they express disease-associated genes under the control of endogenous regulatory sequences. This is crucial not only in complex diseases with a polygenic component but also in Mendelian diseases subjected to genetic disease modifiers such as idiopathic and familial PD respectively.
The first report describing the derivation of patient-specific iPSCs for modeling purposes was published in 2009 by Ebert et al. (2009). iPSCs were generated from a kid with spinal muscular atrophy (SMA). Patient's fibroblast and iPSCs already showed a lack of the SNM1 gene mRNA and a disease-specific phenotype (lack of nuclear gems). Furthermore, a maturation deficit was observed in the disease-relevant cell type, motor neurons. This was also the first report in which patient-iPSCs were used as a tool for drug testing since drugs that were previously described to increase SNM protein levels were proven to be efficacious in this particular SMA model. After this report, the number of publications using iPSC in disease modeling rose exponentially. In 2009, the race of iPSC-based disease modeling started (Fig. 5).

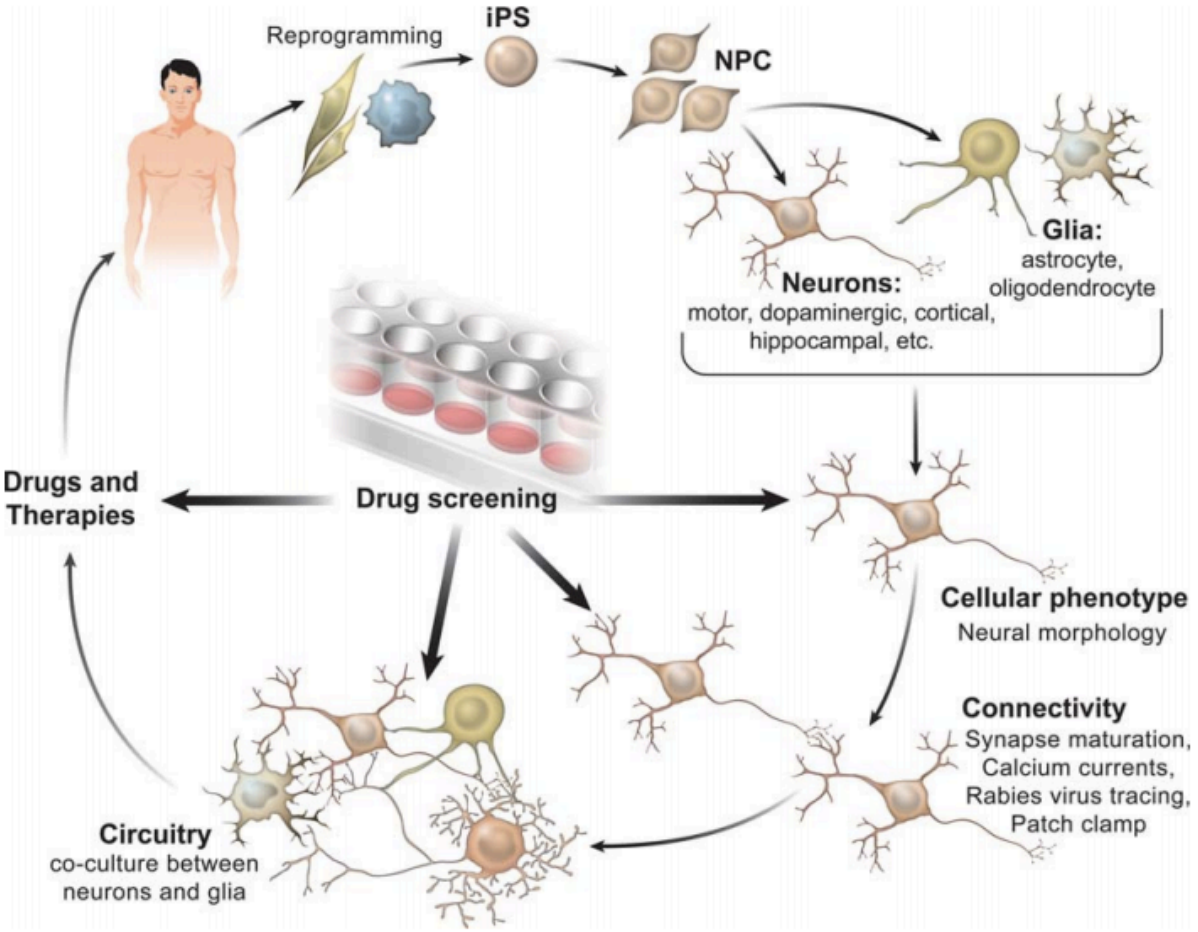

Figure 5: Workflow of iPSC-based disease modeling and its application to drug screening (From Marchetto et al. 2010)

Initial successful attempts focused on early-onset diseases in which the pathological effect of the mutation had been already described. The possibility of modeling multifactorial diseases with a polygenic component or with a known genetic component of unknown function was still uncertain. On the other hand, it was not clear either whether late-onset diseases such as neurodegenerative diseases could be modeled in a dish. It was not until 2011, when several iPSC-based models of genetic PD reported disease related phenotypes. Two groups generated iPSC from patients carrying a triplication of the alpha-synuclein locus. After differentiating those iPSC towards dopaminergic neurons, they observed that alpha-synuclein expression was doubled in comparison with *wild type* controls (Devine et al. 2011; Byers et al. 2011). Furthermore in one of the reports, increased alpha-synuclein expression was associated to increased susceptibility towards oxidative stress (Byers et al. 2011). Increased sensitivity towards oxidative stress was also described in DA neurons differentiated from a patient-specific iPSC carrying the LRRK2 G2019S mutation. Interestingly, this effect was specific to DA neurons, as LRRK2 G2019S TH- cells were not significantly affected by H_2O_2 when compared to control cells. Increased sensitivity in LRRK2 G2019S DA neurons was also observed when treated with other stressors such as the protease inhibitor MG-132 or 6-OHDA.

A very meaningful finding was the one published by Sánchez-Danés et al. (2012). In this work, a PD model was generated in which spontaneous disease-related phenotypes could be observed in DA neurons from iPSC from both LRRK2 G2019S and sporadic PD patients after long-term culture. Given that the present study is based in the model described by Sánchez-Danés et al. (2012), it will be thoroughly described in a separate section. Therefore demonstrating that susceptibility to undergo neurodegeneration in sporadic PD patients is genetically encoded. This is a groundbreaking fact since it implies that iPSC-based models are very well suited for studying the genetic component of both idiopathic and Mendelian diseases. Another important insight is that if the cells are maintained for a relative long span of time, they can present disease-related features spontaneously. In a separate study, this same model was used to corroborate the inhibitory effect of LRRK2 G2019S on CMA, which was shown to decrease alpha-synuclein lysosomal degradation (Orenstein et al. 2013). Other authors have also used iPSC to model LRRK2 G2019S-associated PD. Reinhardt and coworkers (2013), observed similar disease-related phenotypes (reduced neurite extension, increased alpha-synuclein and increase susceptibility towards neurotoxins) in LRRK2 G2019S iPSC-derived neurons. Interestingly, by using gene-editing tools, these phenotypes could be ascribed to the presence of the LRRK2 G2019S mutation. Transcriptional interrogation of differentiated cultures suggested that LRRK2 G2019S exerted its pathogenic effect by deregulating gene expression downstream of ERK signal transduction. The link between LRRK2 and the mitochondrial pathway has also been investigated using iPSC-based models. Aberrant sequestration of mitochondria was found in iPSC-derived dopaminergic neurons from LRRK2 G2019S-associated PD patients, but also from sporadic PD patients. This was caused by defective Miro1 retention on damaged mitochondria. A protein mainly involved in anchoring mitochondria to molecular motors (Hsieh et al. 2016). Enhanced phosphorylation of the mitochondrial fission protein Drp1 has also been suggested as a pathogenic pathway by LRRK2 G2019S. In this regard, phosphorylation insensitive mutant forms of Drp1 or specific inhibitors were shown to abrogate excessive mitochondrial fission and related phenotypes (Su & Qi 2013). LRRK2 has also been shown to phosphorylate ribosomal protein s15 (Rps15). In line with this, the G2019S mutation exacerbated Rps15 phosphorylation causing an overall increase of cap-dependent and independent mRNA transcription both in Drosophila and in iPSC-derived DA and cortical neurons (Martin et al. 2014). In summary, models based on DA neurons differentiated from LRRK2 G2019S patient-specific iPSCs have proven to be very valuable for investigating the pathogenic effects of the mutation.

A model describing spontaneous neurodegeneration phenotypes in patient-specific iPSC

The experimental platform employed in the present thesis was initially described by Sánchez-Danés et al. (2012). It involved the generation of iPSC lines from a cohort of 7 sporadic PD patients, 4 patients carrying the LRRK2 G2019S mutation and 4 healthy controls (Summarized in Table 3). These iPSC lines were differentiated towards ventral midbrain dopaminergic neurons

using a protocol described in previous study (A. Sánchez-Danés et al. 2012). This protocol involved the transduction of the iPSC with a lentiviral vector expressing the floor plate marker LMX1A under the control of the *Nestin* enhancer and the exposure of iPSC aggregates (embryoid bodies or EBs) to the patterning factors SHH and FGF8. In the short-term (3 weeks of *in vitro* culture), iPSC from both cases and controls were shown to differentiate to DA to the same extent. Likewise, these neurons appeared healthy disregarding the parental iPSC line.

Table 3: Summary of iPSC generated in the study by Sánchez-Danés et al. (2012)

	Patient			Disease					iPSC						
	Code	Sex	Age[a]	Age onset	Family history	Mutation	Initial symptoms[b]	LDopa response	# of Lines	Clones selected	Karyotype	Transgene silencing[c]	Pluripotency markers[c]	*In vitro* differentiation[c]	Teratoma assay[c]
CONTROL	SP09	M	66						4	SP09.2	46,XY	Passed	Passed	Passed	N/P
										SP09.4	46,XY	Passed	Passed	Passed	Passed
	SP11	F	48						3	SP11.1	46,XX	Passed	Passed	Passed	Passed
										SP11.4	46,XX	Passed	Passed	Passed	N/P
	SP15	F	47						4	SP15.2	46,XX	Passed	Passed	Passed	Passed
										SP15.3	46,XX	Passed	Passed	Passed	N/P
										SP15.4	47,XX + 20	Passed	Passed	N/P	N/P
	SP17	M	52						3	SP17.1	47,XY + 20	Passed	Passed	Passed	N/P
										SP17.2	46,XY	Passed	Passed	Passed	Passed
										SP17.3	46,XY	Passed	Passed	Failed	N/P
ID-PD	SP01	F	63	58	No	No	T and B	N/A	4	SP01.1	46,XX	Passed	Passed	Passed	Passed
										SP01.4	46,XX	Passed	Passed	Passed	N/P
	SP02	M	55	48	No	No	T	N/A	2	SP02.1	46,XY	Passed	Passed	Passed	Passed
										SP02.2	46,XY	Passed	Passed	Passed	N/P
	SP04	M	46	40	No	No	B	Good	2	SP04.1	46,XY	Passed	Passed	Passed	N/P
										SP04.2	46,XY	Passed	Passed	Passed	Passed
	SP08	F	66	60	No	No	T	Good	4	SP08.1	46,XX	Passed	Passed	Passed	Passed
										SP08.2	46,XX	Passed	Passed	Passed	N/P
										SP08.3	46,XX	Failed	N/P	N/P	N/P
	SP10	M	58	50	No	No	D	Good	2	SP10.1	46,XY	Passed	Passed	Passed	N/P
										SP10.2	46,XY	Passed	Passed	Passed	Passed
	SP14	M	55	51	No	No	B	Good	2	SP14.1	46,XY	Passed	Passed	Passed	Passed
										SP14.2	46,XY	Passed	Passed	Passed	N/P
	SP16	F	51	48	No	No	B	N/A	4	SP16.2	46,XX	Passed	Passed	Passed	Passed
										SP16.3	46,XX	Passed	Passed	Passed	N/P
LRRK2-PD	SP05	M	66	52	Yes	LRRK2	B	Good	2	SP05.1	46,XY	Passed	Passed	Passed	Passed
										SP05.2	46,XY	Passed	Passed	Passed	N/P
	SP06	M	44	33	Yes	LRRK2	T	Good	6	SP06.1	46,XY	Passed	Passed	N/P	N/P
										SP06.2	46,XY	Passed	Passed	Passed	Passed
	SP12	F	63	49	Yes	LRRK2	T	Good	4	SP12.3	46,XX	Passed	Passed	Passed	Passed
										SP12.4	46,XX	Passed	Passed	Passed	N/P
	SP13	F	68	57	Yes	LRRK2	T	Good	4	SP13.2	46,XX	Passed	Passed	Passed	N/P
										SP13.4	46,XX	Passed	Passed	Passed	Passed

N/A, information not available; N/P, test not performed.
[a]Age at biopsy.
[b]T, tremor; B, bradykinesia; D, foot dystonia.
[c]Tests performed as exemplified in Fig 1.

The only disease-related phenotype that was appreciable at that time point was the increased accumulation of alpha-synuclein exclusively in LRRK2 G2019S DA neurons (Fig. 6)

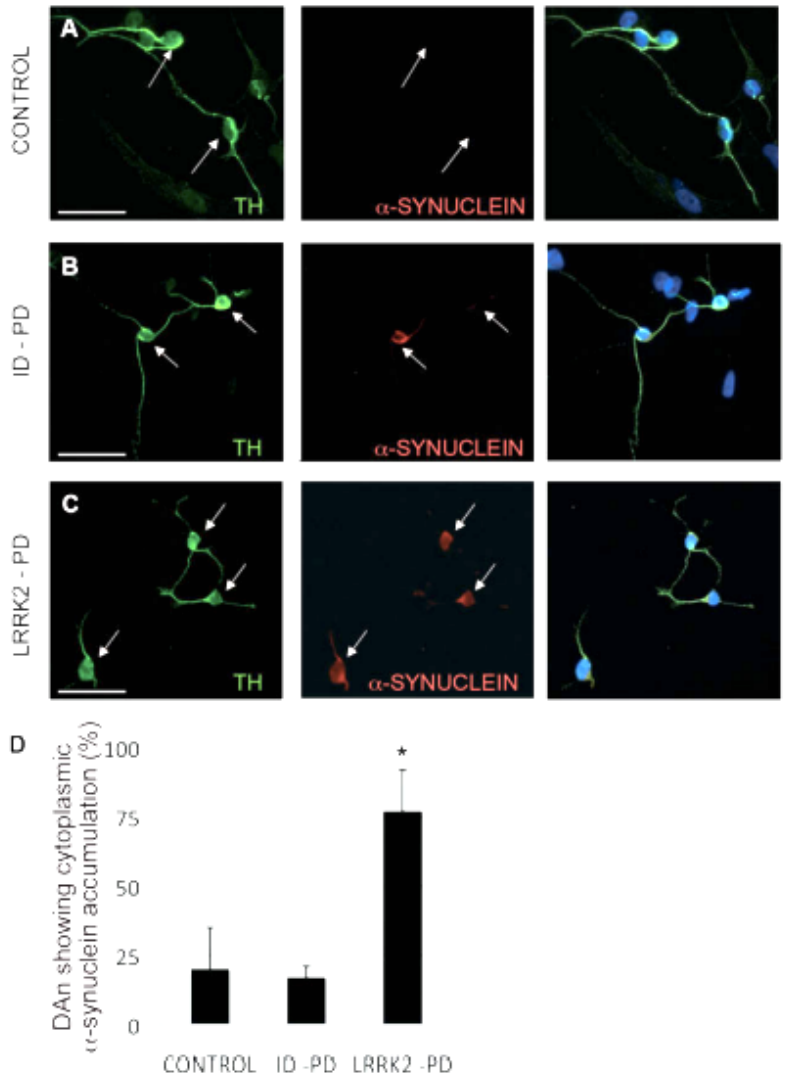

Figure 6: Abnormal accumulation of alpha-synuclein in DA neurons from L2-PD iPSC

In order to be able to maintain and DA neurons for a long span of time, patterned EBs were seeded on a feeder layer of cortical murine astrocytes. Differentiated cultures were maintained for up to 75 days, the moment at which disease-related phenotypes were observed. DA neurons differentiated from patient-specific iPSC presented neuritic pathology (shortening and reduced branching) as well as increased cell death (measured by cleaved-caspase 3 staining) in comparison with control DA neurons (Fig. 6)

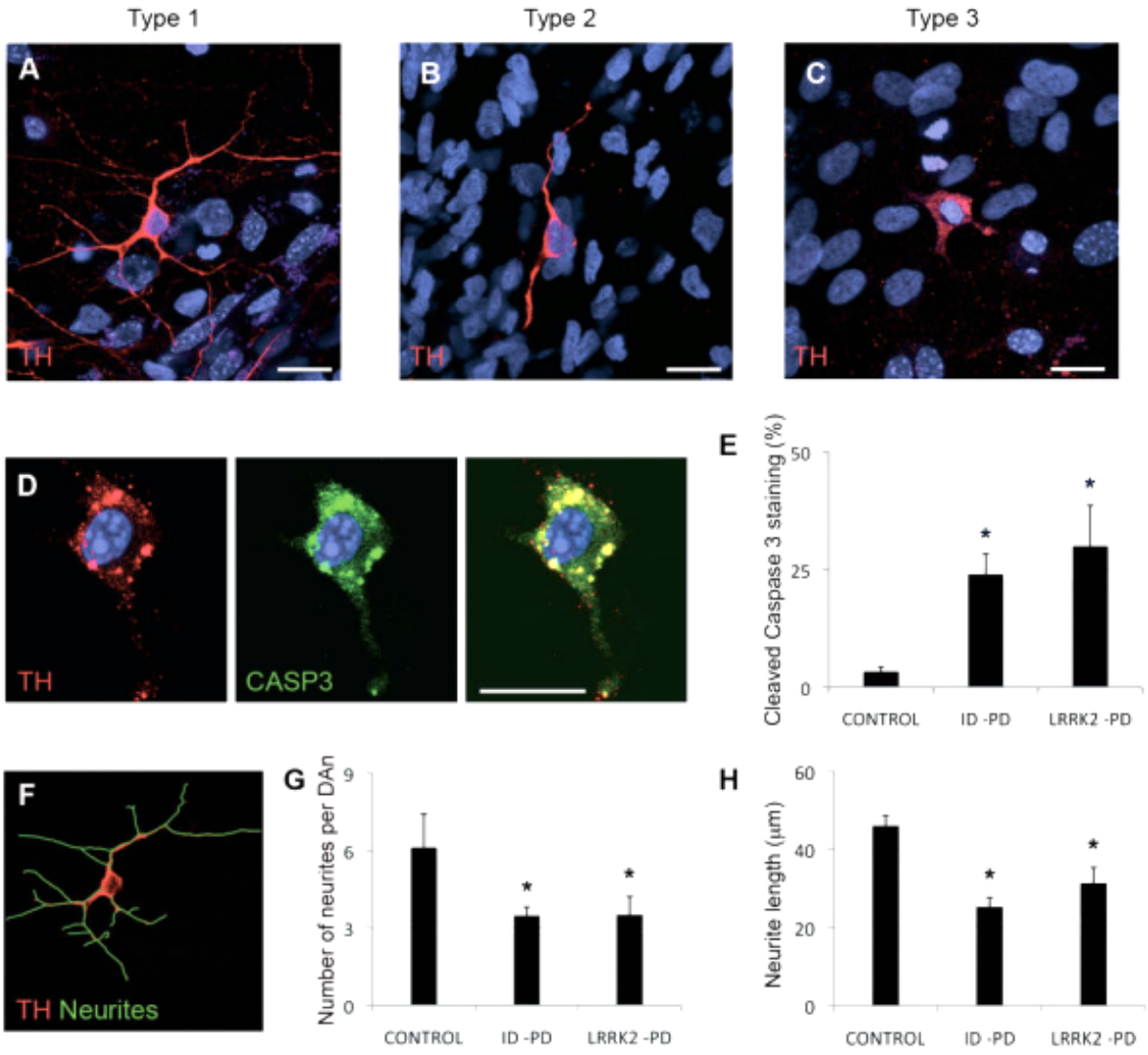

Figure 7: Neurodeneration features observed in patient-specific iPSC derived DA neurons. Adapted from the original research article by Sánchez-Danés et al. (2012)

Delving deeper into the pathological mechanism of degeneration, autophagy flow was studied in DA neurons after 75 days of culture. Western blot and immunofluorescence analyses revealed impaired autophagy. Differentiated DA neurons showed increased amount of P62- and LC3-positive puncta therefore indicating the accumulation of disposal products inside the cells (Fig. 7). Finally, the blockade in autophagy was most probably due to a defective autophagosome to lysosome fusion in patient's DA neurons as judged by reduced co-localization of the lysosomal marker LAMP-1 with the autophagosome marker LC3 (data not shown here).

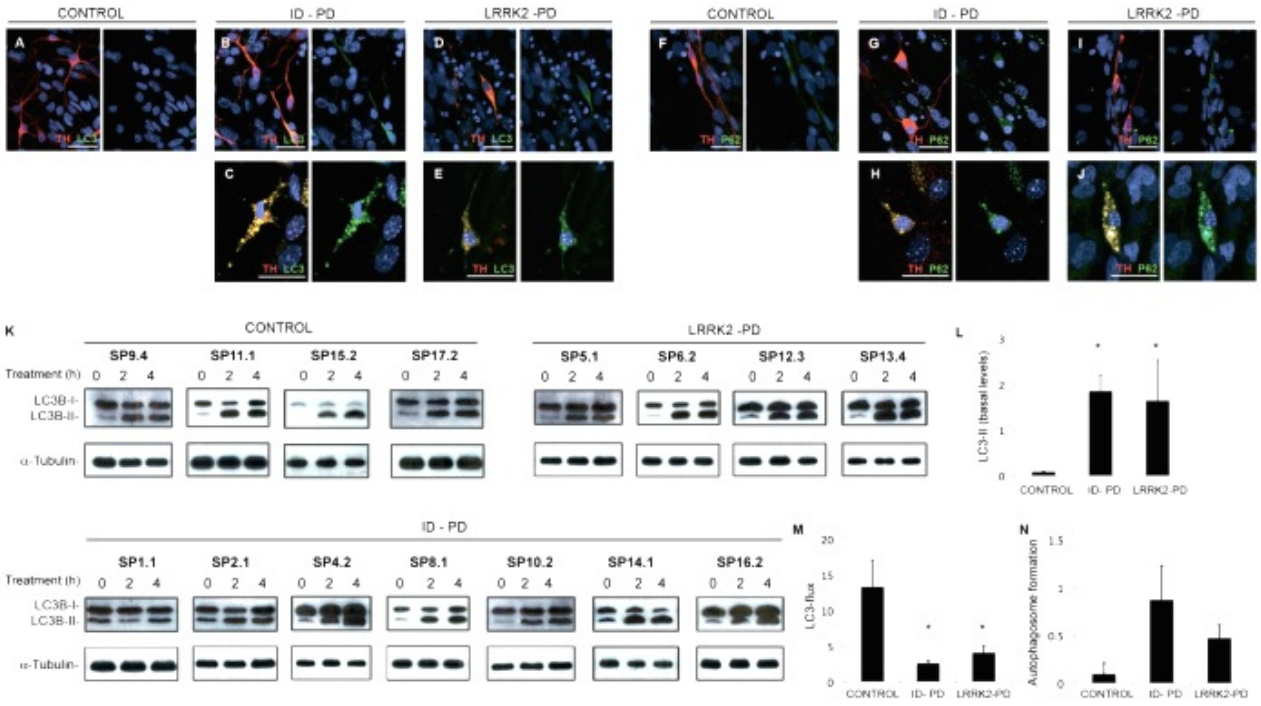

Figure 8: Impaired autophagy in patients' DA neurons after 75 days in culture

In summary, previous work from our lab (2012) demonstrates the PD model generated is a very powerful tool to study the cellular processes implicated in the first steps of the degeneration process. Furthermore, the ability to recapitulate *in vitro* the effect of patient's own genetics suggests that the model could be applied to study the contribution of additional genetic modulators of the disease besides Mendelian mutations.

Gene editing tools in iPSC-based modeling: the importance of genetically-matched controls.

Arguably, the single most important functional characteristic of pluripotent stem cells is their multi-lineage differentiation ability. It is widely accepted that iPSC present considerable variability in differentiation potential among lines derived, not only from different subjects, but also among clones from the same subject (Kajiwara et al. 2012). There have been several attempts to characterize the sources of such variability. Extensive passaging and maintenance of hESC has been shown to induce certain chromosomal alterations, in particular duplication of chromosomes 12 and 17 (Baker et al. 2007). A separate study found that recurrent amplifications in the 17q21.31 chromosomal region specifically affected neural (mesodiencephalic) differentiation properties of hPSCs (Lee, Bendriem, Kindberg, Worden, Williams, et al. 2015). Age-related mutations of the reprogrammed somatic cells (blood cells, fibroblasts, etc) could also be a source of genetic variation. We should take into account that, for many disease conditions, somatic cell samples would be obtained from aged individuals. However, the most in-depth examination of iPSC

variability sources comes from the studies of DeBoever et al. (2017) and Carcamo-Orive et al. (2017). In these two research works, genetic variation was studied among large collections of iPSCs. These authors found that both germ-line and somatic mutations influenced hiPSC-specific gene signature. Moreover, it was observed that the reprogramming process also influenced such variability through the Polycomb repressor complex and the completeness of X chromosome reactivation.

The aforementioned sources of variability may also complicate ascribing disease-related cellular phenotypes to specific genotypes. A straightforward manner to countering that variability would be to utilize (engineer) appropriate controls. In this regard, the use of designer nucleases as gene-editing tools enables researchers to generate isogenic controls that only differ in the presence of one (or more) genetic variant. The realization that DNA double strand breaks (DSB) enhance homology-directed repair (HDR) (Rouet et al. 1994) opened a race for the generation of sequence-specific nucleases for the introduction of sequence-specific DSB. The first two sequence-specific nucleases (SSN) to enter the scene, zinc-finger nucleases (ZFNs) and transcription activator-like effector nucleases (TALENs), were used by some highly skilled laboratories to demonstrate proof-of-concept for targeted gene edition in hiPSC (recently reviewed in Hockemeyer & Jaenisch 2016).
TALENs are based on transcription factors from the bacteria genus Xanthomonas. Contrary to zinc fingers, DNA recognition rationale is much simpler. TAL effectors have a central domain containing an array of repeats each of them recognizing a specific base pair in the genome. Every repeat has a very similar sequence except for two highly variable residues (RVD) located into the central part and are responsible for the base pair specificity (Mussolino & Cathomen 2012). Therefore the generation of an array of repeats each one with a specific central variable di-residue permits to assemble TALE monomers targeting a given sequence of interest. The simple code determining DNA specificity and the lack of context dependent effect of the repeats has allowed that laboratories with little previous experience in protein engineering to be able to design and construct sequence-specific nucleases for their genes of interest. In the case of hPSCs, there are many reports describing successful edition of disease-relevant genes or the generation of lineage-specific reporters using TALENs (Ding et al. 2013; Hockemeyer et al. 2011).

However, actual “democratization” of gene editing procedures in hiPSC was made possible thanks to the development of CRISPR/Cas9 technology. This bacterial immune system consists of two RNA molecules, one of them determining DNA sequence specificity by base pairing, and a nuclease that introduces a DSB in the DNA paired by the RNA. Both RNAs were later joined in a single guide RNA, which could be easily redirected to virtually any DNA sequence (Jinek et al. 2012) by modifying a part of this RNA termed spacer. A graphic representation of the different gene editing tools is depicted in fig 9.

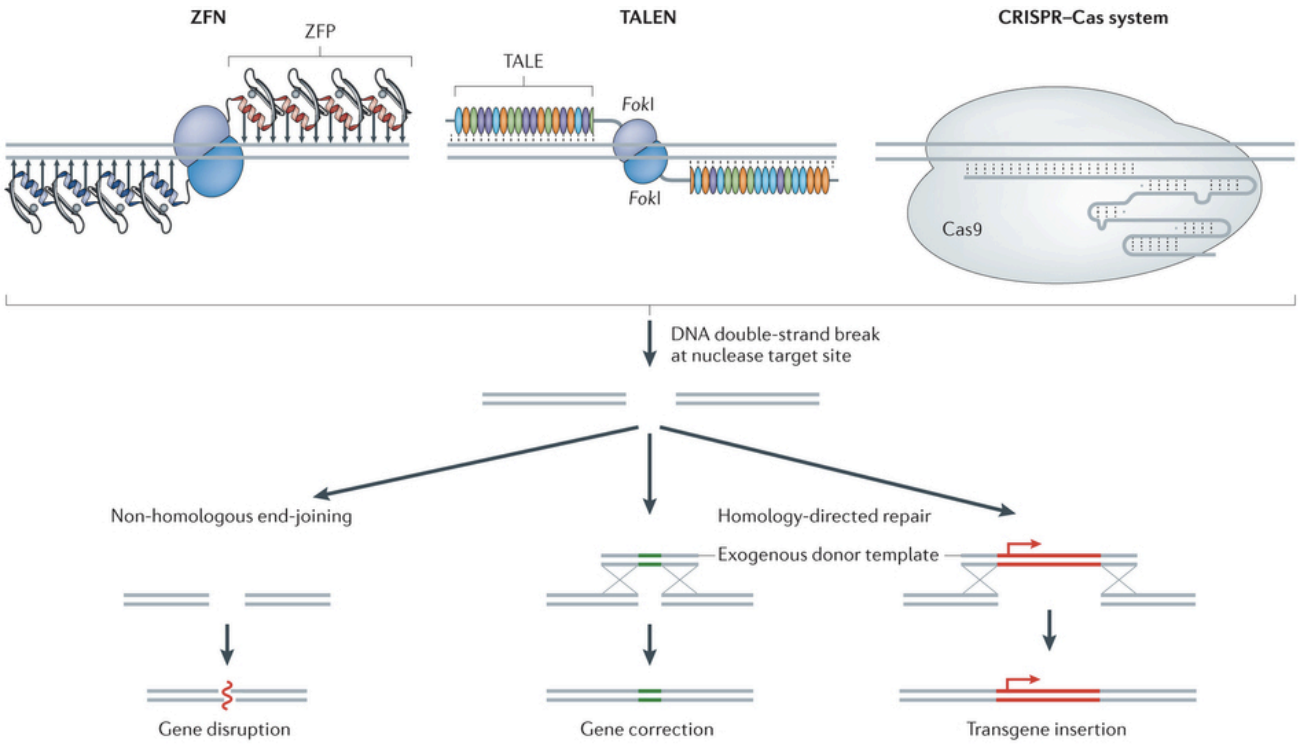

Figure 9: Sequence-specific nuclease employed in gene editing approaches (adapted from (Yin et al. 2014)

The versatility of targeting almost any locus in the genome by simple changing the spacer sequence has enabled any cell biology laboratory with minimal molecular biology equipment to generate their desired targeted genetic modifications. Naturally, the extent of the isogenicity achieved with targeted genome edition becomes crucial for the interpretation of the results. It is not comparable, mutating a coding DNA sequence with editing an enhancer that contains a SNP. In order to strengthen genotype-phenotype relation, the latter (which may have secondary consequences unrelated to the SNP) should be carefully controlled. Indeed, the reproduction of the exact variation under study, allows a much more accurate recapitulation *in vitro* of the disease genetic mechanisms. The very recent introduction of CRISPR/Cas9 and single-stranded oligodeoxynucleotides as donor templates currently allows applying precision gene edition on a routine basis for modeling purposes (Paquet et al. 2016; Richardson et al. 2016).

Generating lineage-specific reporter lines by gene editing

Another complementary approach to circumvent eventual differences in the differentiation efficiency among hiPSC lines is to generate genetic reporter lines. Reporter genes can be used to better identify the specific cell type of interest among the differentiated progeny. A reporter line can be defined as cell line that express a reporter gene under the control of certain regulatory sequences. These regulatory sequences are in turn those that control the transcription of the gene to be reported. In particular, thanks to this technique it is possible to follow and monitor gene

expression, the regulation of that expression and signal transduction pathways. The reporter gene should not be endogenously expressed to reduce the background activity and has to produce a clear, easy detectable, sensitive and reliable signal. To choose a reporter it is necessary to take into account the cell line to use, the type of experiment and the assay to detect the reporter. In this context, the generation of reporter cell lines enables the identification of cells that express certain genes of interest such as those that define a particular cell lineage.

The development of new and easy-to-program gene editing technologies added to the innovative optical imaging platforms allow the real time detection of gene expression at the single cell level. It is now possible to understand when a specific gene is transcribed during development/differentiation process, at which level and where is localized within the cell, what type of cells produce that specific gene, whether the gene is constitutively active or induced by exogenous cues. Furthermore, reporter genes can be used to understand the molecular bases of disease and to perform a large-scale drug screening.

To obtain a reporter cell or animal line it is necessary to link the reporter gene to the regulatory sequences of the gene of interest. Classical approaches consist in fusing selected regulatory sequences (mostly proximal promoters) of the gene to be reported to a reporter gene (fluorescent proteins, luciferase, resistance genes, ß-gal). Many successful cases have been described in the literature. In the case of such as reporters for Synapsin-I (Hioki et al. 2007), GFAP and Dcx (Pei et al. 2015). Recombinant lentiviral vectors were widely used for gene delivery into cells because of the unique advantages of stably integrating transgene into the genome of dividing and non-dividing cells (Naldini et al. 1996). Using neuron-specific promoters for stable neuron-specific expression of transgenes makes possible to track, sort them and even replate neurons. However, the disadvantage associated to the classical approach is that in most of the cases, the proximal promoter does not fully recapitulate the endogenous regulation of the reported gene (Bardy et al. 2016). There is growing evidence that *cis*-regulatory elements could be located not only in the promoter, but also in distal enhancers or in enhancers lying in introns or UTR sequences. In this line the utilization of the endogenous sequences is mandatory to achieve trustworthy gene reporter. This can only be made possible through the introduction of the reporter gene into the locus of the gene to be reported. Fortunately, the development of gene editing techniques allows performing targeted gene modification in cells resilient for classical gene targeting approaches such as human PSCs. A scheme depicting both approaches for reporting gene expression is shown in figure 9.

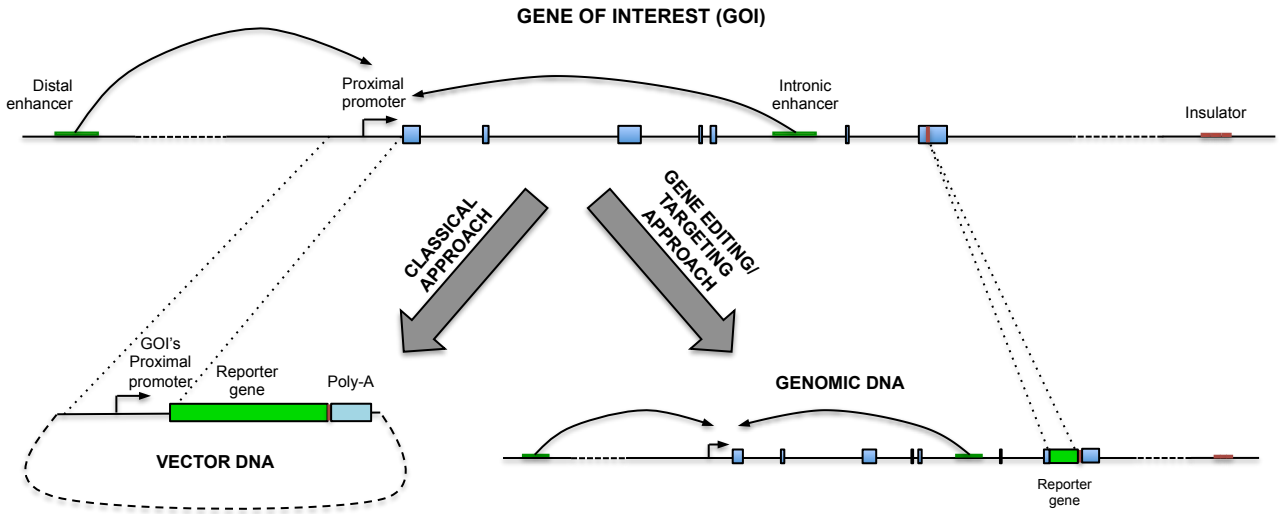

Figure 10: Approaches for generating genetic reporters

In the case of reporters for the dopaminergic neuronal lineage, there are several reporter lines published but just two in hPSC. It is quite necessary to develop these tools since even the gold standard differentiation method does not yield pure populations of DA neurons (Kriks et al. 2011) nor it does work with equal efficiency in different hiPSC lines (Woodard et al. 2014). These reporter lines have been generated using the gene editing toolkit. In 2009, Hockemeyer and collaborators (2009) described an method to target expressed and silent genes in PSCs using ZFNs with the aim to generate genetic reporters. After demonstrating the higher efficiency of this new method compared with the classical gene targeting approach they a gene that is not expressed in PSCs, *PITX3*. This gene is a transcription factor expressed in ventral midbrain dopaminergic neurons among other cell types (eye development). Several years later, this reporter line was used by Watmuff and collaborators (2015) to sort and characterize dopaminergic neurons differentiated from hPSC. They demonstrated that PITX3$^{EGFP/wt}$ neurons differentiated for 70 days with a floor-plate differentiation method are functional (low levels of intracellular chloride and resting calcium) and responsive to a number of pharmacological stimuli. It is also interesting to notice that at maturity the PITX3$^{EGFP/wt}$ neurons show a transcript profile indicative of midbrain DA neurons. This reporter line has obvious implications in neurobiology, neuropharmacology, neurophysiology, and neurotoxicology. (Cui et al. 2016) developed a genetic reporter to monitor the growth of stem cell-derived DA neurons during the differentiation process. By applying TALENs technology they engineered a hESC line by knocking in a secreted Metridia luciferase (Mluc) reporter gene into the endogenous *Tyrosine Hydroxylase* (*TH*) locus. This approach allowed the direct differentiation of the DA neural lineage was monitored non-invasively in real time. This method has many advantages since it provide an effective strategy for tracking gene expression during lineage differentiation and development and can be easily applied in drug testing and screening. The main disadvantage of luciferase reporters is that they does not allow identifying single neurons in the plate (Cui et al. 2016). There is still an urgent need to develop genetic reporters to faithfully track and/or purify dopaminergic neurons. Performing analysis on pure populations will help to reduce experimental noise associated to inefficiency or inter-clonal variation. The availability of trustworthy

genetic reporters will allow to get further insight into the specific dopaminergic susceptibility, PD disease mechanisms and eventually boost drug screening procedures.

OBJECTIVES

The main objective of the present thesis is to investigate the relative contribution of the G2019S mutation in the *LRRK2* gene and the genomic background to the presentation of Parkinson's disease-related phenotypes in our in vitro model of the disease.

To this end, an *in vitro* PD disease model based on patients' cells specifically suited for testing the relative contribution of the mutation and the genomic background was generated. Additionally the thesis project was structured on four specific sub-objectives:

- Recruit non-manifesting carriers (NMC) of the G2019S mutation in the *LRRK2* gene at an advanced age and no signs of prodromal disease and generate iPSC lines from these subjects.

- Generate isogenic hiPSC clones differing in the absence or the presence of the LRRK2 G2019S mutation from both carriers and non-carriers with which to test the specific effect of the mutation.

- Study the *in vitro* penetrance of disease-related phenotypes in dopaminergic neurons derived from the selected cohort of non-manifesting and manifesting carriers, and non-manifesting non-carrier lines along with their isogenic counterparts.

- Investigate the existence of genetic determinants of increased or decreased penetrance of LRRK2 G2019S mutation.

Taking advantage of the abilities and skills developed in the framework of the present thesis, a parallel project was initiated whose main objective was to develop a *TH* gene reporter hiPSC line using CRISPR/Cas9 gene edition.

- Generate a TH reporter hiPSC line using CRISPR/Cas9 gene edition and verify the fidelity of the reporter system.

- Demonstrate its applicability and usefulness in different experimental settings.

MATERIALS AND METHODS

Recruitment of non-manifesting carriers of the LRRK2 G2019S mutation and study of the prodromal features

Studies were approved by the authors' Institutional Review Board and conducted under the Declaration of Helsinki. Patients were encoded to protect their confidentiality, and written informed consent obtained. The generation of human iPSCs was done following a protocol approved by the Spanish competent authorities (Commission on Guarantees concerning the Donation and Use of Human Tissues and Cells of the Carlos III Health Institute). Non-manifesting carriers were recruited from families having members affected by LRRK2-associated PD that attended the Movement Disorder Unit at the Hospital Clinic of Barcelona (Barcelona, Spain). They were selected on the basis of having an advanced age and little or no prodromal signs at the moment of the enrolment.

Generation of iPSC

Using CytoTune iPSC Sendai reprogramming protocol, we converted fibroblasts into transgene-free iPSCs. Briefly, explant cultures were obtained from skin punch biopsies. Primary cultures of fibroblast were expanded and 50,000 to 100,000 cells were transduced with the Sendai vectors. Medium was then sifted to human ESC (hESC) medium, consisting of KO-DMEM (Invitrogen) supplemented with 20% KO-Serum Replacement (Invitrogen), 2 mM Glutamax (Invitrogen), 50 μM 2-mercaptoethanol (Invitrogen), non-essential aminoacids (Lonza) and 10 ng/ml bFGF (Peprotech). Cultures were maintained at 37°C, 5% CO_2, with media changes every other day. Colonies were picked based on morphology 20-30 days after the initial infection and plated onto fresh feeders. Lines of patient-specific iPS cells were maintained by mechanical dissociation of colonies and splitting 1:3 onto feeder cells in hESC medium or by dissociation with EDTA and passaging onto Matrigel-coated plates with hESC medium pre-conditioned by mouse embryonic fibroblasts (chESC medium).

Characterization of iPSC

Expression of Sendai vector transgenes and endogenous pluripotency-associated transcription factors by quantitative Polymerase Chain Reaction (after reverse transcription) (RT-PCR). *In vitro* differentiation towards endoderm, mesoderm and neuroectoderm was carried out essentially as described (Raya et al. 2008)

Generation of TALEN monomers, CRISPR/Cas9 plasmids and donor templates for HDR

TALEN monomers were engineered as described elsewhere (Mussolino et al. 2011) in the Institute for Cell and Gene Therapy & Center for Chronic Immunodeficiency (University of Freiburg). They were composed of 19 RVDs and were fused to *wild type* FokI nuclease domains. Repeats containing the NN RVD were used for Guanidine recognition. Each

monomer was inserted in a plasmid under the control of a modified CMV promoter (Alwin et al. 2005).

CRISPR/Cas9 plasmid pSpCas9(BB)-2A-GFP (PX458)(Ran et al. 2013) was obtained from Addgene (#48138). Original pCbh promoter was exchanged for the full-length pCAGGS promoter in order to achieve higher expression levels in hiPSC. Custom guide RNAs were cloned into the BbsI sites as annealed oligos.

Donor templates for HDR were generated using standard molecular cloning procedures. Briefly, for *LRRK2* donor template, homology arms were amplified using genomic DNA from either *wild-type* or LRRK2 G2019S mutant hiPSC lines and inserted into the KpnI-XhoI (5'HA) and SpeI-NotI (3'HA) sites of pBS-SK(-). pRex1-NeoR-SV40pA cassette was amplified from aMHC-eGFP-Rex-Neo (Kita-Matsuo et al. 2009) (Addgene; #21229) with primers contaning LoxP sites in the proper orientation and inserted into the SalI-BamHI sites. For *TH* donor template, homology arms were amplified from genomic DNA and verified by Sanger sequencing. Resulting sequences matched those of the reference genome GRCh38. They were inserted into the KpnI-ApaI (5'HA) and SpeI-XbaI (3'HA) sites of pBS-SK(-). P2A peptide was added to mOrange with the primers using to amplify the gene and the PCR product was inserted into the ApaI-XhoI sites of the pBS-5'HA-3'HA plasmid. Finally pRex1-Neo-SV40 was inserted between the XhoI and SpeI of the previous plasmid.

Gene edition in iPSC

For correcting the LRRK2 G2019S mutation, mutant iPSC were gene-edited using TALENs. iPSC grown to confluence in 10cm plates were pre-treated for 2-4 hours with 10 μM Y-27632 (RI; Miltenyi-Biotech), disaggregated to small clumps using Accutase (eBiosciences), resuspended in ice-cold chESC medium supplemented with RI and containing 15 μg of each TALEN monomer-coding plasmids and 30 μg HDR donor template and placed in a electroporation cuvette. Cells were electroporated with a Gene Pulser Xcell electroporation system (BioRad) with the following settings: 250 V and 500 μF (time constant should be between 10 and 14 milliseconds). After being pulsed, cell suspension was seeded in 10-cm plates coated with Matrigel containing RI-supplemented chESC medium. 72 hours post-transfection, 50 μg/mL G-418 (Melford Laboratories Ltd.) treatment was initiated and maintained for 2 weeks until resistant colonies attained enough size as to be screened. At that moment, half of each resistant colony was manually picked and site-specific integration was verified by means of PCR and gene correction was assessed by Sanger sequencing. Colonies with the desired genotype were isolated, expanded and cryopreserved.

For inserting the mutation in heterozygosis, *wild-type* iPSC were edited using CRISPR/Cas9. This choice was made based on the difficulty on controlling the zigosity of the edition using TALENs. CRISPR guide RNAs overlapping the selection cassette insertion site were observed to favor biallelic editions (data not shown). The day before transfection, 800.000 iPSC were seeded on Matrigel-coated 10-cm plates. The day after, cells were transfected

using FuGENE HD (Promega) and a mixture. Subsequent steps were carried out as described with TALENs.

For the generation of TH reporter iPSC cell lines, iPSC were transfected and subsequently processed as described for the mutation insertion but with just one HDR plasmid template. CRISPR gRNA overlapped *TH* gene stop codon.

For the excision of the selection cassette, edited iPSC were transfected with CRE recombinase-expressing plasmid (Addgene; #27546). 48 hours post-transfection, cells were singularized and seeded at clonal density on a feeder layer of irradiated human fibroblasts. When colonies attained a certain size they were picked and subcultured in independent matrigel-coated wells. Cells were sampled and checked for cassette excision by PCR and Sanger sequencing. Those clones in which the cassette was excised were expanded, cryopreserved and karyotyped.

iPSC differentiation to DA neurons

For DAn differentiation, iPSC were transduced with LV.NES.LMX1A.GFP and processed as previously described (Sanchez-Danes et al, 2012). For DAn yield analysis cells were co-cultured with PA6 for 3 weeks in N2B27 medium. For short-term SNCA analysis, DAn generated on the top of PA6 for 3 weeks were trypsinized and cultured for 3 days on Matrigel-coated dishes. For long-term culture, neural progenitor cells were seeded onto mouse primary cortical astrocytes, prepared as described elsewhere (Giralt et al. 2010), and maintained in N2B27 medium. After 9 weeks, cells were fixed and processed for immunofluorescence analysis.

Generation of human Neural Progenitor Cells (hNPC)

The hiPSCs colonies were gently disaggregated from the culture plate and plated 6 hours in non-adherent conditions in DMEM/F12, 2% of B27 without vitamin A (12587-010 Gibco) and supplemented with: 1% of N-2 Supplement (17502-048 Gibco), 10 µM of Y-27632 (Milteny-Biotech), 100 nM of LDN 193189 (120-10C Peprotech), 10 µM of SB431542 (S4317-5MG Sigma) and bFGF 2 ng/ml. Cells were plated 10 days on Poly-ornitin/laminin (P4638-1G Sigma; L2020-1MG Sigma) coated dishes in this medium before being detached with accutase and re-plated on Poly-ornitin/laminin coated dishes and cultured in the neural induction medium: 50–50% DMEM/F12 - Neurobasal medium supplemented with 2% of B27, 1% of N-2, 0.5% Glutamax (35050-038 Gibco), 10 ng/ml of Epidermal Growth Factor (EGF; AF-100-15 Peprotech) and bFGF 10 ng/ml. Culture of cells in this neural induction medium generates homogenous cultures of NSCs (more than 95% of the cells).

hNPC differentiation to DA neurons

DA neuron progenitor derivation. NSCs were grown at high confluency (70%) for 7 days on Poly-ornitin/laminin coated dish in N2B27 supplemented with 200 ng/mL of Sonic Hedgehog (SHH); 100 ng/mL of Fibroblast Growth Factor 8 (FGF8; 100-25; Preprotech). This first culture step was required to pattern NPCs as DA neurons progenitors. For terminal

differentiation, DA progenitors were plated on Poly-ornitin/laminin coated dish, in N2B27 supplemented with 20 ng/ml of Brain Derived Neurotrophic Factor (BDNF; 450-02, Peprotech), 20 ng/ml of GDNF (450-10, Peprotech) for the indicated time points.

Immunofluorescence

Cells were fixed with 4% paraformaldehyde in PBS at RT for 15 min and permeabilized for 15 min in 0.3% Triton in TBS. Cells were then blocked in Triton-X100 with 3% donkey serum for 2 h. The following antibodies were used: goat anti-Nanog (R&D Systems; AF1997; 1:50), mouse IgM anti-Tra-1-81 (Merck-Millipore; MAB4381; 1:200), mouse anti-OCT4 (Santa Cruz; sc-5279; 1:30), rat IgM anti-SSEA-3 (Developmental Studies Hybridoma Bank (DSHB); MC-631; 1:10), mouse-SOX2 (R&D Systems; MB2018; 1:50), mouse anti-SSEA-4 (Developmental Studies Hybridoma Bank (DSHB); MC-813-70; 1:100), mouse anti-TUJ1 (Biolegend; 801202; 1:500), rabbit anti-GFAP (Dako; Z0334; 1:1000), rabbit anti-AFP (Dako; A0008; 1:400), goat anti-FOXA2 (R&D Systems; AF2400; 1:50), mouse anti-SMA(Sigma; A5228; 1:400), rabbit anti-GATA4 (Santa Cruz; sc-9053; 1:50), rabbit anti-TH (Santa Cruz; sc14007; 1:500), sheep anti-TH (Pel-Freez P60101-0 1:500), rabbit anti-cleaved caspase-3 (Cell Signaling; 9664; 1:400), mouse anti SNCA (BD transduction laboratories; 610787; 1:500), rabbit anti-SYN-I (Merck-Millipore; 574777; 1:1000), rabbit anti-GM130 (BD transduction laboratories; 610822; 1:100), rabbit anti-mRFP (Abcam; ab34771; 1:400), rabbit anti-PAX6 (Covance; PRB-278P; 1:100) and mouse anti-Nestin (Abcam; ab22035; 1:500). Secondary antibodies used were all the Alexa Fluor Series from Invitrogen (all 1:500). Images were taken using Leica SP5 confocal microscope. To visualize nuclei, slides were stained with 0.5 µg/ml DAPI (4′,6-diamidino-2-phenylindole) and then mounted with PVA/DABCO.

Neurite morphology assessment

Neurite morphology study was performed at the indicated time-point on iPSC-derived DA neurons differentiated on top of cortical mouse astrocytes fixed and stained for TH. We randomly selected fields from differentiated cultures and assessed neurite morphology. Those neurons presenting shortened or thickened neurites in the part most proximal to the soma were considered as having a degenerated phenotype. Images were acquired with a SP5 confocal microscope and cell counts assisted by ImageJ cell counter plug-in (NIH).

Alpha-synuclein assessment

Alpha-synuclein analysis was performed at the indicated time-point on iPSC-derived DA neurons differentiated either on the top of PA6 (early time-point) or cortical mouse astrocytes (late time-point) fixed and stained for TH, alpha-synuclein and synapsin-I antibodies. At early time-points, neurons were classified into high (and detectable) or low (almost undetectable) levels of alpha-synuclein staining, as well as at late-time points, in which we distinguished those showing a punctate pattern of alpha-synuclein *versus* those

presenting a diffuse cytosolic pattern. Images were acquired with a SP5 confocal microscope and cell counts assisted by ImageJ cell counter plug-in (NIH).

Exome sequencing

A total of 3 healthy controls, 7 sporadic PD patients, 4 LRRK2 G2019S PD patients described elsewhere (Sánchez - Danés et al. 2012) plus the 3 non-manifesting carriers of the LRRK2 G2019S described here (Fig. 1A), participated in the genetic study. Genomic DNA was harvested from low passage dermal fibroblast using QIAamp mini DNA kit (Qiagen). Whole exomes were captured with the SureSelect V5 kit (Agilent) and were sequenced on an Illumina 2000/2500 instrument at the Genomics Unit from the Center for Genomic Regulation (Barcelona, Spain). Raw sequencing data quality was assessed using FASTQC and no relevant concerns were observed. The paired-end reads (read size: 125bp) were mapped to the human reference genome GRCh37 using bwa (version 0.5.9), allowing up to five mismatched, inserted or deleted bases (indels). The alignment was refined using GATK (version 1.6) by performing local multiple sequence alignment around inferred putative indels and known ones from 1000 genomes project, and base quality score recalibration. The actual mean base of the samples was 34.09x after the whole process.

Genotyping of candidate protective variants

DNAwas extracted from peripheral blood following standard procedures. Genotyping was performed using a custom TaqMan assays for rs1134921 on a StepOnePlus Real-time PCRSystem(Applied Biosystems, Foster City, CA). Statistical analysis was performed by using the SNPstats software (Sole et al. 2006). Linear regression models were used to assess the AAO variation explained by the different rs356219 SNP genotypes under different possible inheritance models. Akaike's information criterion (AIC) and Bayesian information criterion (BIC) were calculated to define the data that best fitted the model. If binary, the application assumes an unmatched case–control design and unconditional logistic regression models are used.

Sholl Analysis

Cells were cultured under dopaminergic neuron differentiation conditions. After ten days of terminal differentiation fluoresecent cells were FACSorted directly in 48 well plates previously seeded with human astrocytes (ScienCell). They were kept in culture for seven days and before being fixed and stained directly in the tissue culture plate. Cells were stained with TUJ1 (Biolegend; 801202; 1:500), rabbit anti-mRFP (Abcam; ab34771; 1:400) and single neurons were imaged using a Leica AF7000 wide-field automated inverted microscope. Neurites were traced using the Simple Neurite Tracer plugin on FiJi and the neuronal complexity were measured by counting the number of neurite intersections with concentric circles radiating from the cell body with the Sholl Analysis plugin. The number of branching point was manually counted after the analysis.

Live imaging of mitochondrial motility

Differentiated cultures were dissociated after 10 days of initiating terminal differentiation. Cells were then detached using a 1:6 dilution of Accutase (eBioscience). One-twentieth of the total cell amount was re-seeded in a matrigel-coated 35mm µ-Dish (ibidi) in N2B27 medium supplemented with GDNF and BDNF. After additional 10 days of differentiation (medium change every other day), cells were incubated with MitoTracker Green or Red FM (Invitrogen) in a concentration of 100nM. After 1 hour, medium was changed and mitochondrial movement was recorded every 3 seconds in mOrange+ cells for 5 minutes using a confocal microscope (Leica TCS SP5). During the recording process, temperature was kept at 37 degrees and the CO_2 level at 5%. Data was analyzed with the help of the velocity measurement tool of FiJi to create kymographs of the recorded neurites. Kymographs were then used to determine the length of the neurites and the length and speed of all mitochondria in the region of interest. The obtained values enabled the calculation of the mitochondria size distribution, the neurite-mitochondrial-index and the mitochondria motility with Microsoft Excel.

RESULTS

Part I: Investigating the genetic component of Parkinson's disease through the use of human induced pluripotent stem cells and gene editing

Recruitment of candidate protected LRRK2 G2019S carriers and hiPSC generation

We recruited three non-manifesting carriers (NMC) of the LRRK2 G2019S aged 48, 51 and 62 years old, which received the codename SP_19, SP_20 and SP_22. SP_19 and SP_22 were third-degree relatives (cousins). Detailed medical examination performed by a specialized motor disorder unit revealed perfect motor coordination without any signs nor symptoms of ongoing or prodromal disease. At the time of the submission of this thesis, the ages of the NMC were 67, 53 and 57 years old and the three individuals remained free of any parkinsonian sign, with the exception of the oldest NMC which showed a reduced DAT uptake in the left putamen as measured by DaT-SPECT also accompanied by an increased hyperechogenicity in the left SN. These two prodromal markers suggest the beginning of a degeneration process in this subject (Iranzo et al. 2010; Spiegel et al. 2006). Therefore we concluded that these individuals were good candidates to be considered either life-long asymptomatic NMC or at least to be very late converters. Table 4 summarizes the iPSC lines used in the present study plus the observations made after examining the prodromal biomarkers most relevant for LRRK2 G2019S carriers (smell assessment and imaging biomarkers) of the three NMC.

Skin punch biopsies were obtained and explant cultures generated. iPSCs were generated by transducing dermal fibroblast with non-integrative Sendai virus coding for the reprogramming factors. Several clones were obtained and their pluripotency features were assessed. The expression of pluripotency markers was verified both at the protein (Fig. 11B) and RNA level. The expression of reprogramming factors was mediated by the endogenous loci rather than by the Sendai vectors (Fig. 11E and 11F) since vector-mediated expression was lost several passages after initial clonal isolation. They were able to give rise to derivatives of the three germ layers after directed differentiation (Fig. 11C). The karyotype was analysed to discard chromosomal instability confirming the expected number of chromosomes (Fig. 11D). Finally, Sanger sequencing of the exon 41 confirmed the presence of the G>A transition in the position 6055 of the CDS which results in the glycine 2019 to serine substitution (Fig. 11G).

Table 4: Clinical features of PD patients and controls involved in the present study

							Hyposmia		Prodromal Biomarkers DAT-SCAN		Transcranial Sonography		
Cell Line Code	**Disease status**	**Mutation**	**Gender**	**Age at donation**	Current age	**Age at onset**	**Loss of smell**	**UPSIT Score**	**Date**	**Result**	**Right SN**	**Left SN**	**Result**
SP_19	NMC	G2019S LRRK2	Male	48	53	N/A	No	28	19/9/12	Normal	no window	0.15	Normal
SP_20	NMC	G2019S LRRK2	Female	51	57	N/A	No	36	17/10/12	Normal	no window	0.09	Normal
SP_22	NMC	G2019S LRRK2	Female	62	67	N/A	No	32	14/9/12	Reduced uptake in the left putamen	0.11	0.23	Abnormal
SP_11	NMNC	N/A	Female	48	56	N/A							
SP_17	NMNC	N/A	Male	52	60	N/A							
SP_05	MC	G2019S LRRK2	Male	66	74	52							
SP_12	MC	G2019S LRRK2	Female	63	71	49							
SP_13	MC	G2019S LRRK2	Female	68	76	57							

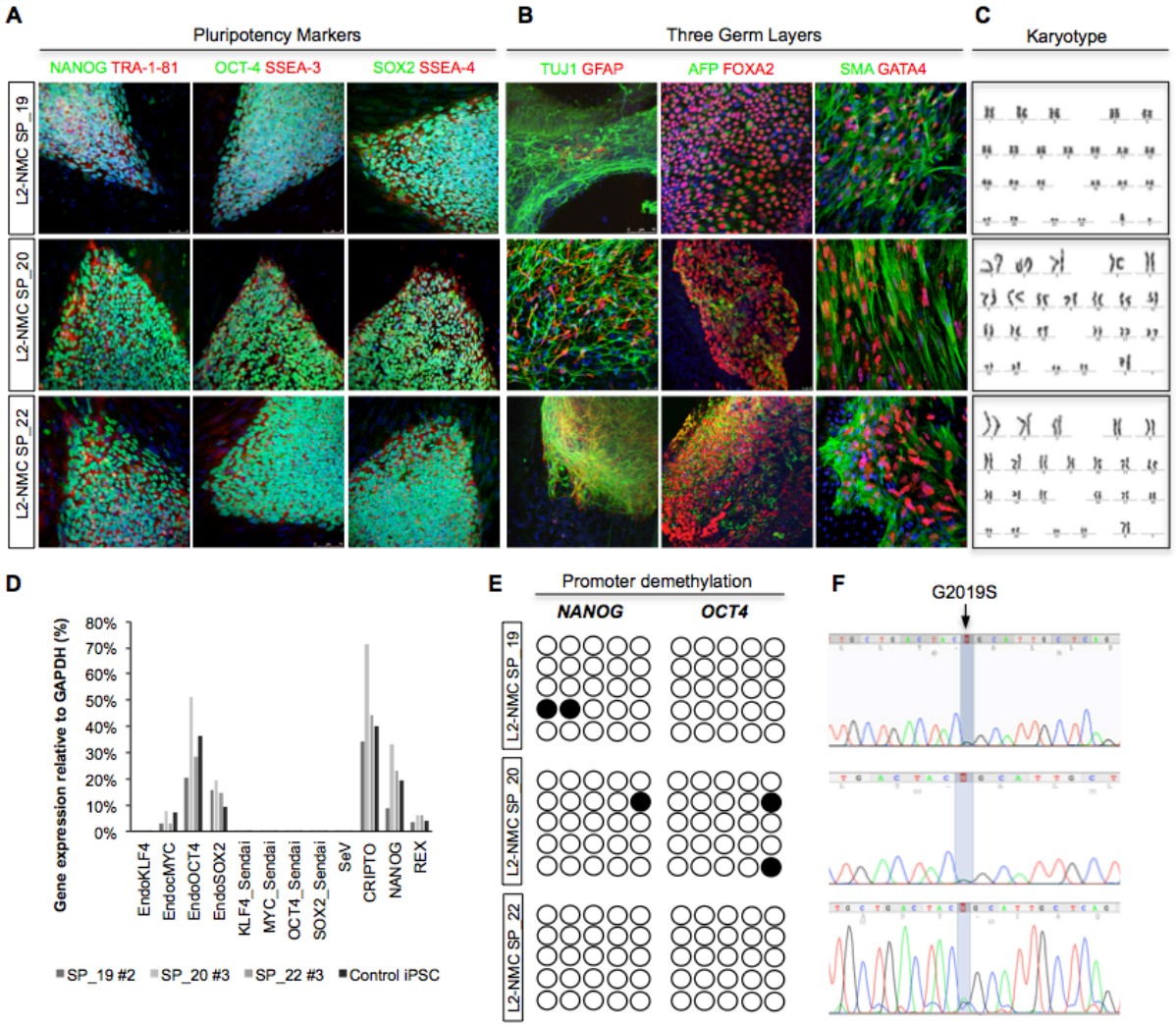

Figure 11: Recruitment of aged NMC of the LRRK2 G2019S mutation and iPSC generation and characterization.

A) Immunofluorescence analysis of representative colonies of L2-NMC SP_19. SP_20 and SP_22 stained positive for the pluripotency-associated markers NANOG. OCT4 and SOX2 (green). TRA-1-81. SSEA3 and SSEA4 (red).

B) Immunofluorescence analyses of L2-NMC iPSC lines differentiated *in vitro* show the potential to generate cell derivatives of all three primary germ cell layers including ectoderm (stained for TUJ1. green and GFAP. red). endoderm (stained for α-fetoprotein. green. and FOXA2. red) and mesoderm (stained for smooth muscle actin. SMA. red).

C) Normal karyotype from selected L2-NMC iPSC clones.

D) RT-qPCR analyses of the expression levels of Sendai Virus-derived reprogramming factors and endogenous expression levels (Endo) of the indicated genes in L2-NMC iPSC lines and a previously validated iPSC line.

E) Bisulphite genomic sequencing of the *NANOG* and *OCT4* promoters showing demethylation in L2-NMC iPSC lines.

F) Sanger sequencing of LRRK2 exon 41 revealed the presence of the G2019S in heterozygosis.

Generation of isogenic controls differing in the presence or absence of the G2019S mutation

The presentation of the disease-related phenotypes by patients DA neurons observed in Sánchez-Danés A. et al. (2012b) is very likely to be the result of the complex interaction between the *in vitro* environment and the genetic particularities of the donor subject. In the case of LRRK2 G2019S carriers, the mutation is supposed to be the major driver of the whole genetic component. However, it cannot be dismissed the participation of many other genetic variants lying in other genes or loci in the phenotypes under study (Nalls et al. 2014a). In order to assess the specific contribution of the LRRK2 mutation, isogenic clones that only differed in the presence (or absence) of the G2019S mutation were generated.
To this end we generated several site-specific nucleases (SSN) that targeted the mutation site in the LRRK2 gene. A plasmid donor template was also generated in order to induce the desired gene edition by means of HDR. The templates contained the specific allele to be introduced plus a *floxed* selection cassette that would be introduced in intron 41 to allow for the selection of the recombined clones. Initially, TALEN monomers were engineered encompassing the position of the mutation. These were mainly employed to both correct and to *knockin* the mutation in mutant and in control lines respectively. However, only gene correction was successfully achieved using these SSN. For the *knockin* setting, CRISPR/Cas9 was used and the guide RNA recognition sequence overlapped selection cassette insertion site (Fig. 12A). The rationale for such choice is explained in the materials and methods section. Once the different SSN were designed, their cleavage efficiency was assayed by means of the T7 endonuclease I assay (Fig. 12B and C).

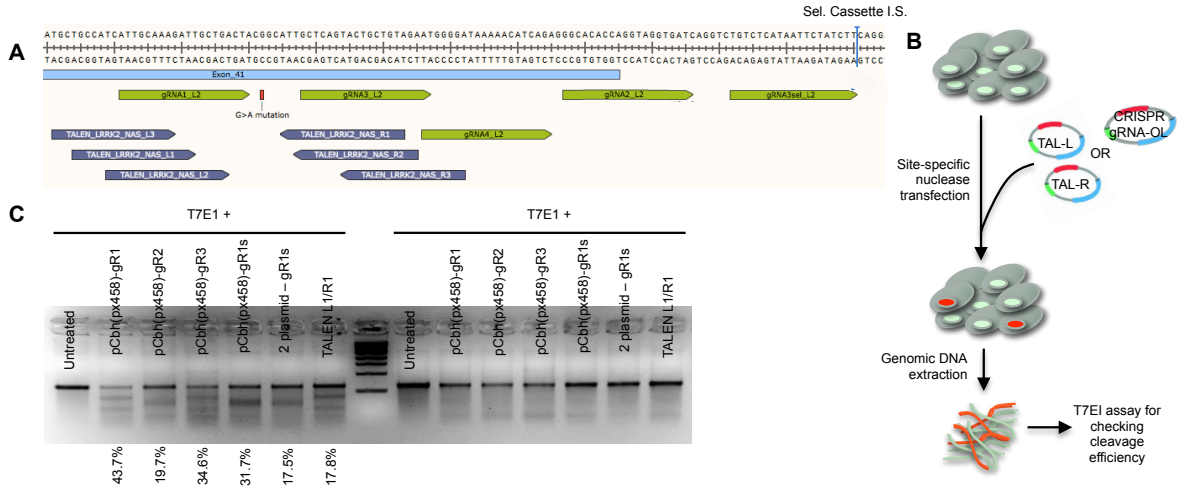

Figure 12: Generation of sequence-specific nucleases.

A) Graphic representation of TALEN monomers and CRISPR guide RNAs overlaying the exon 41 of LRRK2.
B) Scheme of the experimental procedure followed in order to assess the cleavage efficiency of the site-specific nucleases.
C) Assessment of the cleavage efficiency of the different site-specific nucleases through the T7EI assay. Percentages below the image indicate the amount of alleles targeted by the nucleases.

Once having chosen most efficient TALEN monomers, these were co-transfected into iPSC along with a donor template encoding for the *wild type* allele. After applying drug selection, surviving colonies were molecularly characterized in order to ensure site-specific recombination (Fig. 13A and B). This was done using by means of PCR using primers specific for the donor -adjacent genome junctions (Fig. 13B and C). After having detected those colonies that harbored the desired gene modification, they were isolated and expanded and subsequently transfected with a plasmid encoding for the CRE recombinase. Cassette excision left a 50 bp genomic scar reminiscent of the LoxP site that could be observed both by PCR and by Sanger sequencing. Those subclones in which the selection was successfully excised were karyotyped to discard major chromosomal alterations. TALEN-mediated gene edition was applied to correct the mutation in two manifesting carrier iPSC lines (ED-L2-PD SP_12 and SP_13) and in the youngest non-manifesting carrier (ED-L2-NMC SP_19). However, that strategy proved to be very inefficient due to two main reasons: i) edited alleles could be re-targeted by the TALENs therefore introducing undesired indels and ii) donor template contained TALENs target sequences, which favored in-cell linearization and non-specific integration of the selection cassette (Holkers et al. 2014).

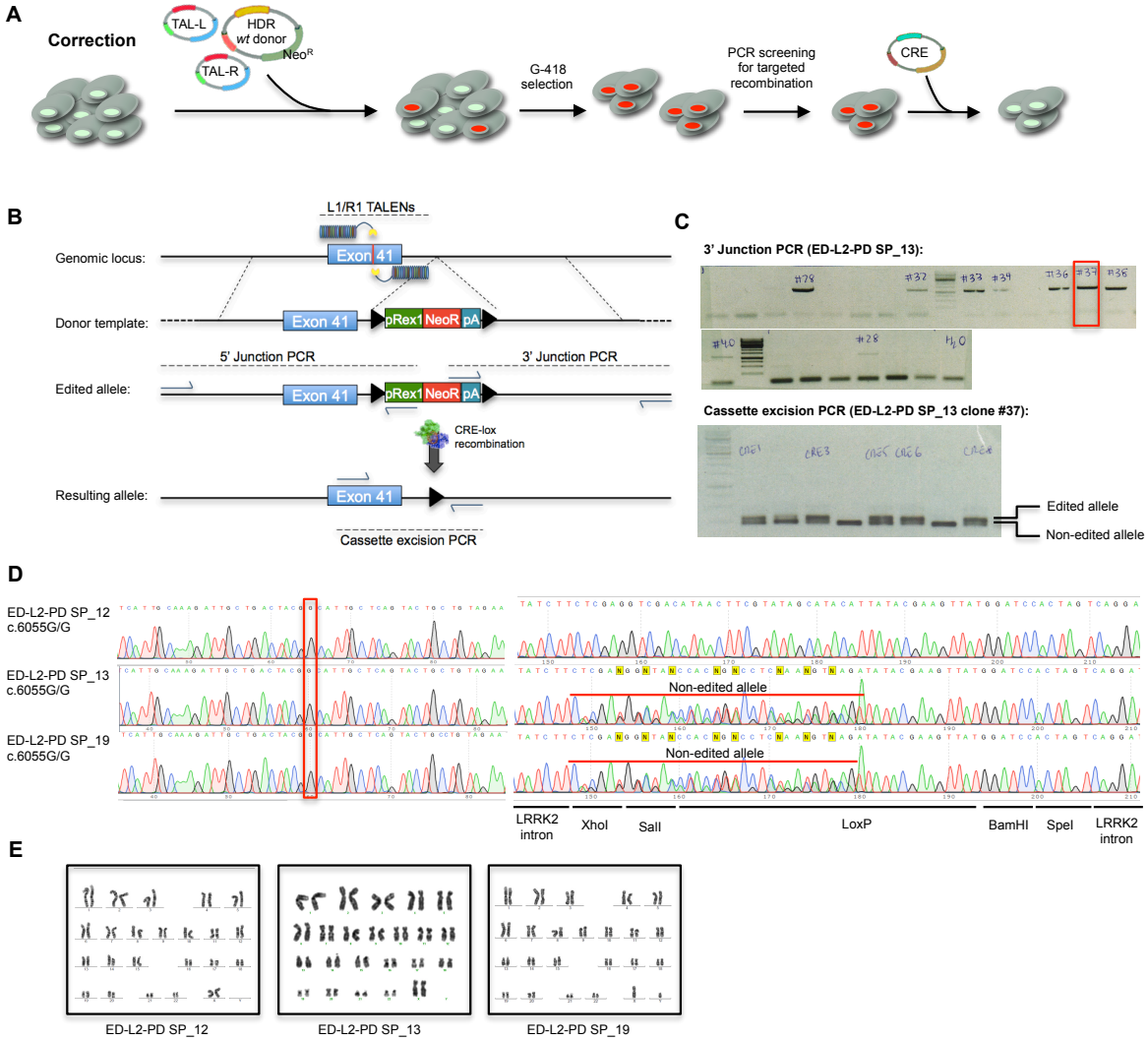

Figure 13: Generation isogenic controls from LRRK2 G2019S mutant iPSC through TALEN-based gene correction.

A) Scheme of the experimental procedure followed in order to correct the G2019S mutation using TALENs.

B) Scheme describing the recombination steps given during the edition process. Blue arrows represent the primers used for the PCR screening procedure. Green or red lines overlying exon 41 represent alternative alleles. Black triangles represent LoxP sites surrounding the selection cassette

C) Molecular analysis of the resistant clones to confirm HDR in the target locus (upper gel) and selection cassette excision (lower gel). In the lower gel, the increase in size of the edited allele is due to the remaining LoxP site.

D) Sanger sequencing of LRRK2 exon 41 and selection cassette insertion site confirmed the desired genotype in each edited line G2019S in heterozygosis and successful excision of the LoxP site-flanked cassette.

E) Normal karyotype from edited iPSC clones.

These two drawbacks associated with the previous design made very difficult to control the zigosity of the edition in the case of the introduction of the mutation in one single allele. To solve this issue, an alternative design combining CRISPR/Cas9 and two donor plasmids, *wild type* and mutant, was used instead. A CRISPR guide RNA overlapping the selection cassette insertion site almost doubled the on-target DNA cutting efficiency of the most efficient TALEN pair (Fig. 12C). Moreover, guide RNA target sequence was absent from

both the donor templates and the edited allele therefore avoiding the two issues raised before. The absence of random recombinants was evident due to the lack of resistant colonies negative for the targeted recombination (Fig.14C, upper panel). This editing strategy was successfully applied to insert the mutation in heterozygosis in a healthy control line (ED-Control SP_11). The gene edition process is depicted in figure 14A-B. Note that biallelic edition could be observed by a single band that is approximately 50 bp longer than the one of the non-edited allele in the cassette excision PCR (Fig. 14C, lower gel).

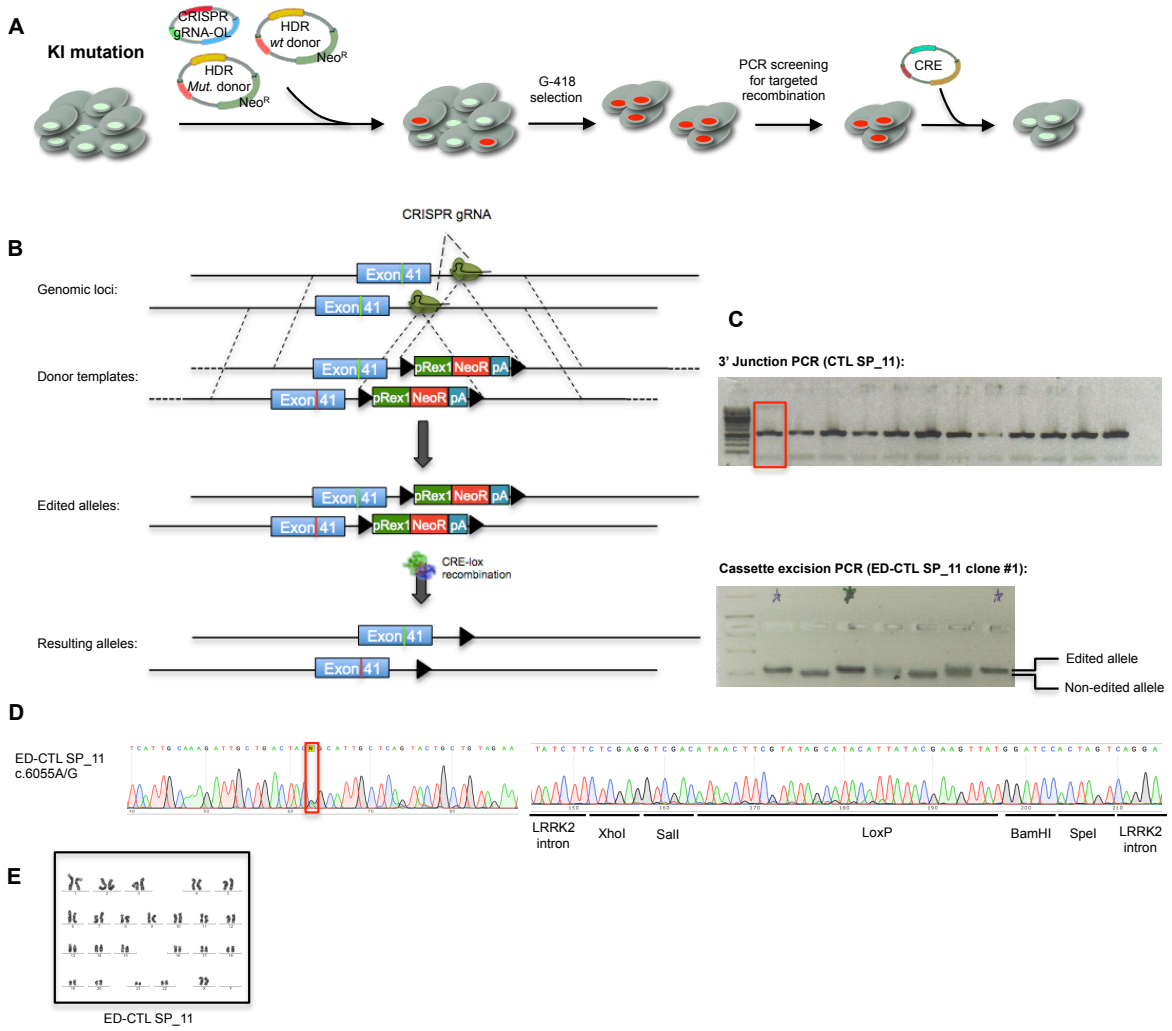

Figure 14: Generation isogenic controls from control iPSC through CRISPR/Cas9-based gene edition.

A) Scheme of the experimental procedure followed in order to *knockin* the mutation in heterozygosis using CRISPR/Cas9.

B) Scheme describing the recombination steps given during the edition process. Blue arrows represent the primers used for the PCR screening procedure. Green or red lines overlying exon 41 represent alternative alleles. Black triangles represent LoxP sites sorrounding the selection cassette

C) Molecular analysis of the resistant clones to confirm HDR in the target locus (upper gel) and selection cassette excision (lower gel). In the lower gel, the increase in size of the edited allele is due to the remaining LoxP site. In the lower gel. the increase in size of the edited is due to the remaining LoxP site.

D) Sanger sequencing of LRRK2 exon 41 and selection cassette insertion site confirmed the desired genotype in each edited line G2019S in heterozygosis and successful excision of the LoxP site-flanked cassette.

E) Normal karyotype from edited iPSC clones.

We then applied our previously established differentiation method (A. Sánchez-Danés et al. 2012) to the newly generated lines (both those of the NMC and the gene-edited clones) (Fig. 15A). After 3 weeks of differentiation, all iPSC lines generated similar numbers of dopaminergic neurons that coexpressed neuronal (TUJ1) and dopaminergic markers (TH) (Fig. 15C). At that early time-point there were not any evident signs of neurodegeneration as judged by the overall morphology of the neuronal net (Fig. 15B).

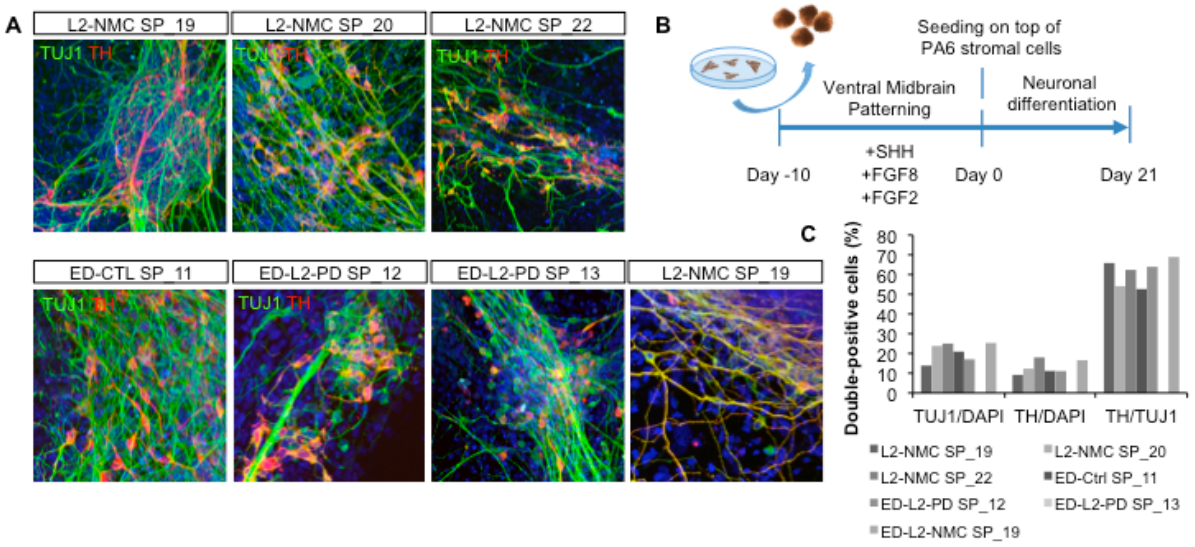

Figure 15: Differentiation of the newly generated iPSC lines to DA neurons

A) Scheme depicting the *in vitro* DA neuron differentiation protocol. Embryoid bodies (EBs) generated by forced aggregation of iPSC colonies were patterned to ventral midbrain in the presence of N2B27 medium supplemented with specific morphogens for 10 days. Neuralized EBs were then seeded on a confluent monolayer of PA6 stromal cells and they were let to differentiate for up to 21 days before they were analyzed for the yield and appearance of DA neurons.

B) Immunofluorescence analysis of DA neurons differentiated from different iPSC lines and cultured for 21 days on the top of PA6 stromal cells. co-stained for TH (red). the pan-neuronal marker TUJ1 (green) and the nuclei were counterstained with DAPI (blue).

C) Quantification of the differentiation efficiency towards dopaminergic neurons of the different iPSC lines.

Long-term culture of L2-NMC-iPSC derived DA neurons does not result in DA cell loss as with L2-PD-iPSC derived DA neurons

We then applied our PD *in vitro* modeling paradigm as described in Sánchez-Danés A. et al (2012b). Briefly, ventral midbrain-patterned embryoid bodies were seeded on the top of cortical murine astrocytes, which facilitated terminal differentiation into mature dopaminergic neurons (Fig. 14A). In addition, murine astrocytes provide a more physiological environment supporting viable cultures of DA neurons for up to 75 days. When neuronal cultures derived from L2-NMC iPSC lines were analyzed for the presence of

apoptotic cells, we found a reduction of the proportion of Caspase-3 (Casp3) positive DA neurons in all three of them compared with the one derived from the L2-PD iPSC lines. Specifically, L2-NMC SP_20 showed the lowest numbers, which were not significantly different from the Control SP_11 line. Interestingly, correction of the mutation in two L2-PD iPSC lines reduced the proportion of apoptotic DA neurons to control levels, suggesting that LRRK2 G2019S is the major driver of the pathology in L2-PD DA neurons. DA cell loss and alpha-synuclein pathological accumulation are considered as the hallmarks of PD (Fig 14B and C). However, some familial forms do not show LB formation and some others do it only in a fraction of cases (such as LRRK2 G2019S manifesting carriers (Kalia et al. 2015)). This result suggests that under an identical environmental setting (*in vitro* culture), the selected L2-NMCs have a lower propensity to undergo neurodegeneration after long term *in vitro* culture.

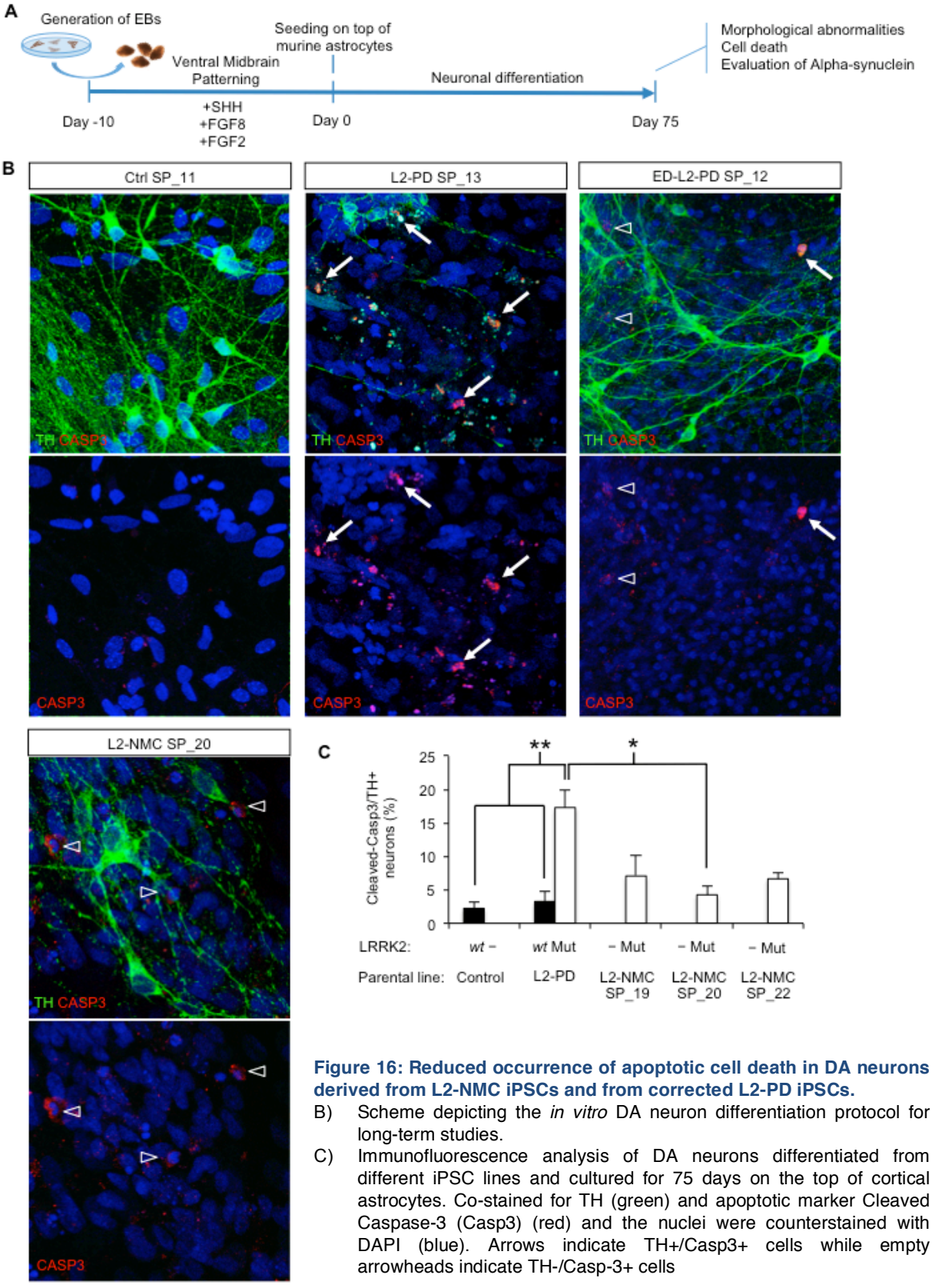

Figure 16: Reduced occurrence of apoptotic cell death in DA neurons derived from L2-NMC iPSCs and from corrected L2-PD iPSCs.

B) Scheme depicting the *in vitro* DA neuron differentiation protocol for long-term studies.

C) Immunofluorescence analysis of DA neurons differentiated from different iPSC lines and cultured for 75 days on the top of cortical astrocytes. Co-stained for TH (green) and apoptotic marker Cleaved Caspase-3 (Casp3) (red) and the nuclei were counterstained with DAPI (blue). Arrows indicate TH+/Casp3+ cells while empty arrowheads indicate TH-/Casp-3+ cells

A) Quantitative analysis of the percentage of DA neurons staining positive for Casp3 at day 75. Data is the average of at least two-independent experiments. Control, 1,064 DA neurons from SP_11; L2-PD is the average of 462 DA neurons from 2 iPSC lines; ED-L2-PD, 1386 DA neurons from 2 iPSC lines; L2-NMC SP_19, 327 DA neurons; L2-NMC SP_20, 510 DA neurons; L2-NMC SP_22, 281 DA neurons. Asterisk denotes statistically significant differences (*:p<0.05; **: p<0.01). [F(5,12) = 8.968; p=0.001].

L2-NMC-iPSC derived DA neurons present a variable degree of morphological abnormalities

LRRK2 mutations and G2019S in particular have been associated to shortening and reduced neurite complexity in diverse disease models (Ramonet et al. 2011; Plowey et al. 2008; MacLeod et al. 2006) including iPSC-based models (Adriana Sánchez-Danés et al. 2012; Reinhardt et al. 2013). To evaluate the impact of LRRK2 G2019S in the process morphology of L2-NMC neurons, 9-weeks old DA cultures were stained for both TH and TUJ1 and neurite morphology was assessed specifically in the DA neurons. We defined two types of DA neurons, those having shortened and/or thickened neurites reminiscent of a degenerative phenotype and those bearing normal processes with an overall healthy appearance (Fig. 17A). Contrary to the generalized reduction in DA neuron death observed among L2-NMC lines, these presented a variable degree of neurite pathology. While L2-NMC SP_20 DA neurons again displayed a phenotype largely resembling that of the control with long and ramified neurites, L2-NMC SP_19 and SP_22 presented a neurite appearance more similar to the L2-PD DA neurons with a considerable proportion of neurons displaying shortened and thickened neurites (Fig. 17B). This latter feature was very frequent in L2-NMC SP_22 DA neurons (see corresponding picture in Fig 17B). Again, isogenic clones from both the control and the L2-PD lines confirmed that the neurite retraction phenotype was mostly dependent on the presence of the LRRK2 G2019S mutation.

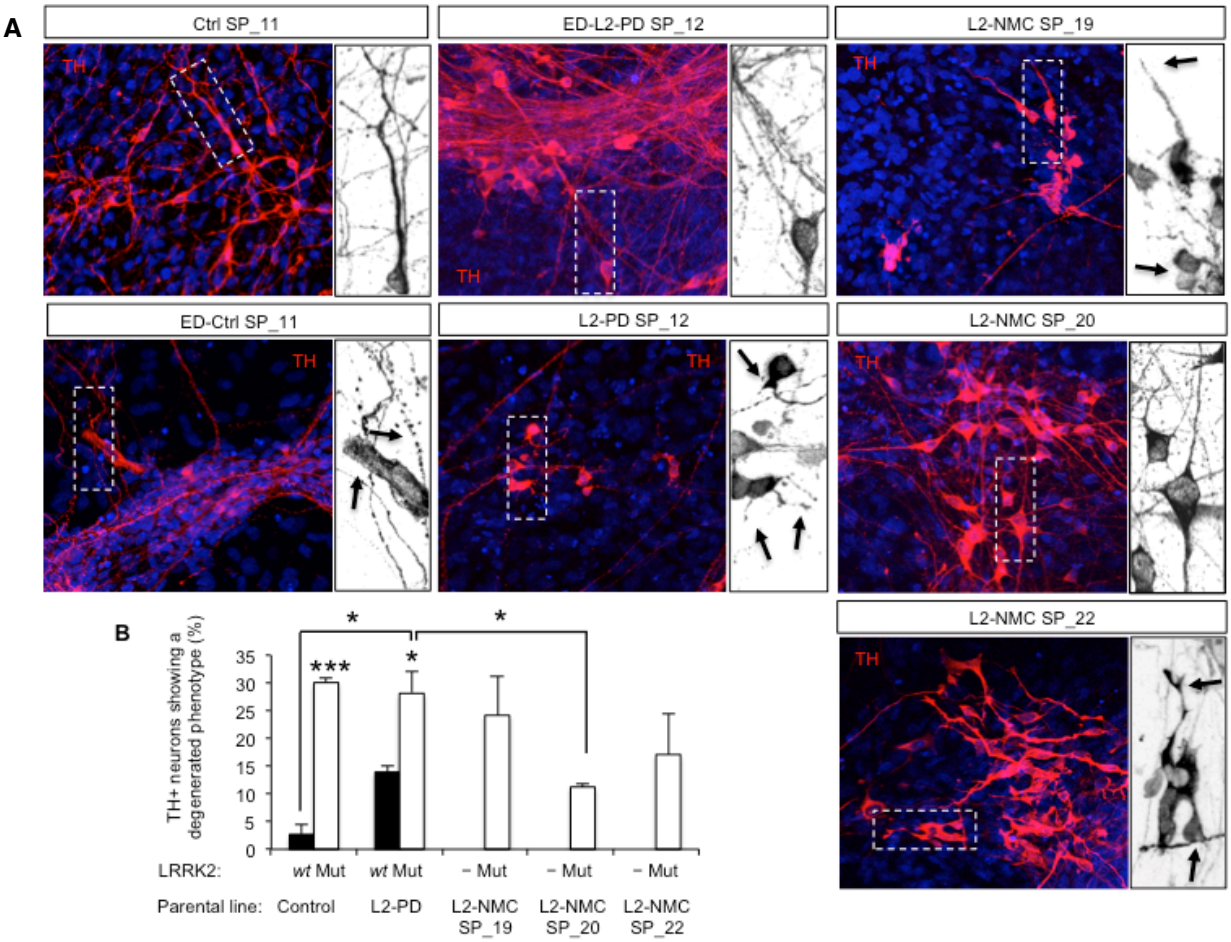

Figure 16: Variable presentation of neuritic aberrations by L2-NMC and corrected L2-PD DA neurons.

A) Immunofluorescence analysis of DA neurons differentiated from different iPSC lines and cultured for 75 days on the top of cortical astrocytes. co-stained for TH (red) and the nuclei were counterstained with DAPI (blue). Insets show representative neurons derived from different iPSC lines presenting either healthy and ramified or shortened/thickened neurites (black arrows)

B) Quantitative analysis of the percentage of DA neurons at day 75. presenting abnormal neuronal processes. Data is the average of at least two-independent experiments. Control, 466 DA neurons from 2 iPSC lines; ED-Control SP_11, 195 DA neurons; L2-PD is the average of 583 DA neurons from 2 iPSC lines; ED-L2-PD, 647 DA neurons from 2 iPSC lines; L2-NMC SP_19, 850 DA neurons; L2-NMC SP_20, 493 DA neurons; L2-NMC SP_22, 211 DA neurons. Asterisk denotes statistically significant differences (*: $p<0.05$; **: $p<0.01$; ***: $p<0.001$). [$F(6,16) = 5,937$; $p=0.002$].

LRRK2 G2019S is a major driver of the accumulation of alpha-synuclein

In our previously published PD model we observed early alpha-synuclein accumulation specifically in L2-PD DA neurons. This finding was further confirmed and mechanistically associated to the inhibitory effect exerted by mutant LRRK2 to chaperon-mediated autophagy (CMA) (Orenstein et al. 2013), the main degradation pathway for alpha synuclein (Cuervo et al. 2004). When the expression of alpha-synuclein was analyzed in the short term, the results confirmed previous results. However L2-NMC SP_20 DA neurons were again an exception since alpha-synuclein levels were similar to those of the control

line. L2-NMC SP_19 and L2-NMC SP_20 DA neurons presented high alpha-synuclein as the L2-PD ones. The correction of the mutation in L2-PD reversed this phenotype while its introduction into the control line recapitulated the rise in alpha-synuclein levels (Fig. 16A and C). We then focused on the evolution of this phenotype in the long term. When we examined alpha-synuclein localization within the DA neurons from the Control iPSC line we could appreciate a punctate pattern along the neurites, which showed extensive co-localization with the synaptic marker Synapsin-I. Physiological alpha-synuclein function is to act as a co-chaperone of SNARE proteins –Synaptobrevin-2 in particular- in vesicle fusion processes (Burré et al. 2010). Therefore, co-localization with pre-synaptic markers can be interpreted as the absence of synucleinopathy. The picture changed when we examined the subcellular localization of alpha-synuclein in L2-PD and L2-NMC SP_19 DA neurons. There was a reduction of the punctate staining accompanied by an increased in cytosol-free alpha-synuclein (Fig. 16B and D). Strikingly, some DA neurons from the L2-PD line showed strong alpha-synuclein nuclear localization suggesting a loss of regulated nucleus-cytosol transport (Rousseaux et al. 2016) (Fig. 16B). L2-NMC SP_20 DA neurons showed a trend ($p=0.053$) towards the conservation of synaptic alpha-synuclein localization and reduced diffuse cytosolic levels (Fig. 16D).

The results from the analysis of the neurite pathology together with the abnormal alpha-synuclein mislocalization and accumulation suggest that L2-NMC does not represent a uniform group. Consequently, different genetic factors may explain the reduced penetrance of LRRK2 parkinsonisms in different aged asymptomatic carriers. Although all three L2-NMC iPSC lines demonstrated to be more resistant to neuronal death after long-term culture, L2-NMC SP_19 and SP_22 presented other neurodegeneration features characteristic of the LRRK2 G2019S mutation.

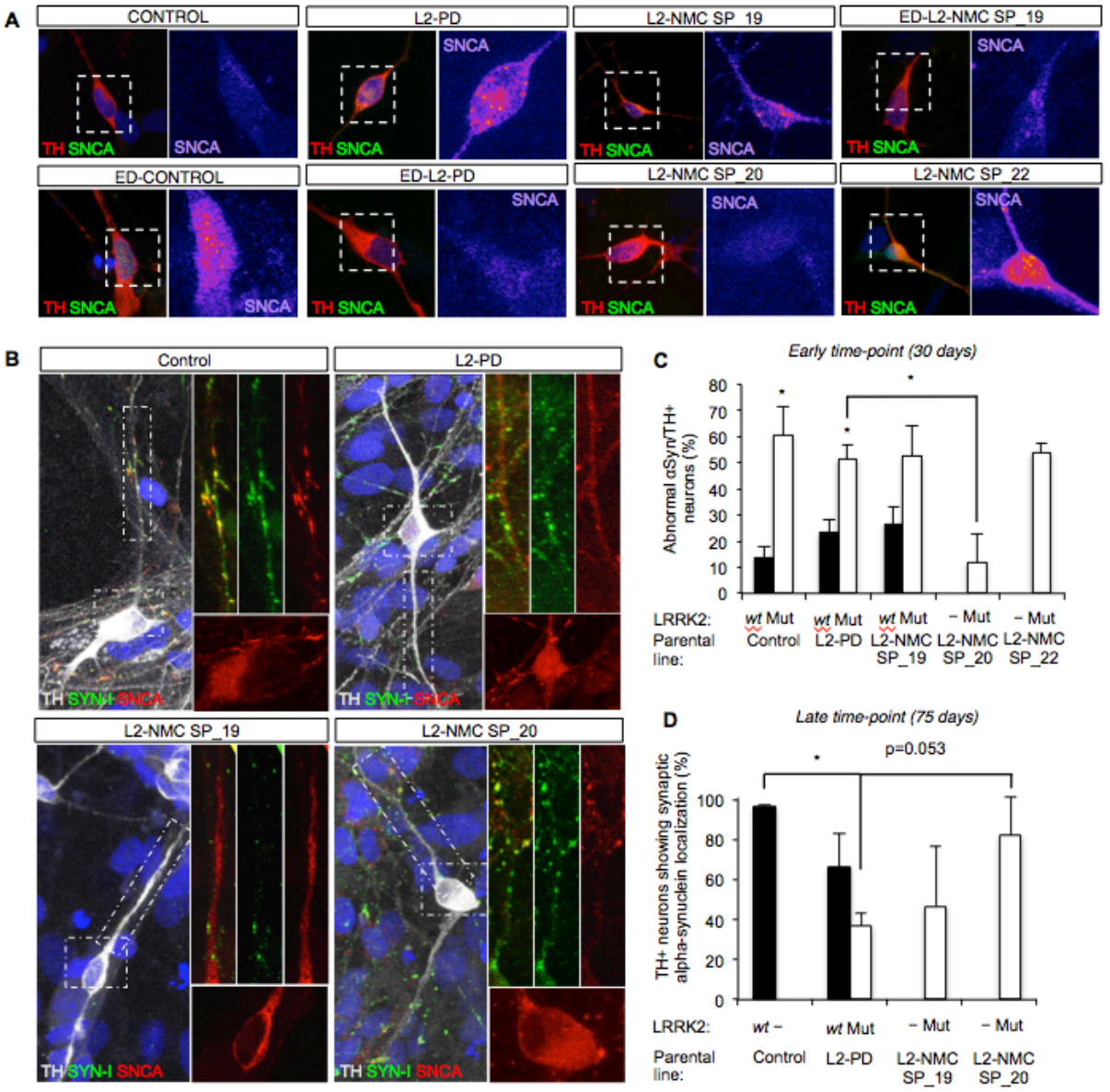

Figure 17: Alpha-synuclein accumulation is a phenotype largely dependent on the presence of LRRK2 G2019S mutation.

A) Immunofluorescence analysis of DA neurons differentiated from different iPSC lines and cultured for 30 days. co-stained for TH (red) and alpha-synuclein (green) the nucleus was counterstained with DAPI (blue). Insets show a pseudo-coloring of alpha-synuclein to facilitate staining intensity apreciation (violet tones represent low intensity whereas red to yellow tones represent increasing intensity).

B) Immunofluorescence analysis of DA neurons differentiated from different iPSC lines and cultured for 75 days. co-stained for TH (grey). synapsin-I and alpha-synuclein (green) the nuclei were counterstained with DAPI (blue). Insets show co-localization of alpha-synuclein with the pre-synaptic marker synapsin-I in the neurites as well as alpha-synuclein levels in the soma.

C) Quantitative analysis of the percentage of DA neurons at day 30 presenting abnormal abnormal alpha-synuclein levels. Data is the average of at least two-independent experiments. Control is the average of 51 DA neurons from 2 iPSC lines; ED-Control is the average of 13 DA neurons from 1 ED-Control SP_11; L2-PD is the average of 80 DA neurons from 2 iPSC lines; ED-L2-PD is the average from 89 DA neurons from 2 iPSC lines; L2-NMC SP_19 is the average of 57 DA neurons; L2-NMC SP_20 is the average of 37 DA neurons; L2-NMC SP_20 is the average of 47 DA neurons. Asterisk denotes statistically significant differences ($p<0.05$). $F(7,19) = 8.926$; $p<0.0001$].

D) Quantitative analysis of the percentage of DA neurons at day 75 presenting synaptic alpha-synuclein localization. Data is the average of at least two-independent experiments. Control, 56 DA neurons from SP_11; L2-PD, 73 DA neurons from SP_12; ED-L2-PD, 183 DA neurons from ED-L2-PD; L2-NMC, 19 DA neurons from SP_19; L2-NMC, 62 DA neurons from SP_20. Asterisk denotes statistically significant differences ($p<0.05$).

Exome interrogation provides clues regarding the increased protection of L2-NMC against LRRK2-related pathogenic effects

One defining feature of disease models based on patient-specific iPSC is that epigenetic marks that are acquired throughout donor's life are erased during the reprogramming process (Mertens et al. 2017). Therefore we reasoned that given that environmental factors were not differing between different cell lines in our *in vitro* model, protective mechanisms should be of genetic nature. The gold standard in the genetics field to address this issue is to conduct GWAS. However the modest sample size does not allow us to perform such approach. On the other hand, GWAS hits only point to genomic regions associated to the trait under scrutiny but does not reveal the actual causal polymorphism. Other authors have successfully employed whole exome sequencing (WES) in order to address complex genetic questions (Woodard et al. 2014; Marchetto et al. 2016). Despite WES would also imply missing important non-coding variation it will inform about common, rare and even *de novo* code-altering variants whose participation in PD is recently gaining more attention (Lubbe et al. 2016; Spataro et al. 2015; Benitez et al. 2016).

We then sequenced the exome of 4 PD patients carrying the LRRK2 G2019S mutation, 7 sporadic patients, 3 non-manifesting carriers of the LRRK2 G2019S mutation and 3 healthy controls. As expected, the pairwise genetic comparison between the different samples was approximately 50,000 per pair (Fig. 17A). In order to narrow down to those variants that could be relevant to the disease process, we focused on those variants lying in genes previously linked to familial and idiopathic PD (Nalls et al. 2014b), those in genes that have been shown to interact either genetically or physically with LRRK2 (Trinh et al. 2017; Steger et al. 2016; Cho et al. 2014; Martin et al. 2014) and those causing either non-synonymous, nonsense or affecting splicing signals (Fig. 17B). After applying these inclusion criteria we still observed a large number of these variants in both patients and controls. Neither pathogenicity predictors (Kircher et al. 2014) (Fig. 17C) nor considering just those variants present only in non-affected individuals provided a clear picture (data not shown). Both L2-NMC subjects and L2-PD patients presented a similar burden of rare variants in Mendelian PD genes as described in Lubbe et al., (2016) (Fig. 17D). Interestingly, the elevated frequency of rare code-altering mutations in the *ATP13A2* was confirmed in our modest cohort and we also observed an equal number of such variants in the *SYNJ1* gene. Given this situation, a hypothesis-driven approach was followed to choose candidates for increased protection in NMC based on the literature. In this regard, two interesting variants found in NMC were selected for further analysis.

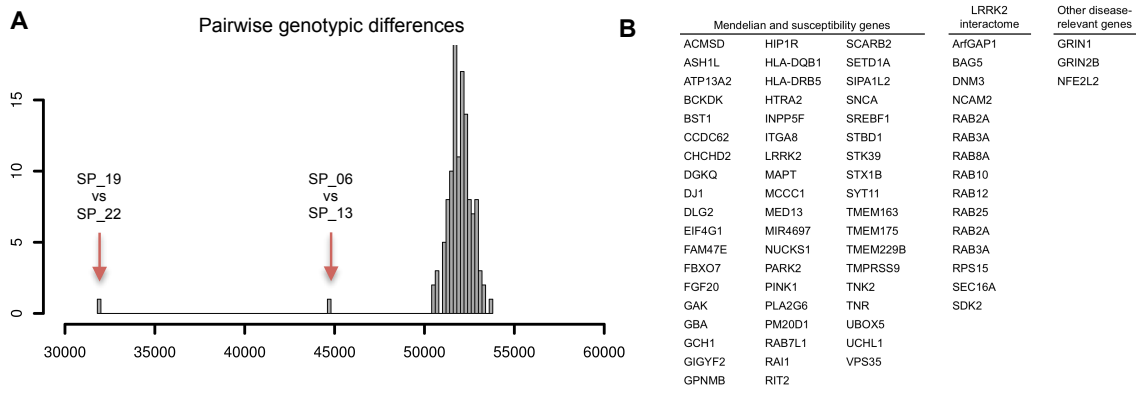

B

Mendelian and susceptibility genes			LRRK2 interactome	Other disease-relevant genes
ACMSD	HIP1R	SCARB2	ArfGAP1	GRIN1
ASH1L	HLA-DQB1	SETD1A	BAG5	GRIN2B
ATP13A2	HLA-DRB5	SIPA1L2	DNM3	NFE2L2
BCKDK	HTRA2	SNCA	NCAM2	
BST1	INPP5F	SREBF1	RAB2A	
CCDC62	ITGA8	STBD1	RAB3A	
CHCHD2	LRRK2	STK39	RAB8A	
DGKQ	MAPT	STX1B	RAB10	
DJ1	MCCC1	SYT11	RAB12	
DLG2	MED13	TMEM163	RAB25	
EIF4G1	MIR4697	TMEM175	RAB2A	
FAM47E	NUCKS1	TMEM229B	RAB3A	
FBXO7	PARK2	TMPRSS9	RPS15	
FGF20	PINK1	TNK2	SEC16A	
GAK	PLA2G6	TNR	SDK2	
GBA	PM20D1	UBOX5		
GCH1	RAB7L1	UCHL1		
GIGYF2	RAI1	VPS35		
GPNMB	RIT2			

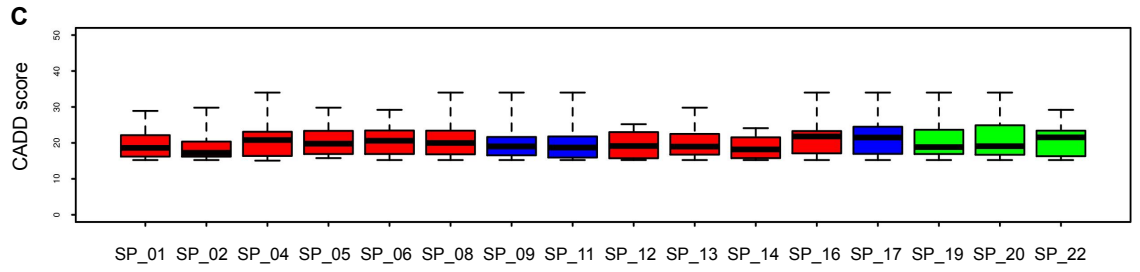

D

Status	iPSC line	Rare variants in mendelian PD genes + GBA
Control	SP_09	
	SP_11	
	SP_17	FBXO7_CodeAlteringDamaging_rs148272407_22_32894389_C_T:C/T
Sporadic PD	SP_01	
	SP_02	
	SP_04	
	SP_08	
	SP_14	PINK1_CodeAltering_._1_20960264_G_T:G/T
	SP_16	
L2-PD	SP_05	
	SP_06	ATP13A2_CodeAlteringDamaging_rs201883464_1_17318282_G_A:G/A
	SP_12	SYNJ1_CodeAlteringDamaging_._21_34100315_C_A:C/A
	SP_13	ATP13A2_CodeAlteringDamaging_rs201883464_1_17318282_G_A:G/A
L2-NMC	SP_19	SYNJ1_CodeAltering_rs145937537_21_34012088_G_A:G/A
	SP_20	PARK2_CodeAlteringDamaging_._6_162394423_G_T:G/T
	SP_22	SYNJ1_CodeAltering_rs145937537_21_34012088_G_A:G/A

Figure 18: Exome sequencing of NMC, L2-PD, sporadic PD and control individuals
A) Pairwise genetic differences among the different subjects.
B) List of genes prioritized.
C) Burden of variants predicted as pathogenic lying in the list of prioritized genes.
D) Code-altering rare variants lying in Mendelian PD genes.

NMC SP_20 harboured a homozygous single nucleotide variant (SNV) (rs1134921) that caused an Asp to Asn substitution in position 1297 in the J-domain of the GAK protein (Fig. 18A). This protein has been shown to participate in a common pathway with LRRK2 whose malfunction results in Golgi apparatus clearance through autophagy. Interestingly, RNA

interference mediated reduction of either *GAK* or *LRRK2* expression mitigates the effects of the overexpression of the other gene. *GAK* mutation is predicted to affect protein functionality (CADDphredScore = 25.1). We crossed the GWAS hit lying in the *GAK/DKGQ/TMEM175* locus (rs34311866) (Nalls et al. 2014b) with the GTEx database in order to determine whether it is associated to higher or to lower *GAK* gene expression. Unfortunately there are no eQTL associations between rs34311866 and *GAK* expression. However, there are other SNPs in the same region for which there is significant association with *GAK* expression. Two SNPs, rs56353809 and rs10902761, reach genome-wide significance association in the PD GWAS with Meta P-values of 6.04e-11 and 2.21e-11 respectively. Both alleles also have OR of 0.90 and 0.89 and have an eQTL effect size on *GAK* expression of -0.19 and -0.16 (which correspond to reduction in gene expression of 19% and 16%). Association studies in the LRRK2 cohort of the Hospital Clinic of Barcelona revealed a trend towards higher AAO in those LRRK2 G2019S carriers that also carried the rs1134921 in homozygosis. When both LRRK2 G2019S and idiopathic patients were combined, the association with AAO almost reached significance (p=0.072) (Fig. 18B). Intriguingly, this mutation was significantly associated with disease status both in idiopathic PD and in LRRK2-carriers (both MC and NMC) in the Catalan population. However, this association with idiopathic PD did not reach significance when queried in the PDgene database.

NMC SP_19 and SP_22 carried a non-synonymous SNV (rs143655258) in homozygosis and heterozygosis respectively, in the *SCARB2* gene. This gene encodes for the lysosomal integral membrane protein-2 (LIMP-2), the receptor that targets GCase into the lysosomes. The SNP causes a Met to Val substitution in position 159. This position lies precisely in the motif that interacts with GCase (Zunke et al. 2016) (Fig. 18D). Previous GWAS have pointed to the presence of protective variation in the locus containing *SCARB2* (Do et al. 2011; Nalls et al. 2014b; Gan-Or 2015). And in line with that, higher GCase activity has been linked to longer disease duration suggesting a milder disease course (Alcalay et al. 2015). Despite we did not find any association of this SNP (and there were no SNPs in linkage disequilibrium) with the disease in PDgene database, we decided to investigate its effect in the penetrance of the mutation. Association studies revealed an almost significant association with the L2-NMC group (p=0.054) (Fig. 18F) although this finding should be taken with caution. L2-NMC may represent both individuals in the initial stages of the disease or actual life-long asymptomatic carriers. However, both L2-PD and the whole PD group (L2-PD + sPD) showed a significant association between increased AAO and the minor allele of rs143655258 (p=0.03 and p=0.028). In the case of the L2-PD group, carriers of the minor allele develop PD on average 14.32 years later than the non-carriers. Again, this finding should be taken with caution. Two out of the 4 L2-PD that carried the SNP in *SCARB2* were symptomatic relatives of L2-NMC SP_19 and SP_22 and the average AAO of that particular family is relatively high. However, the AAO of the other L2-PD carriers of the SNP was also several years higher than the L2-PD group average (71 and 62 years old).

In an attempt of establishing a correlation between the SNP in the *GAK* gene the size and shape of the Golgi apparatus was analyzed in L2-NMC SP_20. Immunofluorescence analysis of the organelle ultrastructure revealed a trend towards increased size in L2-NMC SP_20 and in the non-carriers DA neurons and reduced size in the L2-PD DA neurons (Fig. 19A and B). Therefore, based on the LRRK2 interactome and on the observed genotype-gene expression correlation, we considered *GAK* rs1134921 as a good candidate for being a protective allele.

A

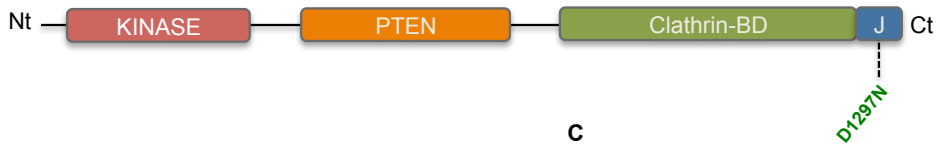

B

GAK rs1134921 association with AAO under a recessive model

Cohort	Genotype	n	AAO mean (S.E.)	Difference (95% CI)	P-value
L2-PD (n=171)	C/C-C/T	166	55.59 (1.02)	-	0.35
	T/T	5	62.8 (1.78)	5.55 (-6.07 - 17.18)	
sPD (n=144)	C/C-C/T	140	56.37 (1.05)	-	0.12
	T/T	4	65.75 (4.91)	9.80 (-2.48 – 22.08)	
L2-PD+sPD (n=315)	C/C-C/T	306	55.95 (0.73)	-	0.072
	T/T	9	64.11 (2.26)	7.69 (-0.67 - 16.06)	

C

GAK rs1134921 association with case-control status

Cohort	Genotype	Frequency Control (n=383)	Frequency Case*	P-value
L2-PD+L2-NMC (n=225)	C/C	0.78	0.75	0.022
	C/T	0.22	0.22	
	T/T	0.01	0.03	
sPD (n=160)	C/C	0.78	0.75	0.016
	C/T	0.22	0.22	
	T/T	0.01	0.03	
L2-PD (n=168)	C/C	0.78	0.75	0.073
	C/T	0.22	0.23	
	T/T	0.01	0.02	
L2-NMC (n=57)	C/C	0.78	0.74	0.017
	C/T	0.22	0.21	
	T/T	0.01	0.05	

* In the case of L2-NMC. they are considered as case despite they are not diagnosed with PD.

D

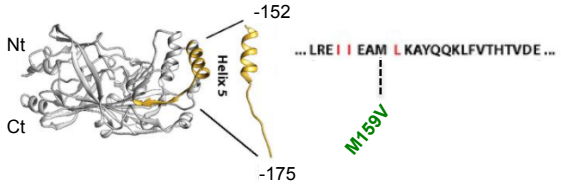

E

SCARB2 rs143655258 association with AAO under a dominant model

Cohort	Genotype	n	AAO mean (S.E.)	Difference (95% CI)	P-value
L2-PD (n=164)	T/T	160	55.69 (1.02)	-	0.03
	C/T	4	71.25 (2.25)	14.32 (1.52 - 27.13)	
sPD (n=143)	T/T	141	56.61 (1.05)	-	0.54
	C/T	2	61.5 (6.5)	5.54 (-12.01 – 23.09)	
L2-PD+sPD (n=307)	C/C-C/T	301	56.12 (0.73)	-	0.028
	T/T	6	68 (3.01)	11.50 (1.31 – 21.70)	

F

SCARB2 rs143655258 association with case-control status

Cohort	Genotype	Frequency Control (n=383)	Frequency Case*	P-value
L2-PD+L2-NMC (n=222)	T/T	0.97	0.96	0.6
	C/T-C/C	0.03	0.04	
sPD (n=160)	T/T	0.97	0.98	0.4
	C/T	0.03	0.02	
L2-PD (n=168)	T/T	0.97	0.98	0.58
	C/T	0.03	0.02	
L2-NMC (n=57)	T/T	0.97	0.91	0.054
	C/T-C/C	0.03	0.09	

* In the case of L2-NMC. they are considered as case despite they are not diagnosed with PD.

Figure 9: Population association studies of GAK rs1134921 and SCARB2 rs143655258

A) Scheme of GAK protein structure with the Asp1297Asn substitution in the J domain indicated in green.
B) Association study of rs1134921 with AAO in different patient groups under a recessive model.
C) Case-control association study of rs1134921 n different patient groups.
D) Graphic representation of the protein domain in which rs143655258 is found. Adapted from *Zunke F. et al (2014) PNAS*
E) Association study of rs143655258 with AAO in different groups under a dominant model.
F) Case-control association study of rs143655258 in different groups.

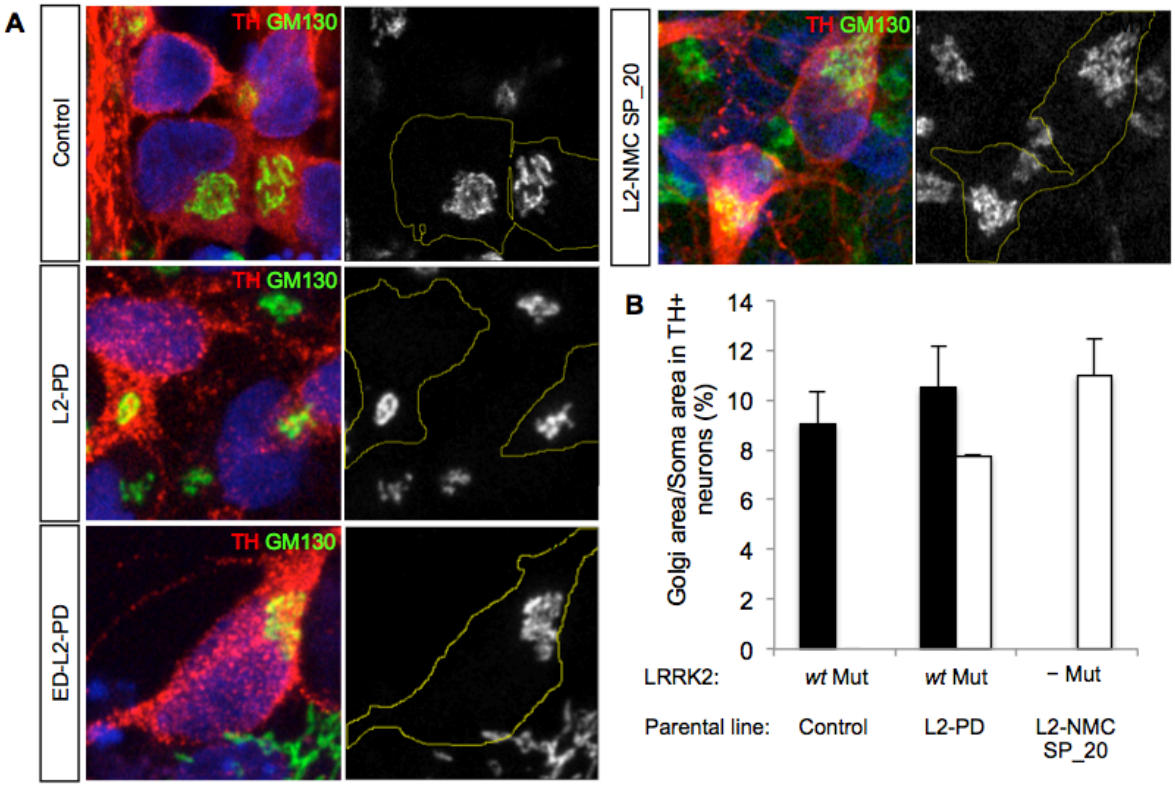

Figure 10: Morphological analysis of the Golgi apparatus.

A) Immunofluorescence analysis of Golgi apparatus in DA neurons differentiated for 75 days. DA neurons were stained for both TH (red) and GM-130 (green). Nuclei were counterstained with DAPI.

B) Quantification of Golgi apparatus surface area. Data is the average of at least two-independent experiments. Control, 27 DA neurons from SP_11; L2-PD, 89 DA neurons from SP_12 and SP_13; ED-L2-PD, 38 DA neurons from ED-SP_12 and ED-SP_13; L2-NMC, 45 DA neurons from SP_20; L2-NMC.

Part II: Generation of a Tyrosine Hydroxylase reporter hiPSC line

Generation of control and L2-PD TH reporter hiPSC lines.

With the aim of generating a reporter system for identifying living dopaminergic neurons in culture, we devised an editing strategy that minimally impacted the endogenous gene. It consisted in the insertion of a self-excisable P2A-mOrange cassette fused to the last exon of the *TH* gene. We chose this protein since it is one of the brightest fluorescent proteins developed to date (Shaner et al. 2004). To this end we co-transfected hiPSC from both control and L2-PD subjects with a CRISPR/Cas9 plasmid expressing a gRNA whose spacer overlapped the *TH* gene stop codon and with a HDR plasmid template (Fig. 20A). After applying selection, resistant clones were molecularly characterized and the selection cassette was excised (Fig 20B and C). Edited hiPSC were expanded and their pluripotency and genomic integrity was verified (Fig. 20D and E).

Edited iPSC were differentiated towards dopaminergic neurons using a simple protocol described by Borgs et al. (2016). This protocol enabled the generation expandable neural progenitor cells that co-expressed PAX6, SOX2 and Nestin, which could be easily and rapidly differentiated into *TH*-expressing DA neurons (Fig. 22A and B). As early as 7-10 days of terminal maturation some TH+ neurons could be observed in the plate. Immunofluorescence analysis confirmed the expression of TH at the protein level in those cells positive for mOrange (both *live* and after probing them with an anti mRFP1 antibody) (Fig. 20B).

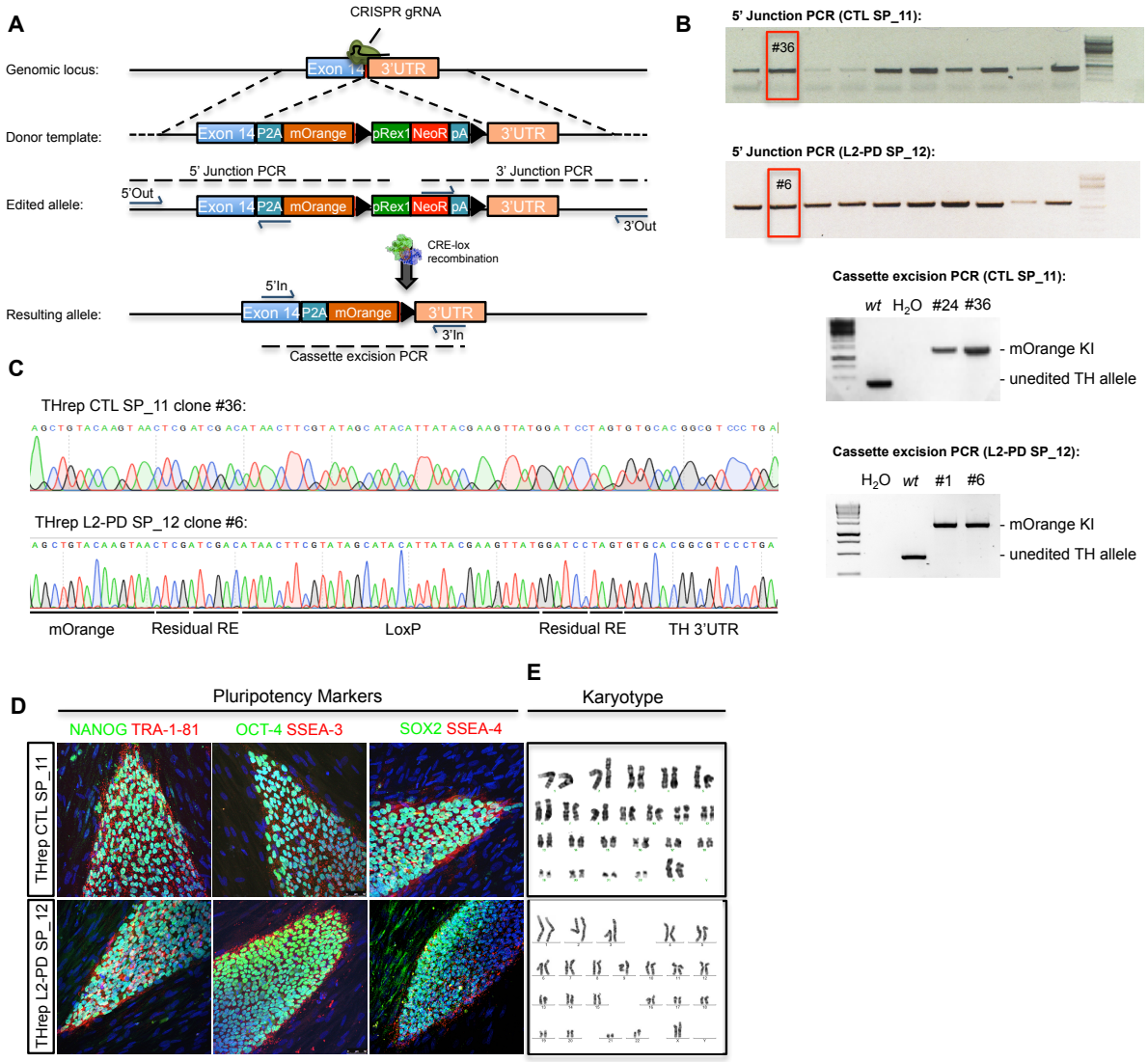

Figure 211: Generation of TH reportes iPSC lines using CRISPR/Cas9-mediated gene editing.

A) Scheme describing the recombination steps given during the edition process. Blue arrows represent the primers used for the PCR screening procedure. Black triangles represent LoxP sites sorrounding the selection cassette

B) Molecular analysis of the correctly targeted clones to confirm proper P2A-mOrange cassette integration and selection cassette excision in a control and a L2-PD iPSC lines. In the lower gel, the increase in size of the edited is due to the P2A-mOrange cassette plus the remaining LoxP site.

C) Sanger sequencing, confirmed successful excision of the LoxP site-flanked cassette.

D) Immunofluorescence analysis of representative colonies of TH reporter control and L2-PD iPSC lines stained positive for the pluripotency-associated markers NANOG. OCT4 and SOX2 (green). TRA-1-81. SSEA3 and SSEA4 (red).

E) Normal karyotype from TH reporter control and L2-PD iPSC clones.

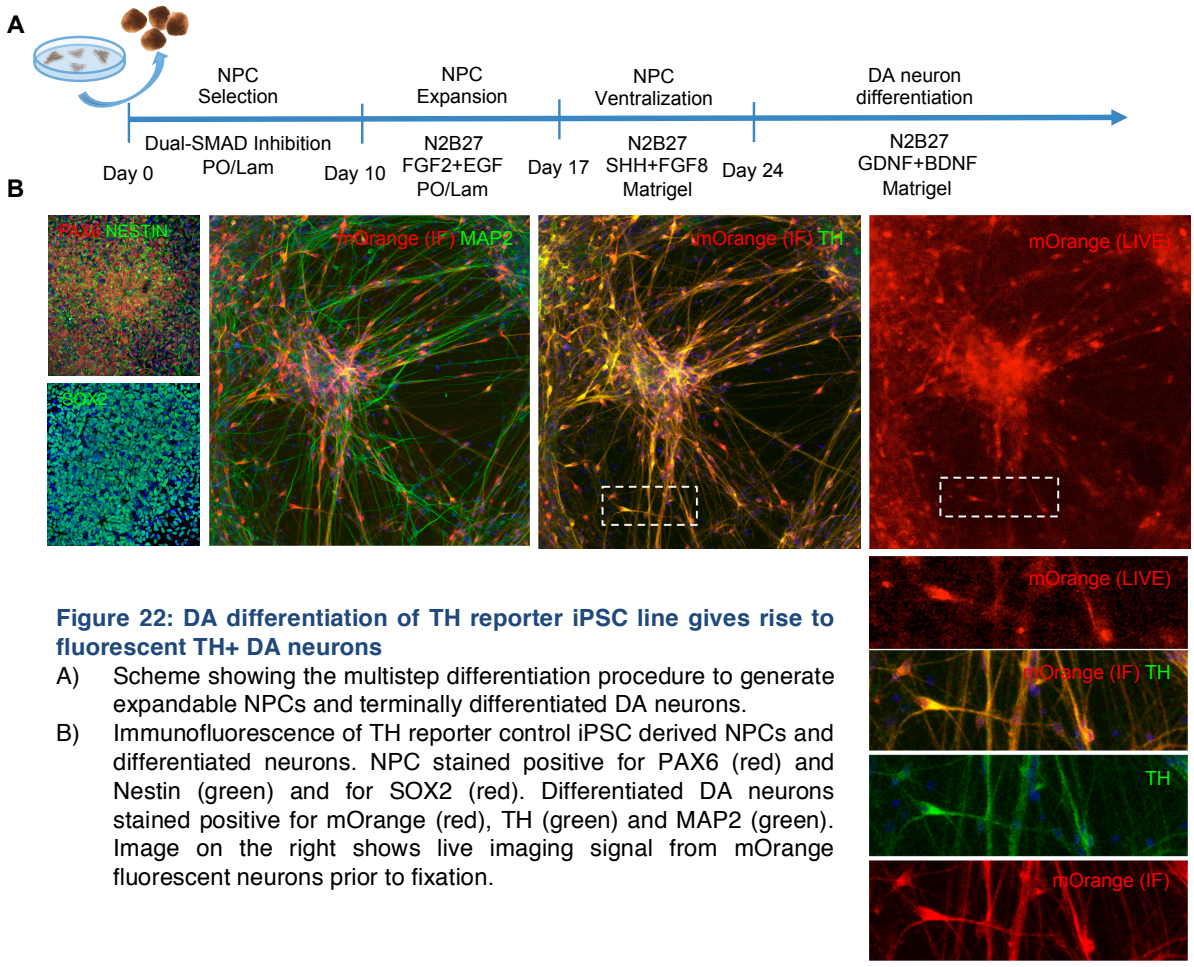

Figure 22: DA differentiation of TH reporter iPSC line gives rise to fluorescent TH+ DA neurons

A) Scheme showing the multistep differentiation procedure to generate expandable NPCs and terminally differentiated DA neurons.

B) Immunofluorescence of TH reporter control iPSC derived NPCs and differentiated neurons. NPC stained positive for PAX6 (red) and Nestin (green) and for SOX2 (red). Differentiated DA neurons stained positive for mOrange (red), TH (green) and MAP2 (green). Image on the right shows live imaging signal from mOrange fluorescent neurons prior to fixation.

Purified mOrange+ cells survive after FAC sorting and restart neuritogenesis.

Following the successful derivation and characterization of the reporter lines, tested whether the reporter could be used to purify DA neurons by fluorescence-activated cell sorting (FACS). After 10 days of terminal differentiation, differentiated neurons were gently disaggregated, FACsorted and subsequently reseeded in a matrigel-coated plate (Fig. 24A-C). Live and immunofluorescence analysis conducted 1 and 7 days post-sorting, confirmed the preservation of the DA phenotype and robust post-sorting survival (Fig. 24C). Newly extended neurites could be readily observed 1 day after sorting and the neuronal network continued gaining complexity during the following days (Fig. 24C), therefore demonstrating that mOrange+ DA neurons are amenable to FAC sorting procedures while remaining viable and conserving their DA phenotype. Flow cytometry analysis of the sorted mOrange+ cells confirmed successful enrichment. While only 5% of the differentiated population was positive for mOrange in the initial cell sorting, it increased to 65% when the sorted cells were reanalysed 7 days after. The negative population may arise from the sorting of false-positive mitotic cells that had proliferated after the first sorting.

After confirming that fluorescent DA neurons could be sorted and successfully replated, the protocol was slightly modified to study neurite branching in sorted neurons. Instead of seeding collected cells in matrigel-coated slides, the DA neurons were directly sorted onto multi-well plates pre-seeded with human astrocytes. They were seeded at clonal density in order to prevent neurite crosslinking. Sorted neurons were fixed and stained 7 days after sorting. Sholl analysis indicated increased branching in DA neurons differentiated from TH reporter L2-PD iPSC (Fig 25A and B) compared to control DA neurons. This increment was more evident for the proximal part (Fig. 25A). Previous studies have observed both, the same (Borgs et al. 2016), and the opposite phenotype (with significantly less branching) in aged neurons (Sánchez-Danés et al., 2012) or upon mutant LRRK2 overexpression in other neuronal subtypes (MacLeod et al, 2007). Further studies are needed to understand this early phenotypic difference between control and L2-PD DA neurons.

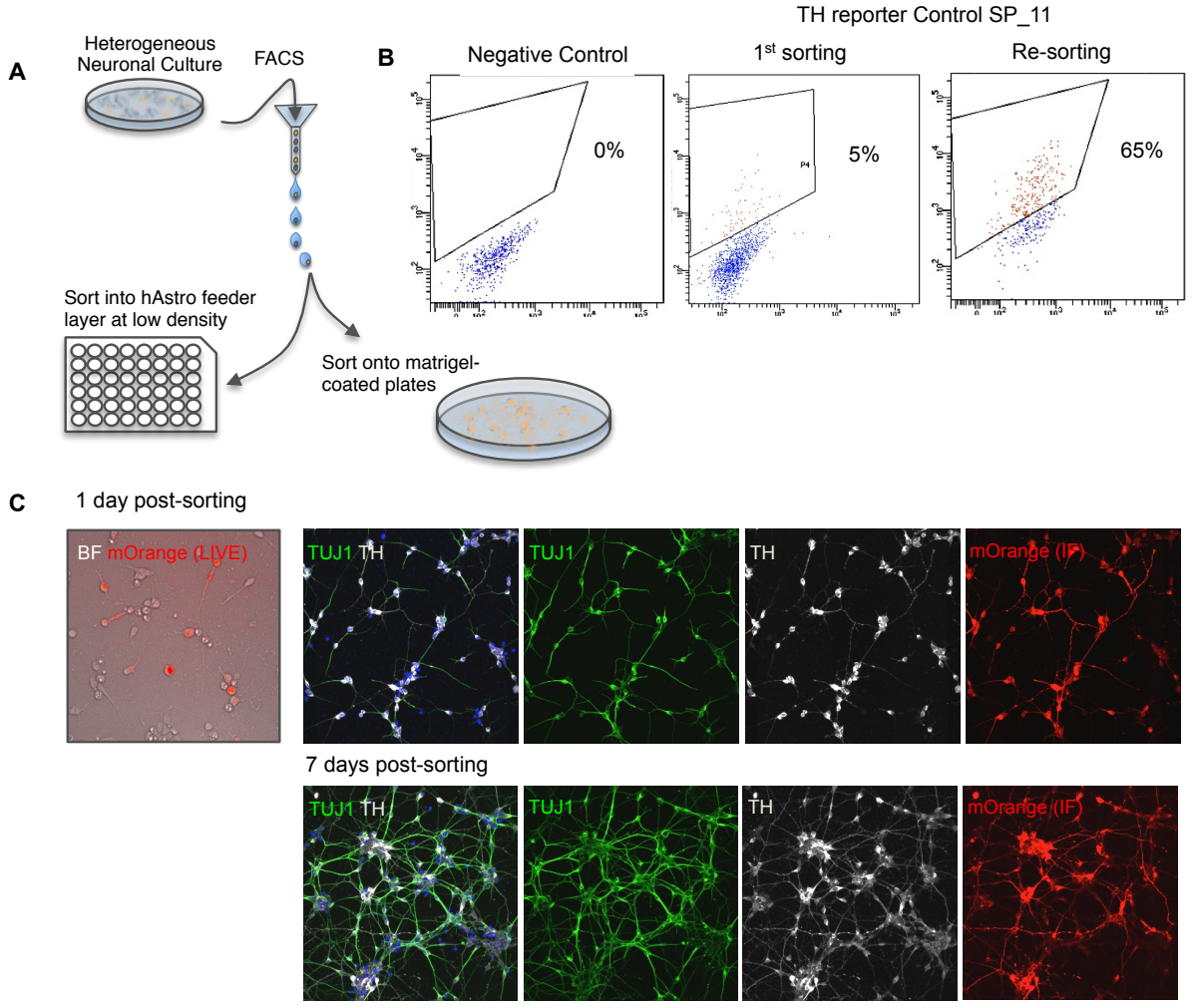

Figure 12: mOrange+ DA neurons are amenable to FACS-mediated purification and survive after sorting.

A) Experimental procedure followed for FACsorting mOrange+ DA neurons in different substrates.

B) Cytograms from FACS of mOrange+ cells from differentiated TH-reporter control SP_11 line. Purified cells were seeded after sorting and re-analyzed after 7 days.

C) Tracking mOrange+ DA neurons sorted and reseeded on matrigel. Neurons were imaged live one day after sorting and after immunofluorescence 1 and 7 days post sorting. For this latter analysis, neurons were co-stained for TUJ1 (green), TH (grey) and mOrange (red). Nuclei were counterstained with DAPI

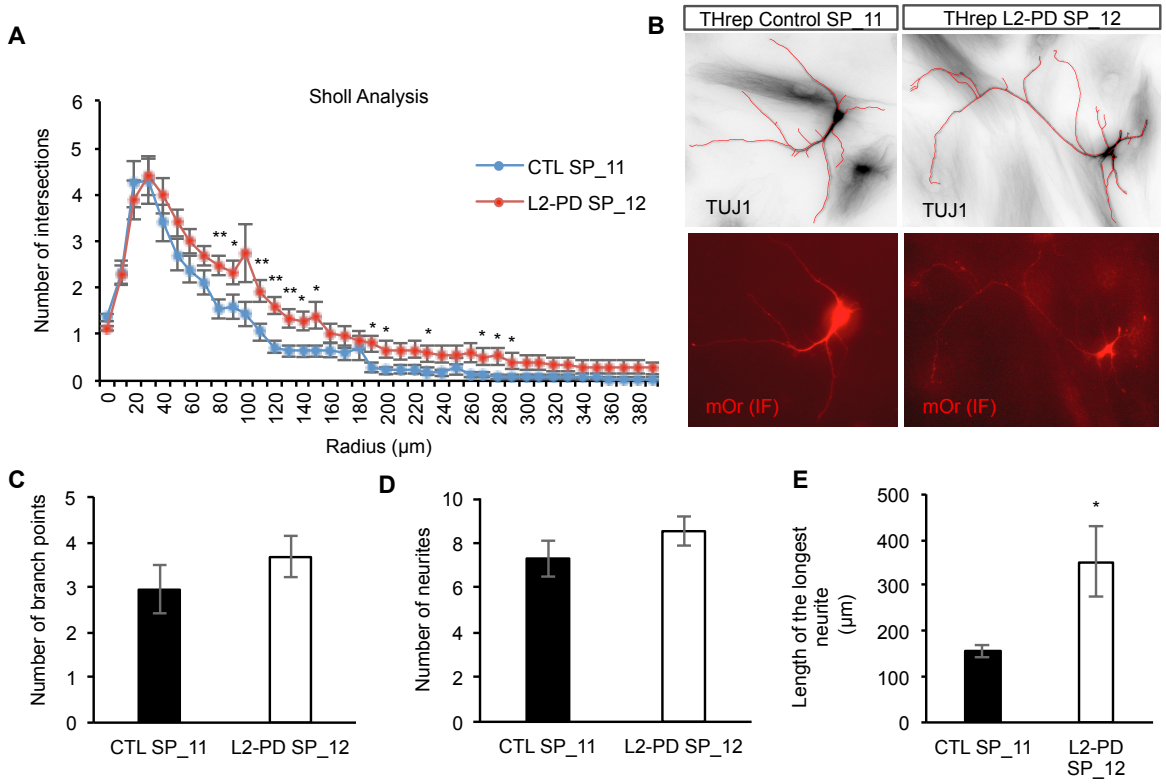

Figure 13: Application of the TH reporter iPSC lines in neurite morphology analysis.

A) Sholl analysis in FACSorted mOrange+ DA neurons and seeded on the top of human astrocytes. Asterisk denotes statistically significant differences (*: p<0.05; **: p<0.01).

B) Immunofluorescence images of FACSorted mOrange+ DA neurons and seeded on the top of human astrocytes and co-stained for TUJ1 (green) and mOrange (red).

C-E) Number of branch points, neurites and length of the longest neurite of FACSorted neurons reseeded on the top of human astrocytes. Asterisk denotes statistically significant differences (*: p<0.05).

mOrange+ DA neurons present less number and slower mitochondria compared to Synapsin-EGFP+ neurons.

The DA neurons derived from TH reporter lines were also used to examine mitochondrial motility. We compared mitochondrial motility using a pan-neuronal marker (LV-Synapsin-EGFP) (Hioki et al. 2007) with that of the mOrange+ DA neurons. Unexpectedly, we observed that mitochondrial motility, but not the proportion of motile mitochondria, was severely reduced specifically in DA neurons in comparison with other neuronal subtypes (Fig 26 A, B). Depending on mitochondrial speed it can be inferred whether these are moving along microtubules (speed > 1 µm/s) or along F-actin filaments (speed = 0.29-1 µm/s). Synapsin-GFP+ neurons had a much higher proportion of mitochondria moving along microtubules while F-actin was the main platform for motile mitochondria in mOrange+ DA neurons (Fig. 26B). Furthermore, mitochondria from mOrange+ neurons had an overall smaller size compared to those of Synapsin-EGFP+ neurons (Fig.26C). Another aspect thath should be noted is the low variability observed among mOrange+ DA neurons in terms of mitochondrial speed. This may be explained in part by the reduced heterogeneity in the sampled neurons. mOrange+ cells reflect just one specific subtype of

neurons (DA neurons). Furthermore, the fact that most visible mOrange+ DA neurons are those that have the highest TH expression, they may also reflect a specific maturation stage. This differential mitochondrial motility suggests that every neuronal subtype may perform very differently in certain biological processes.

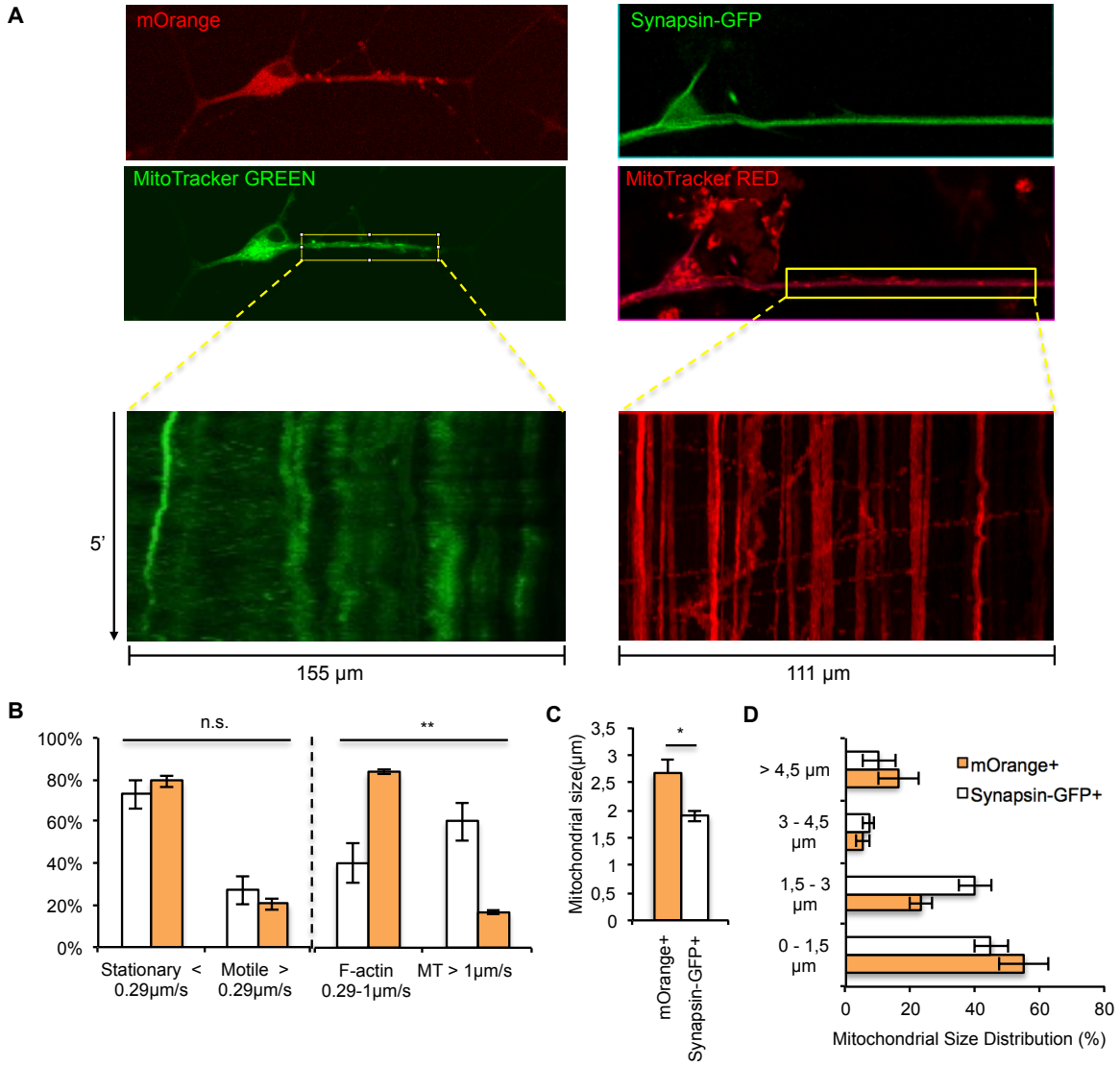

Figure 14: Application of the TH reporter iPSC lines in neurite morphology analysis

A) Live imaging of neurons positive for Synapsin-I expression (green) or DA neurons positive for TH::mOrangeexpression (red). Mitochondrial were labelled with mitotracker red and green respectively.

B) Quantification of mitochondrial motility from kymographs elaborated from recordings of control SP_11 neurons (Synapsin-EGFP+) or in DA neurons (mOrange+). Data is the average of at least three-independent experiments. Synapsin-EGFP+, 19 DA neurons from SP_11; mOrange+, 19 DA neurons from SP_11. Asterisk denotes statistically significant differences (**: $p<0.01$).

C) Quantification of mitochondrial size in those same kymographs recorded from control SP_11 neurons (Synapsin-EGFP+) or in DA neurons (mOrange+). Data is the average of at least three-independent experiments. Synapsin-EGFP+, 19 DA neurons from SP_11; mOrange+, 19 DA neurons from SP_11. Asterisk denotes statistically significant differences (*: $p<0.05$).

DISCUSSION

Patient-specific iPSC for familial PD modeling and the importance of generating genetically-matched controls

Cell models based on hiPSC (and hESC) are becoming an indispensable tool to study the genetic component of complex polygenic diseases (Yoon et al. 2014; Marchetto et al. 2016; Soldner et al. 2016; Young et al. 2015). They are particularly suited for this sort of studies for two main reasons: patient-specific hiPSCs recapitulate the genetic complexity of the donor subject and are free from any epigenetic mark acquired during the life of the individual. The former aspect is of crucial importance since much disease-related genetic variation is not associated to coding sequences and the mechanism of action is commonly ascribed to the regulation of proximal gene expression (Coetzee et al. 2016; Nalls et al. 2014a; Vermunt et al. 2014; Soldner et al. 2016).

To address the contribution of low risk variants there is an urgent need to count on genetically controlled experimental systems. This is relatively recently made possible through the successful application of gene editing techniques to mammalian cells and to human PSC in particular (reviewed in detail in Hockemeyer & Jaenisch, 2016). The possibility of generating genetically-matched controls in which the sole genetic difference is the polymorphism under study allows to detect even very subtle molecular alterations (Soldner et al. 2016).
The generation of isogenic clones also circumvents another drawback associated to iPSC-based disease modeling: the inherent variability associated to the technology. This variability affects crucial experimental parameters such as differentiation efficiency towards the cell type of interest, but also the presentation of specific phenotypes associated to the disease being modeled (mitochondrial activity, autophagy performance, electrophysiology…). The origin of the variability has been investigated thoroughly and has been attributed to several sources such as: extensive *in vitro* cell culture (Lee, Bendriem, Kindberg, Worden, Lupski, et al. 2015; Baker et al. 2007), somatic mutations acquired by the somatic cell before reprogramming, donor subjects genetic background (Rouhani et al. 2014; Burrows et al. 2016) or mutations acquired during the reprogramming process (Carcamo-Orive et al. 2017; DeBoever et al. 2017). Thanks to the gene-editing tools such as TALENs or CRISPR/Cas9, genetically matched controls can be generated allowing to address the specific contribution of certain genetic variants in a uniform genetic background.

An experimental platform for modeling the reduced penetrance of LRRK2 G2019S using non-manifesting carrier-specific hiPSC

In this particular project, a previously described patient-specific iPSC PD model has been adapted to the study of a pressing question: the intriguingly variable penetrance of a

Mendelian PD mutation –LRRK2 G2019S- (Hentati et al. 2014) previously thought to be highly penetrant (Jennifer Kachergus et al. 2005).
In this line, our patient-specific iPSC model has demonstrated not only to be able to model the disease *in vitro*, but also other clinically-relevant disease features such as the reduced penetrance of the mutation in the selected NMC. However, the extent of protection is not the same in the different NMC. While L2-NMC SP_20 presented an overall protection against cell death and against other LRRK2 G2019S pathogenic effects, L2-NMC SP_19 and SP_22 were only resistant to the former but demonstrated to be susceptible to morphological alterations and alpha-synuclein accumulation as the L2-PD lines. Interestingly, we were able to confirm the leader role of the LRRK2 mutation in the phenotypes under study. Correction of the mutation in L2-PD lines reversed the neurodegenerative phenotypes whereas introduction of the mutation recapitulated them. This notion reinforces the idea that L2-NMC subjects carry additional protective genetic variants that prevent or delay disease onset.

Penetrance estimates are often biased due to the fact that these are obtained from studies in affected families in which the penetrance is higher (Sierra et al. 2013; Healy et al. 2008). A recent study designed to avoid such sampling bias by including relatives of sporadic LRRK2 G2019S PD patients, found a penetrance of 42.5% to age 80 for non-Ashkenazi Jewish carriers (Lee et al. 2017). This is the case even in rare and devastating childhood diseases (Chen et al. 2016). These cases may be explained, at least in part, by one or several modulatory variants whose protective effect on disease presentation is at least as potent as the risk conferred to the disease-causing mutation. The identification of such modulatory genetic variants provides precious information that could be harnessed for designing preventive therapies. This is very important in the case of LRRK2 G2019S associated PD, since it is clinically indistinguishable from sporadic disease.

Identification of variants associated with AAO in LRRK2 G2019S non-manifesting carriers

The identification of genetic modulators of the penetrance of LRRK2 G2019S parkinsonism has been assessed by others. Latourelle J. C. and collaborators found association between two LD blocks in 1q32.1 and 16q12.1 and AAO in LRRK2 familial mutation carriers blocks. Unfortunately no SNPs reached genome-wide significance within those regions (Latourelle et al. 2011). Trinh J. and coworkers detected that common variation in the *DNM3* locus explained a large extent of the variation in AAO particularly in the Tunisian Arab Berber population but also in other Caucasian populations (Trinh et al. 2017). A similar approach in the same ethnic group, but focusing in coding variation is being undertaken in the framework of a MJFF-funded project (https://www.michaeljfox.org/foundation/grant-detail.php?grant_id=797). These tasks, despite sharing the same aim, they represent two

different but complementary strategies to unveil modulators of AAO. The former two studies seek for common variation mostly located in non-coding regions while the latter focuses in the coding genome. The genetic approach described here is severely underpowered to find protective variants due to the very low number of NMC involved. This constraint also led us to choose whole exome sequencing to address this issue. Despite that, it benefits from the availability of a genetically customizable cell model that allows testing selected candidate genetic variants. Moreover, other researchers have observed increased frequency of rare code-altering variants not only in sporadic (Spataro et al. 2015) but also in Mendelian PD (Lubbe et al. 2016).

Whole exome sequencing of our cohort provides a large amount of genetic information but its interpretation is rather challenging. Different approaches have been carried out in order to find clues regarding the genetic variants that would explain the picture observed *in vitro*. Disease manifestation does not seem to correlate with a supplementary increase of pathogenic variants in L2-PD *versus* L2-NMC. Though it cannot be ruled out that specific variants in certain genes more than an overall increase in risk is responsible for the effective penetrance of LRRK2 G2019S. In any case, two interesting genetic variants were selected as possible candidates for conferring protection.

The Asp1297Asn variant in the J-domain of GAK represents a firm candidate since this proteins has been previously shown to participate in a pathological pathway leading to Golgi apparatus clearance along with LRRK2 and other PD susceptibility genes (Beilina et al. 2014). The J-domain is responsible for binding Hsc70 and initiate a cascade leading to clathrin disassembly from newly evaginated vesicles either from the Golgi or from the plasma membrane. Several lines of evidence point to the possibility of a reduced function of the GAK protein being protective against PD. The first of them is the fact that surrogate SNPs of the GWAS top-hit with an OR<1 are linked to reduced GAK expression. The second is the experimental confirmation by Beilina and coworkers of the pathological interaction between both proteins. Indeed, silencing of either protein abrogates the pathogenic effect of the overexpression of the other protein. Therefore, explaining why L2-NMC DA neurons present a higher resistance to LRRK2 G2019S pathogenic effects than the other two L2-NMC. Third, despite not reaching significance, the mutation is linked to a later onset of the disease in both sporadic and LRRK2 G2019S almost reaching significance when both groups are analyzed jointly. Indeed, there is a slightly higher frequency of the allele among non-manifesting carriers and those carrying the alternative allele in homozygosis were older than the non-carriers (47.09 *vs*. 56.33 years). Finally we have observed increased Golgi apparatus size in the homozygote for the mutation L2-NMC SP_20 DA neurons.

Despite these promising indications, some other facts should be taken into consideration. Despite showing a trend towards increased AAO for the homozygote carriers of the mutation, the SNP itself is linked to the disease status in the Catalan population but not in the PDgene database. Moreover, transcriptional information derived from PD brains shows

apparently contradictory data. PD brains presented an increased expression of *GAK* 3' exons (*vs.* controls) while carriers of the GWAS risk allele had a reduced expression of 3' proximal exons (coding for the J-domain). In any case, we should take into account that the SNP analyzed here is not in LD disequilibrium with the top-hit described in Nalls *et al*. (2014). Therefore it cannot be discarded that the mechanism of increased risk of the GWAS hit differs from a putative protective mechanism of the Asp1297Asn mutation.
Finally, clathrin disassembly processes have been related to PD genetics in several settings: loss of function *DNAJC6* mutations being responsible for AR-PD (Edvardson et al. 2012) gain-of-function *DNAJC13* mutations being causative for AD-PD (Vilariño-Güell et al. 2014), *GAK* being a susceptibility gene, genetic variation in *DNM3* being a major modifier of LRRK2 G2019S age at onset (Trinh et al. 2017), genetic variation in *AAK1* (a well-known GAK interactor) being associated to AAO in sporadic PD (Latourelle et al. 2009).
Further *in vitro* studies are necessary to ascertain the specific contribution of the GAK mutation described here to the presentation of PD-related phenotypes.

The candidate variant selected for the other L2-NMCs caused a Met159Thr substitution in LIMP-2 (the protein encoded by the *SCARB2* gene). LIMP-2 is the lysosomal receptor for GCase. Variation in this gene has been related both to reduced risk in PD and DLB (Nalls et al. 2014a; Do et al. 2011; Bras et al. 2014), and to disease modification in GD (Velayati et al. 2011). Interestingly, the mutation described in Velayati et al. seems to induce a shift from GD type I to type III, the most severe and with neurological involvement. Mutations in *SCARB2* also cause action myoclonus-renal failure syndrome (AMRF). A disease that presents with myoclonus epilepsy, storage material in the brain and renal failure (Berkovic et al. 2008).
The mutated position lies in the coiled-coil motif that interacts with GCase (Zunke et al. 2016). LIMP-2 binds GCase since very early steps of the secretory pathway until they both are finally targeted to the lysosome, where the drop in pH causes the dissociation of the complex. One of the AA claimed to transduce the effects of the pH drop is Ala158, immediately adjacent to the Met159 residue (Zunke et al. 2016). GCase activity and consequently, overall lysosomal activity closely correlate to alpha-synuclein pathogenic accumulation. Indeed, a bidirectional pathogenic loop has been observed between reduced GCase activity and alpha-synuclein accumulation (Mazzulli et al. 2011). According to this work, pathological alpha-synuclein accumulation blocks GCase import into the lysosomes by blocking ER-to-Golgi transport, therefore causing even lesser alpha-synuclein lysosomal degradation. Likewise, reduced GCase activity caused by either loss of function mutations or by lack of lysosomal targeting reduces lysosomal fitness thereby resulting in alpha-synuclein accumulation. In line with this finding, LIMP-2 dysfunction has been linked to reduced GCase activity and alpha-synuclein accumulation (Rothaug et al. 2014). Studies in patients have proven that slightly higher levels of GCase activity has been correlated with a milder course of PD (Alcalay et al. 2015). Some investigators are also considering the employment of GCase chaperones as a treatment for PD (McNeill et al. 2014; Migdalska-Richards et al. 2016)

Therefore, our hypothesis is that Met159Thr improves GCase targeting to the lysosome and consequently improves overall lysosomal activity. Therefore, despite not specifically protect against LRRK2 G2019S-mediated dysfunction it could be delaying the terminal neurodegeneration by improving proteostasis. If this would be the case, it would be the first report of coding variation in the *SCARB2* gene modifying PD risk.

In any case, we cannot dismiss that these NMC carriers may remain asymptomatic due to the exposure to environmental protective factors. Several habits have been consistently related to a lower incidence of PD. Among them, tobacco, coffee and NSAIDs stand out due to their significative protective effect (see environmental risk factor section in the Introduction). L2-NMC SP_19 and SP_22 declared coffee consumption and L2-NMC smoked too. However, the L2-NMC that revealed as the most protected individual *in vitro* did not smoke nor drink coffee. This means that none of the well-known environmental protective factors could be applied to L2-NMC SP_20. Furthermore, no variants were found in the *GRIN2A* gene. A SNP in this gene has been shown to interact with coffee consumption drastically reducing the risk of suffering PD (OR: 0.43-0.51) (Hamza et al. 2011; Yamada-Fowler et al. 2014). Another alternative mechanism of protection could rely in the simultaneous co-inheritance of two or more specific variants that interact epistatically. This is the case for SNPs in PARK16 and LRRK2 (MacLeod et al. 2013; Pihlstrøm et al. 2015; Gan-Or et al. 2012). However, after sequencing those SNPs we were not able to observe any specific pattern that would suggest protection given what is published in the literature

We strongly believe that the approach described here could be applied to other clinical genetic entities and that the results obtained would be very informative in the design of therapies aimed to counter the molecular mechanism of the disease.

Generation of a genetic reporter of the *TH* gene to circumvent iPSC-inherent variability

The generation of genetic reporter systems is of great usefulness in experimental biology. They allow tracking a myriad of cellular processes ranging from mitochondrial features, autophagy flow or even cell differentiation or the control of gene expression. They make possible to study them in real-time providing a much more detailed information of the temporal execution of those events.
Here, we have described the generation of *Tyrosine Hydroxylase* reporter iPSC lines using gene editing tools. A very bright fluorescent protein preceded by a self-excisable P2A peptide was fused to the last exon of the endogenous *TH* gene. We believe that the exceptional brightness explain the successful visualization of living cells when others failed in a very similar approach (Cui et al. 2016). Another factor that may explain such difference

may be the different *TH* gene expression reached by differentiated DA neurons from different iPSC lines since we also noticed reduced fluorescence in the L2-PD SP_12 DA neurons when compared to the control ones. We have then employed these lines to demonstrate their applicability in different experimental procedures. We have been able to successfully sort mOrange+ DA neurons and resume *in vitro* culture while preserving their dopaminergic identity. We have been able to enrich the culture in DA neurons by 13-fold (5% *versus* 65% 7 days after cells sorting). The lack of 100% purity, 7 days post-sorting, may be due to the presence of autofluorescent mitotic cells with the ability to expand after the initial cell sorting. Several actions can be undertaken to eliminate such contamination: sorting a more mature population, adding cytostatic drugs…
In a separate experiment, these neurons were sorted on the top of human astrocytes, they extended long and branched neurites, which were perfectly suited for Sholl analysis. Using this analysis we have reproduced the increased neurite branching in the short term observed by others (Borgs et al. 2016). Further experiments using isogenic controls will shed more light on the specific contribution of the LRRK2 G2019S to the observed differences between allogeneic iPSC-derived DA neurons. Moreover, we have observed that the performance of DA neurons in mitochondrial motility studies is different to the one presented by other neuronal subtypes. The characterization of these differences is important to understand the increased susceptibility of DA neurons to undergo neurodegeneration (Surmeier et al. 2017) .

We strongly believe that the application of this reporter line in different experimental settings will help to reduce the inherent variability associated to the iPSC technology and to gain further insight into the processes associated to DA biology and disease.

Future directions

The initial aim of the present thesis was to verify whether the model described in Sánchez-Danés *et al*. (2012b) could be applied to model the variable penetrance observed for the LRRK2 G2019S mutation. The successful results obtained in this regard motivate us to interrogate the genome of our cohort in an attempt to ascertain the genetic determinants of the variable penetrance of LRRK2 G2019S mutation. Despite the difficulty in establishing trustworthy prioritization criteria, we selected some variants that could behave as protective due to their link either to LRRK2 biology (GAK) or because of being related to protective variation in GWAS (SCARB2).

Currently, genetically matched isogenic clones are being derived from the homozygotes for the alternative allele, SP_20 for GAK Asp1297Asn and SP_19 for LIMP-2 Met159Thr, in which the alternative allele will be reverted to the reference allele. Likewise, the alternative allele of both genes is being introduced in homozygosis in the *bona-fide* manifesting L2-PD

SP_12 line. This way we will have an experimental platform specifically suited to test the relative effect of both mutations in the phenotypes observed in vitro and to verify the suspected molecular mechanism behind such effect.

Finally, in case we succeed in identifying the mechanisms leading to a decreased penetrance of LRRK2 G2019S we would seek to identify of therapeutic agents that could reproduce the genetic protection and will test them in our *in vitro* model of the disease.

CONCLUSIONS

Part I: Investigating the genetic component of Parkinson's disease through the use of human induced pluripotent stem cells and gene editing.

- We generated 3 iPSC lines representing aged non-manifesting carriers of the LRRK2 G2019S pathogenic mutation.

- We generated isogenic clones differing in the presence of LRRK2 G2019S mutation by gene edition in 3 mutant and 1 control line.

- We found that DAns derived from NMC are more resistant to neurodegeneration compared to those derived from patients carrying LRRK2 mutation:

    - DA neurons from L2-NMC do not die after long-term culture as L2-PD DA neurons do.

    - DA neurons from L2-NMC show a variable degree of neuritic aberration with L2-NMC SP_20 resembling the control lines and L2-NMC SP_19 and SP_22 resembling the L2-PD lines.

    - L2-PD and L2-NMC SP_19 and SP_22 DA neurons present increased alpha-synuclein accumulation in the short term, which results in mislocalization and cytosolic accumulation in the long term. Contrarily, L2-NMC SP_20 alpha-synuclein levels and synaptic localization resembles that of the control line.

    - Correction of the LRRK2 G2019S mutation alleviates the aforementioned phenotypes in L2-PD DA neurons. Conversely, introduction of the mutation in healthy control lines recapitulates the disease phenotypes. Altogether confirming the leading role of LRRK2 G2019S mutation in the phenotypes observed.

- We did not observe any increased burden of variants predicted as pathogenic between L2-PD and L2-NMC. Alternatively, we identified two candidates' variants –in *GAK* and *SCARB2* genes- for conferring protection against LRRK2 G2019S pathogenic effects in L2-NMC subjects.

    - Genetic testing in the Catalan population showed a significant association of the SNP in *GAK* with the case status and a trend towards delayed AAO under a recessive model.

- The SNP in *SCARB2* was associated towards delayed AAO under a dominant model

Part II: Generation of a *Tyrosine Hydroxylase* reporter hiPSC line

- Two TH reporter cell lines have been generated from one parental control and one L2-PD iPSC line respectively.

- The fidelity of the reporting system has been confirmed by verifying its co-expression with the endogenous *Tyrosine Hydroxylase* gene by immunofluorescence.

- We have demonstrated its applicability in purifying DA neurons from heterogeneous cultures and in live imaging studies.

- We have corroborated the importance of performing phenotypical tests in defined and homogenous neuronal populations.

REFERENCES

Abeliovich, A. & Gitler, A.D., 2016. Defects in trafficking bridge Parkinson's disease pathology and genetics. *Nature*, 539(7628), pp.207–216. Available at: http://www.ncbi.nlm.nih.gov/pubmed/27830778 [Accessed May 18, 2017].

Agalliu, I. et al., 2015. Higher Frequency of Certain Cancers in *LRRK2* G2019S Mutation Carriers With Parkinson Disease. *JAMA Neurology*, 72(1), p.58. Available at: http://www.ncbi.nlm.nih.gov/pubmed/25401981 [Accessed May 27, 2017].

Alcalay, R.N. et al., 2015. Glucocerebrosidase activity in Parkinson's disease with and without *GBA* mutations. *Brain*, 138(9), pp.2648–2658. Available at: http://www.ncbi.nlm.nih.gov/pubmed/26117366 [Accessed May 23, 2017].

Alwin, S. et al., 2005. Custom Zinc-Finger Nucleases for Use in Human Cells. *Molecular Therapy*, 12(4), pp.610–617. Available at: http://www.ncbi.nlm.nih.gov/pubmed/16039907 [Accessed June 9, 2017].

Anheim, M. et al., 2012. Penetrance of Parkinson disease in glucocerebrosidase gene mutation carriers. *Neurology*, 78(6), pp.417–420. Available at: http://www.ncbi.nlm.nih.gov/pubmed/22282650 [Accessed June 1, 2017].

Arranz, A.M. et al., 2015. LRRK2 functions in synaptic vesicle endocytosis through a kinase-dependent mechanism. *Journal of Cell Science*, 128(3), pp.541–552. Available at: http://jcs.biologists.org/cgi/doi/10.1242/jcs.158196 [Accessed May 20, 2017].

Backlund, E.-O. et al., 1985. Transplantation of adrenal medullary tissue to striatum in parkinsonism. *Journal of Neurosurgery*, 62(2), pp.169–173. Available at: http://dx.doi.org/10.3171/jns.1985.62.2.0169.

Baker, D.E.C. et al., 2007. Adaptation to culture of human embryonic stem cells and oncogenesis in vivo. *Nat Biotech*, 25(2), pp.207–215. Available at: http://dx.doi.org/10.1038/nbt1285.

Baptista, M.A.S. et al., 2013. Loss of Leucine-Rich Repeat Kinase 2 (LRRK2) in Rats Leads to Progressive Abnormal Phenotypes in Peripheral Organs D. J. Moore, ed. *PLoS ONE*, 8(11), p.e80705. Available at: http://www.ncbi.nlm.nih.gov/pubmed/24244710 [Accessed May 13, 2017].

Bardien, S. et al., 2011. Genetic characteristics of leucine-rich repeat kinase 2 (LRRK2) associated Parkinson's disease. *Parkinsonism & Related Disorders*, 17(7), pp.501–508. Available at: http://www.ncbi.nlm.nih.gov/pubmed/21641266 [Accessed May 5, 2017].

Bardy, C. et al., 2016. Predicting the functional states of human iPSC-derived neurons with single-cell RNA-seq and electrophysiology. *Molecular psychiatry*, 21(11), pp.1573–1588. Available at: http://www.ncbi.nlm.nih.gov/pubmed/27698428 [Accessed June 12, 2017].

Barker, R.A., Drouin-Ouellet, J. & Parmar, M., 2015. Cell-based therapies for Parkinson disease—past insights and future potential. *Nature Reviews Neurology*, 11(9), pp.492–503. Available at: http://www.ncbi.nlm.nih.gov/pubmed/26240036 [Accessed June 8, 2017].

Barrett, J.C. et al., 2008. Genome-wide association defines more than 30 distinct susceptibility loci for Crohn's disease. *Nature Genetics*, 40(8), pp.955–962. Available at: http://www.ncbi.nlm.nih.gov/pubmed/18587394 [Accessed May 27, 2017].

Bartus, R.T. et al., 2015. Post-mortem assessment of the short and long-term effects of the trophic factor neurturin in patients with ?-synucleinopathies. *Neurobiology of Disease*, 78, pp.162–171. Available at: http://www.ncbi.nlm.nih.gov/pubmed/25841760 [Accessed June 11, 2017].

Beilina, A. et al., 2014. Unbiased screen for interactors of leucine-rich repeat kinase 2 supports a common pathway for sporadic and familial Parkinson disease. *Proceedings of the National*

Academy of Sciences of the United States of America, 111(7), pp.2626–31. Available at: http://www.ncbi.nlm.nih.gov/pubmed/24510904 [Accessed April 7, 2017].

Benitez, B.A. et al., 2016. Resequencing analysis of five Mendelian genes and the top genes from genome-wide association studies in Parkinson's Disease. *Molecular Neurodegeneration*, 11(1), p.29. Available at: http://molecularneurodegeneration.biomedcentral.com/articles/10.1186/s13024-016-0097-0 [Accessed May 24, 2017].

Berg, D. et al., 2011. Enlarged Substantia Nigra Hyperechogenicity and Risk for Parkinson Disease. *Archives of Neurology*, 68(7), p.932. Available at: http://www.ncbi.nlm.nih.gov/pubmed/21747034 [Accessed May 15, 2017].

Berg, D. et al., 2015. MDS research criteria for prodromal Parkinson's disease. *Movement Disorders*, 30(12), pp.1600–1611. Available at: http://www.ncbi.nlm.nih.gov/pubmed/26474317 [Accessed May 15, 2017].

Berkovic, S.F. et al., 2008. Array-based gene discovery with three unrelated subjects shows SCARB2/LIMP-2 deficiency causes myoclonus epilepsy and glomerulosclerosis. *American journal of human genetics*, 82(3), pp.673–84. Available at: http://www.ncbi.nlm.nih.gov/pubmed/18308289 [Accessed June 4, 2017].

Bernstein, B.E. et al., 2010. The NIH Roadmap Epigenomics Mapping Consortium. *Nature biotechnology*, 28(10), pp.1045–8. Available at: http://www.ncbi.nlm.nih.gov/pubmed/20944595 [Accessed May 24, 2017].

Lo Bianco, C. et al., 2002. -Synucleinopathy and selective dopaminergic neuron loss in a rat lentiviral-based model of Parkinson's disease. *Proceedings of the National Academy of Sciences*, 99(16), pp.10813–10818. Available at: http://www.ncbi.nlm.nih.gov/pubmed/12122208 [Accessed May 29, 2017].

Biskup, S. et al., 2006. Localization of LRRK2 to membranous and vesicular structures in mammalian brain. *Annals of Neurology*, 60(5), pp.557–569. Available at: http://www.ncbi.nlm.nih.gov/pubmed/17120249 [Accessed May 13, 2017].

Blanca Ramírez, M. et al., 2017. GTP binding regulates cellular localization of Parkinsoṅs disease-associated LRRK2. *Human Molecular Genetics*. Available at: http://www.ncbi.nlm.nih.gov/pubmed/28453723 [Accessed May 13, 2017].

Blesa, J. & Przedborski, S., 2014. Parkinsonâ€™s disease: animal models and dopaminergic cell vulnerability. *Frontiers in Neuroanatomy*, 8, p.155. Available at: http://journal.frontiersin.org/article/10.3389/fnana.2014.00155/abstract [Accessed May 27, 2017].

Boeve, B.F. et al., 2013. Clinicopathologic correlations in 172 cases of rapid eye movement sleep behavior disorder with or without a coexisting neurologic disorder. *Sleep Medicine*, 14(8), pp.754–762. Available at: http://www.sciencedirect.com.sire.ub.edu/science/article/pii/S1389945712003875 [Accessed May 15, 2017].

Bonifati, V. et al., 2005. Early-onset parkinsonism associated with PINK1 mutations: Frequency, genotypes, and phenotypes. *Neurology*, 65(1), pp.87–95. Available at: http://www.neurology.org/cgi/doi/10.1212/01.wnl.0000167546.39375.82 [Accessed May 4, 2017].

Borgs, L. et al., 2016. Dopaminergic neurons differentiating from LRRK2 G2019S induced pluripotent stem cells show early neuritic branching defects. *Scientific reports*, 6(1), p.33377. Available at: http://www.nature.com/articles/srep33377 [Accessed June 12, 2017].

Braak, H. et al., 2003. Idiopathic Parkinson's disease: possible routes by which vulnerable neuronal types may be subject to neuroinvasion by an unknown pathogen. *Journal of Neural Transmission*, 110(5), pp.517–536. Available at: http://link.springer.com/10.1007/s00702-002-0808-2 [Accessed May 28, 2017].

Braak, H. et al., 2003. Staging of brain pathology related to sporadic Parkinson's disease. *Neurobiology of Aging*, 24(2), pp.197–211. Available at: http://www.ncbi.nlm.nih.gov/pubmed/12498954 [Accessed May 15, 2017].

Braak, H. & Del Tredici, K., 2008. Assessing fetal nerve cell grafts in Parkinson's disease. *Nature Medicine*, 14(5), pp.483–485. Available at: http://www.ncbi.nlm.nih.gov/pubmed/18463652 [Accessed May 28, 2017].

Bras, J. et al., 2014. Genetic analysis implicates APOE, SNCA and suggests lysosomal dysfunction in the etiology of dementia with Lewy bodies. *Human Molecular Genetics*, 23(23), pp.6139–6146. Available at: https://academic.oup.com/hmg/article-lookup/doi/10.1093/hmg/ddu334 [Accessed June 4, 2017].

Brüggemann, N. et al., 2010. Recessively Inherited Parkinsonism. *Archives of Neurology*, 67(11), pp.652–662. Available at: http://archneur.jamanetwork.com/article.aspx?doi=10.1001/archneurol.2010.281 [Accessed May 20, 2017].

Brundin, P. et al., 2008. Research in motion: the enigma of Parkinson's disease pathology spread. *Nature Reviews Neuroscience*, 9(10), pp.741–745. Available at: http://www.ncbi.nlm.nih.gov/pubmed/18769444 [Accessed May 28, 2017].

Burke, R.E., Dauer, W.T. & Vonsattel, J.P.G., 2008. A critical evaluation of the Braak staging scheme for Parkinson's disease. *Annals of neurology*, 64(5), pp.485–91. Available at: http://www.ncbi.nlm.nih.gov/pubmed/19067353 [Accessed May 15, 2017].

Burré, J. et al., 2010. Alpha-synuclein promotes SNARE-complex assembly in vivo and in vitro. *Science (New York, N.Y.)*, 329(5999), pp.1663–7. Available at: http://www.ncbi.nlm.nih.gov/pubmed/20798282 [Accessed May 19, 2017].

Burré, J., Sharma, M. & Südhof, T.C., 2014. α-Synuclein assembles into higher-order multimers upon membrane binding to promote SNARE complex formation. *Proceedings of the National Academy of Sciences*, 111(40), pp.E4274–E4283. Available at: http://www.ncbi.nlm.nih.gov/pubmed/25246573 [Accessed May 19, 2017].

Burrows, C.K. et al., 2016. Genetic Variation, Not Cell Type of Origin, Underlies the Majority of Identifiable Regulatory Differences in iPSCs D. J. Gaffney, ed. *PLoS Genetics*, 12(1), p.e1005793.

Butcher, N.J. et al., 2013. Association Between Early-Onset Parkinson Disease and 22q11.2 Deletion Syndrome. *JAMA Neurology*, 70(11), p.1359. Available at: http://www.ncbi.nlm.nih.gov/pubmed/24018986 [Accessed May 31, 2017].

Byers, B. et al., 2011. SNCA triplication parkinson's patient's iPSC-Derived DA neurons accumulate α-Synuclein and are susceptible to oxidative stress W.-C. Chin, ed. *PLoS ONE*, 6(11), p.e26159. Available at: http://dx.plos.org/10.1371/journal.pone.0026159 [Accessed June 11, 2017].

Cao, M. et al., 2017. Parkinson Sac Domain Mutation in Synaptojanin 1 Impairs Clathrin Uncoating at Synapses and Triggers Dystrophic Changes in Dopaminergic Axons. *Neuron*, 93(4), pp.882–896.e5. Available at: http://www.ncbi.nlm.nih.gov/pubmed/28231468 [Accessed May 20, 2017].

Carcamo-Orive, I. et al., 2017. Analysis of Transcriptional Variability in a Large Human iPSC Library

Reveals Genetic and Non-genetic Determinants of Heterogeneity. *Cell Stem Cell*, 20(4), pp.518–532.e9. Available at: http://www.ncbi.nlm.nih.gov/pubmed/28017796 [Accessed June 4, 2017].

Chartier-Harlin, M.-C. et al., 2001. Alpha-synuclein locus duplication as a cause of familial Parkinson's disease. *Lancet (London, England)*, 364(9440), pp.1167–9. Available at: http://www.ncbi.nlm.nih.gov/pubmed/15451224 [Accessed May 4, 2017].

Chen, C.-Y. et al., 2012. (G2019S) LRRK2 activates MKK4-JNK pathway and causes degeneration of SN dopaminergic neurons in a transgenic mouse model of PD. *Cell Death and Differentiation*, 19(10), pp.1623–1633. Available at: http://www.ncbi.nlm.nih.gov/pubmed/22539006 [Accessed May 29, 2017].

Chen, R. et al., 2016. Analysis of 589,306 genomes identifies individuals resilient to severe Mendelian childhood diseases. *Nature biotechnology*, 34(5), pp.531–8. Available at: http://www.nature.com/doifinder/10.1038/nbt.3514 [Accessed April 24, 2017].

Cho, H.J. et al., 2014. Leucine-rich repeat kinase 2 regulates Sec16A at ER exit sites to allow ER-Golgi export. *The EMBO journal*, pp.1–18. Available at: http://www.ncbi.nlm.nih.gov/pubmed/25201882.

Clark, I.E. et al., 2006. Drosophila pink1 is required for mitochondrial function and interacts genetically with parkin. *Nature*, 441(7097), pp.1162–1166. Available at: http://www.ncbi.nlm.nih.gov/pubmed/16672981 [Accessed May 17, 2017].

Coetzee, S.G. et al., 2016. Enrichment of risk SNPs in regulatory regions implicate diverse tissues in Parkinson's disease etiology. *Scientific reports*, 6, p.30509. Available at: http://www.ncbi.nlm.nih.gov/pubmed/27461410.

Cooper, A.A. et al., 2006. -Synuclein Blocks ER-Golgi Traffic and Rab1 Rescues Neuron Loss in Parkinson's Models. *Science*, 313(5785), pp.324–328. Available at: http://www.ncbi.nlm.nih.gov/pubmed/16794039 [Accessed May 19, 2017].

Cooper, O. et al., 2009. Lack of functional relevance of isolated cell damage in transplants of Parkinson's disease patients. *Journal of Neurology*, 256(S3), pp.310–316. Available at: http://www.ncbi.nlm.nih.gov/pubmed/19711122 [Accessed May 28, 2017].

Cuervo, A.M., 2011. Chaperone-mediated autophagy: Dice's "wild" idea about lysosomal selectivity. *Nature Reviews Molecular Cell Biology*, 12(8), pp.535–541. Available at: http://www.nature.com/doifinder/10.1038/nrm3150 [Accessed June 1, 2017].

Cuervo, A.M. et al., 2004. Impaired Degradation of Mutant -Synuclein by Chaperone-Mediated Autophagy. *Science*, 305(5688), pp.1292–1295. Available at: http://www.ncbi.nlm.nih.gov/pubmed/15333840 [Accessed May 21, 2017].

Cui, J. et al., 2016. Quantification of dopaminergic neuron differentiation and neurotoxicity via a genetic reporter. *Scientific Reports*.

DeBoever, C. et al., 2017. Large-Scale Profiling Reveals the Influence of Genetic Variation on Gene Expression in Human Induced Pluripotent Stem Cells. *Cell stem cell*, 20(4), pp.533–546.e7. Available at: http://www.ncbi.nlm.nih.gov/pubmed/28388430 [Accessed June 4, 2017].

Decressac, M. et al., 2011. GDNF fails to exert neuroprotection in a rat α-synuclein model of Parkinson's disease. *Brain*, 134(8), pp.2302–2311. Available at: http://brain.oxfordjournals.org/content/134/8/2302.abstract.

Decressac, M. et al., 2012. Progressive neurodegenerative and behavioural changes induced by AAV-mediated overexpression of α-synuclein in midbrain dopamine neurons. *Neurobiology of Disease*, 45(3), pp.939–953. Available at: http://www.ncbi.nlm.nih.gov/pubmed/22182688 [Accessed May

29, 2017].

Decressac, M. et al., 2012. α-Synuclein–Induced Down-Regulation of Nurr1 Disrupts GDNF Signaling in Nigral Dopamine Neurons. *Science Translational Medicine* , 4 (163), pp.163ra156–163ra156. Available at: http://stm.sciencemag.org/content/4/163/163ra156.abstract.

Deng, H.-X. et al., 2016. Identification of TMEM230 mutations in familial Parkinson's disease. *Nature Genetics*, 48(7), pp.733–739. Available at: http://www.ncbi.nlm.nih.gov/pubmed/27270108 [Accessed May 6, 2017].

DeStefano, A.L. et al., 2002. PARK3 Influences Age at Onset in Parkinson Disease: A Genome Scan in the GenePD Study. *The American Journal of Human Genetics*, 70(5), pp.1089–1095. Available at: http://www.ncbi.nlm.nih.gov/pubmed/11920285 [Accessed May 10, 2017].

Devine, M.J. et al., 2011. Parkinson's disease induced pluripotent stem cells with triplication of the α-synuclein locus. *Nature Communications*, 2, p.440.

Dexter, D.T. et al., 1987. INCREASED NIGRAL IRON CONTENT IN POSTMORTEM PARKINSONIAN BRAIN. *The Lancet*, 330(8569), pp.1219–1220. Available at: http://linkinghub.elsevier.com/retrieve/pii/S0140673687913614 [Accessed May 4, 2017].

Ding, Q. et al., 2013. A TALEN genome-editing system for generating human stem cell-based disease models. *Cell stem cell*, 12(2), pp.238–51.

Do, C.B. et al., 2011. Web-Based Genome-Wide Association Study Identifies Two Novel Loci and a Substantial Genetic Component for Parkinson's Disease G. Gibson, ed. *PLoS Genetics*, 7(6), p.e1002141. Available at: http://dx.plos.org/10.1371/journal.pgen.1002141 [Accessed September 25, 2016].

Dorsey, E.R. et al., 2007. Projected number of people with Parkinson disease in the most populous nations, 2005 through 2030. *Neurology*, 68(5), pp.384–386. Available at: http://www.neurology.org/cgi/doi/10.1212/01.wnl.0000247740.47667.03 [Accessed May 24, 2017].

Dunnett, S.B. et al., 1981. Grafts of embryonic substantia nigra reinnervating the ventrolateral striatum ameliorate sensorimotor impairments and akinesia in rats with 6-OHDA lesions of the nigrostriatal pathway. *Brain Research*, 229(1), pp.209–217. Available at: http://www.sciencedirect.com/science/article/pii/0006899381907599 [Accessed December 16, 2014].

Dusonchet, J. et al., 2011. A rat model of progressive nigral neurodegeneration induced by the Parkinson's disease-associated G2019S mutation in LRRK2. *The Journal of neuroscience : the official journal of the Society for Neuroscience*, 31(3), pp.907–12. Available at: http://www.ncbi.nlm.nih.gov/pubmed/21248115 [Accessed May 22, 2017].

Dzamko, N. et al., 2010. Inhibition of LRRK2 kinase activity leads to dephosphorylation of Ser 910 /Ser 935 , disruption of 14-3-3 binding and altered cytoplasmic localization. *Biochem. J*, 430, pp.405–413. Available at: http://www.biochemj.org/content/ppbiochemj/430/3/405.full.pdf [Accessed May 13, 2017].

Ebert, A.D. et al., 2009. Induced pluripotent stem cells from a spinal muscular atrophy patient. *Nature*, 457(7227), pp.277–280. Available at: http://www.nature.com/doifinder/10.1038/nature07677.

Edvardson, S. et al., 2012. A Deleterious Mutation in DNAJC6 Encoding the Neuronal-Specific Clathrin-Uncoating Co-Chaperone Auxilin, Is Associated with Juvenile Parkinsonism C. Wider, ed. *PLoS ONE*, 7(5), p.e36458. Available at: http://dx.plos.org/10.1371/journal.pone.0036458 [Accessed May 19, 2017].

Espejo, E.F. et al., 1998. Cellular and functional recovery of Parkinsonian rats after intrastriatal transplantation of carotid body cell aggregates. *Neuron*, 20(2), pp.197–206. Available at: http://www.ncbi.nlm.nih.gov/pubmed/9491982 [Accessed May 27, 2017].

Evans, M.J. & Kaufman, M.H., 1981. Establishment in culture of pluripotential cells from mouse embryos. *Nature*, 292(5819), pp.154–6. Available at: http://www.ncbi.nlm.nih.gov/pubmed/7242681 [Accessed July 17, 2016].

Fares, M.-B. et al., 2016. Induction of de novo α-synuclein fibrillization in a neuronal model for Parkinson's disease. *Proceedings of the National Academy of Sciences of the United States of America*, 113(7), pp.E912–21. Available at: http://www.ncbi.nlm.nih.gov/pubmed/26839406 [Accessed May 28, 2017].

Farlow, J.L. et al., 2016. Whole-Exome Sequencing in Familial Parkinson Disease. *JAMA Neurology*, 73(1), p.68.

Ferguson, S.M. & De Camilli, P., 2012. Dynamin, a membrane-remodelling GTPase. *Nature Reviews Molecular Cell Biology*, 13(2), p.75. Available at: http://www.nature.com/doifinder/10.1038/nrm3266 [Accessed May 16, 2017].

Di Fonzo, A. et al., 2005. A frequent LRRK2 gene mutation associated with autosomal dominant Parkinson's disease. *Lancet*, 365(9457), pp.412–415. Available at: http://www.ncbi.nlm.nih.gov/pubmed/15680456 [Accessed May 4, 2017].

Fonzo, A.D. et al., 2009. FBXO7 mutations cause autosomal recessive, early-onset parkinsonian-pyramidal syndrome. *Neurology*, 72(3), pp.240–245. Available at: http://www.ncbi.nlm.nih.gov/pubmed/19038853 [Accessed May 18, 2017].

Freed, C.R. et al., 2001. Transplantation of Embryonic Dopamine Neurons for Severe Parkinson's Disease. *New England Journal of Medicine*, 344(10), pp.710–719. Available at: http://dx.doi.org/10.1056/NEJM200103083441002.

Fuji, R.N. et al., 2015. Effect of selective LRRK2 kinase inhibition on nonhuman primate lung. *Science Translational Medicine*, 7(273), pp.273ra15–273ra15. Available at: http://www.ncbi.nlm.nih.gov/pubmed/25653221 [Accessed May 13, 2017].

Funayama, M. et al., 2015. CHCHD2 mutations in autosomal dominant late-onset Parkinson's disease: a genome-wide linkage and sequencing study. *The Lancet Neurology*, 14(3), pp.274–282. Available at: http://www.ncbi.nlm.nih.gov/pubmed/25662902 [Accessed January 20, 2017].

Gaig, C. et al., 2006. LRRK2 Mutations in Spanish Patients With Parkinson Disease. *Archives of Neurology*, 63(3), p.377. Available at: http://archneur.jamanetwork.com/article.aspx?doi=10.1001/archneur.63.3.377 [Accessed May 14, 2017].

Gan-Or, Z. et al., 2012. Association of Sequence Alterations in the Putative Promoter of <emph type="ital">RAB7L1</emph> With a Reduced Parkinson Disease Risk. *Archives of Neurology*, 69(1), p.105. Available at: http://www.ncbi.nlm.nih.gov/pubmed/22232350 [Accessed January 23, 2017].

Gan-Or, Z. et al., 2015. Differential effects of severe vs mild GBA mutations on Parkinson disease. *Neurology*, 84(9), pp.880–7.

Gan-Or, Z., 2015. PARK16 haplotypes and the importance of protective genetic factors in Parkinson's disease. *Journal of Human Genetics*, 60(8), pp.461–462. Available at: http://www.nature.com/doifinder/10.1038/jhg.2015.73 [Accessed July 19, 2016].

Giasson, B.I. et al., 2002. Neuronal alpha-synucleinopathy with severe movement disorder in mice expressing A53T human alpha-synuclein. *Neuron*, 34(4), pp.521–33. Available at: http://www.ncbi.nlm.nih.gov/pubmed/12062037 [Accessed May 29, 2017].

Giralt, A. et al., 2010. BDNF regulation under GFAP promoter provides engineered astrocytes as a new approach for long-term protection in Huntington's disease. *Gene therapy*, 17(10), pp.1294–308. Available at: http://www.nature.com/doifinder/10.1038/gt.2010.71 [Accessed June 12, 2017].

Gitler, A.D. et al., 2008. The Parkinson's disease protein -synuclein disrupts cellular Rab homeostasis. *Proceedings of the National Academy of Sciences*, 105(1), pp.145–150. Available at: http://www.ncbi.nlm.nih.gov/pubmed/18162536 [Accessed May 19, 2017].

Goker-Alpan, O. et al., 2004. Parkinsonism among Gaucher disease carriers. *Journal of medical genetics*, 41(12), pp.937–40. Available at: http://www.ncbi.nlm.nih.gov/pubmed/15591280 [Accessed January 20, 2017].

Grealish, S. et al., 2014. Human ESC-Derived Dopamine Neurons Show Similar Preclinical Efficacy and Potency to Fetal Neurons when Grafted in a Rat Model of Parkinson's Disease. *Cell Stem Cell*, 15(5), pp.653–665. Available at: http://www.cell.com/cell-stem-cell/abstract/S1934-5909(14)00408-1.

Greenamyre, J.T. et al., 2000a. Chronic systemic pesticide exposure reproduces features of Parkinson's disease. *Nature Neuroscience*, 3(12), pp.1301–1306. Available at: http://www.nature.com/doifinder/10.1038/81834 [Accessed May 3, 2017].

Greenamyre, J.T. et al., 2000b. Chronic systemic pesticide exposure reproduces features of Parkinson's disease. *Nature Neuroscience*, 3(12), pp.1301–1306. Available at: http://www.nature.com/doifinder/10.1038/81834 [Accessed May 27, 2017].

Greene, J.C. et al., 2003. Mitochondrial pathology and apoptotic muscle degeneration in Drosophila parkin mutants. *Proceedings of the National Academy of Sciences of the United States of America*, 100(7), pp.4078–83. Available at: http://www.ncbi.nlm.nih.gov/pubmed/12642658 [Accessed May 17, 2017].

Greener, T. et al., 2000. Role of cyclin G-associated kinase in uncoating clathrin-coated vesicles from non-neuronal cells. *The Journal of biological chemistry*, 275(2), pp.1365–70. Available at: http://www.ncbi.nlm.nih.gov/pubmed/10625686 [Accessed May 19, 2017].

Guttmacher, A.E. et al., 2003. Alzheimer's Disease and Parkinson's Disease. *New England Journal of Medicine*, 348(14), pp.1356–1364. Available at: http://www.ncbi.nlm.nih.gov/pubmed/12672864 [Accessed May 2, 2017].

Hall, H. et al., 2014. Hippocampal Lewy pathology and cholinergic dysfunction are associated with dementia in Parkinson's disease. *Brain*, 137(9), pp.2493–2508. Available at: http://www.ncbi.nlm.nih.gov/pubmed/25062696 [Accessed May 26, 2017].

Hallett, P.J. et al., 2015. Successful Function of Autologous iPSC-Derived Dopamine Neurons following Transplantation in a Non-Human Primate Model of Parkinson's Disease. *Cell Stem Cell*, 16(3), pp.269–274. Available at: http://dx.doi.org/10.1016/j.stem.2015.01.018.

Halliday, G. et al., 2009. No Lewy pathology in monkeys with over 10 years of severe MPTP Parkinsonism. *Movement Disorders*, 24(10), pp.1519–1523. Available at: http://www.ncbi.nlm.nih.gov/pubmed/19526568 [Accessed May 27, 2017].

Hamza, T.H. et al., 2011. Genome-wide gene-environment study identifies glutamate receptor gene GRIN2A as a Parkinson's disease modifier gene via interaction with coffee. *PLoS genetics*, 7(8),

p.e1002237. Available at: http://www.ncbi.nlm.nih.gov/pubmed/21876681 [Accessed July 22, 2016].

Hartmann, A., 2004. Postmortem studies in Parkinson's disease. *Dialogues in clinical neuroscience*, 6(3), pp.281–93. Available at: http://www.ncbi.nlm.nih.gov/pubmed/22033507 [Accessed May 30, 2017].

Healy, D.G. et al., 2008. Phenotype, genotype, and worldwide genetic penetrance of LRRK2-associated Parkinson's disease: a case-control study. *The Lancet Neurology*, 7(7), pp.583–590. Available at: http://www.ncbi.nlm.nih.gov/pubmed/18539534 [Accessed May 5, 2017].

Hely, M.A. et al., 2008. The Sydney multicenter study of Parkinson's disease: The inevitability of dementia at 20 years. *Movement Disorders*, 23(6), pp.837–844. Available at: http://www.ncbi.nlm.nih.gov/pubmed/18307261 [Accessed May 15, 2017].

Hentati, F. et al., 2014. LRRK2 parkinsonism in Tunisia and Norway: a comparative analysis of disease penetrance. *Neurology*, 83(6), pp.568–9. Available at: http://www.ncbi.nlm.nih.gov/pubmed/25008396 [Accessed April 7, 2017].

Hernán, M.A. et al., 2002. A meta-analysis of coffee drinking, cigarette smoking, and the risk of Parkinson's disease. *Annals of Neurology*, 52(3), pp.276–284. Available at: http://doi.wiley.com/10.1002/ana.10277 [Accessed May 3, 2017].

Herzig, M.C. et al., 2011. LRRK2 protein levels are determined by kinase function and are crucial for kidney and lung homeostasis in mice. *Human Molecular Genetics*, 20(21), pp.4209–4223. Available at: http://www.ncbi.nlm.nih.gov/pubmed/21828077 [Accessed May 13, 2017].

Hill, R.W., Wyse, G.A. & Anderson, M., 2012. *Animal physiology*, Sinauer Associates, Inc. Publishers. Available at: http://booksmedicos.org/animal-physiology-3rd-edition/ [Accessed June 10, 2017].

Hinkle, K.M. et al., 2012. LRRK2 knockout mice have an intact dopaminergic system but display alterations in exploratory and motor co-ordination behaviors. *Molecular Neurodegeneration*, 7(1), p.25. Available at: http://molecularneurodegeneration.biomedcentral.com/articles/10.1186/1750-1326-7-25 [Accessed May 13, 2017].

Hioki, H. et al., 2007. Efficient gene transduction of neurons by lentivirus with enhanced neuron-specific promoters. *Gene Therapy*, 14(11), pp.872–882.

Hockemeyer, D. et al., 2009. Efficient targeting of expressed and silent genes in human ESCs and iPSCs using zinc-finger nucleases. *Nature Biotechnology*, 27(9), pp.851–857. Available at: http://www.nature.com/doifinder/10.1038/nbt.1562 [Accessed July 18, 2016].

Hockemeyer, D. et al., 2011. Genetic engineering of human pluripotent cells using TALE nucleases. *Nature biotechnology*, 29(8), pp.731–4.

Hockemeyer, D. & Jaenisch, R., 2016. Induced Pluripotent Stem Cells Meet Genome Editing. *Cell Stem Cell*, 18(5), pp.573–586. Available at: http://linkinghub.elsevier.com/retrieve/pii/S193459091630056X [Accessed February 20, 2017].

Holkers, M. et al., 2014. Adenoviral vector DNA for accurate genome editing with engineered nucleases. *Nature methods*, 11(10). Available at: http://www.ncbi.nlm.nih.gov/pubmed/25152084 [Accessed August 26, 2014].

Hsieh, C.-H. et al., 2016. Functional Impairment in Miro Degradation and Mitophagy Is a Shared Feature in Familial and Sporadic Parkinson's Disease. *Cell Stem Cell*, 19(6), pp.709–724. Available at: http://linkinghub.elsevier.com/retrieve/pii/S1934590916302491 [Accessed January 23, 2017].

Huttenlocher, J. et al., 2015. Heterozygote carriers for CNVs in PARK2 are at increased risk of

Parkinson's disease. *Human molecular genetics*, 24(19), pp.5637–43. Available at: https://academic.oup.com/hmg/article-lookup/doi/10.1093/hmg/ddv277 [Accessed May 16, 2017].

Ibáñez, P. et al., 1998. Causal relation between alpha-synuclein gene duplication and familial Parkinson's disease. *Lancet (London, England)*, 364(9440), pp.1169–71. Available at: http://www.ncbi.nlm.nih.gov/pubmed/15451225 [Accessed May 4, 2017].

INE, 2014. Proyección de la Población de España 2014-2064: Notas de prensa. *Instituto Nacional de Estadística (INE)*, pp.1–9. Available at: http://www.ine.es/prensa/np870.pdf [Accessed May 2, 2017].

Iranzo, A. et al., 2010. Decreased striatal dopamine transporter uptake and substantia nigra hyperechogenicity as risk markers of synucleinopathy in patients with idiopathic rapid-eye-movement sleep behaviour disorder: a prospective study. *The Lancet Neurology*, 9(11), pp.1070–1077. Available at: http://www.sciencedirect.com.sire.ub.edu/science/article/pii/S1474442210702167 [Accessed June 3, 2017].

Ivatt, R.M. et al., 2014. Genome-wide RNAi screen identifies the Parkinson disease GWAS risk locus SREBF1 as a regulator of mitophagy. *Proceedings of the National Academy of Sciences*, 111(23), pp.8494–8499. Available at: http://www.ncbi.nlm.nih.gov/pubmed/24912190 [Accessed May 18, 2017].

Jankovic, J. et al., 1990. Variable expression of Parkinson's disease: a base-line analysis of the DATATOP cohort. The Parkinson Study Group. *Neurology*, 40(10), pp.1529–34. Available at: http://www.ncbi.nlm.nih.gov/pubmed/2215943 [Accessed May 15, 2017].

Jennings, D., Stern, M., Siderowf, A., Eberly, S., Oakes, D., Marek, K., Investigators, P., 2015. Longitudinal Imaging And Phenoconversion In The PARS Prodromal Cohort. In *Longitudinal Imaging And Phenoconversion In The PARS Prodromal Cohort*. San Diego, California, USA: Movement DIsorders, p. 30 Suppl 1:998. Available at: http://www.mdsabstracts.com/abstract.asp?MeetingID=802&id=113533 [Accessed June 3, 2017].

Jinek, M. et al., 2012. A programmable dual-RNA-guided DNA endonuclease in adaptive bacterial immunity. *Science (New York, N.Y.)*, 337(6096), pp.816–21. Available at: http://www.ncbi.nlm.nih.gov/pubmed/22745249 [Accessed July 20, 2016].

Johannessen, J.N. et al., 1985. IV. Differences in the metabolism of MPTP in the rodent and primate parallel differences in sensitivity to its neurotoxic effects. *Life Sciences*, 36(3), pp.219–224. Available at: http://linkinghub.elsevier.com/retrieve/pii/0024320585900621 [Accessed May 27, 2017].

Johnson, W.G., Hodge, S.E. & Duvoisin, R., 1990. Twin studies and the genetics of Parkinson's disease?a reappraisal. *Movement Disorders*, 5(3), pp.187–194. Available at: http://www.ncbi.nlm.nih.gov/pubmed/2388635 [Accessed May 4, 2017].

Kachergus, J. et al., 2005. Identification of a novel LRRK2 mutation linked to autosomal dominant parkinsonism: evidence of a common founder across European populations. *American journal of human genetics*, 76. Available at: http://dx.doi.org/10.1086/429256.

Kachergus, J. et al., 2005. Identification of a Novel LRRK2 Mutation Linked to Autosomal Dominant Parkinsonism: Evidence of a Common Founder across European Populations. *The American Journal of Human Genetics*, 76(4), pp.672–680. Available at: http://linkinghub.elsevier.com/retrieve/pii/S000292970762878X [Accessed May 4, 2017].

Kajiwara, M. et al., 2012. Donor-dependent variations in hepatic differentiation from human-induced pluripotent stem cells. *Proceedings of the National Academy of Sciences*, 109(31), pp.12538–12543.

Kalia, L. V. et al., 2015. Clinical Correlations With Lewy Body Pathology in *LRRK2* -Related Parkinson Disease. *JAMA Neurology*, 72(1), p.100. Available at: http://www.ncbi.nlm.nih.gov/pubmed/25401511 [Accessed June 4, 2017].

Kircher, M. et al., 2014. A general framework for estimating the relative pathogenicity of human genetic variants. *Nature genetics*, 46(3), pp.310–5. Available at: http://www.nature.com/doifinder/10.1038/ng.2892 [Accessed May 22, 2017].

Kirik, D. et al., 2002. Parkinson-like neurodegeneration induced by targeted overexpression of alpha-synuclein in the nigrostriatal system. *The Journal of neuroscience : the official journal of the Society for Neuroscience*, 22(7), pp.2780–91. Available at: http://www.ncbi.nlm.nih.gov/pubmed/11923443 [Accessed May 29, 2017].

Kirkeby, A., Grealish, S., Wolf, D.A., Nelander, J., Wood, J., et al., 2012. Generation of Regionally Specified Neural Progenitors and Functional Neurons from Human Embryonic Stem Cells under Defined Conditions. *Cell Reports*, 1(6), pp.703–714. Available at: http://www.sciencedirect.com/science/article/pii/S2211124712001222 [Accessed May 27, 2017].

Kirkeby, A., Grealish, S., Wolf, D.A., Nelander, J., Wood, J., et al., 2012. Generation of Regionally Specified Neural Progenitors and Functional Neurons from Human Embryonic Stem Cells under Defined Conditions. *Cell Reports*, 1(6), pp.703–714.

Kirkeby, A. et al., 2017. Predictive Markers Guide Differentiation to Improve Graft Outcome in Clinical Translation of hESC-Based Therapy for Parkinson's Disease. *Cell stem cell*, 20(1), pp.135–148. Available at: http://www.ncbi.nlm.nih.gov/pubmed/28094017 [Accessed June 8, 2017].

Kita-Matsuo, H. et al., 2009. Lentiviral Vectors and Protocols for Creation of Stable hESC Lines for Fluorescent Tracking and Drug Resistance Selection of Cardiomyocytes M. V. Blagosklonny, ed. *PLoS ONE*, 4(4), p.e5046. Available at: http://www.ncbi.nlm.nih.gov/pubmed/19352491 [Accessed June 9, 2017].

Kitada, T. et al., 1998. Mutations in the parkin gene cause autosomal recessive juvenile parkinsonism. *Nature, Published online: 09 April 1998; | doi:10.1038/10.1038/33416*, 392(6676), p.605. Available at: https://www.nature.com/nature/journal/v392/n6676/full/392605a0.html [Accessed May 4, 2017].

Klein, C. et al., 2007. Deciphering the role of heterozygous mutations in genes associated with parkinsonism. *The Lancet Neurology*, 6(7), pp.652–662. Available at: http://www.ncbi.nlm.nih.gov/pubmed/17582365 [Accessed May 16, 2017].

Kordower, J.H. et al., 2013. Disease duration and the integrity of the nigrostriatal system in Parkinson?s disease. *Brain*, 136(8), pp.2419–2431. Available at: https://academic.oup.com/brain/article-lookup/doi/10.1093/brain/awt192 [Accessed June 11, 2017].

Kordower, J.H. et al., 2008. Lewy body-like pathology in long-term embryonic nigral transplants in Parkinson's disease. *Nat Med*, 14(5), pp.504–506. Available at: http://dx.doi.org/10.1038/nm1747.

Kordower, J.H. & Bjorklund, A., 2013. Trophic Factor Gene Therapy for Parkinson's Disease. *Movement Disorders*, 28(1), pp.96–109. Available at: http://doi.wiley.com/10.1002/mds.25344 [Accessed June 11, 2017].

Krebs, C.E. et al., 2013. The Sac1 Domain of *SYNJ1* Identified Mutated in a Family with Early-Onset Progressive Parkinsonism with Generalized Seizures. *Human Mutation*, 34(9), pp.1200–1207.

Available at: http://doi.wiley.com/10.1002/humu.22372 [Accessed May 20, 2017].

Kriks, S. et al., 2011. Dopamine neurons derived from human ES cells efficiently engraft in animal models of Parkinson's disease. *Nature*, 480(7378), pp.547–51.

Krüger, R. et al., 1998. AlaSOPro mutation in the gene encoding α-synuclein in Parkinson's disease. *Nature Genetics*, 18(2), pp.106–108. Available at: http://www.nature.com/doifinder/10.1038/ng0298-106 [Accessed May 4, 2017].

Lai, Y. et al., 2015. Phosphoproteomic screening identifies Rab GTPases as novel downstream targets of PINK1. *The EMBO Journal*, 34(22), p.2840. Available at: https://www.ncbi.nlm.nih.gov/pmc/articles/PMC4654935/ [Accessed May 19, 2017].

Langston, J.W. et al., 1983. Chronic Parkinsonism in humans due to a product of meperidine-analog synthesis. *Science (New York, N.Y.)*, 219(4587), pp.979–80. Available at: http://www.ncbi.nlm.nih.gov/pubmed/6823561 [Accessed May 18, 2017].

Langston, J.W. et al., 2015. Multisystem Lewy body disease and the other parkinsonian disorders. *Nature genetics*, 47(12), pp.1378–84. Available at: http://www.ncbi.nlm.nih.gov/pubmed/26620112 [Accessed May 6, 2017].

Latourelle, J.C. et al., 2009. Genomewide association study for onset age in Parkinson disease. *BMC Medical Genetics*, 10(1), p.98. Available at: http://bmcmedgenet.biomedcentral.com/articles/10.1186/1471-2350-10-98 [Accessed May 10, 2017].

Latourelle, J.C. et al., 2011. Genomewide linkage study of modifiers of LRRK2-related Parkinson's disease. *Movement Disorders*, 26(11), pp.2039–2044. Available at: http://www.ncbi.nlm.nih.gov/pubmed/21661047 [Accessed May 16, 2017].

de Lau, L.M.L. et al., 2006. Epidemiology of Parkinson's disease. *The Lancet. Neurology*, 5(6), pp.525–35. Available at: http://www.ncbi.nlm.nih.gov/pubmed/16713924 [Accessed May 27, 2017].

Lazzarini, A.M. et al., 1994. A clinical genetic study of Parkinson's disease: evidence for dominant transmission. *Neurology*, 44(3 Pt 1), pp.499–506. Available at: http://www.ncbi.nlm.nih.gov/pubmed/8145922 [Accessed May 14, 2017].

Lee, A.J. et al., 2017. Penetrance estimate of *LRRK2* p.G2019S mutation in individuals of non-Ashkenazi Jewish ancestry. *Movement Disorders*. Available at: http://www.ncbi.nlm.nih.gov/pubmed/28639421 [Accessed September 4, 2017].

Lee, B.D. et al., 2010. Inhibitors of leucine-rich repeat kinase-2 protect against models of Parkinson's disease. *Nature medicine*, 16(9), pp.998–1000. Available at: http://www.ncbi.nlm.nih.gov/pubmed/20729864 [Accessed May 29, 2017].

Lee, C.-T., Bendriem, R.M., Kindberg, A.A., Worden, L.T., Williams, M.P., et al., 2015. Functional consequences of 17q21.31/WNT3-WNT9B amplification in hPSCs with respect to neural differentiation. *Cell reports*, 10(4), pp.616–32. Available at: http://www.ncbi.nlm.nih.gov/pubmed/25640183 [Accessed April 26, 2017].

Lee, C.-T., Bendriem, R.M., Kindberg, A.A., Worden, L.T., Williams, M.P., et al., 2015. Functional consequences of 17q21.31/WNT3-WNT9B amplification in hPSCs with respect to neural differentiation. *Cell reports*, 10(4), pp.616–32.

Lesage, S. et al., 2016. Loss of VPS13C Function in Autosomal-Recessive Parkinsonism Causes Mitochondrial Dysfunction and Increases PINK1/Parkin-Dependent Mitophagy. *The American Journal of Human Genetics*, 98(3), pp.500–513. Available at:

http://linkinghub.elsevier.com/retrieve/pii/S0002929716000483 [Accessed May 19, 2017].

Li, J.-Y. et al., 2008. Lewy bodies in grafted neurons in subjects with Parkinson's disease suggest host-to-graft disease propagation. *Nat Med*, 14(5), pp.501–503. Available at: http://dx.doi.org/10.1038/nm1746.

Lill, C.M. et al., 2015. Impact of Parkinson's disease risk loci on age at onset. *Movement Disorders*, 30(6), pp.847–850. Available at: http://doi.wiley.com/10.1002/mds.26237 [Accessed May 7, 2017].

Lin, X. et al., 2012. Conditional Expression of Parkinson's Disease-Related Mutant α-Synuclein in the Midbrain Dopaminergic Neurons Causes Progressive Neurodegeneration and Degradation of Transcription Factor Nuclear Receptor Related 1. *Journal of Neuroscience*, 32(27). Available at: http://www.jneurosci.org/content/32/27/9248.long [Accessed May 29, 2017].

Lin, X. et al., 2009. Leucine-Rich Repeat Kinase 2 Regulates the Progression of Neuropathology Induced by Parkinson's-Disease-Related Mutant α-synuclein. *Neuron*, 64(6), pp.807–827. Available at: http://www.ncbi.nlm.nih.gov/pubmed/20064389 [Accessed May 29, 2017].

Lindvall, O. et al., 1990. Grafts of fetal dopamine neurons survive and improve motor function in Parkinson's disease. *Science (New York, N.Y.)*, 247(4942), pp.574–7. Available at: http://www.ncbi.nlm.nih.gov/pubmed/2105529 [Accessed May 31, 2017].

Lindvall, O. et al., 1989. Human Fetal Dopamine Neurons Grafted Into the Striatum in Two Patients With Severe Parkinson's Disease. *Archives of Neurology*, 46(6), p.615. Available at: http://archneur.jamanetwork.com/article.aspx?doi=10.1001/archneur.1989.00520420033021 [Accessed June 7, 2017].

Logan, T. et al., 2017. α-Synuclein promotes dilation of the exocytotic fusion pore. *Nature Neuroscience*, 20(5), pp.681–689. Available at: http://www.nature.com/doifinder/10.1038/nn.4529 [Accessed May 19, 2017].

Lubbe, S.J. et al., 2016. Additional rare variant analysis in Parkinson's disease cases with and without known pathogenic mutations: evidence for oligogenic inheritance. *Human Molecular Genetics*, 57(24), p.ddw348. Available at: https://academic.oup.com/hmg/article-lookup/doi/10.1093/hmg/ddw348 [Accessed May 16, 2017].

Luk, K.C. et al., 2012. Pathological α-Synuclein Transmission Initiates Parkinson-like Neurodegeneration in Nontransgenic Mice. *Science*, 338(6109). Available at: http://science.sciencemag.org.sire.ub.edu/content/338/6109/949.full [Accessed May 28, 2017].

Lupiáñez, D.G. et al., 2015. Disruptions of Topological Chromatin Domains Cause Pathogenic Rewiring of Gene-Enhancer Interactions. *Cell*, 161(5), pp.1012–1025. Available at: http://www.ncbi.nlm.nih.gov/pubmed/25959774 [Accessed May 30, 2017].

Ma, Y. et al., 2002. Dyskinesia after fetal cell transplantation for parkinsonism: A PET study. *Annals of Neurology*, 52(5), pp.628–634. Available at: http://dx.doi.org/10.1002/ana.10359.

MacLeod, D. et al., 2006. The Familial Parkinsonism Gene LRRK2 Regulates Neurite Process Morphology. *Neuron*, 52(4), pp.587–593. Available at: http://dx.doi.org/10.1016/j.neuron.2006.10.008.

MacLeod, D.A. et al., 2013. RAB7L1 interacts with LRRK2 to modify intraneuronal protein sorting and Parkinson's disease risk. *Neuron*, 77(3), pp.425–39.

Madrazo, I. et al., 1987. Open Microsurgical Autograft of Adrenal Medulla to the Right Caudate Nucleus in Two Patients with Intractable Parkinson's Disease. *New England Journal of Medicine*, 316(14), pp.831–834. Available at: http://dx.doi.org/10.1056/NEJM198704023161402.

Manning-Bog, A.B. et al., 2002. The herbicide paraquat causes up-regulation and aggregation of alpha-synuclein in mice: paraquat and alpha-synuclein. *The Journal of biological chemistry*, 277(3), pp.1641–4. Available at: http://www.ncbi.nlm.nih.gov/pubmed/11707429 [Accessed May 27, 2017].

Marchetto, M.C. et al., 2016. Altered proliferation and networks in neural cells derived from idiopathic autistic individuals. *Molecular Psychiatry*. Available at: http://www.nature.com/doifinder/10.1038/mp.2016.95 [Accessed January 27, 2017].

Marchetto, M.C.N. et al., 2010. A model for neural development and treatment of Rett syndrome using human induced pluripotent stem cells. *Cell*, 143(4), pp.527–39. Available at: http://www.pubmedcentral.nih.gov/articlerender.fcgi?artid=3003590&tool=pmcentrez&rendertype=abstract [Accessed July 9, 2014].

Marder, K. et al., 2015. Age-specific penetrance of *LRRK2* G2019S in the Michael J. Fox Ashkenazi Jewish LRRK2 Consortium. *Neurology*, 85(1), pp.89–95. Available at: http://www.ncbi.nlm.nih.gov/pubmed/26062626 [Accessed February 20, 2017].

Marks, W.J. et al., 2010. Gene delivery of AAV2-neurturin for Parkinson's disease: a double-blind, randomised, controlled trial. *The Lancet. Neurology*, 9(12), pp.1164–72. Available at: http://www.ncbi.nlm.nih.gov/pubmed/20970382 [Accessed June 11, 2017].

Martin, I. et al., 2014. Ribosomal Protein s15 Phosphorylation Mediates LRRK2 Neurodegeneration in Parkinson's Disease. *Cell*, 157(2), pp.472–485. Available at: http://www.ncbi.nlm.nih.gov/pubmed/24725412 [Accessed May 22, 2017].

Masliah, E. et al., 2000. Dopaminergic Loss and Inclusion Body Formation in α-Synuclein Mice: Implications for Neurodegenerative Disorders. *Science*, 287(5456). Available at: http://science.sciencemag.org.sire.ub.edu/content/287/5456/1265.full [Accessed May 28, 2017].

Matikainen-Ankney, B.A. et al., 2016. Altered Development of Synapse Structure and Function in Striatum Caused by Parkinson's Disease-Linked LRRK2-G2019S Mutation. *Journal of Neuroscience*, 36(27), pp.7128–7141. Available at: http://www.ncbi.nlm.nih.gov/pubmed/27383589 [Accessed May 29, 2017].

Matsuoka, Y. et al., 2001. *Lack of Nigral Pathology in Transgenic Mice Expressing Human α-Synuclein Driven by the Tyrosine Hydroxylase Promoter*, Available at: http://www.sciencedirect.com.sire.ub.edu/science/article/pii/S0969996101903924 [Accessed May 29, 2017].

Matta, S. et al., 2012. LRRK2 Controls an EndoA Phosphorylation Cycle in Synaptic Endocytosis. *Neuron*, 75(6), pp.1008–1021. Available at: http://www.ncbi.nlm.nih.gov/pubmed/22998870 [Accessed May 20, 2017].

Mazzulli, J.R. et al., 2011. Gaucher disease glucocerebrosidase and α-synuclein form a bidirectional pathogenic loop in synucleinopathies. *Cell*, 146(1), pp.37–52. Available at: http://www.ncbi.nlm.nih.gov/pubmed/21700325 [Accessed January 23, 2017].

McKeran, R.O. et al., 1985. Neurological involvement in type 1 (adult) Gaucher's disease. *Journal of neurology, neurosurgery, and psychiatry*, 48(2), pp.172–5. Available at: http://www.ncbi.nlm.nih.gov/pubmed/3981177 [Accessed January 20, 2017].

McNeill, A. et al., 2012. A clinical and family history study of Parkinson's disease in heterozygous glucocerebrosidase mutation carriers. *Journal of neurology, neurosurgery, and psychiatry*, 83(8), pp.853–4. Available at: http://www.ncbi.nlm.nih.gov/pubmed/22577228 [Accessed June 1, 2017].

McNeill, A. et al., 2014. Ambroxol improves lysosomal biochemistry in glucocerebrosidase mutation-linked Parkinson disease cells. *Brain*, 137(5), pp.1481–1495. Available at: http://www.ncbi.nlm.nih.gov/pubmed/24574503 [Accessed June 4, 2017].

Mendez, I. et al., 2008. Dopamine neurons implanted into people with Parkinson's disease survive without pathology for 14 years. *Nature Medicine*, 14(5), pp.507–509. Available at: http://www.ncbi.nlm.nih.gov/pubmed/18391961 [Accessed May 28, 2017].

Mertens, J. et al., 2017. Directly Reprogrammed Human Neurons Retain Aging-Associated Transcriptomic Signatures and Reveal Age-Related Nucleocytoplasmic Defects. *Cell Stem Cell*, 17(6), pp.705–718. Available at: http://dx.doi.org/10.1016/j.stem.2015.09.001.

Migdalska-Richards, A. et al., 2016. Ambroxol effects in glucocerebrosidase and α-synuclein transgenic mice. *Annals of Neurology*, 80(5), pp.766–775. Available at: http://www.ncbi.nlm.nih.gov/pubmed/27859541 [Accessed June 4, 2017].

Miller, G.W., 2007. Paraquat: The Red Herring of Parkinson's Disease Research. *Toxicological Sciences*, 100(1), pp.1–2. Available at: https://academic.oup.com/toxsci/article/1627080/Paraquat: [Accessed May 27, 2017].

Mittermeyer, G. et al., 2012. Long-Term Evaluation of a Phase 1 Study of AADC Gene Therapy for Parkinson's Disease. *Human Gene Therapy*, 23(4), pp.377–381. Available at: http://online.liebertpub.com/doi/abs/10.1089/hum.2011.220 [Accessed June 11, 2017].

Mok, K.Y. et al., 2016. Deletions at 22q11.2 in idiopathic Parkinson's disease: a combined analysis of genome-wide association data. *The Lancet Neurology*, 15(6), pp.585–596. Available at: http://www.ncbi.nlm.nih.gov/pubmed/27017469 [Accessed May 31, 2017].

Moratalla, R. et al., 1992. Differential vulnerability of primate caudate-putamen and striosome-matrix dopamine systems to the neurotoxic effects of 1-methyl-4-phenyl-1,2,3,6-tetrahydropyridine. *Neurobiology*, 89, pp.3859–3863. Available at: http://www.pnas.org/content/89/9/3859.long [Accessed May 27, 2017].

Morens, D.M., White, L.R. & Davis, J.W., 1996. RE: "THE FREQUENCY OF IDIOPATHIC PARKINSON'S DISEASE BY AGE, ETHNIC GROUP, AND SEX IN NORTHERN MANHATTAN, 1988-1993" *American Journal of Epidemiology*, 144(2), pp.198–198. Available at: https://academic.oup.com/aje/article-lookup/doi/10.1093/oxfordjournals.aje.a008909 [Accessed May 3, 2017].

Morizane, A. et al., 2013. Direct Comparison of Autologous and Allogeneic Transplantation of iPSC-Derived Neural Cells in the Brain of a Nonhuman Primate. *Stem Cell Reports*, 1(4), pp.283–292. Available at: http://linkinghub.elsevier.com/retrieve/pii/S2213671113000738 [Accessed June 8, 2017].

Muñoz, E. et al., 1997. Identification of Spanish familial Parkinson's disease and screening for the Ala53Thr mutation of the alpha-synuclein gene in early onset patients. *Neuroscience letters*, 235(1-2), pp.57–60. Available at: http://www.ncbi.nlm.nih.gov/pubmed/9389595 [Accessed May 4, 2017].

Mussolino, C. et al., 2011. A novel TALE nuclease scaffold enables high genome editing activity in combination with low toxicity. *Nucleic Acids Research* , 39 (21), pp.9283–9293. Available at: http://nar.oxfordjournals.org/content/39/21/9283.abstract.

Mussolino, C. & Cathomen, T., 2012. TALE nucleases: tailored genome engineering made easy. *Current opinion in biotechnology*, 23(5), pp.644–50. Available at:

http://www.sciencedirect.com/science/article/pii/S0958166912000286 [Accessed July 14, 2014].

Naldini, L. et al., 1996. In vivo gene delivery and stable transduction of post mitotic cells by a lentiviral vector. *Science*, 272(5259), pp.263–267.

Nalls, M.A. et al., 2015. Genetic risk and age in Parkinson's disease: Continuum not stratum. *Movement disorders : official journal of the Movement Disorder Society*, 30(6), pp.850–4. Available at: http://doi.wiley.com/10.1002/mds.26192 [Accessed May 7, 2017].

Nalls, M.A. et al., 2014a. Large-scale meta-analysis of genome-wide association data identifies six new risk loci for Parkinson's disease. *Nature Genetics*, 46(9), pp.989–993.

Nalls, M.A. et al., 2014b. Large-scale meta-analysis of genome-wide association data identifies six new risk loci for Parkinson's disease. *Nature genetics*, 46(9), pp.989–93. Available at: http://www.ncbi.nlm.nih.gov/pubmed/25064009 [Accessed July 19, 2016].

Narendra, D.P. et al., 2010. PINK1 Is Selectively Stabilized on Impaired Mitochondria to Activate Parkin D. R. Green, ed. *PLoS Biology*, 8(1), p.e1000298. Available at: http://www.ncbi.nlm.nih.gov/pubmed/20126261 [Accessed May 17, 2017].

Nichols, W.C. et al., 2004. Genetic screening for a single common LRRK2 mutation in familial Parkinson's disease. *Lancet (London, England)*, 365(9457), pp.410–2. Available at: http://www.ncbi.nlm.nih.gov/pubmed/15680455 [Accessed May 4, 2017].

Noyce, A.J. et al., 2017. PREDICT-PD: An online approach to prospectively identify risk indicators of Parkinson's disease. *Movement Disorders*, 32(2), pp.219–226. Available at: http://www.ncbi.nlm.nih.gov/pubmed/28090684 [Accessed June 11, 2017].

Obeso, J.A. et al., 2010. Missing pieces in the Parkinson's disease puzzle. *Nat Med*, 16(6), pp.653–661. Available at: http://dx.doi.org/10.1038/nm.2165.

Obeso, J.A. et al., 2014. The expanding universe of disorders of the basal ganglia. *The Lancet*, 384(9942), pp.523–531. Available at: http://www.sciencedirect.com.sire.ub.edu/science/article/pii/S0140673613624186 [Accessed May 14, 2017].

Okita, K., Ichisaka, T. & Yamanaka, S., 2007. Generation of germline-competent induced pluripotent stem cells. *Nature*, 448(7151), pp.313–317. Available at: http://www.nature.com/doifinder/10.1038/nature05934 [Accessed May 30, 2017].

Olanow, C.W. et al., 2003. A double-blind controlled trial of bilateral fetal nigral transplantation in Parkinson's disease. *Annals of Neurology*, 54(3), pp.403–414. Available at: http://dx.doi.org/10.1002/ana.10720.

Olanow, C.W. & Prusiner, S.B., 2009. Is Parkinson's disease a prion disorder? *Proceedings of the National Academy of Sciences of the United States of America*, 106(31), pp.12571–2. Available at: http://www.ncbi.nlm.nih.gov/pubmed/19666621 [Accessed May 28, 2017].

Orenstein, S.J. et al., 2013. Interplay of LRRK2 with chaperone-mediated autophagy. *Nature Neuroscience*, 16(4), pp.394–406. Available at: http://www.ncbi.nlm.nih.gov/pubmed/23455607 [Accessed May 20, 2017].

Pacelli, C. et al., 2015. Elevated Mitochondrial Bioenergetics and Axonal Arborization Size Are Key Contributors to the Vulnerability of Dopamine Neurons. *Current Biology*, 25(18), pp.2349–2360. Available at: http://www.ncbi.nlm.nih.gov/pubmed/26320949 [Accessed May 17, 2017].

Paisán-Ruíz, C. et al., 2004. Cloning of the gene containing mutations that cause PARK8-linked Parkinson's disease. *Neuron*, 44(4), pp.595–600. Available at:

http://www.ncbi.nlm.nih.gov/pubmed/15541308 [Accessed January 16, 2017].

Palfi, S. et al., 2014. Long-term safety and tolerability of ProSavin, a lentiviral vector-based gene therapy for Parkinson's disease: a dose escalation, open-label, phase 1/2 trial. *The Lancet*, 383(9923), pp.1138–1146. Available at: http://linkinghub.elsevier.com/retrieve/pii/S014067361361939X [Accessed June 11, 2017].

Paquet, D. et al., 2016. Efficient introduction of specific homozygous and heterozygous mutations using CRISPR/Cas9. *Nature*, 533(7601), pp.125–9. Available at: http://www.ncbi.nlm.nih.gov/pubmed/27120160 [Accessed July 20, 2016].

Parisiadou, L. et al., 2014. LRRK2 regulates synaptogenesis and dopamine receptor activation through modulation of PKA activity. *Nature neuroscience*, 17(3), pp.367–76. Available at: http://www.pubmedcentral.nih.gov/articlerender.fcgi?artid=3989289&tool=pmcentrez&rendertype=abstract [Accessed September 19, 2014].

Park, B.-C. et al., 2015. The clathrin-binding and J-domains of GAK support the uncoating and chaperoning of clathrin by Hsc70 in the brain. *Journal of Cell Science*, 128(20), pp.3811–3821. Available at: http://www.ncbi.nlm.nih.gov/pubmed/26345367 [Accessed May 19, 2017].

Park, J. et al., 2006. Mitochondrial dysfunction in Drosophila PINK1 mutants is complemented by parkin. *Nature*, 441(7097), pp.1157–1161. Available at: http://www.ncbi.nlm.nih.gov/pubmed/16672980 [Accessed May 17, 2017].

Parkinson, J., 2002. An Essay on the Shaking Palsy. *The Journal of Neuropsychiatry and Clinical Neurosciences*, 14(2), pp.223–236. Available at: http://www.ncbi.nlm.nih.gov/pubmed/11983801 [Accessed May 31, 2017].

Pei, Y. et al., 2015. A platform for rapid generation of single and multiplexed reporters in human iPSC lines. *Scientific Reports*, 5, p.9205.

Peñas Domingo, E. et al., 2015. El libro blanco del Párkinson en España. Aproximación, anáisis y propuesta de futuro. *Federación Española de Párkinson*. Available at: http://www.fedesparkinson.org/libro_blanco.pdf [Accessed May 31, 2017].

Pezzoli, G. & Cereda, E., 2013. Exposure to pesticides or solvents and risk of Parkinson disease. *Neurology*, 80(22), pp.2035–2041.

Piccini, P. et al., 2005. Factors affecting the clinical outcome after neural transplantation in Parkinson's disease. *Brain*, 128(12), pp.2977–2986. Available at: https://academic.oup.com/brain/article-lookup/doi/10.1093/brain/awh649 [Accessed June 8, 2017].

Pihlstrøm, L. et al., 2015. Fine mapping and resequencing of the PARK16 locus in Parkinson's disease. *Journal of Human Genetics*, 60(7), pp.357–362. Available at: http://www.ncbi.nlm.nih.gov/pubmed/25855069 [Accessed January 23, 2017].

Plowey, E.D. et al., 2008. Role of autophagy in G2019S-LRRK2-associated neurite shortening in differentiated SH-SY5Y cells. *Journal of Neurochemistry*, 105(3), pp.1048–1056. Available at: http://www.ncbi.nlm.nih.gov/pubmed/18182054 [Accessed May 20, 2017].

Politis, M. et al., 2012. Serotonin Neuron Loss and Nonmotor Symptoms Continue in Parkinson's Patients Treated with Dopamine Grafts. *Science Translational Medicine* , 4 (128), pp.128ra41–128ra41. Available at: http://stm.sciencemag.org/content/4/128/128ra41.abstract.

Prusiner, S.B. et al., 2015. Evidence for α-synuclein prions causing multiple system atrophy in humans with parkinsonism. *Proceedings of the National Academy of Sciences of the United States of America*, 112(38), pp.E5308–17. Available at: http://www.ncbi.nlm.nih.gov/pubmed/26324905

[Accessed June 11, 2017].

Puschmann, A. et al., 2017. Heterozygous PINK1 p.G411S increases risk of Parkinson's disease via a dominant-negative mechanism. *Brain*, 140(1), pp.98–117. Available at: http://www.ncbi.nlm.nih.gov/pubmed/27807026 [Accessed May 16, 2017].

van der Putten, H. et al., 2000. Neuropathology in mice expressing human alpha-synuclein. *The Journal of neuroscience : the official journal of the Society for Neuroscience*, 20(16), pp.6021–9. Available at: http://www.ncbi.nlm.nih.gov/pubmed/10934251 [Accessed May 29, 2017].

Quadri, M. et al., 2013. Mutation in the *SYNJ1* Gene Associated with Autosomal Recessive, Early-Onset Parkinsonism. *Human Mutation*, 34(9), pp.1208–1215. Available at: http://doi.wiley.com/10.1002/humu.22373 [Accessed May 20, 2017].

Ramirez, A. et al., 2006. Hereditary parkinsonism with dementia is caused by mutations in ATP13A2, encoding a lysosomal type 5 P-type ATPase. *Nature Genetics*, 38(10), pp.1184–1191. Available at: http://www.nature.com/doifinder/10.1038/ng1884 [Accessed January 16, 2017].

Ramonet, D. et al., 2011. Dopaminergic Neuronal Loss, Reduced Neurite Complexity and Autophagic Abnormalities in Transgenic Mice Expressing G2019S Mutant LRRK2 H. Cai, ed. *PLoS ONE*, 6(4), p.e18568. Available at: http://www.ncbi.nlm.nih.gov/pubmed/21494637 [Accessed May 21, 2017].

Ran, F.A. et al., 2013. Genome engineering using the CRISPR-Cas9 system. *Nat. Protocols*, 8(11), pp.2281–2308. Available at: http://dx.doi.org/10.1038/nprot.2013.143.

Raya, A. et al., 2008. Generation of cardiomyocytes from new human embryonic stem cell lines derived from poor-quality blastocysts. *Cold Spring Harbor symposia on quantitative biology*, 73(0), pp.127–35. Available at: http://symposium.cshlp.org/cgi/doi/10.1101/sqb.2008.73.038 [Accessed June 12, 2017].

Recasens, A. et al., 2014. Lewy body extracts from Parkinson disease brains trigger α-synuclein pathology and neurodegeneration in mice and monkeys. *Annals of Neurology*, 75(3), pp.351–362. Available at: http://doi.wiley.com/10.1002/ana.24066 [Accessed May 28, 2017].

Reinhardt, P. et al., 2013. Genetic correction of a lrrk2 mutation in human iPSCs links parkinsonian neurodegeneration to ERK-dependent changes in gene expression. *Cell Stem Cell*, 12(3), pp.354–367. Available at: http://www.ncbi.nlm.nih.gov/pubmed/23472874 [Accessed July 20, 2016].

Rey, N.L. et al., 2016. Widespread transneuronal propagation of α-synucleinopathy triggered in olfactory bulb mimics prodromal Parkinson's disease. *The Journal of Experimental Medicine*, 213(9), pp.1759–1778. Available at: http://www.jem.org/lookup/doi/10.1084/jem.20160368 [Accessed May 28, 2017].

Richardson, C.D. et al., 2016. Enhancing homology-directed genome editing by catalytically active and inactive CRISPR-Cas9 using asymmetric donor DNA. *Nature biotechnology*, 34(3), pp.339–44. Available at: http://www.nature.com/doifinder/10.1038/nbt.3481 [Accessed June 12, 2017].

Robak, L. et al., 2017. *Excessive burden of lysosomal storage disorder gene variants in Parkinson's disease (S1.001)*, Advanstar Communications. Available at: http://www.neurology.org/content/88/16_Supplement/S1.001 [Accessed May 31, 2017].

Rothaug, M. et al., 2014. LIMP-2 expression is critical for -glucocerebrosidase activity and -synuclein clearance. *Proceedings of the National Academy of Sciences*, 111(43), pp.15573–15578. Available at: http://www.ncbi.nlm.nih.gov/pubmed/25316793 [Accessed June 4, 2017].

Rouet, P., Smih, F. & Jasin, M., 1994. Expression of a site-specific endonuclease stimulates homologous recombination in mammalian cells. *Proceedings of the National Academy of Sciences*

of the United States of America, 91(13), pp.6064–8. Available at: http://www.ncbi.nlm.nih.gov/pubmed/8016116 [Accessed July 18, 2016].

Rouhani, F. et al., 2014. Genetic Background Drives Transcriptional Variation in Human Induced Pluripotent Stem Cells G. Gibson, ed. *PLoS Genetics*, 10(6), p.e1004432.

Rousseaux, M.W. et al., 2016. TRIM28 regulates the nuclear accumulation and toxicity of both alpha-synuclein and tau. *eLife*, 5. Available at: http://elifesciences.org/lookup/doi/10.7554/eLife.19809 [Accessed May 21, 2017].

Sacino, A.N. et al., 2014. Intramuscular injection of α-synuclein induces CNS α-synuclein pathology and a rapid-onset motor phenotype in transgenic mice. *Proceedings of the National Academy of Sciences* , 111 (29), pp.10732–10737. Available at: http://www.pnas.org/content/111/29/10732.abstract.

Sánchez-Danés, A. et al., 2012. Disease-specific phenotypes in dopamine neurons from human iPS-based models of genetic and sporadic Parkinson's disease. *EMBO molecular medicine*, 4(5), pp.380–95. Available at: http://www.pubmedcentral.nih.gov/articlerender.fcgi?artid=3403296&tool=pmcentrez&rendertype=abstract [Accessed September 22, 2014].

Sánchez-Danés, A. et al., 2012. Efficient Generation of A9 Midbrain Dopaminergic Neurons by Lentiviral Delivery of LMX1A in Human Embryonic Stem Cells and Induced Pluripotent Stem Cells. *Human Gene Therapy*, 23(1), pp.56–69. Available at: http://www.ncbi.nlm.nih.gov/pubmed/21877920 [Accessed April 7, 2017].

Sánchez-Danés, A. et al., 2012. Disease-specific phenotypes in dopamine neurons from human iPS-based models of genetic and sporadic Parkinson's disease. *EMBO Molecular Medicine*, 4(5), pp.380–395. Available at: http://embomolmed.embopress.org/content/4/5/380.abstract.

Satake, W. et al., 2009. Genome-wide association study identifies common variants at four loci as genetic risk factors for Parkinson's disease. *Nature Genetics*, 41(12), pp.1303–1307. Available at: http://www.nature.com/doifinder/10.1038/ng.485 [Accessed May 7, 2017].

Saunders-Pullman, R. et al., 2015. REM sleep behavior disorder, as assessed by questionnaire, in G2019S LRRK2 mutation PD and carriers. *Movement Disorders*, 30(13), pp.1834–1839. Available at: http://doi.wiley.com/10.1002/mds.26413 [Accessed May 15, 2017].

Scott, W.K. et al., 1997. Genetic complexity and Parkinson's disease. Deane Laboratory Parkinson Disease Research Group. *Science (New York, N.Y.)*, 277(5324), pp.387–8; author reply 389. Available at: http://www.ncbi.nlm.nih.gov/pubmed/9518366 [Accessed May 4, 2017].

Seaman, M.N.J., Gautreau, A. & Billadeau, D.D., 2013. Retromer-mediated endosomal protein sorting: all WASHed up! *Trends in cell biology*, 23(11), pp.522–8. Available at: http://www.ncbi.nlm.nih.gov/pubmed/23721880 [Accessed May 20, 2017].

Seidel, K. et al., 2015. The brainstem pathologies of Parkinson's disease and dementia with Lewy bodies. *Brain pathology (Zurich, Switzerland)*, 25(2), pp.121–35. Available at: http://www.ncbi.nlm.nih.gov/pubmed/24995389 [Accessed May 24, 2017].

Seniuk, N.A., Tatton, W.G. & Greenwood, C.E., 1990. *Dose-dependent destruction of the coeruleus-cortical and nigral-striatal projections by MPTP*, Available at: http://www.sciencedirect.com.sire.ub.edu/science/article/pii/000689939091055L [Accessed May 27, 2017].

Shaner, N.C. et al., 2004. Improved monomeric red, orange and yellow fluorescent proteins derived

from Discosoma sp. red fluorescent protein. *Nature Biotechnology*, 22(12), pp.1567–1572. Available at: http://www.nature.com/doifinder/10.1038/nbt1037 [Accessed June 12, 2017].

Shendelman, S. et al., 2004. DJ-1 Is a Redox-Dependent Molecular Chaperone That Inhibits α-Synuclein Aggregate Formation Huda Y. Zoghbi, ed. *PLoS Biology*, 2(11), p.e362. Available at: http://www.ncbi.nlm.nih.gov/pubmed/15502874 [Accessed May 17, 2017].

Shimoji, M. et al., 2005. Absence of inclusion body formation in the MPTP mouse model of Parkinson's disease. *Molecular Brain Research*, 134(1), pp.103–108. Available at: http://www.ncbi.nlm.nih.gov/pubmed/15790534 [Accessed May 27, 2017].

Shojaee, S. et al., 2008. Genome-wide Linkage Analysis of a Parkinsonian-Pyramidal Syndrome Pedigree by 500 K SNP Arrays. *The American Journal of Human Genetics*, 82(6), pp.1375–1384. Available at: http://dx.doi.org/10.1016/j.ajhg.2008.05.005.

Sidransky, E. et al., 2009. Multicenter analysis of glucocerebrosidase mutations in Parkinson's disease. *The New England journal of medicine*, 361(17), pp.1651–61. Available at: http://www.ncbi.nlm.nih.gov/pubmed/19846850 [Accessed January 20, 2017].

Sierra, M. et al., 2011. High frequency and reduced penetrance of lRRK2 g2019S mutation among Parkinson's disease patients in Cantabria (Spain). *Movement Disorders*, 26(13), pp.2343–2346. Available at: http://dx.doi.org/10.1002/mds.23965.

Sierra, M. et al., 2013. Olfaction and imaging biomarkers in premotor LRRK2 G2019S-associated Parkinson disease. *Neurology*, 80(7), pp.621–6. Available at: http://www.ncbi.nlm.nih.gov/pubmed/23325906 [Accessed May 15, 2017].

Simón-Sánchez, J. et al., 2009. Genome-wide association study reveals genetic risk underlying Parkinson's disease. *Nature Genetics*, 41(12), pp.1308–1312. Available at: http://www.nature.com/doifinder/10.1038/ng.487 [Accessed January 17, 2017].

Singleton, A.B. et al., 2003. α-Synuclein Locus Triplication Causes Parkinson's Disease. *Science* , 302 (5646), p.841. Available at: http://www.sciencemag.org/content/302/5646/841.short.

Soldner, F. et al., 2016. Parkinson-associated risk variant in distal enhancer of α-synuclein modulates target gene expression. *Nature*, 533(7601), pp.95–99.

Sole, X. et al., 2006. SNPStats: a web tool for the analysis of association studies. *Bioinformatics*, 22(15), pp.1928–1929. Available at: http://www.ncbi.nlm.nih.gov/pubmed/16720584 [Accessed June 9, 2017].

Soukup, S.-F. et al., 2016. A LRRK2-Dependent EndophilinA Phosphoswitch Is Critical for Macroautophagy at Presynaptic Terminals. *Neuron*, 92(4), pp.829–844. Available at: http://www.ncbi.nlm.nih.gov/pubmed/27720484 [Accessed May 20, 2017].

Spataro, N. et al., 2015. Mendelian genes for Parkinson's disease contribute to the sporadic forms of the disease†. *Human Molecular Genetics*, 24(7), pp.2023–2034. Available at: https://academic.oup.com/hmg/article-lookup/doi/10.1093/hmg/ddu616 [Accessed May 22, 2017].

Spiegel, J. et al., 2006. Transcranial sonography and [123I]FP-CIT SPECT disclose complementary aspects of Parkinson's disease. *Brain*, 129(5), pp.1188–1193. Available at: http://www.ncbi.nlm.nih.gov/pubmed/16513685 [Accessed June 4, 2017].

Spillantini, M.G. et al., 1997. [alpha]-Synuclein in Lewy bodies. *Nature*, 388(6645), pp.839–840.

Steger, M. et al., 2016. Phosphoproteomics reveals that Parkinson's disease kinase LRRK2 regulates a subset of Rab GTPases. *eLife*, 5. Available at: http://www.ncbi.nlm.nih.gov/pubmed/26824392 [Accessed May 19, 2017].

Su, Y.-C. & Qi, X., 2013. Inhibition of excessive mitochondrial fission reduced aberrant autophagy and neuronal damage caused by LRRK2 G2019S mutation. *Human Molecular Genetics*, 22(22), pp.4545–4561. Available at: https://academic.oup.com/hmg/article-lookup/doi/10.1093/hmg/ddt301 [Accessed June 12, 2017].

Sumikura, H. et al., 2015. Distribution of α-synuclein in the spinal cord and dorsal root ganglia in an autopsy cohort of elderly persons. *Acta neuropathologica communications*, 3, p.57. Available at: http://www.ncbi.nlm.nih.gov/pubmed/26374630 [Accessed May 24, 2017].

Surmeier, D.J., Obeso, J.A. & Halliday, G.M., 2017. Selective neuronal vulnerability in Parkinson disease. *Nature Reviews Neuroscience*, 18(2), pp.101–113. Available at: http://www.ncbi.nlm.nih.gov/pubmed/28104909 [Accessed May 2, 2017].

Takahashi, K. et al., 2007. Induction of Pluripotent Stem Cells from Adult Human Fibroblasts by Defined Factors. *Cell*, 131(5), pp.861–872. Available at: http://www.ncbi.nlm.nih.gov/pubmed/18035408 [Accessed May 30, 2017].

Takahashi, K. et al., 2006. Induction of pluripotent stem cells from mouse embryonic and adult fibroblast cultures by defined factors. *Cell*, 126(4), pp.663–76.

Takahashi, K. & Yamanaka, S., 2006. Induction of pluripotent stem cells from mouse embryonic and adult fibroblast cultures by defined factors. *Cell*, 126(4), pp.663–76. Available at: http://www.ncbi.nlm.nih.gov/pubmed/16904174 [Accessed July 9, 2014].

Tanner, C.M. et al., 1999. Parkinson disease in twins: an etiologic study. *JAMA*, 281(4), pp.341–6. Available at: http://www.ncbi.nlm.nih.gov/pubmed/9929087 [Accessed May 4, 2017].

Thiruchelvam, M.J. et al., 2004. Risk factors for dopaminergic neuron loss in human α-synuclein transgenic mice. *European Journal of Neuroscience*, 19(4), pp.845–854. Available at: http://doi.wiley.com/10.1111/j.0953-816X.2004.03139.x [Accessed May 29, 2017].

Tong, Y. et al., 2010. Loss of leucine-rich repeat kinase 2 causes impairment of protein degradation pathways, accumulation of -synuclein, and apoptotic cell death in aged mice. *Proceedings of the National Academy of Sciences*, 107(21), pp.9879–9884. Available at: http://www.ncbi.nlm.nih.gov/pubmed/20457918 [Accessed May 29, 2017].

Trinh, J. et al., 2017. DNM3 and genetic modifiers of age of onset in LRRK2 Gly2019Ser parkinsonism: a genome-wide linkage and association study. *The Lancet Neurology*, 15(12), pp.1248–1256. Available at: http://dx.doi.org/10.1016/S1474-4422(16)30203-4.

Trinh, J. & Farrer, M., 2013. Advances in the genetics of Parkinson disease. *Nature Reviews Neurology*, 9(8), pp.445–454. Available at: http://www.nature.com/doifinder/10.1038/nrneurol.2013.132 [Accessed May 5, 2017].

Trinh, J., Vilariño-Güell, C. & Ross, O.A., 2015. A commentary on fine mapping and resequencing of the PARK16 locus in Parkinson's disease. *Journal of Human Genetics*, 60(8), pp.405–406. Available at: http://www.nature.com/doifinder/10.1038/jhg.2015.76 [Accessed May 14, 2017].

Tsika, E. et al., 2015. Adenoviral-mediated expression of G2019S LRRK2 induces striatal pathology in a kinase-dependent manner in a rat model of Parkinson's disease. *Neurobiology of Disease*, 77, pp.49–61. Available at: http://www.ncbi.nlm.nih.gov/pubmed/25731749 [Accessed May 22, 2017].

Ungerstedt, U., 1968. 6-Hydroxy-dopamine induced degeneration of central monoamine neurons. *European journal of pharmacology*, 5(1), pp.107–10. Available at: http://www.ncbi.nlm.nih.gov/pubmed/5718510 [Accessed May 27, 2017].

Valente, E.M. et al., 2004. Hereditary Early-Onset Parkinson's Disease Caused by Mutations in PINK1.

Science, 304(5674).

Vanhauwaert, R. et al., 2017. The SAC1 domain in synaptojanin is required for autophagosome maturation at presynaptic terminals. *The EMBO Journal*, 36(10), pp.1392–1411. Available at: http://emboj.embopress.org/lookup/doi/10.15252/embj.201695773 [Accessed May 20, 2017].

Vaughan, J. et al., 1998. The ?-synuclein Ala53Thr mutation is not a common cause of familial Parkinson's disease: A study of 230 European cases. *Annals of Neurology*, 44(2), pp.270–273. Available at: http://www.ncbi.nlm.nih.gov/pubmed/9708553 [Accessed May 4, 2017].

Velayati, A. et al., 2011. A mutation in SCARB2 is a modifier in gaucher disease. *Human Mutation*, 32(11), pp.1232–1238. Available at: http://www.ncbi.nlm.nih.gov/pubmed/21796727 [Accessed June 4, 2017].

Vermunt, M.W. et al., 2014. Large-Scale Identification of Coregulated Enhancer Networks in the Adult Human Brain. *Cell Reports*, 9(2), pp.767–779. Available at: http://www.ncbi.nlm.nih.gov/pubmed/25373911 [Accessed June 4, 2017].

Vilariño-Güell, C. et al., 2014. DNAJC13 mutations in Parkinson disease. *Human Molecular Genetics*, 23(7), pp.1794–1801. Available at: https://academic.oup.com/hmg/article-lookup/doi/10.1093/hmg/ddt570 [Accessed May 6, 2017].

Vilariño-Güell, C. et al., 2011. VPS35 Mutations in Parkinson Disease. *The American Journal of Human Genetics*, 89(1), pp.162–167. Available at: http://www.ncbi.nlm.nih.gov/pubmed/21763482 [Accessed May 6, 2017].

Vives-Bauza, C. et al., 2010. PINK1-dependent recruitment of Parkin to mitochondria in mitophagy. *Proceedings of the National Academy of Sciences of the United States of America*, 107(1), pp.378–83. Available at: http://www.ncbi.nlm.nih.gov/pubmed/19966284 [Accessed May 17, 2017].

Volakakis, N. et al., 2015. Nurr1 and Retinoid X Receptor Ligands Stimulate Ret Signaling in Dopamine Neurons and Can Alleviate -Synuclein Disrupted Gene Expression. *Journal of Neuroscience*, 35(42), pp.14370–14385. Available at: http://www.ncbi.nlm.nih.gov/pubmed/26490873 [Accessed May 29, 2017].

Watmuff, B. et al., 2015. Human pluripotent stem cell derived midbrain PITX3(eGFP/w) neurons: a versatile tool for pharmacological screening and neurodegenerative modeling. *Frontiers in cellular neuroscience*, 9, p.104.

Woodard, C.M. et al., 2014. iPSC-Derived Dopamine Neurons Reveal Differences between Monozygotic Twins Discordant for Parkinson's Disease. *Cell Reports*, 9(4), pp.1173–1182. Available at: http://www.cell.com/cell-reports/abstract/S2211-1247(14)00877-8.

Yamada-Fowler, N. et al., 2014. Caffeine Interaction with Glutamate Receptor Gene GRIN2A: Parkinson's Disease in Swedish Population V. Grolmusz, ed. *PLoS ONE*, 9(6), p.e99294. Available at: http://dx.plos.org/10.1371/journal.pone.0099294 [Accessed June 16, 2017].

Yin, H. et al., 2014. Non-viral vectors for gene-based therapy. *Nature Reviews Genetics*, 15(8), pp.541–555. Available at: http://www.nature.com/doifinder/10.1038/nrg3763 [Accessed June 12, 2017].

Yoon, K.-J. et al., 2014. Modeling a Genetic Risk for Schizophrenia in iPSCs and Mice Reveals Neural Stem Cell Deficits Associated with Adherens Junctions and Polarity. *Cell Stem Cell*, 15(1), pp.79–91. Available at: http://linkinghub.elsevier.com/retrieve/pii/S1934590914001908 [Accessed August 17, 2016].

Young, J.E. et al., 2015. Elucidating molecular phenotypes caused by the SORL1 Alzheimer's disease

genetic risk factor using human induced pluripotent stem cells. *Cell stem cell*, 16(4), pp.373–85.

Yu, J. et al., 2007. Induced Pluripotent Stem Cell Lines Derived from Human Somatic Cells. *Science*, 318(5858), pp.1917–1920. Available at: http://www.ncbi.nlm.nih.gov/pubmed/18029452 [Accessed May 30, 2017].

Zarranz, J.J. et al., 2004. The new mutation, E46K, of α-synuclein causes parkinson and Lewy body dementia. *Annals of Neurology*, 55(2), pp.164–173. Available at: http://doi.wiley.com/10.1002/ana.10795 [Accessed May 4, 2017].

Zavodszky, E. et al., 2014. Mutation in VPS35 associated with Parkinson's disease impairs WASH complex association and inhibits autophagy. *Nature communications*, 5(May), p.3828. Available at: http://www.pubmedcentral.nih.gov/articlerender.fcgi?artid=4024763&tool=pmcentrez&rendertype=abstract [Accessed November 27, 2014].

Zhang, F.-R. et al., 2009. Genomewide Association Study of Leprosy. *New England Journal of Medicine*, 361(27), pp.2609–2618. Available at: http://www.ncbi.nlm.nih.gov/pubmed/20018961 [Accessed May 27, 2017].

Zhang, Q. et al., 2015. Commensal bacteria direct selective cargo sorting to promote symbiosis. *Nature Immunology*, 16(9), pp.918–926. Available at: http://www.ncbi.nlm.nih.gov/pubmed/26237551 [Accessed May 29, 2017].

Zhao, X. et al., 2009. iPS cells produce viable mice through tetraploid complementation. *Nature*, 461(7260), pp.86–90. Available at: http://www.ncbi.nlm.nih.gov/pubmed/19672241 [Accessed May 30, 2017].

Zijdeman, R. & Ribeira da Silva, F., 2015. Life Expectancy at Birth (Total). Available at: http://hdl.handle.net/10622/LKYT53.

Zimprich, A. et al., 2011. A Mutation in VPS35, Encoding a Subunit of the Retromer Complex, Causes Late-Onset Parkinson Disease. *The American Journal of Human Genetics*, 89(1), pp.168–175. Available at: http://www.ncbi.nlm.nih.gov/pubmed/21763483 [Accessed May 6, 2017].

Zimprich, A. et al., 2004. Mutations in LRRK2 cause autosomal-dominant parkinsonism with pleomorphic pathology. *Neuron*, 44(4), pp.601–7. Available at: http://www.ncbi.nlm.nih.gov/pubmed/15541309 [Accessed January 16, 2017].

Zunke, F. et al., 2016. Characterization of the complex formed by β-glucocerebrosidase and the lysosomal integral membrane protein type-2. *Proceedings of the National Academy of Sciences*, 113(14), pp.3791–3796. Available at: http://www.ncbi.nlm.nih.gov/pubmed/27001828 [Accessed May 20, 2017].

ANNEXES

Annex I: Review article

Available online at www.sciencedirect.com

ScienceDirect

Current Opinion in Genetics & Development

Modeling the genetic complexity of Parkinson's disease by targeted genome edition in iPS cells

Carles Calatayud[1,2,3], Giulia Carola[2,3], Antonella Consiglio[2,3,4] and Angel Raya[1,5,6]

Patient-specific iPSC are being intensively exploited as experimental disease models. Even for late-onset diseases of complex genetic influence, such as Parkinson's disease (PD), the use of iPSC-based models is beginning to provide important insights into the genetic bases of PD heritability. Here, we present an update on recently reported genetic risk factors associated with PD. We discuss how iPSC technology, combined with targeted edition of the coding or noncoding genome, can be used to address clinical observations such as incomplete penetrance, and variability in phenoconversion or age-at-onset in familial PD. Finally, we also discuss the relevance of advanced iPSC/CRISPR/Cas9 disease models to ascertain causality in genotype-to-phenotype correlation studies of sporadic PD.

Addresses
[1] Center of Regenerative Medicine in Barcelona (CMRB), Hospital Duran i Reynals, 3rd Floor, Av. Gran Via 199-203, 08908 Hospitalet de Llobregat (Barcelona), Spain
[2] Institute of Biomedicine (IBUB) of the University of Barcelona (UB), 08028 Barcelona, Spain
[3] Department of Pathology and Experimental Therapeutics, School of Medicine, University of Barcelona, 08908 Barcelona, Spain
[4] Department of Molecular and Translational Medicine, University of Brescia and National Institute of Neuroscience, 25123 Brescia, Italy
[5] Center for Networked Biomedical Research on Bioengineering, Biomaterials and Nanomedicine (CIBER-BBN), 28029 Madrid, Spain
[6] Institució Catalana de Recerca i Estudis Avançats (ICREA), 08010 Barcelona, Spain

Corresponding authors: Consiglio, Antonella (aconsiglio@ibub.pcb.ub.es) and Raya, Angel (araya@cmrb.eu)

Current Opinion in Genetics & Development 2017, **46**:123–131
This review comes from a themed issue on **Cell reprogramming**
Edited by **Jianlong Wang** and **Miguel Esteban**

http://dx.doi.org/10.1016/j.gde.2017.06.002

iPSC-based modeling of human diseases

The groundbreaking discovery of induced pluripotent stem cells (iPSC) by Kazutoshi Takahashi and Shinya Yamanaka [1] is revolutionizing many aspects of biology and medicine. The ability to generate virtually unlimited amounts of patient-specific cells has opened new vistas for the design of cell replacement therapies and drug/toxicity testing, as well as for the creation of genuinely human models of disease (reviewed in [2,3]). In the case of disease modeling, the possibility of capturing the genetic peculiarities of a patient in a dish is changing the way in which genetic diseases may be approached. Monogenic diseases of early onset or congenital have proved to be especially amenable to iPSC-based modeling, as shown by the success of this strategy with dozens of diseases thus far (reviewed in [2,3]). In spite of the shortcomings of this approach, such as the relative simplicity of cell-based models and immaturity of iPSC-derivatives, the generation of disease-relevant cell types from patient-specific iPSC provides disease models that, in many cases, supersede previously available alternatives. In this way, it is now possible to recapitulate the onset and progression of diseases with a strong genetic contribution, in the specific cell type(s) affected by the disease, and having the precise genetic makeup (including mutations and variants) of the patients themselves. This is in sharp contrast with previously available animal-based or cell-based models, in which researchers most often had to choose either studying disease-relevant cells/tissues, or maintaining the patient's genetic complexity. Whereas iPSC-based models of monogenic, early-onset diseases appear relatively straightforward, modeling late-onset diseases of complex genetic influence is much more challenging [4], but potentially more rewarding as well. Successful efforts in this regard will be discussed below.

Limitations inherent to iPSC technology

Arguably, the single most important functional characteristic of pluripotent stem cells is their multi-lineage differentiation ability. It is widely accepted that iPSC present considerable variability in differentiation potential among lines derived, not only from different subjects, but also among clones from the same subject [5,6]. There have been several attempts to characterize the sources of such variability. Extensive passaging and maintenance of hESC has been shown to induce certain chromosomal alterations, in particular duplication of chromosomes 12 and 17 [7]. A separate study found that recurrent amplifications in the 17q21.31 chromosomal region specifically affected neural (mesodiencephalic) differentiation properties of hPSCs [8]. Age-related mutations of the reprogrammed somatic cells (blood cells, fibroblasts, etc.) could also be a source of genetic variation. We should take into account that, for many disease conditions, somatic

cell samples would be obtained from aged individuals. However, the most in-depth examination of iPSC variability sources comes from the studies of DeBoever *et al.* [9] and Carcamo-Orive *et al.* [10].

DeBoever *et al.* performed a genome-wide characterization of the eQTL present in a compilation of 215 iPSC genomes, and found that these influenced the transcription of nearby stem cell-related genes such as *NANOG* and *POU5F1*. In most of the cases, these eQTL, both SNV and indels, were located in putative transcription factor binding sites. The authors also observed that other types of polymorphisms, such as CNV and rare variants, also affected gene expression in these cells. This fact is interesting given that rare variants are more likely to arise during the reprogramming process or the subsequent cell culture expansion. In line with these findings, X chromosome reactivation was found to be not complete among the different lines, the extent of completion potentially representing an extra source of variation among iPSC lines [9].

Carcamo-Orive *et al.* pursued a similar approach using 317 iPSC lines from 101 individuals. The authors were able to ascribe ~50% of the variation found among different lines to inter-individual variation, associated to eQTL mostly controlling the expression of pluripotency-related genes [10]. They also identified the differential retention allelic imbalance at imprinted and other loci to be a source of inter-individual variability, since clones from the same individual displayed a more constant pattern. Regarding intra-individual variability, the authors found that it mostly affects gene networks related to differentiation processes. Network analysis identified targets of the Polycomb repressor complex as key drivers of those processes. Given that the role of this complex is of central importance for the erasure of somatic cell identity during reprogramming, the authors hypothesized that the reprogramming process is a primary determinant of both inter-individual and intra-individual variation [10]. In the light of these findings, controlling the sources of genetic variability would be of the utmost importance when it comes to study complex diseases in which the different genetic components confer relatively low risk.

The advent of CRISPR/Cas9

The aforementioned sources of variability may also complicate ascribing disease-related cellular phenotypes to specific genotypes. A straightforward manner to countering that variability would be to utilize (engineer) appropriate controls. In this regard, the use of designer nucleases as gene-editing tools enables researchers to generate isogenic controls that only differ in the presence of one (or more) genetic variants. The realization that DNA double strand breaks (DSB) enhance homology-directed repair (HDR) [11] opened a race for the generation of sequence-specific nucleases for the introduction of sequence-specific DSB. The first two sequence-specific nucleases to enter the scene, zinc-finger nucleases (ZFNs) and transcription activator-like effector nucleases (TALENs), were used by some highly skilled laboratories to demonstrate proof-of-concept for targeted gene edition in iPSC (recently reviewed in [12]). However, actual democratization of gene editing procedures in human iPSC was made possible thanks to the development of CRISPR/Cas9 technology. This bacterial immune system consists on two RNA molecules, one of them determining DNA sequence specificity by base pairing, and a nuclease that introduces a DSB in the DNA paired by the RNA. Both RNAs were later joined in a single guide RNA, which could be easily redirected to virtually any DNA sequence [13] by modifying a part of this RNA termed spacer.

The versatility of targeting almost any locus in the genome by simple changing the spacer sequence has enabled any cell biology laboratory with minimal molecular biology equipment to generate their desired targeted genetic modifications. Naturally, the extent of the isogenicity achieved with targeted genome edition becomes crucial for the interpretation of the results. It is not comparable, neither in terms of technical simplicity nor in the mechanistic interpretation, mutating a coding DNA sequence with editing an enhancer that contains a SNP. In order to strengthen genotype-phenotype relation, the latter (which may have secondary consequences unrelated to the SNP) should be carefully controlled. The reproduction of the exact variation under study, indeed, allows a much more accurate reproduction of the genetic mechanisms *in vitro*. The very recent introduction of CRISPR/Cas9 and single-stranded oligodeoxynucleotides as donor templates currently allows applying precision gene edition on a routine basis for modeling purposes [14,15].

Mendelian forms of PD

Parkinson's disease was long believed to have an environmental etiology. However, the discovery that rare mutations in *SNCA*, the gene encoding the α-synuclein protein that is found accumulated in PD, caused familial forms of the disease brought about a paradigm shift in the study of PD etiology. Since then, over a dozen of genes — *LRRK2*, *SNCA*, *VPS35*, *PINK1*, *PARK2*, *DJ-1*, *ATP13A2*, *PLA2G6*, *FBXO7*, *DNAJC6*, *SYNJ1*, *UCHL1*, *GIGYF2*, *HTRA2*, and *EIF4G1* — have been shown to cause PD with a Mendelian pattern of inheritance [16]. And the list keeps growing thanks to the application of new sequencing techniques [17–19] (Table 1).

Despite the initial debate on the suitability of iPSC-based models to model a late onset neurodegenerative disease such as PD [4], numerous reports have shown the appearance of disease-specific phenotypes in patient-specific iPSC-derived neurons carrying pathogenic familial PD

Table 1

Genes linked to Mendelian PD

PARK CODE	Gene name	Chromosome location	Inheritance	Onset
PARK1, PARK4	*SNCA*	4q22.1	AD	EOPD
PARK2	*PRKN*	6q26	AR	EOPD
PARK5[a]	*UCHL1*	4q13	AD	LOPD
PARK6	*PINK1*	1p36.12	AR	EOPD
PARK7	*DJ-1*	1p36.23	AR	EOPD
PARK8	*LRRK2*	12q12	AD	LOPD
PARK9	*ATP13A2*	1p36.13	AR	JPD
PARK11[a]	*GIGYF2*	2q37.1	AD	LOPD
PARK13[a]	*HTRA2*	2p13.1	AD	LOPD
PARK14	*PLA2G6*	22q13-1	AR	JPD
PARK15	*FBXO7*	22q12.3	AR	JPD
PARK17	*VPS35*	16q11.2	AD	LOPD
PARK18[a]	*EIF4G1*	3q27.1	AD	LOPD
PARK19A/B	*DNAJC6*	1p31.3	AR	JPD (A), EOPD (B)
PARK20	*SYNJ1*	21q22.2	AR	EOPD
PARK21[b]	*DNAJC13*	3q22.1	AD	LOPD
PARK21[b]	*TMEM230*	20p12	AD	LOPD
PARK22[a]	*CHCHD2*	7p11.2	AD	LOPD
PARK23	*VPS13C*	15q22.2	AR	EOPD
–	*TNR*	1q25.1	AD	LOPD
–	*TNK2*	3q29	AD	LOPD

[a] These associations are controversial; some of them have not being confirmed in separate replication studies. However reduced penetrance could account for the discordances in most cases.
[b] These associations are conflicting since they were found in the same large multiplex kindred. Further studies are advised.

mutations (recently reviewed in [20]). However, the number of PD cases explained by mutations in these genes is very limited and most cases remain classified as idiopathic. Altogether, these Mendelian mutations only account for approximately 30% of familial and 3–5% of sporadic cases of PD [21]. Among sporadic PD cases, mutations in *GBA* are gaining special attention due to their relatively high prevalence and their associated risk. Cellular models have demonstrated how mutant GBA reduces lysosomal function, thus favoring α-synuclein accumulation, which in turn disrupts ER-to-Golgi transport of newly synthesized proteins, such as the lysosomal ones including GCase [22]. This 'toxic bi-directional loop' has also been observed in patient-specific iPSC-derived neurons and importantly, the model has been used to assay new drugs to counter the decline in ER-to-Golgi transport [23].

It should be noted that some of the aforementioned familial PD mutations are not fully penetrant. This is the case for the most common mutation found in familial PD: $LRRK2^{G2019S}$. Furthermore, there is wide variation in terms of age-at-onset (AAO) among different carriers of the mutation, and even among different ethnic groups [24]. AAO variability may be explained by genetic and/or environmental factors. In the case of gene-gene interactions, AAO modifiers of PD associated to $LRRK2^{G2019S}$ have been found, as well as risk modifiers of *LRRK2* risk variants. Certain haplotypes at the *PARK16* locus have been shown to protect against PD in certain populations, and to epistatically interact with *LRRK2 rs1491942*, reducing risk [25,26]. This genetic interaction was experimentally explored in a study by MacLeod *et al.* [27]. In that study and a later work by Beilina *et al.* [28•], an interaction network dealing with vesicle trafficking and sorting was drawn around LRRK2. Surprisingly, it incriminated other PD genes such as *VPS35*, *RAB7L1* and *GAK* [27,28•]. Genetic variability in *DNM3* has been linked to protection against PD associated to $LRRK2^{G2019S}$ in the North-African Arab-Berber population, and replicated in $LRRK2^{G2019S}$ carriers from different origins [29•].

Genetic bases of sporadic PD forms

The familial PD forms discussed above — Mendelian and GBA-related — have a strong and defined genetic component that is sufficient to manifest *in vitro*. But, what happens with the majority of sporadic PD cases that are not associated to (known) penetrant disease-causing mutations? To which extent their genetic component could also be captured *in vitro* in iPSC-based models? There are very few reports describing the derivation of iPSC from sporadic PD patients, and even less recapitulating disease-related phenotypes *in vitro*. In this regard, the first study showing PD-related cellular phenotypes in neurons from sporadic PD patient-specific iPSC was reported by our laboratories [30•]. In this work, a large collection of iPSC lines derived from $LRRK2^{G2019S}$-associated PD patients, sporadic PD patients, and healthy individuals were differentiated towards dopaminergic neurons. Neurons derived from sporadic PD patients

showed increased susceptibility to undergo neurodegeneration after long-term culture, similar to neurons derived from *LRRK2*^{G2019S}-associated PD patients [30•]. Independent evidence for PD-related cellular phenotypes in iPSC derived from sporadic PD patients came from the analysis of mitochondrial dynamics. Aberrant sequestration of mitochondria was found in iPSC-derived dopaminergic neurons from *LRRK2*^{G2019S}-associated PD patients, but also from sporadic PD patients [31]. Moreover, features of neurodegeneration and dysregulated expression of the splicing factor RBFOX1 were found in iPSC-derived dopaminergic neurons carrying familial PD mutations (in *LRRK2*, *SNCA*, or *PARK2*), as well as from a sporadic PD patient [32]. Taken together, these reports demonstrate that, at least for the sporadic PD patients being modeled, the predisposition to suffer the disease is genetically encoded and, importantly, it can be captured in iPSC and manifest as measurable PD-related cellular phenotypes in iPSC-derived neurons. Table 2 summarizes these and other reports in which sporadic PD patient-specific iPSC were investigated.

Modern genome interrogation techniques such as whole-genome genotyping, or whole-exome/genome sequencing have identified a large list of genetic loci associated to sporadic PD. A meta-analysis of different GWAS described 28 independent risk loci that reached genome-wide significance [33••]. Many of these loci contain genes that had been previously linked to familial PD, supporting the idea that familial and sporadic PD share to some extent their genetic component. Moreover, the analysis of copy number variation (CNV) in the context of PD has found linkage of specific CNVs to both familial and sporadic forms of the disease [34,35•]. Overall, these approaches seek for common genomic variations that confer a very small risk of suffering PD, or rare dominant variants that segregate with the disease. Alternatively, a recent study analyzed the participation of very rare or even *de novo* variants in disease-related genes. By using targeted in-depth sequencing of 38 PD-related genes, the authors found an enrichment of rare and low frequency variants specifically of familial PD genes in sporadic PD cases, compared with healthy individuals [36•], revealing an even greater degree of complexity in the genetic bases of PD.

Interestingly, most of the genetic variation linked to PD risk is not found in coding regions [37]. Results from recent reports support the notion that some GWAS hits lying in the non-coding genome affect the function of gene regulatory regions such as enhancers or promoters. Vermunt and colleagues generated a vast library of distal enhancer regions that are active in diverse regions in the human brain as judged by ChIP-seq results [38••]. To gain insight into how these enhancers were collectively regulated, the authors studied whether there were patterns of co-regulation of different sets of enhancers, either in multiple regions or specifically in particular brain areas. They found enhancer networks associated to certain neuroglial functions that could be general or cell

Table 2

iPSC-based models of sporadic PD

Report	Patients included	Phenotypes observed
Park *et al.*, 2008 [50]	1 idiopathic PD patient and patients from other conditions	Not studied
Soldner *et al.*, 2009 [51]	7 idiopathic PD patients and patients from other conditions	Not studied
Sánchez-Danés *et al.*, 2012 [30•]	7 idiopathic and 4 LRRK2 G2019S PD patients and 4 healthy controls	Increased apoptosis, reduced neurite length and branching and impaired autophagosome-to-lysosome fusion in DA neurons
Woodard *et al.*, 2014 [52]	1 idiopathic PD patient, 2 monozygotic twins carrying N370S GBA mutation and discordant for PD diagnosis and 2 healthy controls	Alpha-synuclein and GCase levels similar to those of the control and reduced dopamine synthesis ability in DA neurons
Fernández-Santiago *et al.*, 2015 [53]	6 idiopathic and 4 LRRK2 G2019S PD patients and 4 healthy controls	Aberrant DNA methylation in DA neurons derived from both idiopathic and LRRK2 PD iPSC
Nenasheva *et al.*, 2016 [54]	1 idiopathic, 1 LRRK2 G2019S, 1 LRRK2 G2019S and GBA N370S, 1 GBA N370S and 1 Parkin compound heterozygote PD patients and 3 healthy controls	Different expression of different *trim* genes during the transition from fibroblast to iPSC, NPC and neurons
Hsieh *et al.*, 2016 [31]	5 idiopathic, 3 LRRK2 G2019S, 1 LRRK2 Y1699C 1 LRRK2 R1441G, 1 LRRK2 R1441C PD patients and 4 healthy controls	Failure to arrest and clear mitochondria after depolarization
Chang *et al.*, 2016 [55]	1 idiopathic (EOPD) carrying a heterozygous Ex5del PARK2 and 1 healthy control	Abnormal alpha-synuclein accumulation and down-regulation of the proteasome and anti-oxidative pathways rendering them more sensitive to these insults
Lin *et al.*, 2016 [32]	1 idiopathic, 6 LRRK2 G2019S, 1 SNCA triplication, 1 Parkin c.255delA PD patients and 3 healthy controls	Increased cell death, increased alpha-synuclein expression (RNA) and deregulated expression of the splicing factor *RBFOX1*

type-, region-, or context-specific (such as response to hypoxia or nutrient levels). With this catalogue of brain enhancers at hand, the authors checked if two of the major PD-related loci, the one containing the *SNCA* gene and *PARK16*, lied within any brain-specific enhancer region. In the case of *SNCA*, GWAS hits were in tight linkage disequilibrium (LD = 1) with other two SNPs located in a putative enhancer in intron 4. The analysis of 3D interactions by chromosome conformation capture-on-chip (4C-seq) showed that this putative enhancer not only regulated the transcription from the *SNCA* promoter, but also regulated the expression of nearby genes. Moreover, the authors used a murine reporter system and found overall enhancer activity at E11.5 throughout the mouse brain, with greater signal in the posterior hindbrain-midbrain boundary and dorsal root ganglia, two regions with evident implications in the disease process [38**].

Surprisingly, other PD GWAS hits fall in enhancer regions with no evident activity in the brain. Coetzee *et al.* [39**] analyzed 21 PD risk SNPs from previous GWAS studies [33**], of which 12 were related to gene regulatory regions (enhancer or promoter) in any one of the 77 cell types or tissues from the Roadmap Epigenomics Mapping Consortium (REMC [40]). Finally, only four enriched loci passed the authors' very stringent significance criteria: 4q21.1 (enrichment in liver and fat cells), 8p22 (BMP4 treated ES-derived mesoendoderm), 12q12 (CD19-B lymphocytes), and 14q24.1 (CD19-B lymphocytes and dopaminergic neurons). Crossing data from the Genotype-Tissue Expression consortium (GTEx) with REMC data allowed establishing Expression Quantitative Trait Loci (eQTL) for two of the loci. In the case of the risk allele *4q21.1 rs6812193*, correlation with decreased expression of *CCDC158*, *FAM47E*, *NAAA*, and *NUP54* in different tissues, including liver and fat, was found. For risk allele *14q24.1 rs76904798*, the authors found correlation with increased expression of the familial PD gene *LRRK2* [39**]. These findings highlight the importance of considering the involvement of tissues other than the brain when investigating PD pathogenesis.

The results of Vermunt *et al.* [38**] (but also those of Coetzee *et al.* [39**]) underscore the notion that 3D chromatin structure is critically important for appropriate transcriptome orchestration. Chromatin is organized in megabase-scale regions known as 'topologically associated domains' (TADs). The spatial organization imposes a certain transcriptional regulation of the genes contained within a given TAD. Disruption of TAD spatial boundaries (associated to transcriptional insulators) can cause diverse pathogenic conditions, and might represent an alternative disease mechanism for GWAS hits located in non-coding regions. Fortunately, CRISPR/Cas9-based strategies can also be exploited to investigate the causative role this type of polymorphisms [41]. Another insight gained from the study of Vermunt *et al.* [38**] is that many enhancer networks appear to be 'context-dependent'. In other words, their epigenetic state and transcription factor occupancy is also a result of the interaction with the environment. Many environmental factors have been described to modulate PD risk, and some of them have even been described to interact with specific polymorphisms, such as the case of caffeine and a SNP located near the glutamate receptor *GRIN2A* gene [42,43]. Therefore, a conceivable alternative disease mechanism could be that risk variants render regulatory elements unresponsive to environmental cues. In any case, studies addressing such putative alternative disease mechanisms will require a great deal of attention to avoid influence from eventual genetic aberrations acquired during reprogramming and/or expansion of cell cultures.

Approaching complex genetic questions by combining gene editing and iPSC

The neuropsychiatric field has pioneered the use of iPSC-based models to address the complex genetics of disease (Table 3), on account of the very few cases of Mendelian inheritance and the availability of many risk loci associated to this type of diseases [44]. As early as 2014, patient-specific iPSC were used to characterize risk loci associated to schizophrenia [45**]. Specifically, Yoon *et al.* dissected a risk locus for schizophrenia and autism that is commonly affected by CNVs in these disorders. Of the several genes present in the locus, *CYFIP1* was identified as the one responsible for the abnormal cytoskeleton dynamics that caused defective apical polarization in neural rosettes *in vitro* and the cortical developmental defects *in vivo* [45**].

Taking this approach one step further, Marchetto *et al.* [46**] investigated the genetic bases of some specific cases of autism stratified by the presence of macroencephaly during the three first years of life, and subsequent normalization of the brain size. CNV analysis and exome sequencing identified an enrichment of mutations in several members of the Wnt/β-catenin pathway as well as in genes previously linked with autism. Patient-specific iPSC-derived neural progenitor cells showed increased proliferation rates compared to controls, concomitant with reduced Wnt/β-catenin transcriptional activity, and reduced synaptogenesis and functional alterations in neuronal networks. The availability of an iPSC-based model of the disease enabled the authors to dissect the molecular mechanisms underlying the various cellular phenotypes. The overall picture that emerged from those studies suggests that autistic neural progenitor cells undergo premature differentiation, but do not complete maturation as normal progenitors do [46**]. The stratification of a heterogeneous patient group according to specific disease signs made possible in this case the identification of genetic defects in specific ontologies. Deriving iPSC from those patients allowed the authors to

Table 3

Using iPSC to disentangle genetic risk

Reference	Disease	Locus/variant	Gene	Associated effect	PSCs	Gene editing
Shcheglovitov *et al.*, 2013 [56]	Phelan-McDermid Syndrome (PMDS)	22q13del	*SHANK3*	Impaired excitatory transmission due to reduced glutamate receptors and synapse number	6 clones from 2 PMDS patient iPSC and 2 control iPSC and 1 control ESC	No (LV-mediated gene complementation)
Yoon *et al.*, 2014 [45••]	Schizophrenia	15q11.2del	*CYFIP1*	CYFIP1 loss negatively regulates the stability of the WAVE complex, impairing the formation of adherens junctions, and neural precursor polarity	3 iPSC lines from carriers of the deletion and 3 control lines	No (LV-mediated gene complementation)
Young *et al.*, 2015 [57]	Sporadic Alzheimer Disease (SAD)	*SORL1* gene region	*SORL1*	Protective alleles in 3 linked SNPs reduced *SORL1* expression	7 SAD and 6 control lines	No (Piggy-back/ LV-mediated gene complementation/ silencing)
Griesi-Oliveira *et al.*, 2015 [58]	Non-syndromic autism	Translocation t(3;11)(p21;q22)	*TRPC6*	*TRPC6* reduction or haploinsufficiency causes developmental defects and neuronal morphological and functional deficits	1 iPSC line from a carrier of the translocation and 6 control lines	No (LV-mediated gene complementation)
Soldner *et al.*, 2016 [47••]	Sporadic Parkinson's Disease	SNPs in a distal enhancer of the 4th intron of the *SNCA* gene	*SNCA*	1.06-fold increase in alpha-synuclein expression	WIBR3 hESC	Yes Deletion of enhancer and exchange of variants
Li *et al.*, 2016 [59]	Schizophrenia	Risk alleles along the 10q24.32 locus	AS3MT and BORCS7	Increased expression of BORCS7 and of a specific isoform of AS3MT termed d2d3	1 control iPSC and 1 hESC lines	No
Marchetto *et al.*, 2016 [46••]	Non-syndromic autism	High mutational load detected in genes of the Wnt/β-catenin pathway and other ASD genes	Genes of the Wnt/β-catenin pathway and other ASD genes	Abnormal proliferation rates of NPC and misbalanced generation of excitatory vs. inhibitory	8 ASD patient and 5 control iPSC lines	No

test the specific hypotheses raised from the genetic studies.

In the field of PD research, Soldner and colleagues very recently described a strategy to unveil the effect of a PD-related SNP in the *SNCA* locus [47••]. By crossing GWAS data from SNPs spanning the *SNCA* locus with epigenetic signatures characteristic of enhancer elements, the authors identified a candidate variant in a distal enhancer located in intron 4. Using CRISPR/Cas9-mediated gene editing of a control hESC line, they generated a collection of isogenic lines representing an allelic series of the SNP of interest, including clones hemizygotic for both enhancer variants and enhancer-depleted clones. Increased *SNCA* expression in neurons was associated to the presence of the G allele in rs356168, consistent with the GWAS protective signal detected for the alternative A allele (OR = 0.79). Further investigation by ChIP-RT-qPCR of the transcription factors differentially binding the risk alleles revealed two possible candidates: EMX2 and NKX6-1. Both of them showed preferential binding for the A allele, suggesting that the risk allele results in increased *SNCA* expression by decreasing the binding and transcriptional repression of EMX2/NKX6-1 [47••].

Complementary strategies to address complex genetic traits in PD may benefit from high-throughput screening approaches. Commercially available libraries of CRISPR/Cas9 guide RNAs could be employed to screen for modifiers of PD phenotypes (expressivity, penetrance, etc.). No studies have been published to date using such strategies, but high-throughput screens have identified

Figure 1

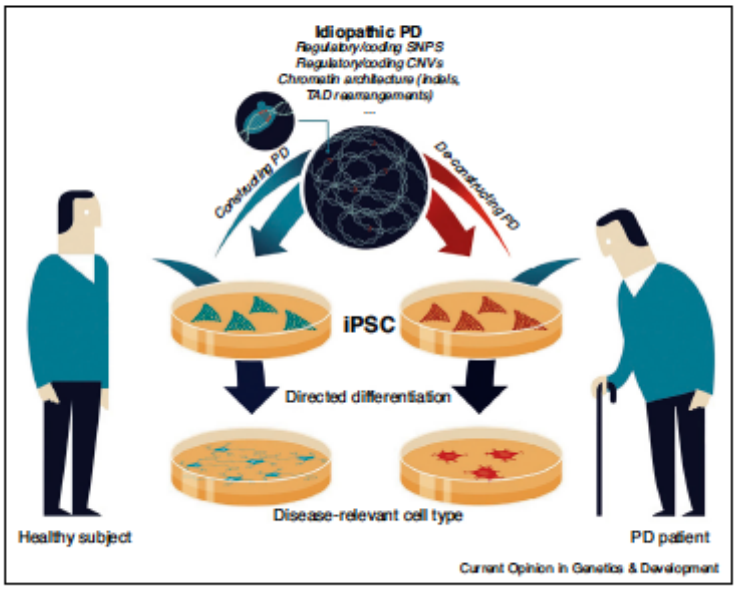

Strategies to dissect the genetic contribution to sporadic PD. Sporadic PD results from a complex interplay between multiple small-effect genetic and environmental factors. The former imply genetic variation of different nature, ranging from single nucleotide variation to large genomic rearrangements. The genetic contribution is amenable to investigation using iPSC models combined with CRISPR/Cas9. However, given the polygenic nature of the genetic predisposition, each genetic variant may contribute to the disease phenotypes to a different extent. Two alternative approaches have been highlighted in this review to dissect the genetic component. The first one (PD construction) represents the approach followed by Soldner *et al.* [38••] to dissect the association signal in the 3′ region of the *SNCA* gene. By using a 'naïve' hPSC line, the introduction of disease-related variants in a controlled genomic background provides information about the specific contribution of such variant. The opposite approach (PD de-construction) would consist on editing the genome of sporadic PD patient-specific iPSC to replace PD risk-associated variants with those of low risk. Causality would be then assessed by the presence/absence of PD-related cellular or molecular phenotypes in this case.

interesting correlations between genes related to GWAS hits and disease-related phenotypes, including altered mitophagy [48] and mitochondrial fragmentation [49].

Future directions: constructing and deconstructing PD

The study by Soldner *et al.* [47••] demonstrates the power of combining PSC-based models and directed genome edition to examine the causal link between GWAS signals — either SNPs or CNVs — and disease phenotypes. In their approach, which we refer to as 'constructing PD' in Figure 1, small-effect genetic variants are introduced into a healthy genome, and the resulting cellular and/or molecular phenotypes analyzed. It should be possible, and perhaps even more sensitive, to address causality with the opposite approach, that is 'deconstructing PD' (Figure 1). In this case, editing putative small-effect risk variants from sporadic PD patient-specific iPSC into their low-risk counterparts, could prevent the appearance of PD-relevant cellular/molecular phenotypes, thus supporting causality. In either approach, the combination of CRISPR/Cas9-mediated genome edition and patient-specific iPSC will surely accelerate the pace at which genetic risk (or protective) factors are put together to complete the current jigsaw that is the missing heritability of PD.

Conflict of interest statement

Nothing declared.

Acknowledgements

The authors are indebted to all the members of our laboratories for fruitful discussions, and to David Maynar for excellent artwork. Research from the authors' laboratories is supported by the European Research Council-ERC (2012-StG-311736-PD-HUMMODEL), the Spanish Ministry of Economy and Competitiveness-MINECO (SAF2015-69706-R and BFU2013-49157-P), Instituto de Salud Carlos III-ISCIII/FEDER (Red de Terapia Celular – TerCel RD16/0011/0024), AGAUR (2014-SGR-1460), and CERCA Programme/Generalitat de Catalunya. C.C. and G.C. are partially supported by pre-doctoral fellowships from the Spanish Ministry of Education-MEC (FPU12/03332) and Economy and Competitiveness-MINECO (BES-2014-069603), respectively.

References and recommended reading

Papers of particular interest, published within the period of review, have been highlighted as:

• of special interest
•• of outstanding interest

1. Takahashi K, Yamanaka S: **Induction of pluripotent stem cells from mouse embryonic and adult fibroblast cultures by defined factors**. *Cell* 2006, **126**:663-676.

2. Cherry AB, Daley GQ: **Reprogrammed cells for disease modeling and regenerative medicine**. *Annu Rev Med* 2013, **64**:277-290.

3. Zeltner N, Studer L: **Pluripotent stem cell-based disease modeling: current hurdles and future promise**. *Curr Opin Cell Biol* 2015, **37**:102-110.

4. Lee G, Studer L: **Induced pluripotent stem cell technology for the study of human disease**. *Nat Methods* 2010, **7**:25-27.

5. Kajiwara M, Aoi T, Okita K, Takahashi R, Inoue H, Takayama N, Endo H, Eto K, Toguchida J, Uemoto S *et al.*: **Donor-dependent variations in hepatic differentiation from human-induced pluripotent stem cells**. *Proc Natl Acad Sci U S A* 2012, **109**:12538-12543.

6. Hu BY, Weick JP, Yu J, Ma LX, Zhang XQ, Thomson JA, Zhang SC: **Neural differentiation of human induced pluripotent stem cells follows developmental principles but with variable potency**. *Proc Natl Acad Sci U S A* 2010, **107**:4335-4340.

7. Baker DE, Harrison NJ, Maltby E, Smith K, Moore HD, Shaw PJ, Heath PR, Holden H, Andrews PW: **Adaptation to culture of human embryonic stem cells and oncogenesis in vivo**. *Nat Biotechnol* 2007, **25**:207-215.

8. Lee CT, Bendriem RM, Kindberg AA, Worden LT, Williams MP, Drgon T, Mallon BS, Harvey BK, Richie CT, Hamilton RS *et al.*: **Functional consequences of 17q21.31/WNT3-WNT9B amplification in hPSCs with respect to neural differentiation**. *Cell Rep* 2015, **10**:616-632.

9. DeBoever C, Li H, Jakubosky D, Benaglio P, Reyna J, Olson KM, Huang H, Biggs W, Sandoval E, D'Antonio M *et al.*: **Large-scale profiling reveals the influence of genetic variation on gene expression in human induced pluripotent stem cells**. *Cell Stem Cell* 2017, **20**:533-546 e537.

10. Carcamo-Orive I, Hoffman GE, Cundiff P, Beckmann ND, D'Souza SL, Knowles JW, Patel A, Papatsenko D, Abbasi F, Reaven GM *et al.*: **Analysis of transcriptional variability in a large human iPSC library reveals genetic and non-genetic determinants of heterogeneity**. *Cell Stem Cell* 2017, **20**:518-532 e519.

11. Rouet P, Smih F, Jasin M: **Expression of a site-specific endonuclease stimulates homologous recombination in mammalian cells**. *Proc Natl Acad Sci U S A* 1994, **91**:6064-6068.

12. Hockemeyer D, Jaenisch R: **Induced pluripotent stem cells meet genome editing**. *Cell Stem Cell* 2016, **18**:573-586.

13. Jinek M, Chylinski K, Fonfara I, Hauer M, Doudna JA, Charpentier E: **A programmable dual-RNA-guided DNA endonuclease in adaptive bacterial immunity**. *Science* 2012, **337**:816-821.

14. Richardson CD, Ray GJ, DeWitt MA, Curie GL, Corn JE: **Enhancing homology-directed genome editing by catalytically active and inactive CRISPR-Cas9 using asymmetric donor DNA**. *Nat Biotechnol* 2016, **34**:339-344.

15. Paquet D, Kwart D, Chen A, Sproul A, Jacob S, Teo S, Olsen KM, Gregg A, Noggle S, Tessier-Lavigne M: **Efficient introduction of specific homozygous and heterozygous mutations using CRISPR/Cas9**. *Nature* 2016, **533**:125-129.

16. Bras J, Guerreiro R, Hardy J: **SnapShot: genetics of Parkinson's disease**. *Cell* 2015, **160**:570 e571.

17. Farlow JL, Robak LA, Hetrick K, Bowling K, Boerwinkle E, Coban-Akdemir ZH, Gambin T, Gibbs RA, Gu S, Jain P *et al.*: **Whole-exome sequencing in familial Parkinson disease**. *JAMA Neurol* 2016, **73**:68-75.

18. Funayama M, Ohe K, Amo T, Furuya N, Yamaguchi J, Saiki S, Li Y, Ogaki K, Ando M, Yoshino H *et al.*: **CHCHD2 mutations in autosomal dominant late-onset Parkinson's disease: a genome-wide linkage and sequencing study**. *Lancet Neurol* 2015, **14**:274-282.

19. Deng HX, Shi Y, Yang Y, Ahmeti KB, Miller N, Huang C, Cheng L, Zhai H, Deng S, Nuytemans K *et al.*: **Identification of TMEM230 mutations in familial Parkinson's disease**. *Nat Genet* 2016, **48**:733-739.

20. Torrent R, De Angelis Rigotti F, Dell'Era P, Memo M, Raya A, Consiglio A: **Using iPS cells toward the understanding of Parkinson's disease**. *J Clin Med* 2015, **4**:548-566.

21. Kumar KR, Djarmati-Westenberger A, Grunewald A: **Genetics of Parkinson's disease**. *Semin Neurol* 2011, **31**:433-440.

22. Mazzulli JR, Xu YH, Sun Y, Knight AL, McLean PJ, Caldwell GA, Sidransky E, Grabowski GA, Krainc D: **Gaucher disease glucocerebrosidase and alpha-synuclein form a bidirectional pathogenic loop in synucleinopathies**. *Cell* 2011, **146**:37-52.

23. Mazzulli JR, Zunke F, Tsunemi T, Toker NJ, Jeon S, Burbulla LF, Patnaik S, Sidransky E, Marugan JJ, Sue CM *et al.*: **Activation of beta-glucocerebrosidase reduces pathological alpha-synuclein and restores lysosomal function in Parkinson's patient midbrain neurons**. *J Neurosci* 2016, **36**:7693-7706.

24. Marder K, Wang Y, Alcalay RN, Mejia-Santana H, Tang MX, Lee A, Raymond D, Mirelman A, Saunders-Pullman R, Clark L *et al.*: **Age-specific penetrance of LRRK2 G2019S in the Michael J. Fox Ashkenazi Jewish LRRK2 Consortium**. *Neurology* 2015, **85**:89-95.

25. Gan-Or Z, Bar-Shira A, Dahary D, Mirelman A, Kedmi M, Gurevich T, Giladi N, Orr-Urtreger A: **Association of sequence alterations in the putative promoter of RAB7L1 with a reduced Parkinson disease risk**. *Arch Neurol* 2012, **69**:105-110.

26. Pihlstrom L, Berge V, Rengmark A, Toft M: **Parkinson's disease correlates with promoter methylation in the alpha-synuclein gene**. *Mov Disord* 2015, **30**:577-580.

27. MacLeod DA, Rhinn H, Kuwahara T, Zolin A, Di Paolo G, McCabe BD, Marder KS, Honig LS, Clark LN, Small SA *et al.*: **RAB7L1 interacts with LRRK2 to modify intraneuronal protein sorting and Parkinson's disease risk**. *Neuron* 2013, **77**:425-439.

28. • Beilina A, Rudenko IN, Kaganovich A, Civiero L, Chau H, Kalia SK, Kalia LV, Lobbestael E, Chia R, Ndukwe K *et al.*: **Unbiased screen for interactors of leucine-rich repeat kinase 2 supports a common pathway for sporadic and familial Parkinson disease**. *Proc Natl Acad Sci U S A* 2014, **111**:2626-2631.
In this study, a network of LRRK2 interactors is identified using an unbiased proteomic screen. Interestingly, up to 2 PD genes were identified in this network.

29. • Trinh J, Gustavsson EK, Vilarino-Guell C, Bortnick S, Latourelle J, McKenzie MB, Tu CS, Nosova E, Khinda J, Milnerwood A *et al.*: **DNM3 and genetic modifiers of age of onset in LRRK2 Gly2019Ser parkinsonism: a genome-wide linkage and association study**. *Lancet Neurol* 2016, **15**:1248-1256.
Large-scale GWAS screening for age-at-onset modifiers in *LRRK2*^{G2019S}-associated PD. Interestingly, the highest-ranked locus contained a gene implicated in vesicle dynamics.

30. • Sanchez-Danes A, Richaud-Patin Y, Carballo-Carbajal I, Jimenez-Delgado S, Caig C, Mora S, Di Guglielmo C, Ezquerra M, Patel B, Giralt A *et al.*: **Disease-specific phenotypes in dopamine neurons from human iPS-based models of genetic and sporadic Parkinson's disease**. *EMBO Mol Med* 2012, **4**:380-395.
First experimental evidence that sporadic PD can be recapitulated *in vitro* using patient-specific iPSC.

31. Hsieh CH, Shaltouki A, Gonzalez AE, Bettencourt da Cruz A, Burbulla LF, St Lawrence E, Schule B, Krainc D, Palmer TD, Wang X: **Functional impairment in Miro degradation and mitophagy is a shared feature in familial and sporadic Parkinson's disease**. *Cell Stem Cell* 2016, **19**:709-724.

32. Lin L, Goke J, Cukuroglu E, Dranias MR, VanDongen AM, Stanton LW: **Molecular features underlying neurodegeneration identified through in vitro modeling of genetically diverse Parkinson's disease patients**. *Cell Rep* 2016, **15**:2411-2426.

33. •• Nalls MA, Pankratz N, Lill CM, Do CB, Hernandez DG, Saad M, DeStefano AL, Kara E, Bras J, Sharma M *et al.*: **Large-scale meta-analysis of genome-wide association data identifies six**

new risk loci for Parkinson's disease. *Nat Genet* 2014, **46**:989-993.
This meta-analysis has yielded the largest collection to date of loci associated to PD risk.

34. Ambroziak W, Koziorowski D, Duszyc K, Gorka-Skoczylas P, Potulska-Chromik A, Slawek J, Hoffman-Zacharska D: **Genomic instability in the PARK2 locus is associated with Parkinson's disease**. *J Appl Genet* 2015, **56**:451-461.

35. • Mok KY, Sheerin U, Simón-Sánchez J, Salaka A, Chester L, Escott-Price V, Mantipragada K, Doherty KM, Noyce AJ, Mencacci NE *et al.*: **Deletions at 22q11.2 in idiopathic Parkinson's disease: a combined analysis of genome-wide association data**. *Lancet Neurol* 2016, **15**:585-596.
This report demonstrates that chromosomal structural variation can also modify PD risk.

36. • Spataro N, Calafell F, Cervera-Carles L, Casals F, Pagonabarraga J, Pascual-Sedano B, Campolongo A, Kulisevsky J, Lleo A, Navarro A *et al.*: **Mendelian genes for Parkinson's disease contribute to the sporadic forms of the disease**. *Hum Mol Genet* 2015, **24**:2023-2034.
First report describing an increased incidence of rare (MAF < 1%) code-altering variants of genes associated with Mendelian forms of the disease in sporadic PD cases.

37. Chai C, Lim KL: **Genetic insights into sporadic Parkinson's disease pathogenesis**. *Curr Genomics* 2013, **14**:486-501.

38. •• Vermunt MW, Reinink P, Korving J, de Bruijn E, Creyghton PM, Basak O, Geeven G, Toonen PW, Lansu N, Meunier C *et al.*: **Large-scale identification of coregulated enhancer networks in the adult human brain**. *Cell Rep* 2014, **9**:767-779.
Report describing the generation of a brain region-specific catalogue of active enhancer regions and networks of co-regulated enhancers, which are used to identify enhancers affected by PD-related risk variants.

39. •• Coetzee SG, Pierce S, Brundin P, Brundin L, Hazelett DJ, Coetzee GA: **Enrichment of risk SNPs in regulatory regions implicate diverse tissues in Parkinson's disease etiology**. *Sci Rep* 2016, **6**:30509.
In this study, a systematical approach is conducted in order to identify the cell types in which several non-coding PD risk variants exert their effect.

40. Roadmap Epigenomics C, Kundaje A, Meuleman W, Ernst J, Bilenky M, Yen A, Heravi-Moussavi A, Kheradpour P, Zhang Z, Wang J *et al.*: **Integrative analysis of 111 reference human epigenomes**. *Nature* 2015, **518**:317-330.

41. Lupianez DG, Kraft K, Heinrich V, Krawitz P, Brancati F, Klopocki E, Horn D, Kayserili H, Opitz JM, Laxova R *et al.*: **Disruptions of topological chromatin domains cause pathogenic rewiring of gene-enhancer interactions**. *Cell* 2015, **161**:1012-1025.

42. Hamza TH, Chen H, Hill-Burns EM, Rhodes SL, Montimurro J, Kay DM, Tenesa A, Kusel VI, Sheehan P, Eaaswarkhanth M *et al.*: **Genome-wide gene-environment study identifies glutamate receptor gene GRIN2A as a Parkinson's disease modifier gene via interaction with coffee**. *PLoS Genet* 2011, **7**:e1002237.

43. Yamada-Fowler N, Fredriksson M, Soderkvist P: **Caffeine interaction with glutamate receptor gene GRIN2A: Parkinson's disease in Swedish population**. *PLOS ONE* 2014, **9**:e99294.

44. Gratten J, Wray NR, Keller MC, Visscher PM: **Large-scale genomics unveils the genetic architecture of psychiatric disorders**. *Nat Neurosci* 2014, **17**:782-790.

45. •• Yoon KJ, Nguyen HN, Ursini G, Zhang F, Kim NS, Wen Z, Makri G, Nauen D, Shin JH, Park Y *et al.*: **Modeling a genetic risk for schizophrenia in iPSCs and mice reveals neural stem cell deficits associated with adherens junctions and polarity**. *Cell Stem Cell* 2014, **15**:79-91.
Report describing the use of patient-specific iPSC to identify the gene that increases the risk of suffering from schizophrenia and autism in patients carrying a chromosomal microdeletion.

46. •• Marchetto MC, Belinson H, Tian Y, Freitas BC, Fu C, Vadodaria KC, Beltrao-Braga PC, Trujillo CA, Mendes AP, Padmanabhan K *et al.*: **Altered proliferation and networks in neural cells derived from idiopathic autistic individuals**. *Mol Psychiatry* 2016.
Excellent example from the neuropsychiatric field of how to address genotype-to-phenotype correlation in a complex and heterogeneous disease such as autism. In this study, the authors stratified a group of patients with specific clinical features which helped narrowing down the genetic bases.

47. •• Soldner F, Stelzer Y, Shivalila CS, Abraham BJ, Latourelle JC, Barrasa MI, Goldmann J, Myers RH, Young RA, Jaenisch R: **Parkinson-associated risk variant in distal enhancer of alpha-synuclein modulates target gene expression**. *Nature* 2016, **533**:95-99.
First study combining hPSC and CRISPR/Cas9 technologies for investigating the genetic bases of sporadic PD. The authors identified the actual variant responsible for association signal in GWAS.

48. Ivatt RM, Sanchez-Martinez A, Godena VK, Brown S, Ziviani E, Whitworth AJ: **Genome-wide RNAi screen identifies the Parkinson disease GWAS risk locus SREBF1 as a regulator of mitophagy**. *Proc Natl Acad Sci U S A* 2014, **111**:8484-8499.

49. Jansen IE, Ye H, Heetveld S, Lechler MC, Michels H, Seinstra RI, Lubbe SJ, Drouet V, Lesage S, Majounie E *et al.*: **Discovery and functional prioritization of Parkinson's disease candidate genes from large-scale whole exome sequencing**. *Genome Biol* 2017, **18**:22.

50. Park IH, Arora N, Huo H, Maherali N, Ahfeldt T, Shimamura A, Lensch MW, Cowan C, Hochedlinger K, Daley GQ: **Disease-specific induced pluripotent stem cells**. *Cell* 2008, **134**:877-886.

51. Soldner F, Hockemeyer D, Beard C, Gao Q, Bell GW, Cook EG, Hargus G, Blak A, Cooper O, Mitalipova M *et al.*: **Parkinson's disease patient-derived induced pluripotent stem cells free of viral reprogramming factors**. *Cell* 2009, **136**:964-977.

52. Woodard CM, Campos BA, Kuo SH, Nirenberg MJ, Nestor MW, Zimmer M, Mosharov EV, Sulzer D, Zhou H, Paull D *et al.*: **iPSC-derived dopamine neurons reveal differences between monozygotic twins discordant for Parkinson's disease**. *Cell Rep* 2014, **9**:1173-1182.

53. Fernandez-Santiago R, Carballo-Carbajal I, Castellano G, Torrent R, Richaud Y, Sanchez-Danes A, Vilarrasa-Blasi R, Sanchez-Pla A, Mosquera JL, Soriano J *et al.*: **Aberrant epigenome in iPSC-derived dopaminergic neurons from Parkinson's disease patients**. *EMBO Mol Med* 2015, **7**:1529-1546.

54. Nenasheva VV, Novosadova EV, Makarova IV, Lebedeva OS, Grefenshtein MA, Arsenyeva EL, Antonov SA, Grivennikov IA, Tarantul VZ: **The transcriptional changes of trim genes associated with Parkinson's disease on a model of human induced pluripotent stem cells**. *Mol Neurobiol* 2016.

55. Chang KH, Lee-Chen GJ, Wu YR, Chen YJ, Lin JL, Li M, Chen IC, Lo YS, Wu HC, Chen CM: **Impairment of proteasome and anti-oxidative pathways in the induced pluripotent stem cell model for sporadic Parkinson's disease**. *Parkinsonism Relat Disord* 2016, **24**:81-88.

56. Shcheglovitov A, Shcheglovitova O, Yazawa M, Portmann T, Shu R, Sebastiano V, Krawisz A, Froehlich W, Bernstein JA, Hallmayer JF *et al.*: **SHANK3 and IGF1 restore synaptic deficits in neurons from 22q13 deletion syndrome patients**. *Nature* 2013, **503**:267-271.

57. Young JE, Boulanger-Weill J, Williams DA, Woodruff G, Buen F, Revilla AC, Herrera C, Israel MA, Yuan SH, Edland SD *et al.*: **Elucidating molecular phenotypes caused by the SORL1 Alzheimer's disease genetic risk factor using human induced pluripotent stem cells**. *Cell Stem Cell* 2015, **16**:373-385.

58. Griesi-Oliveira K, Acab A, Gupta AR, Sunaga DY, Chailangkarn T, Nicol X, Nunez Y, Walker MF, Murdoch JD, Sanders SJ *et al.*: **Modeling non-syndromic autism and the impact of TRPC6 disruption in human neurons**. *Mol Psychiatry* 2015, **20**:1350-1365.

59. Li M, Jaffe AE, Straub RE, Tao R, Shin JH, Wang Y, Chen Q, Li C, Jia Y, Ohi K *et al.*: **A human-specific AS3MT isoform and BORCS7 are molecular risk factors in the 10q24.32 schizophrenia-associated locus**. *Nat Med* 2016, **22**:649-656.

Annex II: Research article (Under review process)

Molecular Neurobiology

The small GTPase RAC1/CED-10 is essential in maintaining dopaminergic neuron function and survival against α-synuclein-induced toxicity

--Manuscript Draft--

Manuscript Number:	
Article Type:	Original Article
Keywords:	Parkinson's disease; dopaminergic neurons; alpha-synuclein accumulation; autophagy impairment; RAC1/ced-10
Corresponding Author:	Esther Dalfo, Ph.D Universitat Autònoma de Barcelona Institut de Neurociències Bellaterra, Catalunya SPAIN
First Author:	Hannah Kim
Order of Authors:	Hannah Kim
	Carles Calatayud
	Sanjib Kumar-Guha, PhD
	Irene Fernández-Carasa
	Laura Berkowitz, PhD
	Iria Carballo-Carbajal, PhD
	Mario Ezquerra, PhD
	Rubén Fernández-Santiago, PhD
	Pankaj Kapahi, PhD
	Ángel Raya, MD, PhD
	Antonio Miranda-Vizuete, PhD
	Jose Miguel Lizcano, PhD
	Miquel Vila, MD, PhD
	Kimberlee Caldwell, PhD
	Guy Alexander Caldwell, PhD
	Antonella Consiglio, PhD
	Esther Dalfo, Ph.D
Abstract:	Parkinson's disease is associated with intracellular α-synuclein accumulation and ventral midbrain dopaminergic neuronal death in the Substantia Nigra of brain patients. The Rho GTPase pathway, mainly linking surface receptors to the organization of the actin and microtubule cytoskeletons, has been suggested to participate to Parkinson's disease pathogenesis. Nevertheless, its exact contribution remains obscure. To unveil the participation of the Rho GTPase family to the molecular pathogenesis of Parkinson's disease, we first used C elegans to demonstrate the role of the small GTPase RAC1 (ced-10 in the worm) in maintaining dopaminergic function and survival in the presence of alpha-synuclein. In addition, ced-10 mutant worms determined an increase of alpha-synuclein inclusions in comparison to control worms as well as an increase in autophagic vesicles. We then used a human neuroblastoma cells (M17) stably over-expressing alpha-synuclein, and found that RAC1 function decreased the amount of amyloidogenic alpha-synuclein. Further, by using dopaminergic neurons derived from patients of familial LRRK2-Parkinson's disease we report that human RAC1 activity is essential in the regulation of dopaminergic cell death, alpha-synuclein accumulation, participates in neurite arborization and modulates autophagy. Thus we determined for the first time that RAC1/ced-10 participates in Parkinson's Disease associated pathogenesis and established RAC1/ced-10 as a new candidate for further investigation of Parkinson's Disease associated mechanisms, mainly focused on

	dopaminergic function and survival against α-synuclein-induced toxicity.

Cover Letter

Click here to download Cover Letter COVER LETTER MNBG.docx

Dear Editor in chief Dr. Nicolas G. Bazan,

we hereby submit a manuscript entitled **The small GTPAse RAC1/CED-10 is essential in maintaining dopaminergic neuron function and survival against α-synuclein-induced toxicity** to be considered for publication as original paper in Molecular Neurobiology.

There are four files in all: the abstract, the manuscript (containing 2 tables), the figures (containing 7 figures), and the online resources files (containing 4 figures, 3 video files, 1 Table, 1 methodology section and 1 reference).

In this article the simple organism *C elegans* was primarily used to demonstrate a relevant role of the small GTPase *RAC1* (*ced-10* in the worm) in maintaining dopaminergic function and survival in the presence of alpha-synuclein, in addition to decreasing alpha-synuclein inclusions. Furthermore, *ced-10* function is associated with autophagy impairment. Thioflavin S staining in human neuroblastoma cells expressing constitutively alpha-synuclein, reveals that *RAC1* function decreased the amount of amyloidogenic alpha-synuclein. Finally, all these results are compiled altogether in induced pluripotent stem cell–derived dopaminergic neurons from Parkinson's disease patients with *LRRK2* mutation. In this model we show that human RAC1 activity is essential in the regulation of dopaminergic neuron cell death, alpha-synuclein accumulation, participates in neurite arborization and modulates autophagy.

This manuscript describes original work and is not under consideration by any other journal. All authors approved the manuscript and this submission.

The small GTPase RAC1/CED-10 is essential in maintaining dopaminergic neuron function and survival against α-synuclein-induced toxicity

Hanna Kim[1] (*), Carles Calatayud[2,3] (*), Sangib K Guha[4] (*), Irene Fernández-Carasa[2,3], Laura Berkowitz[1], Iria Carballo-Carbajal[5], Mario Ezquerra[6], Rubén Fernández-Santiago[6], Pankaj Kapahi[4], Ángel Raya[7], Antonio Miranda-Vizuete[8], Jose Miguel Lizcano[9], Miquel Vila [5,8,10], Kimberlee Caldwell [1], Guy A Caldwell [1], Antonella Consiglio[2,3] and Esther Dalfo (**) [9].

(1) Department of Biological Sciences, The University of Alabama, Tuscaloosa, Alabama 35487, USA.

(2) Institute for Biomedicine (IBUB) University of Barcelona (UB), Barcelona 08028, Spain.

(3) Department of Pathology and Experimental Therapeutics, School of Medicine, University of Barcelona, 08908 Barcelona, Spain

(4) Buck Institute for Research on Aging, 8001 Redwood Boulevard, Novato, CA 94945, USA

(5) Neurodegenerative Diseases Research Group, Vall d'Hebron Research Institute-Center for Networked Biomedical Research on Neurodegenerative Diseases (CIBERNED), 08035 Barcelona, Spain.

(6) Laboratory of Parkinson Disease and Other Neurodegenerative Movement Disorders, Department of Neurology: Clinical and Experimental Research, IDIBAPS – Hospital Clínic de Barcelona, 08036, Barcelona, Spain

(7) Center of Regenerative Medicine in Barcelona (CMRB), Hospital Duran i Reynals, 3rd Floor, Av. Gran Via 199-203, 08908 Hospitalet de Llobregat (Barcelona), Spain

(8) Instituto de Biomedicina de Sevilla, Hospital Universitario Virgen del Rocío/CSIC/ Universidad de Sevilla, Sevilla 41013, Spain.

(9) Department of Biochemistry and Molecular Biology, Institut de Neurociències, Faculty of Medicine, M2 , Universitat Autònoma de Barcelona (UAB), Bellaterra Campus , Cerdanyola del Vallés, Barcelona, Spain. ORCID: 0000-0003-4677-8515

(10) Catalan Institution for Research and Advanced Studies (ICREA), 08010 Barcelona, Spain

(**) Corresponding author: esther.dalfo@uab.cat +34935811624//+34676136881

Carles Calatayud Aristoy, ORCID ID: 0000-0003-0032-4198

Iria Carballo-Carbajal, ORCID ID: 0000-0002-4403-8006

Mario Ezquerra, ORCID ID: 0000-0003-3246-6641

Rubén Fernández-Santiago, ORCID ID: 0000-0002-4582-0702

Pankaj Kapahi, ORCID ID: 0000-0002-5629-4947

Ángel Raya, ORCID ID: 0000-0003-2189-9775

Antonio Miranda-Vizuete, ORCID ID: 0000-0002-6856-5396

Jose Miguel Lizcano, ORCID ID: 0000-0002-3154-5383

Guy Caldwell, ORCID ID: 0000-0002-8283-9090

Antonella Consiglio, ORCID ID: 0000-0002-3988-6254

Esther Dalfó, ORCID ID: 0000-0003-4677-8515

Acknowledgements

The genetic strain BR3579 was kindly provided by Dr Ralf Baumeister (Albert-Ludwing University, Freiburg/Brisgau, Germany). Plasmids Rac1-GFP WT and Rac1-GFP (CA) HYM772 were kindly provided by Dr Francisco Sánchez-Madrid (Spanish National Center for Cardiovascular Research (CNIC), Madrid, Spain). The construct P*ced-10*::CFP::CED-10 was a generous gift provided by Erik Lundquist (University of Kansas, Lawrence, KS, USA). Human neuroblastoma cell line BE(2)-M17 over-expressing wild type α-SYN was provided by Dr B. Wolozin (Boston University School of Medicine).

Funding: This work was supported the following grants: ED was supported by the grant PH613883 from The Instituto de Salud Carlos III. AMV was supported by grants from the Spanish Ministry of Economy and Competitiveness (MINECO) (BFU2015-64408-P) and the Instituto de Salud Carlos III (PI11/00072, cofinanced by the Fondo Social Europeo). MV was supported by a grant from the MINECO (SAF2016-77541-R). This work was also supported by BFU2016-80870-P and RETIC TerCel grants from MINECO and the European Research Council (ERC) 2012-StG (311736- PD-HUMMODEL) to AC. C C is the recipient of a Spanish FPU fellowship of the MINECO. ED and AV are members of the GENIE and EU-ROS Cost Action of the European Union.

Abstract

Parkinson's disease is associated with intracellular α-synuclein accumulation and ventral midbrain dopaminergic neuronal death in the *Substantia Nigra* of brain patients. The Rho GTPase pathway, mainly linking surface receptors to the organization of the actin and microtubule cytoskeletons, has been suggested to participate to Parkinson's disease pathogenesis. Nevertheless, its exact contribution remains obscure. To unveil the participation of the Rho GTPase family to the molecular pathogenesis of Parkinson's disease, we first used *C elegans* to demonstrate the role of the small GTPase *RAC1* (*ced-10* in the worm) in maintaining dopaminergic function and survival in the presence of alpha-synuclein. In addition, *ced-10* mutant worms determined an increase of alpha-synuclein inclusions in comparison to control worms as well as an increase in autophagic vesicles. We then used a human neuroblastoma cells (M17) stably over-expressing alpha-synuclein, and found that *RAC1* function decreased the amount of amyloidogenic alpha-synuclein. Further, by using dopaminergic neurons derived from patients of familial LRRK2-Parkinson's disease we report that human RAC1 activity is essential in the regulation of dopaminergic cell death, alpha-synuclein accumulation, participates in neurite arborization and modulates autophagy. Thus we determined for the first time that *RAC1/ced-10* participates in Parkinson's Disease associated pathogenesis and established *RAC1/ced-10* as a new candidate for further investigation of Parkinson's Disease associated mechanisms, mainly focused on dopaminergic function and survival against α-synuclein-induced toxicity.

Keywords: Parkinson's disease; dopaminergic neurons; alpha-synuclein accumulation; autophagy impairment; *RAC1/ced-10*

Introduction

Parkinson's disease (PD) is the second most frequent neurodegenerative disorder in the elderly. While most of cases are sporadic, monogenic PD caused by pathogenic point mutations in PD-associated genes occurs in less than 10% of cases (reviewed in [1]). The common neuropathological hallmarks of PD include a selective loss of the dopaminergic neurons (DAn) in the *Substantia Nigra pars compacta* and aggregation of the protein alpha-synuclein (α-SYN) in the surviving DAn and in the so called Lewy bodies (LB) and Lewy neurites (LN) which are found in the few surviving DAn (reviewed in [2]). α-SYN is intrinsically misfolded in pathological conditions such as PD [3] and forms multiple conformations, including amyloidogenic oligomers [4, 5] implicated in α-SYN toxicity [6].

There exist evidences of an essential role of actin cytoskeleton disruptions in both DAn cell death [7, 8] and α-SYN accumulation [9]. In fact, the cytoskeleton is an important target of α-SYN [10] and neuronal microtubule-kinesin function could be impaired by α-SYN oligomers [11]. Actin cytoskeletal organization is regulated by small GTPases of the Rho family encompassing Rho, Cdc42 and Rac subfamily members [7]. More specifically, RAC1 activity is mainly associated with cellular processes involving the regulation of actin polymerization such as cell migration, lamellipodia extension or the phagocytosis of dead cells or engulfment [12]. In addition, RAC1 participates in the extension and retraction of neurites [13] and, together with other members of the Rho family, govern changes in neuronal morphology and the dynamics of neuronal processes (reviewed in [8])

RAC1 function has been associated with two PD-related genes. We have previously shown in *C elegans* that RAC1 is ubiquitylated by PARKIN [14], mutated in the juvenile variant of PD. Likewise, Leucine-rich repeat kinase 2 (LRRK2), in which mutations cause the most common form of familial PD [15], strongly and selectively binds to RAC1 [16]. Furthermore, neuronal apoptosis induced in DAn *in vitro* is correlated with decreased RAC1 activity [17]. In contrast, in a monkey model of PD, it was suggested

136 that aberrant activation of RAC1 in microglia may contribute to enhanced production of
137 ROS underlying the death of neighboring DAn [18]. Therefore understanding the
138 cytoskeletal mechanisms associated with DA cell death and α-SYN degradation is
139 important to elucidate other causative agents of the PD pathophysiology.
140 Autophagic flux is profoundly disrupted in PD patients (reviewed in *[1]* and α-SYN is
141 normally degraded by autophagy [19]. Indeed, autophagy has been associated with PD
142 pathogenesis through several genes, such as *LRRK2* [20], *ATG9A* [21] or *ATG8/LC3*
143 [22], and cellular processes such as lysosomal disruption [23, 24]. In addition,
144 autophagy-related gene products are required for apoptotic clearance, either in dying
145 cells or through a role in engulfment, in where *RAC1* has a pivotal role [25-27].
146 In the present study we have systematically investigated *RAC1* function in three
147 disease models of PD including: a) *C elegans* models of PD, b) human derived
148 neuroblastoma BE(2) (M17) cells stably over-expressing α-SYN, wherein amyloidigenic
149 accumulation of α-SYN is induced by sodium butyrate, and c) iPSC-derived DAn
150 generated by cell reprogramming of somatic skin cells from patients with monogenic
151 LRRK2-associated PD [20]. Using these models we determine for the first time that
152 *RAC1/ced-10* participates specifically in PD associated pathogenesis and establish
153 *RAC1/ced-10* as a new candidate to be considered for the investigation of PD
154 associated mechanisms, mainly focused on DA function and survival against α-SYN-
155 induced toxicity.
156 **Results**
157 ***RAC1/ced-10* cell-autonomous depletion in DAn hampers dopamine- associated**
158 **behavior in the presence of α-SYN and accelerates α-SYN induced DAn death in**
159 ***C elegans***
160 We first investigated the role of *RAC1/ced-10* in DAn function, by performing behavioral
161 assays through analyzing the DA behavior in *ced-10(n3246)* mutant animals. The
162 mutation *ced-10(n3246)* is a G-to-A transition resulting in a change of glycine 60 of
163 CED-10 to arginine (G60R) which results in non-null altered function [28, 29]. The

164 severity of this allele is stronger in contrast to other *ced-10* alleles (11). To explore the
165 role of *ced-10* in PD pathogenesis, all the experiments included in this study involving
166 the *ced-10* gene were performed in a *ced-10(n3246)* mutant background. To simplify,
167 *ced-10(n3246)* is named *ced-10* from here on.
168 The basal slowing response is a DA dependent behavior widely used in *C elegans* for
169 analyzing the functionality of the DA system [30-32]. Briefly, worms decrease
170 locomotion speed when in physical contact with a food source whereas the turn
171 frequency increases when worms leave the food source [31, 33]. The *cat-2* gene
172 encodes the enzyme tyrosine hydroxylase required for the synthesis of dopamine.
173 Accordingly, *cat-2(e1112)* mutant worms have decreased levels of dopamine and
174 altered DA behavior [30, 33] and were used as positive control.
175 The locomotion speed of the nematodes, represented by the body bends every 20
176 seconds, was measured in the absence/presence of bacteria (+/-) (**Fig 1a**). In a wild
177 type background (wt background), both wild type and *ced-10* animals decreased the
178 locomotion speed in the presence of food, thus showing unaltered basal slowing
179 response. In contrast, in *cat-2(e1112)* mutants the locomotion speed was not
180 significantly decreased by the presence of food (**Fig 1a** wt background, **and Table 1**).
181 Similarly to the slow basal response, avoidance against ethanol is a sensory
182 behavior associated with DA signaling [34]. A slight decrease was observed in the
183 ethanol avoidance test performed in *ced-10* mutant animals in a wt background (**Fig**
184 **1b** wt background and **Table 2**).
185 The absence of significant dopaminergic behavioral alterations observed in *ced-10*
186 mutants might be the consequence of compensating mechanisms existing in the
187 worm that mask the effect of *ced-10* function specifically in DAn. To discard any
188 effect of *ced-10* function onto DA responses, *ced-10* was depleted conditionally in
189 DAn by RNAi, in a *C. elegans* PD model in which DAn undergo age-dependent
190 neurodegeneration following human α-SYN overexpression [35]. In this model, animals
191 express both α-SYN and GFP in DAn. Importantly, this is a neuronal-sensitive RNAi

192 strain whereby the impact of RNAi knockdown targeting gene candidates can be
193 selectively examined exclusively in the DAn [36] To simplify, this strain is called P*dat-*
194 *1*::α-SYN + P*dat-1*::GFP herein. Animals exposed to *ced-10* RNAi showed a mild but
195 significant altered slow response assay (**Fig 1a** and **Table 1**). In addition, selective
196 depletion of *ced-10* in DAn resulted in similar avoidance against ethanol as *cat-2*
197 depleted animals in the ethanol avoidance test (**Fig 1b** and **Table 2**). Therefore, in the
198 presence of α-SYN, *ced-10* function is specifically necessary in *C elegans* DAn to
199 execute a correct DA behavioral response.
200 This negative impact of *ced-10* depletion on DAn behavior brought us to explore the
201 relevance of *ced-10* deficiency in DAn cell death in the above mentioned strain P*dat-*
202 *1*::α-SYN + P*dat-1*::GFP. There exist 4 pairs of DAn in *C elegans* hermaphrodites, 3 of
203 them (CEPD, CEPV and ADE) located in the anterior part, and 1 pair, the PDE, located
204 in the posterior part of the nematode [37]. In this nematode, when human α-SYN is
205 expressed in DAn, the six DAn within the anterior region of the worm display
206 progressive degenerative characteristics [38]. To draw parallels between human PD
207 evidenced in aged populations and this worm model, we sought to determine the
208 relevance of *ced-10* depletion at 9 days (L4+7) post hatching. Cell bodies and neuronal
209 processes were assessed to determine whether these structures were normal or
210 displayed degenerative changes, and consequently considered wild type neurons (**Fig**
211 **2**). After feeding worms with EV RNAi, 24.93 % ± 2.54 of animals showed the six
212 anterior wild type DAn. In contrast, *ced-10* RNAi knockdown significantly enhanced DA
213 neurodegeneration (8.33 % ± 1.67 (*** $P< 0.001$)) in comparison with EV control (**Fig**
214 **2a-b**). Animals expressing the fusion protein, CFP::CED-10, under *ced-10* promoter,
215 rescued α-SYN induced-neurodegeneration (*** $P< 0.001$) (**Fig 2a-b**). We found that
216 neurodegeneration was accelerated already at days 3 and 5 (L4+1 and L4+3
217 respectively) post-hatching (**Online Resource 1**) thus corroborating the impact of *ced-*
218 *10* in α-SYN-induced DA cell death at younger ages.
219 **CED-10 expression decreases α-SYN inclusions formation in *C elegans***

220 The term phagocytosis refers also to the mechanism by which certain cells engulf and
221 digest other cells and also larger particles or even anomalous inclusions or aggregates
222 [39, 40]. *RAC1/ced-10* is the converging gene of the engulfment machinery mobilizing
223 actin pseudopodia in phagocytic cells [12]. Therefore, we considered the possibility of
224 *ced-10* playing a role in the clearance/phagocytosis of α-SYN inclusions. We used a
225 nematode model of PD, in which human α-SYN is fused to the yellow fluorescent
226 protein (YFP) under control of the body wall muscle *unc-54* promoter, transgene
227 *pkIs2386* [P*unc-54*::*α-SYN*::*YFP*] [41]. With this approach we examined changes in
228 apparent aggregate density or aggregate count of pathogenic α-SYN conjugated to
229 fluorescent YFP in muscle cells [42], without considering neuronal side effects.
230 Accordingly, *ced-10* animals were crossed with *pkIs2386* worms and the number of α-
231 SYN aggregates was evaluated in aged worms at 7 days post hatching. This *ced-10*
232 mutation increased to 1.5 units the apparent density of α-SYN inclusions in comparison
233 to control worms (0.9 ± 0.06 vs 1.49 ± 0.06 respectively; *** $P < 0.001$) (**Fig 3 a-b**) thus
234 suggesting a deleterious effect of the *ced-10* mutation in the generation of α-SYN
235 aggregates. Importantly, the increase in α-SYN apparent aggregates was abolished in
236 transgenic *ced-10* mutants expressing the CFP::CED-10 fusion protein (array
237 *baEx167[*P*ced-10*::CFP::*ced-10]*) (0.42 ± 0.03 in worms expressing CED-10 wild type
238 vs 1.49 ± 0.06 in *ced-10* mutant worms respectively and **Fig 3a-b**, *** $P < 0.001$),
239 showing that the lack of *ced-10* is contributing to α-SYN accumulation.
240 The number of body thrashes or thrashing have been used extensively to identify
241 modifiers of protein aggregation [41, 43]. Thrashing in *C elegans* can be measured in
242 liquid media by counting the number of body bends per unit of time [44]. Using this
243 method, we confirmed the observed damaged motility (**Fig 3c** and **Online Resources**
244 **2-4**) of the PD worms in a *ced-10* background. Whereas a decrease of 27 % in the
245 bending are observed in animals expressing YFP::α-SYN in comparison to the wild
246 type N2 wild type strain (55.01±7.5 vs 75.96 ± 2.8 bends/min respectively), the number
247 of bends decreases almost 90% in animals harboring the *ced-10* mutation in a

YFP::SYN background in comparison with N2 wild type animals (7.93 ±4.4 vs 75.96 ± 2.8 bends/min respectively) and 70% in comparison with worms expressing YFP::SYN, without the *ced-10* mutation (7.93 ±4.4 vs 55.01±7.5 bends/min respectively). Thus, increased α-SYN in muscle with its concomitant locomotion decrease in *ced-10* mutants, indicate the involvement of *RAC1/ced-10* in the process of α-SYN accumulation in *C. elegans*.

α-SYN variants that form oligomers and protofibrils are associated to the most severe DAn nigral loss in PD models [1, 6]. To identify the biochemical nature of the apparent α-SYN aggregates increased by this *ced-10* mutation, worm lysates from *pkIs2386* worms without and with the *ced-10* mutation at L4+ 5 days of development, were sequentially extracted by detergent-containing buffers [45] and the amount of α-SYN extracted in each fraction was assessed by immunoblotting (**Fig 3d**). A faint band of 19 kDa was detected in the Tris-HCl fraction, most probably corresponding to the α-SYN monomer staining. The number of oligomeric species is increased in *ced-10* mutant animals within all analyzed fractions.

Autophagic markers are increased in *ced-10* mutant animals

Autophagy is considered one of the main pathways involved in α-SYN clearance [19, 46]. Given the role of *RAC1/ced-10* detected in α-SYN levels and in α-SYN-induced DAn cell death, we further sought to determine the participation of *ced-10* in the modulation of autophagy in *C elegans*. To this end, we first crossed *ced-10* mutant animals with those carrying the array *adIs2122 [Plgg-1::gfp::lgg-1]*. The gene *lgg-1* encodes a ubiquitin-like protein belonging to the Atg8/LC3 protein family, and the respective GFP::LGG-1 translational fusion thus allows to monitor autophagosome formation via fluorescence microscopy [47]. To explore the role of *ced-10* in autophagy, we manually counted the number of GFP::LGG-1 puncta present in the seam cells [48]. At the L3 stage, the number of puncta present in the seam cells were increased in animals harboring the *ced-10* mutation, in comparison to animals without the mutation, in where the GFP::LGG-1 pattern is mainly diffuse (**Fig 4a** and **b**). An increase in the

276 number of GFP::LGG-1 puncta may result from either elevated or impaired autophagic
277 flux [48, 49]. Therefore, we investigated the involvement of *RAC1/ced-10* in autophagic
278 pathways by analyzing the impact of the *ced-10* mutation in the autophagy- associated
279 reporter strain *bpIs51* [P*sqst-1*::*sqst-1*::*gfp* + *unc-76*(+)] . The *C.*
280 *elegans* SeQueSTosome-related protein, SQST-1, exhibits sequence similarity to
281 mammalian SQSTM1/p62 and is degraded by autophagy [48, 50]. As such, autophagy
282 impairment is often associated with SQST-1::GFP accumulation [48-50]. Similarly to
283 the results obtained with the GFP::LGG-1 reporter, *ced-10* mutant animals displayed
284 increased SQST-1::GFP internal density (**Fig 4c-e**). Whereas SQST-1::GFP staining
285 was barely detected in wild type animals (**Fig 4 c,d** upper panels, and **e**), *ced-10*
286 worms displayed SQST-1::GFP accumulation (**Fig 4 c,d** bottom panels, and **e**).
287 Cumulatively, these results suggest a role of *RAC1/ced-10* in the regulation of
288 autophagy.

289 **Human RAC1 expression reduces α-SYN accumulation and amyloidogenic**
290 **aggregation in a neuroblastoma cell line**

291 We further explored the effect of *RAC1* on α-SYN accumulation using a stable BE(2)-
292 M17 neuroblastoma cell line over-expressing wild type α-SYN. As previously reported
293 [51], differentiation with retinoic acid (RA) and treatment with the histone deacetylases
294 inhibitor sodium butyrate (SB) increased α-SYN expression by 2-fold and induced the
295 accumulation of small α-SYN cytoplasmic aggregates (**Online Resource 5a-b**).
296 Differentiated cells treated with SB were transduced with a lentiviral vector (LV)
297 expressing either RAC1 wild type (WT)-GFP or RAC1 constitutively active (CA)-GFP
298 and analyzed 4 days post-transduction, using the empty vector (Control-GFP) as a
299 control. Infection with both, RAC1 (WT) and RAC 1(CA) decreased α-SYN expression
300 level (**Online Resource 5b**) and aggregation, as shown by Thioflavin S (ThyoS) dye
301 (**Fig 5**), which specifically stains cross-beta sheet fibrils, such those forming amyloid
302 aggregates [52]. The area covered by ThyoS -positive α-SYN aggregates per cell was

303 decreased by 90 % in RAC1(WT) and RAC1(CA) infected cultures (**Fig 5**) thus
304 suggesting a role of RAC1 in either the formation or clearance of toxic α-SYN species
305 and corroborating the data obtained by western blot in the nematode.

306 **High RAC1 activity reduces α-SYN levels and increases neurite arborization in**
307 **PD patient-specific midbrain iPSC-derived DAn**

308 Lastly, to connect the nematode data with the human PD, we differentiated DAn upon
309 cell reprogramming of skin fibroblasts into induced pluripotent stem cells (iPSC) from
310 PD patients carrying the G2019S (G/S) mutation in the *LRRK2* gene. While preserving
311 the patient genetic background, this model exhibits some characteristic features and
312 cellular phenotypes of PD including reduced axonal outgrowth, α-SYN accumulation,
313 α-SYN-induced DAn cell death, and impaired autophagy [20]. Therefore, it represents
314 a suitable tool to contextualize and compare the nematode encountered data.
315 At 30 days of differentiation, patient iPSC-derived DAn do not show overt
316 morphological signs of neurodegeneration [20]. However, almost 40% of DAn positive
317 for the DA marker tyrosine hydroxylase (TH) showed detectable amounts of α-SYN
318 [20]. For this reason, and to explore early events affecting PD, we next investigated the
319 contribution of RAC1 in PD by rescuing α-SYN accumulation in DAn. For this purpose,
320 PD-iPSC derived midbrain DAn (at 30 days of differentiation when α-SYN accumulation
321 is already evident), were transduced with lentivirus (LV) expressing either RAC1 wild
322 type (RAC1 (WT)-GFP or a highly active form of RAC1 (RAC1 (CA-GFP), and LV-GFP
323 as control (Control-GFP) (**Online Resource 6a**, **c** and **d**), and analyzed 7 days after
324 transduction. We found that LRR2-PD derived DAn, transduced with Control-GFP
325 showed significant increase in α-SYN content in comparison with non-PD derived DAn
326 (**Fig 6a**, first and second panels, and scatter dot plot) confirming previous results [20].
327 A 18% decrease in α-SYN accumulation was observed in PD-derived cells infected
328 with RAC1 (WT)-GFP, and it was even stronger (48.15%) in PD-derived cells infected
329 with RAC1 (CA)-GFP (**Fig 6a**, third and fourth panels, and scatter dot plot, *** P <

0.001). By analyzing the number and length of neurites, to explore the capacity of Rac1 in rescuing neuronal degeneration (**Online Resource 7**), we found a decrease in neurite arborization in PD-derived DAn (**Fig 6b**), confirming previous reports showing reduction in neurite length/branching and defects of Rac signaling in LRRK2-associated parkinsonism (53). Importantly, overexpression of RAC1 (CA)-GFP, but not RAC1 (WT)-GFP, was associated with significant increase of neurite arborization (**Fig 6b**, fourth panel and left graph), consistent with a role for RAC1 in organizing the actin cytoskeleton (58). The neurite length was not rescued in any of the conditions tested (**Fig 6b**, right graph).

By transcriptome analysis we have previously reported that iPSC-derived DAn from PD patients exhibited a large number of gene expression changes. More specifically, we identified 437 differentially expressed genes (DEGs) in PD vs. controls of which 254 were up-regulated in PD patients and 183 were down-regulated [54]. Here, to gain further insight into the canonical pathways affected by differential gene expression detected at early PD, we performed a biological enrichment analysis at 30 days of differentiation, by using the software and databases of Ingenuity Pathway Analysis (IPA). We found that the signaling by Rho family GTPases pathway was the top-1 statistically most significant canonical pathway in PD patients compared to controls ($P = 2.56x10^{-4}$) (**Online Resource 8**). From the total of 245 members comprised in this pathway, we found 16 DEGs of which 9 genes were up-regulated and 7 down-regulated in PD DAn (**Online Resource 9**). Interestingly, the top-2 statistically most significant canonical pathway was the related Rho GDI pathway ($P = 7.91x10^{-4}$). Overall, the results from this unbiased biological enrichment analysis identifies Rho family GTPases as top deregulated canonical pathway in iPSC-derived DAn from PD patients.

RAC1 activity increases the long-term survival of PD-patient derived DAn and alleviates the impairment of autophagy

To assess whether the protective effect of RAC1 in reducing α-SYN levels correlated with increased survival rates over time, neurons were further cultured for 75 days (**Online Resource 6b**) by co-culturing them over a monolayer of mouse post-natal cortical astrocytes [55], which supported viable cultures of DAn for up to 75 days [20]. After this time span, differentiated cultures from genetic LRRK2-PD- patient derived DAn showed higher numbers of apoptotic DAn when compared to those derived from healthy subjects [20] and **Fig 7a-b** and **e**. Overexpression of both RAC1 (CA)-GFP and RAC1 (WT)-GFP prevented cell death by reducing the amount of DAn positively stained for cleaved caspase-3 to the levels of the non-PD patient derived DA cells (**Fig 7 c-d** and **e**). We and others have described that LRRK2 G2019S mutation has negative effects in the autophagic flux by seemingly impairing autophagosome-lysosome fusion [20]. In this specific case, RAC1 CA (LV-RAC1-(CA) but not RAC1 wild type (LV-RAC1-(WT) displayed autophagosome vesicle numbers similar to those of the non-PD patient derived neurons (**Fig 7**). Therefore, these results suggest a mechanism by which a better performance of the autophagic clearance promoted by RAC1 alleviates the accumulation of aggregation-prone proteins, such as α-SYN, thus contributing to increase the survival of DAn.

In conclusion, these results obtained in DAn derived from LRRK2-associated PD patients are in line with findings in the nematode models of PD, where RAC1 activity is directly involved with DAn survival in the presence of α-SYN, α-SYN inclusions formation and autophagic mechanisms.

Discussion

Here we demonstrate in *C elegans* and in human-derived PD cells that *RAC1/ced-10* participates in the main pathogenic manifestations of PD such as DAn death, α-SYN accumulation and impaired autophagy. Besides, the results obtained in the nematode, suggest a role of *ced-10* modulating DA behavior in the presence of α-SYN. Furthermore, *RAC1* function is associated with the considered toxic α-SYN species.

384 Overall, in this manuscript we propose *RAC1/ced-10* as a potential therapeutic target
385 for the treatment of PD-related disorders.

386 ***RAC1/ced-10* and DAn death**

387 Previous research has shown that Rac GTPases play an essential neuroprotective and
388 pro-survival role in neuronal models and diseases [17, 56-58]. Indeed, our in depth
389 analysis of the RAC1 signaling pathway arose from the transcriptomic data in human
390 iPSC-derived DAn from PD patients, showing altered Rho signaling as top deregulated
391 pathway, points to this same direction (**Online Resources 8-9**). However, Rac
392 GTPases modulation in different cell types is much more complex. Loss of RAC
393 GTPase activity may contribute to the death of DAn while increased Rac-GTP activity
394 in microglia may contribute to the formation of toxic ROS [59]. Hence, this complicated
395 RAC1 modulation depending upon the tissue and the ROS state, might explain the
396 behavioral differences observed between whole *ced-10* mutant animals and *RAC1/ced-*
397 *10* specifically depleted in DAn in the presence of α-SYN (**Fig 1**). Interestingly, a cell
398 non-autonomous function for hypodermal *RAC1/ced-10* in the maintenance of axonal
399 survival has been recently proposed in *C. elegans* [60]. Consequently, the influence of
400 RAC1 activity in the neighboring tissues cannot be obviated.

401 There exist positive correlation between neuronal apoptosis and decreased RAC1
402 GTPase activity [17]. Very different cellular models, such as human lymphoma cells or
403 primary cerebellar granule neurons, suggest the inhibition of caspase-induced
404 apoptosis by RAC1, whereby AKT-dependent pro-survival pathways and the
405 consequent Bcl-2-associated death protein (BAD) phosphorylation were downstream
406 and activated by RAC1 [59, 61].

407 The activation of the AKT by RAC1, also participates in the cytoskeleton reorganization
408 and cellular growth [62, 63] and a failure to maintain the integrity of DAn after they are
409 formed could cause DAn death [64]. Accordingly, RAC1-modulated processes involved
410 in the maintenance of cell integrity, might be crucial for cell survival.

411 LRRK2-PD patient derived DAn show increased neurite numbers after being
412 transduced with RAC1 (**Fig 7**), thus expanding the role of this GTPase in the
413 maintenance and in the generation of new neurites [13], and thus contributing
414 accordingly to DAn survival (**Fig 7**). Therefore, our results are in accordance with
415 LRRK2 inducing neurite retraction through diminished RAC1 GTPase activity [16].
416 Surprisingly, neurite length was not rescued with any of the infected RAC1 constructs
417 in the present manuscript. Differences between results can be explained based on the
418 different cellular models used in both laboratories, since our results are provided
419 directly from PD-derived cells, whereas the neuroblastoma cell line SHSY5Y is the
420 model used by Chan et al. [16]. In addition, the existing actin-microtubule cross talk in
421 the process of neurite outgrowth and elongation has to be considered [65, 66].
422 Microtubules are the main cytoskeletal components of neurites [66] and decreased
423 stability of microtubules is a common feature of neurodegenerative diseases [67].
424 Interestingly, LRRK2-PD variants are characterized by defects in microtubule
425 associated processes [68] and LRRK2 regulates microtubule stability [69].However,
426 extension and navigation of neurites are normally driven by actin-rich growth cones and
427 inhibition of microtubules dynamics does not stop neurite outgrowth [66]. Thus, our
428 results are consistent with cellular dysfunction in PD, with RAC1 modulating actin-
429 associated mechanisms better than in microtubule linked processes.

430 ***RAC1/ced-10* and α-SYN accumulation**

431 One of the main factors linked with DAn death in PD progression is α-SYN
432 accumulation. α-SYN overexpression in model systems, and its concomitant
433 aggregation and deposition precede neuronal cell death. In the case of DAn, its
434 degeneration is influenced by intracellular and extracellular α-SYN accumulation,
435 mainly in its oligomeric form [70]. Interestingly, extracellular oligomeric α-SYN impairs
436 RAC1 activity in neuroblastoma cells [70]. Considering the increased intracellular α-
437 SYN aggregates together with increased oligomeric α-SYN species observed in *ced-*
438 *10* mutant animals, we hypothesize that altered *RAC1/ced-10* function might accelerate

α-SYN accumulation and the formation of α-SYN oligomers which might bind concurrently *RAC1/ced-10* [70] thus increasing the severity of *RAC1/ced-10* altered function. Moreover, and considering the modulation of the actin cytoskeletal dynamics by α-SYN [71], a synergistic regulation between RAC1 and α-SYN cannot be excluded. Additional experiments, where the amount of α-SYN could be tightly controlled, will provide some clues about the relevance of RAC1/α-SYN interaction in the progress of PD.

α-SYN accumulation in PD patients is associated with failure of the two major protein breakdown pathways, the ubiquitin proteasome system (UPS) and autophagy [72-74], which , in cooperation, reduce the misfolded protein burden [75]. Stably increased levels of α-SYN can lead to impaired proteasome function [76] and *ced-10* is proteasome regulated in the phagocytosis of dead cells [14]. Hence, we hypothesize that increased α-SYN in a *ced-10* mutant background might reinforce the severity of the *ced-10* mutation in the degradation of α-SYN, due to the interaction of α-SYN with the proteasomal machinery.

Overexpression of α-SYN results in the inhibition of autophagy [77]. Here we suggest *RAC1/ced-10* being necessary for autophagy to occur (**Fig 3** and **7**). Accordingly, α-SYN accumulation, due to *ced-10* impairment, might increase the severity of *ced-10* mutation. Therefore we add RAC1 to the already proposed feedback loop between proteasome activity and autophagy [1] and we propose that a tight regulation of RAC1 function is required to avoid excess of α-SYN accumulation and the concomitant cell death.

Impaired autophagy associated with LRRK2 mutations are already reported [78, 79], with the G2019S mutation showing less autophagic activity [80]. In the context of LRRK-2 induced phenotypes, we propose RAC1-LRRK2 interaction as relevant factor favoring autophagy to occur, and helping in the clearance of α-SYN aggregates, thus warranting the proper neurite growth and maintenance.

466 Future scientific research is needed to unravel the mechanisms associated with PD-
467 related disorders for finding efficient therapies. In light of our results the
468 pharmacological modulation of RAC1 and RAC1-derived signaling pathways could be
469 of therapeutic value.

470 **Experimental procedures**

471 **Worm experiments:**

472 ***C. elegans* strains**

473 Nematodes were maintained using standard procedures [81]. We obtained the strains
474 CB1112 *cat-2(e1112)*, NL5901, *unc-119(ed3) III;* [*pkIs2386* (P*unc-54*::*α-SYN*::*YFP;*
475 *unc-119(+)*)]; DA2123 *adIs2122* [P*lgg-1*::*lgg-1*::*GFP*; *rol-6(su1006)]* and HZ589,
476 *bpIs151* [P*sqst-1*::*sqst-1*::GFP*; unc-76(+)*] *IV; him-5(e1490) V* from the *Caenorhabditis*
477 *elegans* Genetic Center (CGC). The strain BR3579, *ced-10(n3246)* was a generous gift
478 from Dr Ralf Baumeister (Albert-Ludwing University, Freiburg/Breisgau, Germany).
479 The strain BR3579 was crossed with NL5901 animals to generate the strain EDC101,
480 *unc-119(ed3) III; pkIs2386* [P*unc-54*::*α-SYN*::YFP*; unc-119(+)*]*; ced-10(n3246).*
481 The following strains is used to analyze the DAn degeneration as reported in
482 Harrington et al., 2010 [36]: P*dat-*$_1$::α-SYN +P*dat-1*::GFP from the main text is named
483 UA196, with the genotype*: sid-1(pk3321); baIn33* [P*dat-1*::*sid-1*; P*myo-2*::*mCherry*];
484 *baIn11* [P*dat-1*::α-SYN*; Pdat-1*::GFP].
485 For autophagy experiments, males from the DA2123 strain [P*lgg-1*::*lgg-1*::GFP*; rol-*
486 *6(su1006)]* were crossed with *ced-10(n3246)* hermaphrodites. Males a from the HZ589
487 *bpIs151* [P*sqst-1*::*sqst-1*::GFP*; unc-76*(+) *IV*]*; him-5*(*e1490*) *V*] strain, expressing
488 SQST-1::GFP crossed with *ced-10* (*n3246*) hermaphrodites.
489 N2 (Bristol) was used as the *C. elegans* wild-type (wt) strain. Hermaphrodites were
490 used throughout of the study.
491 **RNAi feeding**

For feeding RNAi bacteria, egg lay from gravid adults were directly transferred to NGM plates containing 1 mM of isopropyl β-D-1-thiogalactopyranoside/ IPTG (referred to as RNAi plates) seeded with 20X concentrated bacteria containing 50 µg/ml ampicillin, carrying desired plasmid for RNAi of a specific gene (*ced-10* or *cat-1*, depending upon the experiment) or bacteria carrying empty (EV) pL4440 as control and allowed to grow on plates for approximately 50 h to reach the L4 stage and then another 16 h for the conduction of actual experiment.

Note: Bacterial clones for RNAi feeding protocol were obtained from the Ahringer library (Source Bioscience, Nottingham, UK) [82] and were then streaked on LB-Tetracycline-Ampicillin plate which was then incubated at 37°C. Individual colonies from this freshly streaked plate were grown for 10-12h constantly shaking at 37°C in LB medium containing 50 µg/ml ampicillin.

Blinding of experiments and replicates

All behavioral studies were completed such that the experimenter was blind to the genotype of the worms. Strains were given letter codes by another member of the laboratory and the code was not broken until all of the replicates for a particular assay were completed. For all assays, we completed a minimum of three biological replicates per strain.

Behavioral experiments

Locomotor rate assay

Locomotor rate assay was performed as described in [33]. Briefly, assay plates were prepared by spreading the *E. coli* strain OP50-1 in a ring on NGM agar [81] in 5 cm petri plates. Assay plates were always freshly spread with bacteria, incubated overnight at 37°C, and allowed to cool to room temperature before use. Plates for measuring locomotor rate in the absence of bacteria were also incubated at 37°C. Only synchronized young adult hermaphrodites (16 h after the late L4 larval stage) were tested. For well-fed animals, locomotor rate was measured by removing 5 animals from plates with ample bacteria, washing the animals twice in S basal buffer [81], and

520 transferring them to an assay plate in a drop of buffer using a capillary pipette. The
521 drop of buffer used to transfer the animals was absorbed with a Kimwipe. Five minutes
522 after transfer, the number of body bends in 20 s intervals was sequentially counted for
523 each of the 5 animals on the assay plate and then repeated the same thing for next set
524 of animals in a different assay plate.

525 **Ethanol avoidance assay**

526 Ethanol avoidance assay was performed as described [34]Cooper et a, 2015).
527 Synchronized young adult hermaphrodites (16 h after the late L4 larval stage) were
528 transferred to assay plates, which are divided into four quadrants: two quadrants
529 seeded with 50 µl of 100% ethanol and the others without. Worms are placed in the
530 center of the assay plate and allowed to move for 30min at which point the entire plate
531 is imaged and the worms are scored for their quadrant of preference. Ethanol
532 avoidance is calculated as [(number of worms in control quadrants) – (number of
533 worms in ethanol quadrants)]/ total number of worms.

534 **Generation of the rescue construct P*ced-10*:: CFP::*ced-10***

535 P*ced-10* ::CFP::*ced-10* plasmids were co-injected into worm strain EDC101 and UA196
536 to generate UA281, *baEx167* [P*ced-10* ::CFP::*ced-10, rol-6(su1006)*]; [P*unc-54*::α-
537 SYN::YFP*;ced-10(n3246)*] and UA282, *baEx167* [P*ced-10*::CFP::*ced-10; rol-*
538 *6(su1006)*]; *sid-1(pk3321)*; *baIn33* [P*dat-1*::*sid-1,* P*myo-2*::*mCherry*]; *baIn11*[P*dat-1* ::α-
539 SYN; P*dat-1* ::GFP]). Hermaphrodites were used throughout of the study.

540 **Site-directed mutagenesis**

541 The construct P*ced-10*::GFP::*ced-10* was provided by Erik Lundquist (University of
542 Kansas, Lawrence, KS, USA) as a gift. TagMaster Site-directed mutagenesis (GM
543 Biosciences, Rockville, USA) was used to create mutations (Y66W, Y145F, and
544 M153T) in GFP sequence for changing fluorescence marker as CFP. The product
545 plasmid P*ced-10*::CFP::*ced-10* was sequenced (Eurofins Genomics, Huntsville, AL,
546 USA) to confirm the presence of the desired mutations.

547 ***C. elegans* neurodegeneration assays.**

548 Worms were analyzed for DA neurodegeneration as described previously [38]. Briefly,
549 10 L1-stage worms (neuron-specific RNAi worm strain with α-Syn UA196 were
550 transferred to the plates (empty vector (EV) and *ced-10* RNAi) and grown at 20°C until
551 adulthood. Adult worms were then transferred to corresponding freshly made RNAi
552 plates and allowed to lay eggs for 6 h to synchronize. α-SYN-induced DA
553 neurodegeneration was scored at the indicated days after hatching (L4+7; L4+3; L4+1).
554 To investigate the effect of CED-10 overexpression on α-SYN –induced DA
555 degeneration, the strain UA282 was analyzed at L4+7 days of aging. Worms were
556 considered normal when all six anterior DA neurons (four CEP (cephalic) and two ADE
557 (anterior deirid)) were present without any visible signs of degeneration. If a worm
558 displayed degeneration in at least one of the six neurons, it was scored as exhibiting
559 degeneration. In total, at least 50 adult worms were analyzed for each independent
560 transgenic line or RNAi treatment.

561 **Aggregate quantification**

562 The quantification of aggregates was performed as previously described [83]. Briefly,
563 NL5901animals without and with *ced-10(n3246)* mutation, together with the EDC101,
564 were age-synchronized by bleaching with NaOCl and left overnight to hatch. L1
565 animals were transferred onto individual NGM plates seeded with *Escherichia coli*.
566 Aggregates were counted for each animal staged at L4 + 5 days. Images were
567 captured using a Leica SP5 confocal microscope with an x40 oil immersion lens (HCX
568 PL APO CS). The number of α-syn aggregates was determined in the mid body of each
569 animal, taking the vulva position (V) as a reference. Aggregates were defined as
570 discrete, bright structures, with boundaries distinguishable from surrounding
571 fluorescence. Measurements on inclusions were performed using ImageJ software
572 taking into consideration the area dimensions.

573 **Thrashing assays.**

574 At L4 + 5 days, animals from the strains N2 wild type, NL5901 [*unc-119(ed3) III;*
575 *pkIs2386* [P*unc-54*::α-SYN::YFP*; unc-119(+)*] and EDC01 *unc-119(ed3) III; pkIs2386*

576 [P*unc-54*::α-SYN::YFP*; unc-119(+)*] ; *ced-10 (n3246)* were placed in a drop of M9
577 buffer and allowed to recover for 120 s (to avoid observing behavior associated with
578 stress) after which the number of body bends was counted for 1 min. Movies of
579 swimming worms were recorded using a Leica MZFFLIII stereomicroscope at nominal
580 magnification of 30X and the Hamamatsu ORCA-Flash 4.0LT camera at 17 frames per
581 second (17 fps) for 1 min. Bends per minute were obtained with the Worm Tracker
582 pluggin (wrMTrck), from the ImageJ software [84]. Thirty animals were counted in each
583 experiment unless stated otherwise. Experiments were carried out in triplicate.
584 Statistical analysis was performed using Graphpad Prism version 6.00 for Windows,
585 GraphPad Software, La Jolla California USA).

586 **Detergent fractionation**

587 α-SYN oligomeric species were isolated by detergent fractionation as described
588 (Kuwahara et al, 2012) with slight modifications. Briefly, worms were washed three
589 times with M9 buffer, collected as a 100 µl pellet, and the pellet was snap-frozen in
590 liquid nitrogen. The pellets were homogenized in 1 mL of 50 mM Tris-HCl buffer at pH
591 7.5 with complete protease inhibitor mixture (Roche Applied Science) by brief
592 sonication. Sonicates were centrifuged two times at 1000 X g for 5 min to remove
593 debris of worm tissue. The supernatant was then ultracentrifuged at 350,000 X g for 15
594 min, and the supernatant was collected as a Tris-HCl soluble fraction. The resulting
595 pellet was subsequently extracted by sonication in 500 µl of Triton X-100 (Tris-HCl
596 buffer with 1% TritonX-100), 200 µl of Sarkosyl (Tris-HCl with 1% Sarkosyl), and µl 100
597 of SDS (TrisHCl with SDS sample buffer containing 2% SDS) followed by centrifugation
598 at 350,000 X g for 15 min. The Tris-HCl fraction containing 20 µg of total proteins,
599 along with equal volumes of Triton X-100, Sarkosyl, and SDS fractions to the Tris-HCl
600 fraction, were loaded onto the acrylamide gel and separated by SDS-PAGE.

601 **Immunoblotting**

602 20 µl of protein per strain were loaded from each sample and fraction on Novex
603 NuPAGE 4-12% Bis-Tris Gels (Thermo Fisher) an run in MES SDS buffer at 200 V for

604 40 min. Resolved proteins were transferred onto 0.45 µm nitrocellulose membranes
605 (Amersham) at 200 mA for 1 h. Blocking was done in 5% milk powder in PBS for 1 h,
606 followed by overnight incubation at 4ºC with a mouse monoclonal antibody against α-
607 synuclein (1:1000, BD Biosciences, #610787) diluted in 2% bovine serum albumin
608 (BSA)/PBS. Incubation with a donkey anti-mouse (1:5000, Amersham) secondary
609 antibody diluted in 1% milk powder/PBS was performed for 1 h at room temperature.
610 Membranes were developed using Supersignal West Femto (Thermo Scientific) in a
611 ImageQuant RT ECL Imager (GE Healthcare).

612 **Autophagy measurements**

613 For measuring the involvement of *ced-10(n3246)* mutation in autophagy, we followed
614 specific *C elegans* protocols [48, 85]. LGG-1::GFP foci were analyzed in the
615 hypodermal seam cells at L3 stage of development. Images were not considered for
616 quantification where the hypodermis was not clear. In total, at least 40 total regions
617 were quantified from 30 different worm samples per genotype.
618 To confirm the involvement of *ced-10* in impairing autophagy, we followed the protocol
619 described in [86]. Pictures of L1 animals (whole animal) and L4 animals (whole
620 intestine), were analyzed by using a 63X objective. The GFP internal intensity (FI),
621 corresponding to SQST-GFP foci, was quantified at L4 stage of development. The
622 presence of the *ced-10* mutation was checked by PCR as described [14]. The
623 presence of the GFP reporter was double checked by PCR using the *gfp* primers, and
624 under the fluorescence microscope.

625 **Microscopy and imaging**

626 For neurodegeneration assays and aggregates quantification animals were mounted
627 with a coverslip on a 4% agarose pad in M9, containing 10 mM of sodium azide.
628 Confocal microscopy was performed using a Leica TCS-SP5 confocal spectral
629 microscope (Leica, Barcelona, Spain) and analyzed using ImageJ software (NIH, ver.
630 1.43, Schindelin, 2015). Animals were examined at 100X magnification to examine α-
631 SYN induced DA cell death and at 40X to examine α-SYN apparent aggregates.

For autophagy measurements, animals were placed in a 5 µL drop of 10 mM solution of levamisole (Sigma-Aldrich, Madrid, Spain). For each independent experiment, between 20-30 7-days old worms of each treatment were examined under a Nikon EclipseTE2000-E epifluorescence microscope equipped with a monochrome camera (Hamamatsu ORCA-ER) coupled to the Metamorph software (Molecular Devices Corp., Sunnyvale, CA). The system acquires a series of frames at specific Z-axis position (focal plane) using a Z-axis motor device.

Cell culture experiments in BE(2)-M17 neuroblastoma cell line

Cell culture

Human neuroblastoma cell line BE(2)-M17 over-expressing wild type α-SYN were maintained at 37ºC and 5% CO_2 in Optimem medium (Gibco) (Thermo-Fisher Scientific, Madrid, Spain) supplemented with 10% fetal bovine serum (Gibco) (Thermo-Fisher Scientific, Madrid, Spain) , 500 µg/ml G418 (Geneticin) (Sigma-Aldrich, Madrid, Spain) and Penicillin/Streptomycin (Sigma-Aldrich, Madrid, Spain). For immunofluorescence, $2x10^4$ cells/ well were seeded in 24-well plates on coverslips coated with poly-D-lysine. α-SYN aggregation was induced as previously reported ([51] by differentiation with 10 µM retinoic acid (Sigma-Aldrich, Madrid, Spain) for 10 days, followed by treatment with the histone deacetylases inhibitor sodium butyrate (SB) (Sigma-Aldrich, Madrid, Spain) at a concentration of 10 mM for 36 h. To analyze the effect of RAC1 on α-SYN aggregation, cells were transduced 24 h before SB treatment with either the lentiviral empty vector or with the wild type or the constitutively active isoforms of RAC1 at an estimated multiplicity of infection (MOI) of 5.

Immunofluorescence

BE(2)-M17 cells were fixed in 4% paraformaldehyde (PFA) (Sigma-Aldrich, Madrid, Spain) in phosphate saline buffer (PBS) for 30 min at 4ºC and permeabilized with Tris-buffered saline (TBS) containing 0.5% Triton X-100 (Sigma-Aldrich, Madrid, Spain) for 5 min. Cells were then blocked with 3% normal goat serum (NGS) (Vector

659 Laboratories, Palex Medical, Sant Cugat del Vallès, Spain) in TBS for 1 h and
660 subsequently incubated with the corresponding primary antibody in in 1%NGS/TBS
661 overnight at 4ºC. The following primary antibodies were used: mouse anti-α-SYN
662 (610787; 1:500) (BD Biosciences, Madrid, Spain), rabbit anti-α-SYN (2642; 1:500) (Cell
663 Signaling, Leiden, The Netherlands). Incubation with goat secondary antibodies
664 conjugated with Alexa488 (anti-mouse, A11001; or Alexa594 (anti-mouse, A11005;
665 anti-rabbit, A11012) (Thermo-Fisher Scientific, Madrid, Spain) was done in 1%
666 NGS/TBS for 1h at RT. Between each incubation period cells were rinsed three times
667 in TBS.

668 **Thioflavin S staining**

669 After incubation with the antibodies, coverslips were immersed in 0.005% thioflavin S
670 (Sigma-Aldrich, Madrid, Spain) in PBS for 8 min and then rinsed twice in ethanol 70%
671 and once in PBS. Only after thioflavin S staining, nuclei were counterstained with
672 Hoechst 33342 (Thermo Fisher Scientific, Madrid, Spain, 1:10000 in PBS) for 10 min.

673 **Microscopy and IF quantification**

674 Cells were coverslipped using Dako Cytomation Fluorescent Mounting Medium (Dako,
675 Sant Just Desvern, Spain). Immunofluorescence images were acquired using standard
676 filter sets using an Olympus FluoView TM FV1000 confocal microscope and the
677 FV10_ASW 4.2 visualization software.
678 α-SYN fluorescence intensity for each condition was analyzed in an average of 150
679 cells from 6 different random fields at an objective magnification of 40x. Quantification
680 of Thioflavin S positive aggregates in each condition was analyzed in an average of 20
681 cells from 3 different random fields by measuring the fluorescent area per cell. All
682 quantification analyses were done using ImageJ software (NIH, USA).

683 **Cell culture experiments with iPSC cell lines derived from human patients**

684 Previously generated iPSC lines SP-11.1 (from control) and SP-12.3 (from patients
685 with familial PD with the LRRK2 G2019S mutation) were used and culture and
686 differentiation were carried out as described, (34), following a protocol approved by the

687 Spanish competent authorities (Commission on Guarantees concerning the Donation
688 and Use of Human Tissues and Cells of the Carlos III Health Institute). Briefly, hiPSC
689 were cultured on matrigel (Corning Limited, Life Sciences, UK) and maintained in
690 hESC medium, consisting on KO-DMEM (Invitrogen, Thermo Fisher Scientific, Madrid,
691 Spain) supplemented with 20% KO-Serum Replacement (Invitrogen, Thermo Fisher
692 Scientific, Madrid, Spain), 2 mM Glutamax (Invitrogen, Thermo Fisher Scientific,
693 Madrid, Spain), 50 µM 2-mercaptoethanol (Invitrogen, Thermo Fisher Scientific,
694 Madrid, Spain), non-essential aminoacids (Cambrex, Nottingham, UK) and 10 ng/ml
695 bFGF (Peprotech, London, UK)). Medium was preconditioned overnight by irradiated
696 mouse embryonic fibroblast and hiPSC were maintained on Matrigel (Corning Limited,
697 Life Sciences, UK) at 37°C, 5% CO2.
698 For DAn differentiation, iPSC were transduced with LV.NES.LMX1A.GFP and
699 processed as previously described (79). Briefly, confluent iPSC 10 cm dishes were
700 disaggregated with accutase and embryoid bodies (EB) were generated using forced
701 aggregation method in V-shaped 96 well plates. Two days later, EBs were patterned as
702 ventral midbrain by culturing them in suspension for 10 days in N2B27 supplemented
703 with 100ng/ml SHH (Peprotech, London, UK), 100ng/ml FGF8 (Peprotech, London,
704 UK) and 10ng/ml FGF2 (Peprotech, London, UK). Then, for α-SYN and neurite
705 analysis, differentiation to midbrain DAn was performed on the top of PA6 murine
706 stromal cells for 3 weeks (79). To analyze α-SYN levels, neuronal cultures were gently
707 trypsinized and re-plated in matrigel-coated slides for 3 days, then transduced with the
708 two different RAC1 isoforms or the control LV, at an estimated MOI of 10. Cells were
709 fixed and analyzed 7 days after transduction. For long-term culture studies, EBs were
710 mechanically dissociated by repeated pipetting after the induction step. Salient EB
711 fragments were transduced with the two different RAC1 isoforms or the control LV at
712 an estimated MOI of 3. 3 days post transduction, the aggregates were seeded on
713 primary murine astrocytes and cultured for 9 weeks.
714 **Lentiviral vectors**

715 RAC1 wild type (WT) and constitutively active (V12) (CA) forms were amplified by
716 means of PCR from expression plasmids kindly provided by (Dr Francisco Sánchez-
717 Madrid; Spanish National Center for Cardiovascular Research (CNIC), Madrid, Spain).
718 Subsequently, RAC1-(WT) and RAC1-(CA) cDNA were cloned under the human
719 phosphoglycerate kinase (PGK) promoter of pCCL.cPPT-hPGK-IRES.eGFP-WPRE
720 lentiviral transfer vector. High-titer vesicular stomatitis virus (VSV)–pseudotyped LV
721 stocks were produced in 293T cells by calcium phosphate–mediated transient
722 transfection of the transfer vector, the late generation packaging construct pMDL, and
723 the VSV envelope–expressing construct pMD2.G, and purified by ultracentrifugation as
724 previously described [87]. Expression titers, determined on HeLa cells by fluorescence-
725 activated cell sorter (FACS) analysis (FACSCalibur, Becton Dickinson), were: LV-
726 RAC1 (WT): 2,60 · 10^8 TU/mL; LV-RAC1 (CA): 2,24 · 10^8 TU/mL; LV-PGK-GFP:
727 5,08 · 10^9 TU/mL

728 **Immunofluorescence for iPSC-derived cells**

729 iPSC-derived cells were fixed with 4% paraformaldehyde (PFA) in Tris-buffered saline
730 (TBS) buffer for 20 min and blocked in 0.3% Triton X-100 (Sigma-Aldrich, Madrid,
731 Spain) with 3% donkey serum for 2 h. In the case of α-SYN and LC3 staining, Triton X-
732 100 was kept at 0.01% for the blocking and antibody incubation steps. The following
733 primary antibodies were used: mouse anti-α-SYN (610787; 1:500) (BD Biosciences,
734 Madrid, Spain), rabbit anti-TH (sc-14007; 1:500) (Santa Cruz Biotechnology, Madrid,
735 Spain), chicken anti-GFP (1020; 1:250) from Aves Labs (Cosmo Bio, AbBcn S.L.,
736 Bellaterra, Spain), rabbit anti-cleaved Caspase3 (9664; 1:400) (Cell Signaling) and
737 LC3B (2775; 1:100) (Cell Signaling). Images were acquired using a Leica SP5 confocal
738 microscope.

739 **α-SYN and neurite analysis**

740 α-SYN and neurite analysis were performed after a total of 4 weeks of differentiation
741 plus 1 week after LV transduction on iPSC-derived DA neurons. DA neurons were
742 randomly selected, using a Leica SP5 confocal microscope, and analyzed with ImageJ

743 for α-SYN intensity levels and with the ImageJ plugin NeuronJ to determine the number
744 of neurites per cell, number of terminals and branch points.

745 **Apoptotic cell number and autophagosome accumulation and analysis**

746 Autophagosome accumulation and apoptotic cell number analysis were performed after
747 a total of 9 weeks of differentiation on iPSC-derived DAn grown on murine astrocytes.
748 DA neurons were randomly selected, using a Leica SP5 confocal microscope, and
749 analysed with ImageJ to determine the fraction of the neuronal soma area covered by
750 LC3-positive particles.

751 **Statistical analysis**

752 All data are presented as mean ± SEM as stated. Group means were compared with
753 either the Student's t-test or ANOVA. All *P* values were two tailed, and a *P* value of less
754 than 0.05 was considered statistically significant. All statistical analyses were analyzed
755 using GraphPad Prism (San Diego, CA, USA) software.
756 Outlier values were identified with the Grubbs' tests and excluded from the analysis.
757 Differences among means were analyzed either by 1- or 2-way analysis of variance
758 (ANOVA), as appropriate, using the post-hoc Tukey's multiple comparison test. In all
759 cases, the null hypothesis was rejected at the 0.05 level.

760 **Biological enrichment analysis**

761 Transcriptomic analysis of iPSC-derived DAn from PD patients (n=10) and healthy
762 controls (n=4) was done as previously described [54]. Identified differentially expressed
763 genes (DEGs) after multiple testing adjustment of P values (n=437) were subjected to
764 biological enrichment analysis. To this end, we used the Core Analysis module of the
765 Ingenuity® Pathway Analysis (IPA) software (Qiagen, Redwood City,
766 www.qiagen.com/ingenuity) to identify biological enrichment of canonical pathways
767 deregulated in iPSC-derived DAn from PD patients. More specifically, we used the
768 Ingenuity Knowledge Base of Genes, and considered only direct molecules and/or
769 relationships for humans. Statistical significance of canonical pathways was computed
770 by using the Fischer's exact test and significance levels were set at P below 0.05.

771 Using IPA we also calculated Z-score values which consider the directional effect of
772 one molecule on another molecule or on a process, and also the direction of change of
773 molecules in the dataset and provide predictions about whether the pathway
774 is predicted to be activated or inhibited, or if the pathway is ineligible for such an
775 assessment.

776 **Tables**

777 **Table 1:**

Genotype	w/o food (body bends/20 sec)	with food (body bends/20 sec)	Significance (*P* value)
wild type	20.00± 0.423	9.55 ± 0.328	$P < 0.001$
ced-10(n3246)	19.05 ± 0.211	13.00 ± 0.145	$P < 0.001$
cat-2 (e1112)	21.00 ± 0.191	20.00 ± 0.162	ns
UA196 on EV	18.40 ± 0.255	9.20 ± 0.257	$P < 0.001$
UA196 on *ced-10* RNAi	16.00 ± 0.254	13.15 ± 0.392	$P < 0.001$
UA196 on *cat-2* RNAi	17.25 ± 0.502	16.40 ± 0.689	ns

778

779 **Table 1: Slow dose response quantifications**: Mean and SEM reported, n=20. One-
780 way ANOVA

781 **Table 2: Ethanol avoidance**

Genotype	Avoidance (% of worms)	N	Significance (*P* value)
wild type	71.21± 2.120	155	--
ced-10(n3246)	57.80 ± 3.957	94	$P < 0.05$
cat-2 (e1112)	26.67 ± 3.335	80	$P < 0.001$
UA196 on EV	70.35 ± 1.213	122	--
UA196 on *ced-10* RNAi	12.95 ± 1.328	95	$P < 0.001$
UA196 on *cat-*	10.902 ± 1.524	175	$P < 0.001$

2 RNAi			

782

783 **Table 2: Ethanol avoidance quantifications:** Mean and SEM reported. One-way
784 ANOVA

785 **Figure legends**

786 **Figure 1: DAn function is hampered by specific depletion of *RAC1/ced-10* in DAn**
787 **expressing α-SYN in *C elegans*: (A)** Modulation of the locomotor rate. Well-fed
788 animals were transferred to assay plates without or with a bacterial lawn (- /+) and 5
789 minutes later, the locomotor rate (body bends every 20 seconds) of each animal was
790 analyzed. Statistical significance shows comparison of the bending within same
791 genotype animals (wild type, *ced-10(n3246)* and *cat-2 (e1112)*) without (-) or with (+)
792 bacteria. RNAi experiments indicate P*dat-1*::α-SYN +P*dat-1*:: GFP worms fed with EV
793 (empty vector) or with the indicated RNAi clones **(B)** Test of ethanol avoidance. The
794 percentage (%) of ethanol avoidance was analyzed at the indicated genotypes.
795 Statistical analysis shows comparisons between wild type animals and mutants, and
796 P*dat-1*::α-SYN +P*dat-1*:: GFP worms fed either with EV (empty vector) or with the
797 indicated RNAi clones. *cat-2 (e1112)* mutant worms were included as positive controls
798 for both assays. Slow response assay and ethanol avoidance behaviors were
799 hampered in *ced-10* depleted animals and not in *ced-10(n3246)* mutants. Data are
800 mean ± SEM. * P <0.05, ** P<0.01, *** P<0.001, ns: non-significant. Statistics: One
801 way-ANOVA, Tukey *post hoc* test for multiple comparisons. Between 20- 30 worms
802 were used in three independent replicates.

803 **Figure 2: CED-10 protects DAn from α-SYN-induced DA cell death in *C elegans*.**
804 Representative RNAi empty vector (EV) fed worms expressing GFP and α-SYN
805 specifically in DAn (P*dat-1*:: α-SYN + P*dat-1*:: GFP) at L4 + 7 days (9 days post
806 hatching) and fed with empty vector (EV) or *ced-10* RNAi clones. Filled white
807 arrowhead labels healthy neurons whereas degenerated or missing neurons are
808 labeled with an open arrow. **(A)** *ced-10* depletion reduces the amount of DAn per worm
809 and the expression of the CED-10::CFP transgene {*baEx167* [P*ced-10*::CFP::*ced-10*]}

delays the DA cell death at the same age. Magnification bar is 30 µm. **(B)** Percentage of P*dat-1*:: α-SYN + P*dat-1*:: GFP worms non- depleted and *ced-10* depleted by RNAi, that had the full complement of six anterior DAn at day 7 post L4. The transgenic derivative strain UA281 expressing CFP::CED-10 (CED-10 wild type), carrying the array *baEx167* [P*ced-10*::CFP::*ced-10*] ameliorates the DA cell death. Data are mean ± SEM. Statistics were obtained by comparing *ced-10* RNAi depleted worms or worms containing the CFP::CED-10 array with the corresponding EV fed animals. Statistics: *** $P< 0.001$, one way ANOVA, Tukey's *post hoc* test. Number of animals is 30-35 per condition, and the experiment was repeated 3 times independently.

Figure 3: *ced-10* decreases α-SYN inclusions in *C elegans* **(A)** Representative confocal pictures obtained from animals containing the genomic array *pkIs2386* [*Punc-54*_α-SYN::YFP] expressing α-SYN in body wall muscle cells at L4 + 5 days of development (7 days posthatching). Green staining in all figures represents α-SYN::YFP inclusions in muscle cells. The vulva (V, thick arrow) was used as a reference to analyze the same central section in all worms. A representative area was highlighted and expanded in each panel, to better visualize the α-SYN::YFP accumulation. (A, first panel) α-SYN inclusions were detected in a *C. elegans* model of α-SYN miss folding in which α-SYN is expressed under the control of the *unc-54* promoter. (A, second panel) α-SYN apparent aggregates are increased in *ced-10*(*n3246*) mutant nematodes. (A, third panel) CFP::CED-10 expression (array *baEx167* [P*ced-10*::CFP::CED-10]) decreased the number of α-SYN inclusions in a *ced-10*(*n3246*) background. (A, fourth panel) The blue fluorescence marker (CFP) represented the endogenous expression of CED-10 in a *ced-10*(*n3246*) background for rescuing α-SYN accumulation. Magnification bar is 10 µm **(B)** Quantification of the number of α-SYN inclusions per area. Data are mean ± SEM. Between 30-35 animals were analyzed per genotype. Three different transgenic lines expressing CFP::CED-10 were generated and analyzed independently. Statistics: One-way ANOVA with a Tukey post hoc test. *** $P < 0.005$ **(C)** The movement of YFP::α-SYN animals is hampered by

838 the mutation *ced-10n(3246)*. Thrashing behavior (bends/minute) was video recorded
839 and the resulting images were analyzed by the ImageJ software. Data are mean ±
840 SEM. Between 20 and 30 animals were recorded per experiment and the same
841 experiment was repeated 3 independent times. **(D)** Immunoblotting analysis of protein
842 extracts from 5 days post L4 old YFP::α-SYN synchronized animals, using anti-α- SYN
843 antibody without and with the *ced-10(n3246)* mutation (wild type and *ced-10*
844 respectively). The amount of α- SYN insoluble species was increased by the *ced-*
845 *10(n3246)* mutation.

846 **Figure 4: Autophagic markers accumulate in *ced-10* mutant worms (A)** L4 worms
847 expressing the reporter GFP::LGG-1 (*adIs2122* [P*lgg-1*::GFP::*lgg-1; rol-6(su1006)*] in
848 hypodermal seam cells, without (left panel, wild type) and with (right panel) the *ced-*
849 *10(n3246)* mutation. GFP::LGG-1 puncta are labeled with an filled arrow. Magnification
850 bar is 5 µm. **(B)** The bar graph indicates the number of GFP::LGG-1 foci per cell at the
851 indicated genotypes. These results are mean ± SEM of three independent experiments
852 performed in triplicate. Statistics is Student's t-test. *** $P \leq 0.001$. **(C-D)** Worms
853 expressing the autophagy reporter SQST-1::GFP (*bpIs151*[P*sqst-1*::*sqst-1*::GFP]) were
854 crossed with *ced-10(3246)* animals and the GFP fluorescence intensity (FI) was
855 analyzed under a fluorescence (C) or a confocal (D) microscope. (D, upper panel) L4
856 animals expressing the array SQST-1::GFP without induction of the GFP reporter in
857 normal conditions. (D, bottom panel) The *ced-10*(*n3246*) mutation increased GFP
858 intensity and aggregation. Magnification bar is 20 µm. **(E)** Normalized fluorescence
859 intensity (FI) observed in SQST-1::GFP animals without and with the *ced-10*(*n3246*)
860 mutation. 30 animals were analyzed per genotype. Data are represented as the mean
861 ± SEM and were obtained by comparing wild type animals (without the *ced-10(n3246)*
862 mutation) with *ced-10* mutated animals. Statistics, *** $P < 0.001$, Student's t-test.

863 **Figure 5: Rac1 activity decreases α-SYN accumulation and aggregation in the**
864 **neuroblastoma cell line BE(2)-M17. (A)** Representative confocal images of α-SYN
865 over-expressing cells induced with 10 µM retinoic acid (RA) and treated with 10 mM

sodium butyrate (SB) for 36 h. Cells were transduced with Control -GFP (upper row), RAC1 (WT)-GFP (middle row) and RAC1 (CA)-GFP (bottom row) and co-stained for Thioflavin S (green) and α-SYN (red). Arrows indicate Thioflavin S positive aggregates with amyloidal structure. **(B)** Bar graph showing the quantitative analyses of the neuronal soma area (in percentage %) covered by Thioflavin S positive stain in individual cells transduced with (WT)- or (CA) RAC1 or with the corresponding control. N = 14 (EV), N = 25 (WT) and N = 24 (CA), from at least 3 independent experiments. Data are presented as mean ± SEM. Statistics, *** P<0.001, One-way ANOVA with Bartlett's test correction followed by post hoc Tukey test. Scale bars represent 10 µm.

Figure 6: Rac1 activity rescues α-SYN accumulation and neurite degeneration in early LRRK2-PD-derived DAcells. (A) First row: Confocal images of non-PD (first panel) and LRRK2-PD iPSC-derived DAn (second, third and fourth panels) at 30 days of differentiation transduced with Control -GFP (first and second panels), RAC1 (WT)-GFP (third panel) and RAC1 (CA)-GFP (fourth panel), and co-stained for GFP (green), Tyrosine hydroxylase (TH) (red) and α-SYN (grey). Second row: Confocal images representing the expanded pictures of the corresponding above neurons highlighted within the white dashed square, evidencing α-SYN staining. Dot plot shows the quantification of the average (in %) of α-SYN fluorescent intensity in every analyzed neuron positive for TH and GFP. Statistical analysis is the result of comparing α-SYN staining intensity of non-PD with LV-transduced DAn. Data are presented as mean ± SEM. Statistics is One-way ANOVA with a Tukey's post hoc analysis ** P<0.01. **(B)** Representative confocal micrographs of single DAn derived from non-PD (first panel) and LRRK-2PD patients, transfected with Control-GFP (second panel), RAC1 (WT)-GFP (third panel) or RAC1 (CA)-GFP (fourth panel). Extension bars are 10 µm. (Left graph) This bar graph represents the number of neurites per neuron (primary, secondary and tertiary), according to the indicated transduction, in non-PD and in PD-derived cells. Statistical analysis is the result of comparing neurite number non-PD with LRRK2-PD derived DA cells transduced with RAC1 (WT)-GFP or RAC1 (CA)-

GFP. Data are presented as mean ± SEM. Statistics is One-way ANOVA * P <0.05 and ** P<0.01. (Right graph) Quantitative analyses of the neurite length (in µm) in DAn derived from non-PD and LRRK2-PD derived patients. Statistical analysis is the result of comparing neurite number non-PD with LRRK2-PD derived DA cells transduced with RAC1 (WT)-GFP or RAC1 (CA)-GFP. Data are presented as mean ± SEM. Statistics is One-way ANOVA. *** P <0.001.

Figure 7: RAC1 activity increases the long-term survival of PD-derived DAn and alleviates autophagy impairment. (A-D) Confocal images of non- PD (A) and PD-iPSC derived DA cultures transduced with Control -GFP (B), RAC1 (WT)-GFP (C), and RAC1 (CA)-GFP (D), stained for GFP (green), TH (red) and cleaved Caspase-3 (grey). PD derived cells transduced with Control -GFP (second panel) showed increased numbers of triple positive TH/GFP/Caspase 3 staining in TH+ neurons in comparison to the other conditions tested, where cells were non-PD (first panel left) or transduced with RAC1 (WT)-GFP and RAC1 (CA)-GFP (third and fourth panels respectively). Extension bar from A-D is 20 µm. **(E)** Bar graph showing the quantification of the number of TH/GFP double-positive neurons presenting cleaved Caspase-3 staining from 2 independent experiments. Data are presented as mean ± SEM. Statistics, * P<0.05, ** P < 0.01 and *** P< 0.001, Two-way ANOVA, Tukey post hoc test. **(F)** Confocal images of non-PD (left panel) and PD iPSC derived DA cultures transduced with Control-GFP (second row), RAC1 (WT)-GFP (third row), and RAC1 (CA)-GFP (fourth row), stained for GFP (green), TH (red) and LC3 (grey). Non-PD cells (first row) and PD cells transduced with RAC1 (CA)-GFP (fourth row) showed similar amount of LC3-II positive vesicles in TH+/GFP+ neurons. Extension bar is 5 µm. **(G)** Bar graph showing the quantification of the neuronal soma area (in percentage %) covered by LC3-II positive vesicles in at least 15 DA neurons from 2 independent experiments. Data are presented as mean ± SEM. Statistics, * P<0.05, Two-way ANOVA, post hoc Tukey test

Compliance with Ethical Standards

All experiments were performed under the guidelines and protocols of the Ethical Committee for Animal Experimentation (CEEA) of the University of Barcelona. All procedures adhered to internal and EU guidelines for research involving derivation of pluripotent cell lines. All subjects gave informed consent for the study using forms approved by the Ethical Committee on the Use of Human Subjects in Research at Hospital Clinic in Barcelona, Spain. Generation of iPSC lines was approved by the Advisory Committee for Human Tissue and Cell Donation and Use, by the Commission on Guarantees concerning the Donation and Use of Human Tissues and Cells of the Carlos III Health Institute, Madrid, Spain. All procedures were done in accordance with institutional guidelines following the Spanish legislation.

Conflict of Interest: The authors declare that they have no conflict of interest.

References

1. Michel, P.P., E.C. Hirsch, and S. Hunot, *Understanding Dopaminergic Cell Death Pathways in Parkinson Disease*. Neuron, 2016. **90**(4): p. 675-91.
2. Dehay, B., et al., *Targeting α-synuclein for treatment of Parkinson's disease: mechanistic and therapeutic considerations*. Lancet Neurol, 2015. **14**(8): p. 855-66.
3. Weinreb, P.H., et al., *NACP, a protein implicated in Alzheimer's disease and learning, is natively unfolded*. Biochemistry, 1996. **35**(43): p. 13709-15.
4. Iwai, A., et al., *The precursor protein of non-A beta component of Alzheimer's disease amyloid is a presynaptic protein of the central nervous system*. Neuron, 1995. **14**(2): p. 467-75.
5. Wong, Y.C. and D. Krainc, *α-synuclein toxicity in neurodegeneration: mechanism and therapeutic strategies*. Nat Med, 2017. **23**(2): p. 1-13.

947 6. Winner, B., et al., *In vivo demonstration that alpha-synuclein oligomers are*
948 *toxic*. Proc Natl Acad Sci U S A, 2011. **108**(10): p. 4194-9.
949 7. Hall, A. and G. Lalli, *Rho and Ras GTPases in axon growth, guidance, and*
950 *branching*. Cold Spring Harb Perspect Biol, 2010. **2**(2): p. a001818.
951 8. Musilli, M., et al., *Therapeutic effects of the Rho GTPase modulator CNF1 in a*
952 *model of Parkinson's disease*. Neuropharmacology, 2016. **109**: p. 357-65.
953 9. Schnack, C., et al., *Protein array analysis of oligomerization-induced changes in*
954 *alpha-synuclein protein-protein interactions points to an interference with Cdc42*
955 *effector proteins*. Neuroscience, 2008. **154**(4): p. 1450-7.
956 10. Koch, J.C., et al., *Alpha-Synuclein affects neurite morphology, autophagy,*
957 *vesicle transport and axonal degeneration in CNS neurons*. Cell Death Dis,
958 2015. **6**: p. e1811.
959 11. Prots, I., et al., *α-Synuclein oligomers impair neuronal microtubule-kinesin*
960 *interplay*. J Biol Chem, 2013. **288**(30): p. 21742-54.
961 12. Kinchen, J.M., et al., *Two pathways converge at CED-10 to mediate actin*
962 *rearrangement and corpse removal in C. elegans*. Nature, 2005. **434**(7029): p.
963 93-9.
964 13. Hou, S.T., S.X. Jiang, and R.A. Smith, *Permissive and repulsive cues and*
965 *signalling pathways of axonal outgrowth and regeneration*. Int Rev Cell Mol Biol,
966 2008. **267**: p. 125-81.
967 14. Cabello, J., et al., *PDR-1/hParkin negatively regulates the phagocytosis of*
968 *apoptotic cell corpses in Caenorhabditis elegans*. Cell Death & Disease, 2014.
969 **5**.
970 15. Paisán-Ruíz, C., et al., *Cloning of the gene containing mutations that cause*
971 *PARK8-linked Parkinson's disease*. Neuron, 2004. **44**(4): p. 595-600.
972 16. Chan, D., et al., *Rac1 protein rescues neurite retraction caused by G2019S*
973 *leucine-rich repeat kinase 2 (LRRK2)*. J Biol Chem, 2011. **286**(18): p. 16140-9.

17. Pesaresi, M.G., et al., *Mitochondrial redox signalling by p66Shc mediates ALS-like disease through Rac1 inactivation.* Hum Mol Genet, 2011. **20**(21): p. 4196-208.

18. Philippens, I.H., et al., *Oral treatment with the NADPH oxidase antagonist apocynin mitigates clinical and pathological features of parkinsonism in the MPTP marmoset model.* J Neuroimmune Pharmacol, 2013. **8**(3): p. 715-26.

19. Vogiatzi, T., et al., *Wild type alpha-synuclein is degraded by chaperone-mediated autophagy and macroautophagy in neuronal cells.* J Biol Chem, 2008. **283**(35): p. 23542-56.

20. Sánchez-Danés, A., et al., *Disease-specific phenotypes in dopamine neurons from human iPS-based models of genetic and sporadic Parkinson's disease.* EMBO Mol Med, 2012. **4**(5): p. 380-95.

21. Zavodszky, E., et al., *Mutation in VPS35 associated with Parkinson's disease impairs WASH complex association and inhibits autophagy.* Nat Commun, 2014. **5**: p. 3828.

22. Huang, Y., et al., *Macroautophagy in sporadic and the genetic form of Parkinson's disease with the A53T α-synuclein mutation.* Transl Neurodegener, 2012. **1**(1): p. 2.

23. Ramirez, A., et al., *Hereditary parkinsonism with dementia is caused by mutations in ATP13A2, encoding a lysosomal type 5 P-type ATPase.* Nat Genet, 2006. **38**(10): p. 1184-91.

24. Schapira, A.H., *Glucocerebrosidase and Parkinson disease: Recent advances.* Mol Cell Neurosci, 2015. **66**(Pt A): p. 37-42.

25. Qu, X., et al., *Autophagy gene-dependent clearance of apoptotic cells during embryonic development.* Cell, 2007. **128**(5): p. 931-46.

26. Li, W., et al., *Autophagy genes function sequentially to promote apoptotic cell corpse degradation in the engulfing cell.* J Cell Biol, 2012. **197**(1): p. 27-35.

1001 27. Cheng, S., et al., *Autophagy genes coordinate with the class II PI/PtdIns 3-*
1002 *kinase PIKI-1 to regulate apoptotic cell clearance in C. elegans*. Autophagy,
1003 2013. **9**(12): p. 2022-32.
1004 28. Reddien, P.W. and H.R. Horvitz, *CED-2/CrkII and CED-10/Rac control*
1005 *phagocytosis and cell migration in Caenorhabditis elegans*. Nat Cell Biol, 2000.
1006 **2**(3): p. 131-6.
1007 29. Shakir, M.A., J.S. Gill, and E.A. Lundquist, *Interactions of UNC-34 Enabled with*
1008 *Rac GTPases and the NIK kinase MIG-15 in Caenorhabditis elegans axon*
1009 *pathfinding and neuronal migration*. Genetics, 2006. **172**(2): p. 893-913.
1010 30. Ezcurra, M., et al., *Food sensitizes C. elegans avoidance behaviours through*
1011 *acute dopamine signalling*. EMBO J, 2011. **30**(6): p. 1110-22.
1012 31. Hills, T., P.J. Brockie, and A.V. Maricq, *Dopamine and glutamate control area-*
1013 *restricted search behavior in Caenorhabditis elegans*. J Neurosci, 2004. **24**(5):
1014 p. 1217-25.
1015 32. Sanyal, S., et al., *Dopamine modulates the plasticity of mechanosensory*
1016 *responses in Caenorhabditis elegans*. EMBO J, 2004. **23**(2): p. 473-82.
1017 33. Sawin, E.R., R. Ranganathan, and H.R. Horvitz, *C. elegans locomotory rate is*
1018 *modulated by the environment through a dopaminergic pathway and by*
1019 *experience through a serotonergic pathway*. Neuron, 2000. **26**(3): p. 619-31.
1020 34. Lee, J., C. Jee, and S.L. McIntire, *Ethanol preference in C. elegans*. Genes
1021 Brain Behav, 2009. **8**(6): p. 578-85.
1022 35. Hamamichi, S., et al., *Hypothesis-based RNAi screening identifies*
1023 *neuroprotective genes in a Parkinson's disease model*. Proc Natl Acad Sci U S
1024 A, 2008. **105**(2): p. 728-33.
1025 36. Harrington, A.J., et al., *C. elegans as a model organism to investigate molecular*
1026 *pathways involved with Parkinson's disease*. Dev Dyn, 2010. **239**(5): p. 1282-
1027 95.

1028 37. Sulston, J., M. Dew, and S. Brenner, *Dopaminergic neurons in the nematode*
1029 *Caenorhabditis elegans*. J Comp Neurol, 1975. **163**(2): p. 215-26.
1030 38. Cao, S., et al., *Torsin-mediated protection from cellular stress in the*
1031 *dopaminergic neurons of Caenorhabditis elegans*. J Neurosci, 2005. **25**(15): p.
1032 3801-12.
1033 39. Hochreiter-Hufford, A. and K.S. Ravichandran, *Clearing the dead: apoptotic cell*
1034 *sensing, recognition, engulfment, and digestion*. Cold Spring Harb Perspect
1035 Biol, 2013. **5**(1): p. a008748.
1036 40. Oczypok, E.A., T.D. Oury, and C.T. Chu, *It's a cell-eat-cell world: autophagy*
1037 *and phagocytosis*. Am J Pathol, 2013. **182**(3): p. 612-22.
1038 41. van Ham, T.J., et al., *C. elegans model identifies genetic modifiers of alpha-*
1039 *synuclein inclusion formation during aging*. PLoS Genet, 2008. **4**(3): p.
1040 e1000027.
1041 42. Martinez, B.A., et al., *A bacterial metabolite induces glutathione-tractable*
1042 *proteostatic damage, proteasomal disturbances, and PINK1-dependent*
1043 *autophagy in C. elegans*. Cell Death Dis, 2015. **6**: p. e1908.
1044 43. van der Goot, A.T., et al., *Delaying aging and the aging-associated decline in*
1045 *protein homeostasis by inhibition of tryptophan degradation*. Proc Natl Acad Sci
1046 U S A, 2012. **109**(37): p. 14912-7.
1047 44. Gidalevitz, T., et al., *Destabilizing protein polymorphisms in the genetic*
1048 *background direct phenotypic expression of mutant SOD1 toxicity*. PLoS Genet,
1049 2009. **5**(3): p. e1000399.
1050 45. Kuwahara, T., et al., *Phosphorylation of α-synuclein protein at Ser-129 reduces*
1051 *neuronal dysfunction by lowering its membrane binding property in*
1052 *Caenorhabditis elegans*. J Biol Chem, 2012. **287**(10): p. 7098-109.
1053 46. Cuervo, A.M., et al., *Impaired degradation of mutant alpha-synuclein by*
1054 *chaperone-mediated autophagy*. Science, 2004. **305**(5688): p. 1292-5.

1055 47. Büttner, S., et al., *Spermidine protects against α-synuclein neurotoxicity.* Cell
1056 Cycle, 2014. **13**(24): p. 3903-8.
1057 48. Zhang, H., et al., *Guidelines for monitoring autophagy in Caenorhabditis*
1058 *elegans.* Autophagy, 2015. **11**(1): p. 9-27.
1059 49. Guo, B., et al., *Genome-wide screen identifies signaling pathways that regulate*
1060 *autophagy during Caenorhabditis elegans development.* EMBO Rep, 2014.
1061 **15**(6): p. 705-13.
1062 50. Tian, Y., et al., *C. elegans screen identifies autophagy genes specific to*
1063 *multicellular organisms.* Cell, 2010. **141**(6): p. 1042-55.
1064 51. Jiang, P., et al., *ER stress response plays an important role in aggregation of α-*
1065 *synuclein.* Mol Neurodegener, 2010. **5**: p. 56.
1066 52. Raiss, C.C., et al., *Functionally different α-synuclein inclusions yield insight into*
1067 *Parkinson's disease pathology.* Sci Rep, 2016. **6**: p. 23116.
1068 53. MacLeod, D., et al., *The familial Parkinsonism gene LRRK2 regulates neurite*
1069 *process morphology.* Neuron, 2006. **52**(4): p. 587-93.
1070 54. Fernández-Santiago, R., et al., *Aberrant epigenome in iPSC-derived*
1071 *dopaminergic neurons from Parkinson's disease patients.* EMBO Mol Med,
1072 2015. **7**(12): p. 1529-46.
1073 55. Johnson, M.A., et al., *Functional neural development from human embryonic*
1074 *stem cells: accelerated synaptic activity via astrocyte coculture.* J Neurosci,
1075 2007. **27**(12): p. 3069-77.
1076 56. Tahirovic, S., et al., *Rac1 regulates neuronal polarization through the WAVE*
1077 *complex.* J Neurosci, 2010. **30**(20): p. 6930-43.
1078 57. Lorenzetto, E., et al., *Rac1 selective activation improves retina ganglion cell*
1079 *survival and regeneration.* PLoS One, 2013. **8**(5): p. e64350.
1080 58. Kanekura, K., et al., *A Rac1/phosphatidylinositol 3-kinase/Akt3 anti-apoptotic*
1081 *pathway, triggered by AlsinLF, the product of the ALS2 gene, antagonizes*

Cu/Zn-superoxide dismutase (SOD1) mutant-induced motoneuronal cell death. J Biol Chem, 2005. **280**(6): p. 4532-43.

59. Stankiewicz, T.R. and D.A. Linseman, *Rho family GTPases: key players in neuronal development, neuronal survival, and neurodegeneration.* Front Cell Neurosci, 2014. **8**: p. 314.

60. Nichols, A.L., et al., *The Apoptotic Engulfment Machinery Regulates Axonal Degeneration in C. elegans Neurons.* Cell Rep, 2016. **14**(7): p. 1673-83.

61. Zhang, B., Y. Zhang, and E. Shacter, *Rac1 inhibits apoptosis in human lymphoma cells by stimulating Bad phosphorylation on Ser-75.* Mol Cell Biol, 2004. **24**(14): p. 6205-14.

62. Cheng, C., et al., *Trihydrophobin 1 Interacts with PAK1 and Regulates ERK/MAPK Activation and Cell Migration.* J Biol Chem, 2009. **284**(13): p. 8786-96.

63. Cicenas, J., *The potential role of Akt phosphorylation in human cancers.* Int J Biol Markers, 2008. **23**(1): p. 1-9.

64. Nagarajan, A., et al., *Progressive degeneration of dopaminergic neurons through TRP channel-induced cell death.* J Neurosci, 2014. **34**(17): p. 5738-46.

65. Coles, C.H. and F. Bradke, *Coordinating neuronal actin-microtubule dynamics.* Curr Biol, 2015. **25**(15): p. R677-91.

66. Chia, J.X., N. Efimova, and T.M. Svitkina, *Neurite outgrowth is driven by actin polymerization even in the presence of actin polymerization inhibitors.* Mol Biol Cell, 2016.

67. Dubey, J., N. Ratnakaran, and S.P. Koushika, *Neurodegeneration and microtubule dynamics: death by a thousand cuts.* Front Cell Neurosci, 2015. **9**: p. 343.

68. Godena, V.K., et al., *Increasing microtubule acetylation rescues axonal transport and locomotor deficits caused by LRRK2 Roc-COR domain mutations.* Nat Commun, 2014. **5**: p. 5245.

1110 69. Gandhi, P.N., et al., *The Roc domain of leucine-rich repeat kinase 2 is sufficient*
1111 *for interaction with microtubules.* J Neurosci Res, 2008. **86**(8): p. 1711-20.
1112 70. Okada, T., et al., *Impairment of PDGF-induced chemotaxis by extracellular α-*
1113 *synuclein through selective inhibition of Rac1 activation.* Sci Rep, 2016. **6**: p.
1114 37810.
1115 71. Sousa, V.L., et al., *{alpha}-synuclein and its A30P mutant affect actin*
1116 *cytoskeletal structure and dynamics.* Mol Biol Cell, 2009. **20**(16): p. 3725-39.
1117 72. Crews, L., et al., *Selective molecular alterations in the autophagy pathway in*
1118 *patients with Lewy body disease and in models of alpha-synucleinopathy.* PLoS
1119 One, 2010. **5**(2): p. e9313.
1120 73. Mak, S.K., et al., *Lysosomal degradation of alpha-synuclein in vivo.* J Biol
1121 Chem, 2010. **285**(18): p. 13621-9.
1122 74. Vijayakumaran, S., et al., *Direct and/or Indirect Roles for SUMO in Modulating*
1123 *Alpha-Synuclein Toxicity.* Biomolecules, 2015. **5**(3): p. 1697-716.
1124 75. Ahmed, I., et al., *Development and characterization of a new Parkinson's*
1125 *disease model resulting from impaired autophagy.* J Neurosci, 2012. **32**(46): p.
1126 16503-9.
1127 76. Ebrahimi-Fakhari, D., et al., *Distinct roles in vivo for the ubiquitin-proteasome*
1128 *system and the autophagy-lysosomal pathway in the degradation of α-*
1129 *synuclein.* J Neurosci, 2011. **31**(41): p. 14508-20.
1130 77. Winslow, A.R., et al., *α-Synuclein impairs macroautophagy: implications for*
1131 *Parkinson's disease.* J Cell Biol, 2010. **190**(6): p. 1023-37.
1132 78. Orenstein, S.J., et al., *Interplay of LRRK2 with chaperone-mediated autophagy.*
1133 Nat Neurosci, 2013. **16**(4): p. 394-406.
1134 79. Alegre-Abarrategui, J., et al., *LRRK2 regulates autophagic activity and localizes*
1135 *to specific membrane microdomains in a novel human genomic reporter cellular*
1136 *model.* Hum Mol Genet, 2009. **18**(21): p. 4022-34.

80. Saha, S., L. Liu-Yesucevitz, and B. Wolozin, *Regulation of autophagy by LRRK2 in Caenorhabditis elegans*. Neurodegener Dis, 2014. **13**(2-3): p. 110-3.

81. Brenner, S., *The genetics of Caenorhabditis elegans*. Genetics, 1974. **77**(1): p. 71-94.

82. Kamath, R.S. and J. Ahringer, *Genome-wide RNAi screening in Caenorhabditis elegans*. Methods, 2003. **30**(4): p. 313-21.

83. Nollen, E.A., et al., *Genome-wide RNA interference screen identifies previously undescribed regulators of polyglutamine aggregation*. Proc Natl Acad Sci U S A, 2004. **101**(17): p. 6403-8.

84. Schindelin, J., et al., *The ImageJ ecosystem: An open platform for biomedical image analysis*. Mol Reprod Dev, 2015. **82**(7-8): p. 518-29.

85. Palmisano, N.J. and A. Meléndez, *Detection of Autophagy in Caenorhabditis elegans*. Cold Spring Harb Protoc, 2016. **2016**(2): p. pdb.top070466.

86. Lapierre, L.R., et al., *The TFEB orthologue HLH-30 regulates autophagy and modulates longevity in Caenorhabditis elegans*. Nat Commun, 2013. **4**: p. 2267.

87. Consiglio, A., et al., *Robust in vivo gene transfer into adult mammalian neural stem cells by lentiviral vectors*. Proc Natl Acad Sci U S A, 2004. **101**(41): p. 14835-40.

Figure

Click here to download Figure FIGURE 1.tif

Figure 1

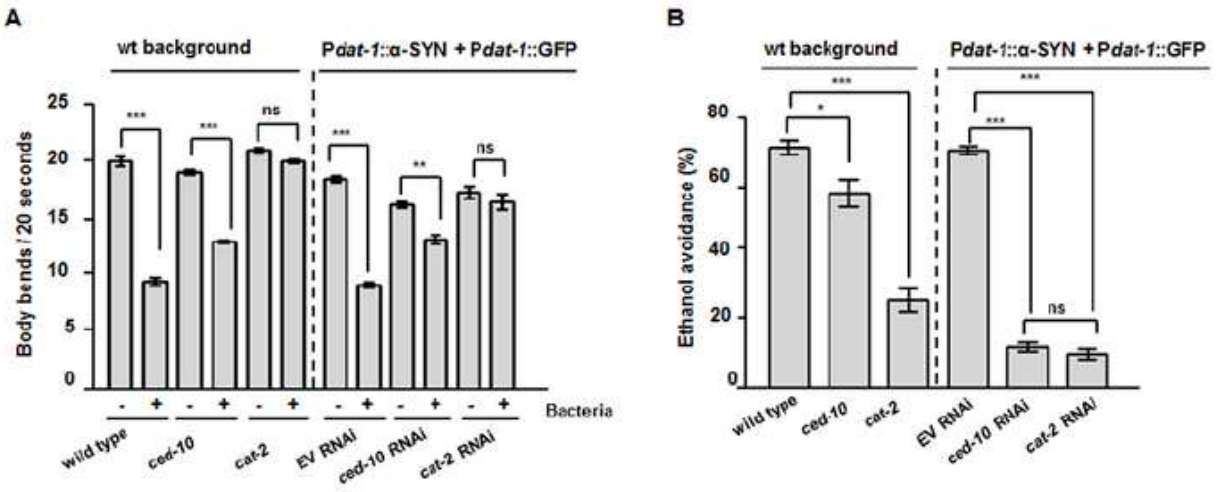

Figure

Click here to download Figure FIGURE 2.tif

Figure 2

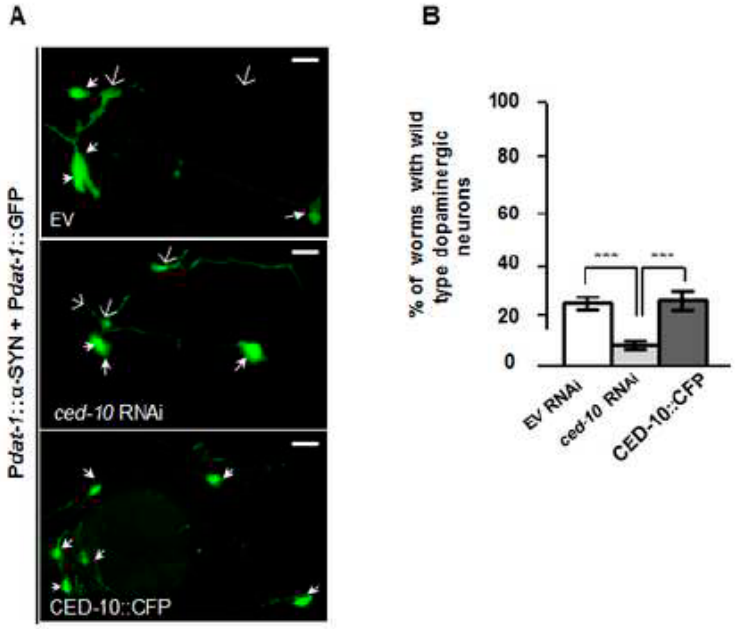

Figure

Click here to download Figure FIGURE 3.tif

Figure 3

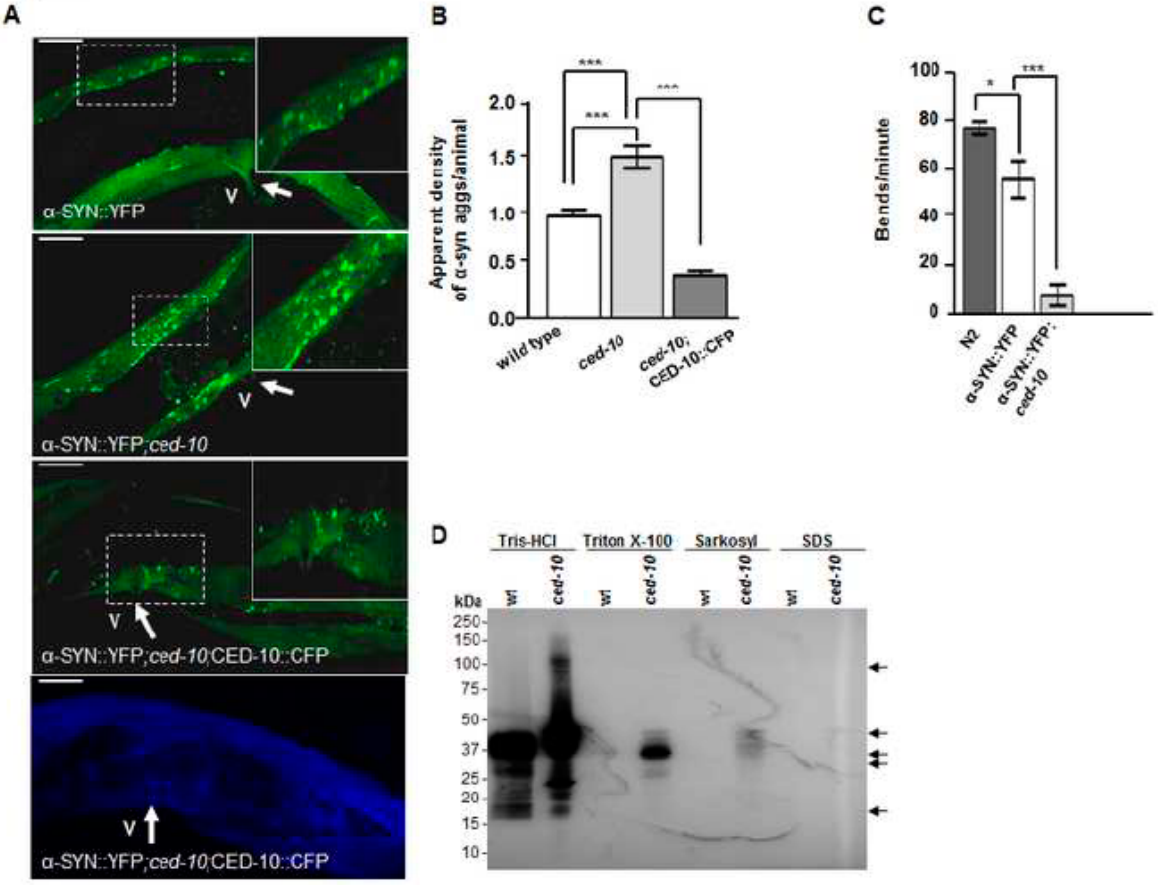

Figure

Click here to download Figure FIGURE 4.tif

Figure 4

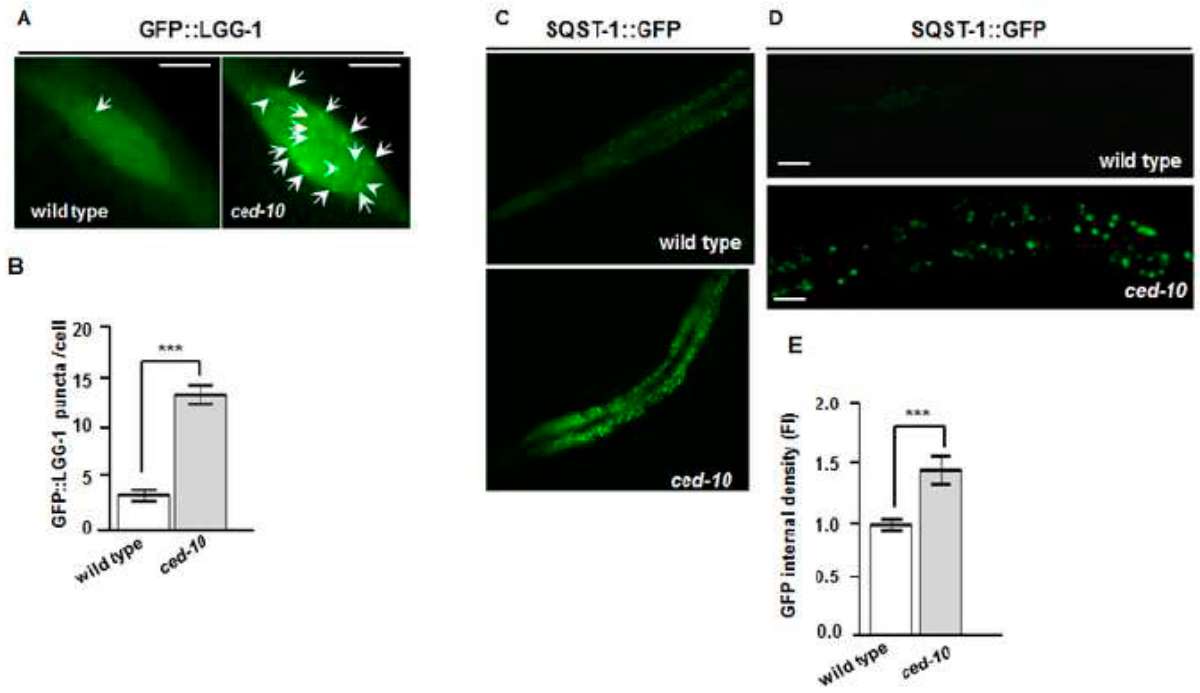

Figure

Click here to download Figure FIGURE 5.jpg

Figure 5

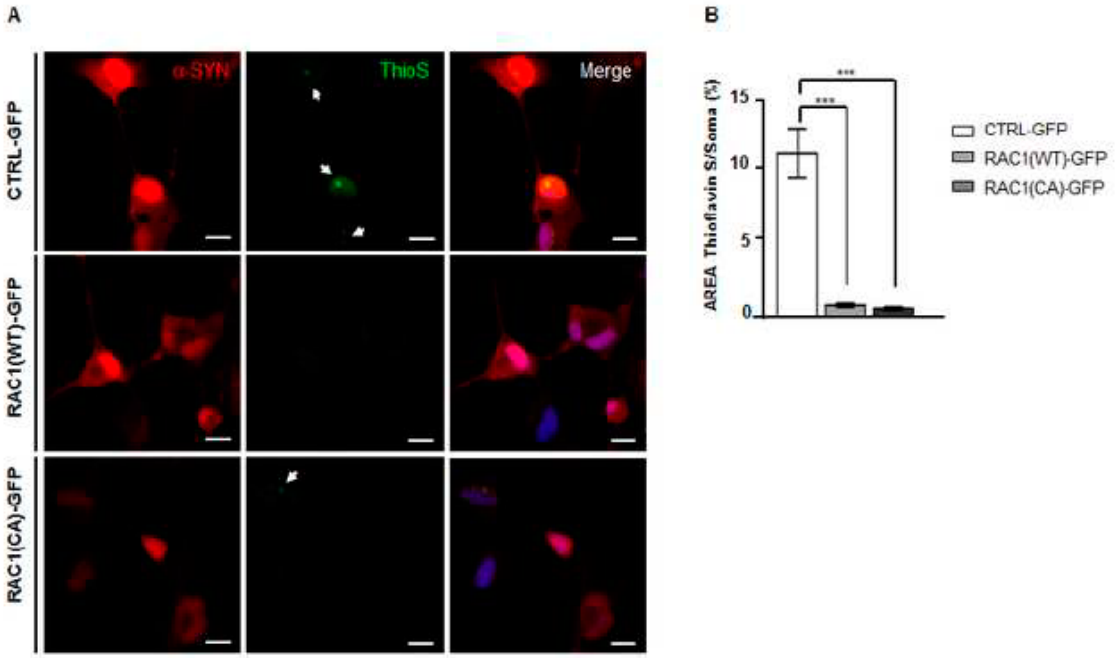

Figure

Click here to download Figure FIGURE 6.tif

Figure 6

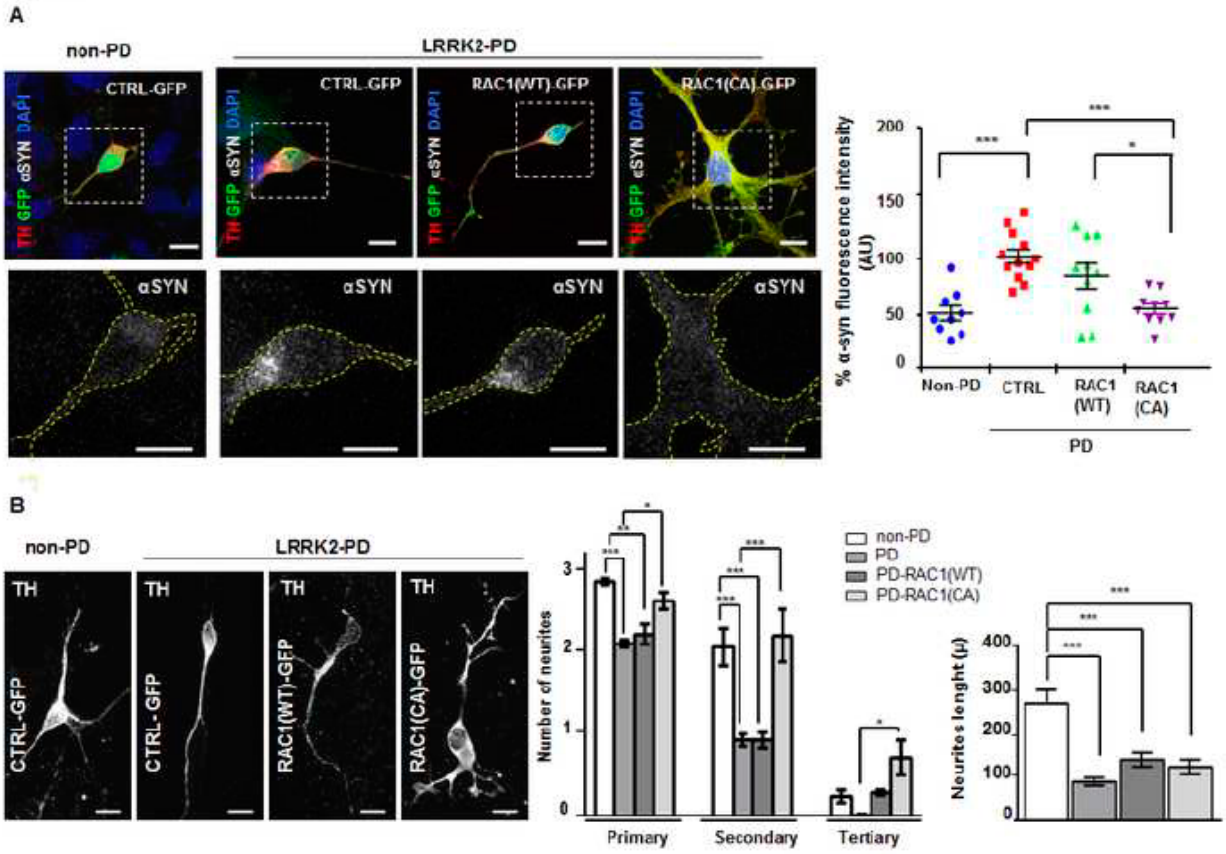

Figure

Click here to download Figure Figure 7.tif

Figure 7

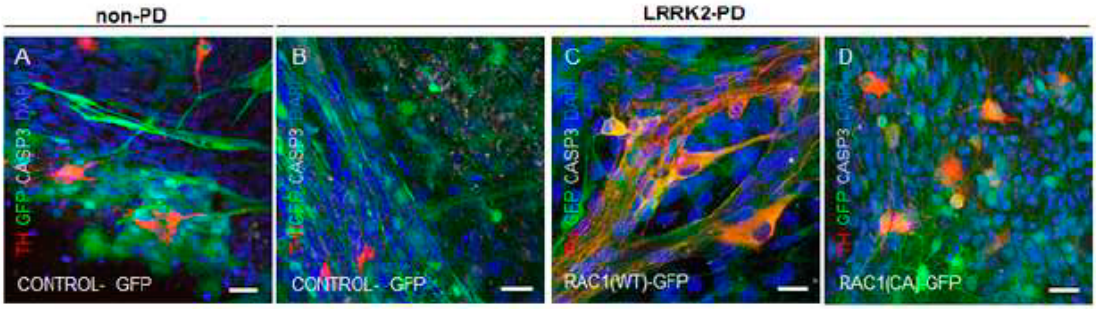

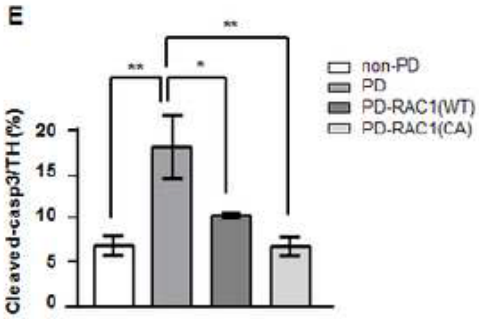

Figure

Click here to download Figure FIGURE 7 CONT.tif

Figure 7 (cont.)

F

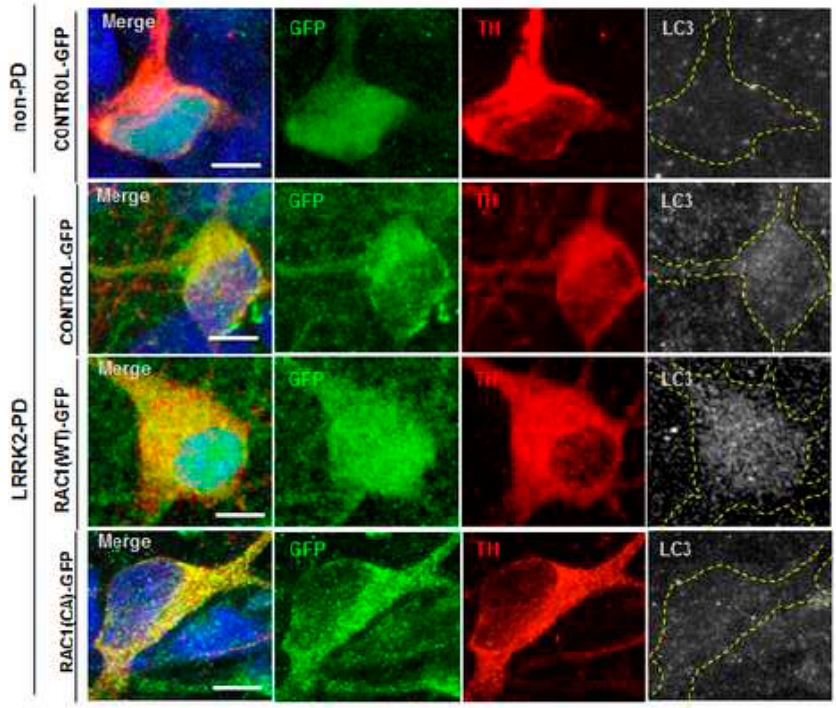

G

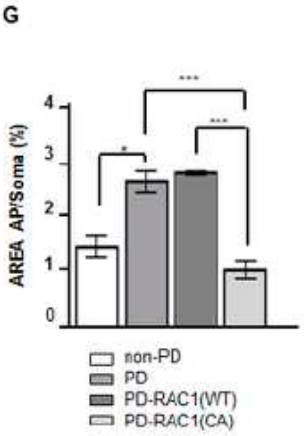

Annex III: Research article (Under review process)

REGULAR MANUSCRIPT

MicroRNA alterations in iPSC-derived dopaminergic neurons from Parkinson disease patients

Eduard Tolosa [a,b], Teresa Botta-Orfila [c,d], Xavier Morató [e,f], Carles Calatayud [g], Raquel Ferrer-Lorente [h,i], María-José Martí [a,b], Carles Gaig [a,b,j], Ángel Raya [h,i,k], Antonella Consiglio [g,l,m,*], Mario Ezquerra [a,b,*], Rubén Fernández-Santiago [a,b,*]

[a] Laboratory of Neurodegenerative Disorders, Department of Neurology, Hospital Clínic de Barcelona, Institut d'Investigacions Biomèdiques August Pi i Sunyer (IDIBAPS), University of Barcelona (UB), 08036 Barcelona, Spain. [b] Centro de Investigación Biomédica en Red de Enfermedades Neurodegenerativas (CIBERNED), 28031 Madrid, Spain. [c] Gene Function and Evolution Group, Centre for Genomic Regulation (CRG), 08003 Barcelona, Spain. [d] Universitat Pompeu Fabra (UPF), 08003 Barcelona, Spain. [e] Unitat de Farmacologia, Departament Patologia i Terapèutica Experimental, Facultat de Medicina, IDIBELL-Universitat de Barcelona, L'Hospitalet de Llobregat, 08907 Barcelona, Spain. [f] Institut de Neurociències, Universitat de Barcelona, 08035 Barcelona, Spain. [g] Institute for Biomedicine (IBUB), University of Barcelona (UB), 08028 Barcelona, Spain. [h] Center of Regenerative Medicine in Barcelona (CMRB), Barcelona Biomedical Research Park, 08003 Barcelona, Spain. [i] Centre for Networked Biomedical Research on Bioengineering, Biomaterials and Nanomedicine (CIBER-BBN), 28029 Madrid, Spain. [j] Multidisciplinary Sleep Unit, Department of Neurology, Hospital Clínic of Barcelona, Institut d'Investigacions Biomèdiques August Pi i Sunyer (IDIBAPS), University of Barcelona, 08036 Barcelona, Spain. [k] Institució Catalana de Recerca i Estudis Avançats (ICREA), 08010 Barcelona, Spain. [l] Department of Pathology and Experimental Therapeutics, Faculty of Medicine, IDIBELL- University of Barcelona, 08907 Barcelona, Spain. [m] Department of Molecular and Translational Medicine, University of Brescia and National Institute of Neuroscience, 25123 Brescia, Italy. *Contributed equally as co-senior and co-corresponding authors.

R. Fernández-Santiago and M. Ezquerra
Laboratory of Neurodegenerative Diseases
CELLEX building, Faculty of Medicine (UB)
Institut d'Investigacions Biomèdiques August Pi i Sunyer
(IDIBAPS), Hospital Clínic Universitari de Barcelona
University of Barcelona
Casanova 143, Floor 3B, 08036, Barcelona
Phone: +34-932-275-400 ext. 4814
ruben.fernandez.santiago@gmail.com
ezquerra@clinic.ub.es

A.Consiglio
Department of Neural Commitment and Differentiation
Institute for Biomedicine of the University of Barcelona (IBUB)
Barcelona Science Park, University of Barcelona
Barcelona, 08028 Spain
Baldiri Reixac 15-21
Phone: +34-934-039-842
aconsiglio@ibub.pcb.ub.es

Running head:
Genome-wide microRNA analysis of induced dopaminergic neurons from PD patients

Journal instructions
Nr. of characters in title (max. 85 incl. spaces): 85
Nr. of words abstract (max. 170): 170
Nr. of keywords 3-12: 4
Nr. of pages: 22
(Regular manuscript 30 double-spaced pages,
incl. references, figures and tables)

ABSTRACT

MicroRNA (miRNA) misregulation in peripheral blood has been linked to Parkinson disease (PD) but its role in the disease progression remains elusive. We performed an explorative genome-wide study of miRNA expression levels in dopaminergic neurons (DAn) from PD patients generated by somatic cell reprogramming and induced pluripotent stem cells (iPSC) differentiation. We quantified expression levels of 377 miRNAs in DAn from three sporadic PD patients (sPD), three monogenic LRRK2-associated PD patients (L2PD) (total six PD), and four healthy controls. We identified differential expression of ten miRNA of which five were up-regulated in PD (miR-9-5p, miR-135a-5p, miR-135b-5p, miR-449a, and miR-449b-5p) and five down-regulated (miR-141-3p, miR-199a-5p, miR-299-5p, miR-518e-3p, and miR-519a-3p). Changes were similar in sPD and L2PD. Integrative analysis revealed significant correlations between miRNA/mRNA expression. Moreover, up-regulation of miR-9-5p and miR-135b-5p was associated with down-regulation of transcription factors related to DNA hypermethylation of enhancer elements in PD DAn (*FOXA1* and *NR3C1*). In summary, miRNA changes are associated with monogenic L2PD and sPD and co-occur with epigenetic changes in DAn from PD patients.

KEYWORDS

Parkinson disease (PD); microRNA (miRNA); leucine-rich repeat kinase 2 (LRRK2); dopaminergic neuron (DAn); transcription factor (TF)

1. INTRODUCTION

Parkinson disease (PD) is a progressive neurodegenerative disorder characterized by dopaminergic neural loss in the substantia nigra pars compacta (SNpc) and a related striatal dopamine (DA) deficit leading to the classical motor symptoms of bradykinesia, rigidity, and tremor (Lang and Lozano, 1998a, b). The vast majority of PD cases are sporadic (sPD) and are believed to result from a complex interplay between genetic and environmental risk factors of which aging is considered the most important known disease risk (Reeve et al., 2014). Yet around 5% encompass monogenic cases caused by Mendelian mutations segregating with disease in affected families (Gasser, 2009). Of these, missense mutations in the leucine-rich repeat kinase 2 (*LRRK2*) gene including the toxic gain-of-function G2019S located in the kinase domain are the most frequent cause of monogenic PD. Interestingly, *LRRK2* mutations have been identified not only in familial LRRK2-associated PD (L2PD) but also in many sPD cases suggesting reduced penetrance determined by additional modifiers of their pathogenic expressivity (Healy et al., 2008). Since L2PD can resemble clinically and neuropathologically sPD (Marras et al., 2016) this form is being widely used to model common sPD and to gain novel insights into the molecular alterations occurring in disease.

MicroRNAs (miRNAs) are small non-coding regulatory RNAs controlling gene expression by the translational inhibition and degradation of their target mRNAs (Bartel, 2009). MiRNA alterations have been shown to contribute to the pathophysiology of neurodegenerative disorders (Abe and Bonini, 2013; Dimmeler and Nicotera, 2013). Mounting evidence has demonstrated differential miRNA expression changes in peripheral tissues from PD patients such as whole blood (Alieva et al., 2015; Margis et al., 2011; Martins et al., 2011; Serafin et al., 2015; Soreq et al., 2013), plasma (Cardo et al., 2014; Khoo et al., 2012), and serum (Botta-Orfila et al., 2012; Vallelunga et al., 2014) even at PD prodromal stages before clinical manifestation of motor symptoms (Fernandez-Santiago et al., 2015b). These studies have suggested a potential role of miRNAs as candidate biomarkers for the diagnosis and prognosis

of PD (Danborg et al., 2014). However, miRNA studies in the central nervous system (CNS) have been hindered by the inaccessibility to dopaminergic neurons (DAn) from live patients. Yet reports in post-mortem PD brain tissue have also shown that miRNA deregulation of at least some specific miRNAs also occurs at advanced stages of disease (Fuchs et al., 2009; Kim et al., 2007). Due to this limiting cell inaccessibility, the miRNA expression profile of DAn from PD patients at more initial stages of the neurodegenerative process remains unknown until date.

Upon cell reprogramming of skin fibroblasts from patients with sPD and L2PD into induced pluripotent stem cells (iPSC) and their differentiation into dopaminergic neurons (DAn) we have previously generated and characterized a patient-derived disease-specific DAn model of PD (Fernandez-Santiago et al., 2015a; Sanchez-Danes et al., 2012b). In these iPSC-derived DAn cells, we have reported large epigenomic changes consisting in an aberrant DNA methylation profile which was associated with both sPD and L2PD as compared to healthy subjects (Fernandez-Santiago et al., 2015a). We also reported that epigenomic changes detected in these PD iPSC-derived DAn antedated disease-specific phenotypes emerging upon long-term culture which included reduced axonal outgrowth, impaired autophagic vacuole clearance, and accumulation of alpha-synuclein (SNCA) (Sanchez-Danes et al., 2012b). The same patient DAn cell lines from these two previous studies were used here to further perform an unbiased genome-wide miRNA expression study interrogating the expression levels of 377 miRNAs in three sPD patients, three L2PD patients, and four healthy controls. More specifically here we have investigated whether specific miRNA expression modifications occur in iPSC-derived DAn from sPD as well as familial L2PD and concurrently we have also explored a potential functional relation between miRNA and global gene expression changes observed in our model.

2. MATERIAL AND METHODS

2.1 Study Approval

The study conformed to the principles of the Declaration of Helsinki and the Belmont Report. All participants gave written informed consent, and the study was approved by the Commission on Guarantees for Donation and Use of Human Tissues and Cells of the Instituto de Salud Carlos III (ISCIII) and the ethics committee from the Hospital Clínic de Barcelona. Personal data was anonymized and subject samples were codified to preserve confidentiality.

2.2 Subjects and generation of iPSC-derived DAn cell lines

Studied individuals included three patients with sPD reporting no family history of disease who were negative in the *LRRK2* mutational screening, three patients with familial L2PD who carried the *LRRK2* G2019S mutation, and four genetically unrelated healthy controls without familial history of neurological disease. Clinical details from the patients and controls are summarized in **Table 1**. Skin biopsies of 3 mm of diameter were performed in the alar surface of the forearm of subjects and primary cultures of somatic skin cells (keratinocytes and fibroblasts) were established. Cell reprogramming of somatic cells into iPSC was done based on the retroviral delivery of a cocktail of three reprogramming factors including *OCT4*, *KLF4*, and *SOX2*. Differentiation of iPSCs into DAn was carried out by the lentiviral delivery of the A9-subtype DAn pattering factor *LMX1A* which enriches by 4-fold the yield of DAn, and co-culture with mouse PA6 feeding cells. Reprogramming and differentiation protocol (Sanchez-Danes et al., 2012a) and cell line characterization of the DAn used in the present study have been previously described elsewhere by our group (Fernandez-Santiago et al., 2015a; Sanchez-Danes et al., 2012b). After 30-days of differentiation, resulting iPSC-derived DAn were subjected to miRNA expression profiling and also to the genome-wide gene expression and DNA methylation analyses previously published (Fernandez-Santiago et al., 2015a).

79 **2.3 miRNA isolation**

80 Total RNA containing enriched small RNAs (18 nucleotides upwards) was isolated from one
81 million cells using the miRNeasy Kit (QIAGEN) according to manufacturer instructions, and
82 resuspended in 30 µl of RNase-free water. Total RNA concentration and quality were
83 determined in a Nanodrop instrument. Average RNA yield using this method was of 10 µg at a
84 mean concentration of 300 ng/ µl per sample.
85
86 **2.4 miRNA expression analysis**
87 Retro-transcription of 400 ng of RNA samples enriched in miRNA into cDNA was performed
88 using the Megaplex RT Primer Pools - Human Pool A (Applied Biosystems, product datasheet:
89 https://tools.thermofisher.com/content/sfs/manuals/4399721c.pdf) in a PTC-200 thermocycler
90 (MJ Research). We mixed 6 µl of each cDNA product with a total of 394 µl of nuclease-free
91 water and 400 µl of TaqMan Master Mix and loaded 100 µl of the RT-PCR reaction mix in each
92 port of the TaqMan Array Human MicroRNA A Cards v2.0 (Applied Biosystems, product
93 datasheet: https://tools.thermofisher.com/content/sfs/manuals/cms_042326.pdf), also known as
94 TaqMan Low Density Array (TLDA). Samples were centrifuged two times at 110 g during 1 min
95 and miRNA amplification was performed in a Viia7 1.0 Real-Time PCR system (Applied
96 Biosystems). Raw data was filtered out using the Expression Suite v1.0 software (Applied
97 Biosystems). Out of the 377 miRNAs included in the array, we considered for subsequent
98 analyses only the Cq values from miRNAs expressed below cycle 35 resulting in 240 miRNAs.
99 Relative quantification of miRNA expression levels was done using the -ΔCt algorithm in the
100 DataAssist software v3.0 (Applied Biosystems). As endogenous normalizating controls, we
101 selected miRNAs showing the best normalization score (MammU6, RNU48, miR-26a, miR-484,
102 miR-744, and miR-26b) according to a method which has been previously described
103 (Vandesompele et al., 2002).
104

105 **2.5 Identification of differentially expressed miRNAs**

106 We performed pair-wise comparisons between the groups of study - sPD, L2PD, total PD, and
107 controls - using a 2-tailed Student T-test. For each miRNA, we calculated the difference
108 between the expression levels in the two groups under comparison as relative quantity (RQ)
109 values (equivalent to fold-change values). We set the statistical significance threshold for
110 differential miRNA expression at *P* below 0.05 after multiple testing adjustment of raw *P* values
111 by false discovery rate (FDR) correction (**Table 2**). We used the DataAssist v3.0 pipeline for
112 hierarchical clustering analysis of differentially expressed miRNAs (DEmiR) using the average
113 linkage as clustering algorithm and the Pearson correlation coefficient as distance measure
114 (**Figure 1**).
115
116 **2.6 Biological enrichment analysis of genes targeted by miRNAs**
117 We explored the genes targeted by the identified DEmiR using the software DIANA-miRPath
118 v3.0 (Vlachos et al., 2015b). The tool predicts miRNA / target gene interactions
119 (http://www.microrna.gr/miRPathv3) and is based on more than half a million of experimentally
120 reported interactions and the DIANA-TarBase v7 algorithm (Vlachos et al., 2015a).
121 Subsequently, we performed a miRNA-target gene biological enrichment analysis and identified
122 affected canonical pathways using the DAVID extension (https://david.ncifcrf.gov) of DIANA-
123 miRPath v3.0. To this end, we used both the union analysis mode including the summatory
124 effect of independent miRNAs, and also the more conservative gene intersection mode
125 considering only genes simultaneously targeted by at least three different miRNAs
126 (**Supplemental Table 1**).
127
128 **2.7 Association of miRNA and gene expression changes**
129 We overlapped DEmiR expression data with global gene expression data from 437 differentially
130 expressed genes (DEGs) identified previously in the same DAn cell lines from PD patients by a

genome-wide transcriptomic analysis covering 96% of the transcriptome (Fernandez-Santiago et al., 2015a). These DEG data are deposited in the Gene Expression Omnibus (GEO) under accession number GSE51922. For identifying specific DEmiR / DEG pairs, we used the MAGIA software (Sales et al., 2010) (http://genc.omp.bio.unipd.it/magia/start/). The MAGIA pipeline detects miRNA / mRNA significant correlations based on both predictive and experimentally observed correlations. We considered only DEmiR / DEG interactions identified simultaneously by three independent algorithms including miRanda (stringency score 20), PITA (stringency score 300), and Targetscan, with a Spearman correlation coefficient (r) above |0.60|, and with a multiple testing adjusted *P* below 0.05 (**Supplemental Table 2**).

2.8 Functional network analysis of miRNA and gene expression changes

We used the DEmiR and DEG interaction data described above to build interaction networks by using the MAGIA software. For network visualization we used the Cytoscape software (www.cytoscape.org) (Shannon et al., 2003). In the DEmiR / DEG network, yellow nodes represent DEmiRs whereas white nodes represent DEGs, the size of nodes are proportional to the number of direct interactions, and the thickness of edges are proportional to the degree of correlation (**Figure 2**). We also performed a biological enrichment analysis of identified DEmiR / DEG pairs by using the DAVID software (https://david.ncifcrf.gov) (**Table 3**).

3. RESULTS

We performed a comprehensive genome-wide analysis of miRNA expression levels in iPSC-derived DAn from PD patients and controls. Out of the 377 screened miRNAs, a total of 240 miRNAs showed detectable and quantifiable expression levels in our samples. Prior to statistical analysis, unsupervised hierarchical clustering of expression values from these 240 miRNAs showed expression profiles which mostly differentiated between PD patients (L2PD and sPD) and healthy controls suggesting overall miRNA expression differences between these two groups (**Supplemental Figure 1**). We then first compared the sPD and L2PD groups under a multiple testing adjusted *P* below 0.05 and found no differentially expressed miRNA (DEmiR) in between these two forms of disease indicating similar miRNA expression profiles. Using the same conditions of above, we further identified ten differentially expressed microRNA (DEmiR) in the PD group as a whole as compared to controls (**Table 2**). Of these, five DEmiR were significantly up-regulated in PD (miR- miR-9-5p, 135a-5p, miR-135b-5p, miR-449a, and miR-449b-5p) whereas five were down-regulated (miR-141-3p, miR-199a-5p, miR-299-5p, miR-518e-3p, and miR-519a-3p) (**Figure 1**). Collectively, these data indicate that DAn from PD patients show alterations in miRNA expression compared to healthy controls. They also indicate that sPD and L2PD share similar miRNA expression changes.

We next explored the molecular functions regulated by the identified DEmiR by performing an in-silico biological enrichment analysis of their predicted target genes. To this end, we overlapped the PD-associated DEmiR data with experimentally validated miRNA / target-gene interaction data which are publically available at the DIANA-miRPath database (Vlachos et al., 2015b). We used the union analysis mode which considers the summatory effect of independent DEmiR, and also the more conservative intersection mode considering only genes simultaneously targeted at least by three different DEmiRs. Significantly enriched gene ontology (GO) biological processes and Kyoto Encyclopedia of Genes and Genomes (KEGG) pathways included canonical pathways involved in cancer including melanoma, extracellular matrix (ECM),

cytoskeleton dynamics, and PI3K kinase / Akt cell signalling (**Supplemental Table 1**). These results suggest an effect of the PD-associated miRNA expression changes on the cytoskeleton, axonal transport, cell adhesion, and cell survival in PD.

We then analyzed the relationship between PD differential miRNA expression and previously observed gene expression changes from the same DAn lines (Fernandez-Santiago et al., 2015a). We found a significant association of 590 DEmiR / differentially expressed gene (DEG) pairs under a Spearman correlation coefficient (r) above |0.6| and a multiple testing adjusted *P* below 0.05 (See Material and Methods). Of these, 285 associations were inverse and affected to a total of 167 different genes, whereas 305 were positive (**Supplemental Table 2**). On the other hand, apart from expected direct negative associations mediated by the direct binding of DEmiR to specific motifs at the 3'-UTR of regulated genes, positive associations have also been previously reported in the literature (Ritchie et al., 2009). These positive associations are thought to operate by indirect interactions through the binding and degradation of DEmiR to intermediate molecules such as transcription inhibitors operating between the DEmiR and the controlled genes, thus leading to their up-regulation (Ritchie et al., 2009). Overall, our findings suggest that miRNA expression changes occurring in PD play a role in regulating gene expression, both inversely and positively.

We further performed a functional network analysis of DEmiR and DEG correlating pairs. We focused only in inverse DEmiR / DEG associations to specifically analyze classical direct down-regulation effects of miRNA on RNAs. We found two independent clusters (**Figure 2**). Cluster 1 encompassed the PD down-regulated DEmiRs miR-141-3p, miR-199a-5p, miR-299-5p, miR-518e-3p, and miR-519a-3p, and associated DEGs which interestingly, were largely involved in specific neural functions such as neuron differentiation, neural projection development, or axonogenesis among others (**Table 3**). In addition, cluster 2 included the PD up-regulated DEmiRs miR-135a, miR-135b, miR-449a, miR-449b-5p, miR-9-5p, and associated DEGs which were related to diverse homeostatic functions such as regulation of response to

external stimulus, endocytosis, or metabolic processes. Previously we have shown that PD up-regulated DEGs were overall involved in neural functions whereas down-regulated DEGs in different homeostasis processes (Fernandez-Santiago et al., 2015a). Thus our miRNA data here complements these previous expression observations in PD DAn by adding a new layer of molecular data suggesting that the down-regulation of specific miRNA is related to enhancement of specific neural functions, whereas the up-regulation of other miRNA is associated with the down-regulation of basic homeostasis in PD.

We then dissected specific DEmiR / DEG inversely associated pairs. We found that the PD up-regulation of miR-9-5p was associated with the expression down-regulation of the transcription factor (TF) *FOXA1* (r=-0.87, adj. P=0.0052) whereas, in the same direction, the up-regulation of miR-135b-5p was related to the down-regulation of the TF *NR3C1* (r=-0.71, adj. P=0.0308) (**Supplemental Table 2**). We previously showed that the gene expression deficit of *FOXA1* and *NR3C1*, among other TFs, was related to the DNA hypermethylation of enhancer elements in iPSC-derived DAn from PD patients (Fernandez-Santiago et al., 2015a). Contrariwise, we also found that the down-regulation of miR-199a-5p was associated with the gene expression up-regulation of *ZIC1* (r=-0.93, adj. P=0.0012), *NELL2* (r=-0.90, adj. P=0.0024), and *OTX1* (r=-0.87, adj. P=0.0052) whereas, in the same direction, the down-regulation of miR-519a-3p was related to the up-regulation of *DCC* (r=-0.90, adj. P=0.0062). Previously we reported that *ZIC1*, *NELL2*, *OTX1*, and *DCC* among others are top DEGs involved in neural functions showing differential gene expression up-regulation in PD (top-20 list of 437 DEGs) (Fernandez-Santiago et al., 2015a). Altogether these data suggest that the specific miRNA expression changes in PD could be related to the aberrant DNA methylation mediated by the deficit of key TFs *FOXA1* and *NR3C1* and also to specific gene expression changes observed in our DAn model.

4. DISCUSSION

We report the first explorative genome-wide study of miRNA expression levels in iPSC-derived DAn from PD patients, with either sPD or monogenic L2PD, and unrelated healthy controls. After multiple-testing adjustment, we identified differential expression of ten miRNA in PD patients as compared to controls of which five DEmiR were up-regulated in PD (miR- miR-9-5p, 135a-5p, miR-135b-5p, miR-449a, and miR-449b-5p) whereas five were down-regulated (miR-141-3p, miR-199a-5p, miR-299-5p, miR-518e-3p, and miR-519a-3p).

Among PD up-regulated DEmiR, changes in miR-9-5p and miR-135b-5p expression were previously associated with PD in samples from patients but miR-135a-5p, miR-449a, and miR-449b-5p have also been linked to disease in earlier studies. MicroRNA miR-9-5p was found to be up-regulated in peripheral blood from PD patients (Alieva et al., 2015). Moreover, up-regulation of miR-9 was associated with down-regulated expression of glial cell line-derived neurotrophic factor (*GDNF*), a key neurotrophin which increases the number of adult DAn in the SNpc and promotes survival of DAn both in-vivo and in-vitro (Kumar et al., 2015). MicroRNA miR-135a-5p is involved in delimiting the dorso-ventral extent and allocation of DAn progenitors by targeting *LMX1B* and other genes of the Wnt signalling pathway during midbrain development (Anderegg et al., 2013). Also, this miRNA has been reported to be compensatorily protective in adult DAn of a 1-methyl-4-phenyl-1,2,3,6-tetrahydropyridine (MPTP) subacute mouse model of PD (Liu et al., 2016). In addition, expression levels of the functionally closely related miR-135b-5p (Anderegg et al., 2013) were found to be deregulated in SNpc from PD patients (Cardo et al., 2014) and also in cerebrospinal fluid (CSF) from Alzheimer disease (AD) patients (Liu et al., 2014). Finally, miR-449a and miR-449b are involved in normal brain development and microtubule dynamics (Wu et al., 2014) and have been predicted to target a-synuclein, the major aggregating protein found in Lewy bodies (LB) from PD patients (Heman-Ackah et al., 2013). In addition, another study has shown deregulation of miR-9 and miR-449b in putamen and also in CSF from PD patients (Hesse and Arenz, 2014).

Regarding DEmiR down-regulated in PD, abnormally reduced expression of miR-141-3p, miR-199a-5p, and miR-299-5p was already reported in biological samples from PD patients in recent studies whereas miR-518e-3p and miR-519a-3p misregulation have not been earlier related to PD. MicroRNA miR-141 expression levels were significantly reduced in serum samples from PD patients at early Hoehn&Yahr motor stages I and II (Dong et al., 2016). Moreover, a recent study applying a systems biology approach has identified miR-141-3p as hub miRNA in a TF-miRNA-mRNA regulatory network involved in PD and postulated this miRNA as potential biomarker and therapeutic target in PD (Chatterjee et al., 2014). MicroRNA miR-199a-5p has been shown to be down-regulated in peripheral blood mononuclear cells (PBMCs) from PD patients (Martins et al., 2011) and this miRNA was also predicted to target a-synuclein (Heman-Ackah et al., 2013). In addition, expression levels of miR-299-5p have also been found to be down-regulated in SNpc from PD patients (Cardo et al., 2014). Finally, miR-518e-3p and miR-519a-3p have shown up-regulated expression in specific types of cancer (Flor et al., 2016; Wei et al., 2016) but their potential involvement in neurodegenerative diseases has not been previously reported.

We showed that genes targeted by the identified DEmiR were involved in regulating cytoskeleton dynamics, axonal transport, cell adhesion and cell survival, comprising canonical pathways previously shown to be altered in PD (Edwards et al., 2011; Grunblatt et al., 2004; Mandel et al., 2005; Mutez et al., 2011). This is in line with reports linking LRRK2 function to Rho GTPases which play a critical role in neurite growth by the remodeling of actin cytoskeleton (Chan et al., 2011; Habig et al., 2013) and also imbalances in the related Akt/ PI3k pathway regulating survival in PD (Romani-Aumedes et al., 2014). For instance, miR-135a-5p has been shown to target the 3'-UTR and inhibit mRNA translation of Rho-associated protein kinase 2 (ROCK2) which promotes neurodegeneration during the progression of PD in neuronal cells, acting as a compensatory mechanism (Liu et al., 2016; Saal et al., 2017). It is important to mention that the PD DAn cells studied here showed reduced axonal outgrowth and survival via

287 caspase 3 cleavage, among others phenotypes, upon the 75-days long-term culture (Sanchez-
288 Danes et al., 2012b). Although we do not provide a functional link of these long-term funtional
289 alterations with early miRNA deregulation at 30-days culture, it is plausible that these processes
290 could be related.

291 We also found that DEmiR identified in PD are associated with gene expression
292 changes suggesting a role in regulating gene expression, which we observed can occur both
293 inversely and positively. Focusing in classical direct inverse DEmiR / DEG associations, we
294 found two miRNA / mRNA clusters including Cluster 1 which encompassed PD down-regulated
295 DEmiRs and associated DEGs which were largely involved in specific neural functions, and
296 cluster 2 comprising PD up-regulated DEmiRs and associated DEGs which were related to
297 diverse homeostatic functions. This finding adds a new layer of complexity to our PD DAn
298 system providing additional molecular changes of miRNA expression correlating with previously
299 observed gene expression changes (Fernandez-Santiago et al., 2015a). Our data also show
300 that PD DEmiR alterations co-occur in early 30-days DAn cultures with large PD-associated
301 DNA methylation changes encompassing an hypermethylation of genomic enhancer elements
302 which was related to a deficit of a network of TF relevant to PD (*FOXA1*, *NR3C1*, *HNF4A* and
303 *FOSL2*) (Fernandez-Santiago et al., 2015a). More specifically, we found that up-regulation of
304 miR-9-5p and of miR-135b-5p were associated with down-regulation of *FOXA1* and *NR3C1*
305 respectively, suggesting a functional link between miRNA changes of gene expression of TF
306 which are important for the correct epigenetic patterning of DAn in PD.

307 miRNA profiles were largely similar in sPD and L2PD which overall did not show
308 differences in miRNA expression between each other. This finding is in line with previous
309 transcriptomic, epigenomic (Fernandez-Santiago et al., 2015a), and phenotypic changes
310 (Sanchez-Danes et al., 2012b) previously observed in PD DAn which were also largely common
311 in sPD and L2PD. Our results also agree with previous reports showing that, yet with specific
312 differences (Marras et al., 2016), L2PD largely resembles common sPD clinically and

313 neuropathologically (Healy et al., 2008). In addition, our study uncovers changes of miRNA
314 expression which are associated with PD and co-occur with transcriptomic and epigenomic
315 changes antedating late PD neurodegenerative phenotypes. Altogether these data suggest that
316 multi-layered molecular changes occur simultaneously in PD, a concept which is compatible
317 with the well-accepted complex multifactorial character of disease. Moreover, our PD DAn
318 model exhibited miRNA expression alterations which were previously reported in other
319 biological samples from PD patients such as PD peripheral blood (miR-9-5p), PD serum (miR-
320 141-3p), PBMCs (miR-199a-5p), SNpc (miR-135b-5p, miR-299-5p), and putamen and CSF
321 (miR-9 and miR-449b). Finally, our study also indicates that iPSC-derived DAn from PD patients
322 can prove a useful humanized cell system which, while preserving the patient genomic
323 background, can recapitulate molecular alterations occurring in PD providing a unique tool to
324 model disease at the cellular level.

DISCLOSURE STATEMENT

The authors report no actual or potential conflict of interest including any financial, personal or other relationships with other people or organizations within three years of beginning the work submitted that could inappropriately influence this work.

ACKNOWLEDGEMENTS

The authors thank the patients who participated in the study and their family members. The authors also thank Yvonne Richaud-Patin, Adriana Sánchez-Danés, Iria Carballo-Carbajal, and Miquel Vila, who contributed in the generation and characterization of the induced dopaminergic neurons from PD patients. This work was supported by funds from the Spanish Ministry of Economy and Competitiveness (MINECO) to R.F.-S. (grant # SAF2015-73508-JIN (AEI/FEDER/UE), the Fondo de Investigaciones Sanitarias of the Instituto de Salud Carlos III (ISCIII) to M.E. (grant # PI14/00426), the Centro de Investigación Biomédica en Red de Enfermedades Neurodegenerativas (CIBERNED) to the Movement Disorders Unit of the Neurology Service from the Hospital Clínic de Barcelona to E.T., M.-J.M., R.F.-S., M.E., and C.G. (grant # PRI-16-207). This work was also supported by BFU2013-49157-P and RETIC TerCel grants from MINECO and the European Research Council (ERC) 2012-StG (311736-PD-HUMMODEL) to A.C. The authors also thank the CERCA Program from the Generalitat de Catalunya and the FEDER Program from the European Union to IDIBAPS. Part of this work was developed at the Centre de Recerca Biomèdica Cellex (CRBC) from IDIBAPS / Hospital Clínic de Barcelona, Barcelona, Spain. R.F.-S. was supported by a Jóvenes Investigadores grant of the Spanish Ministry of Economy and Competitiveness (MINECO) (grant # SAF2015-73508-JIN (AEI/FEDER/UE), and M.E. by a Miguel Servet contract of the ISCIII/IDIBAPS.

APPENDIX A. SUPPLEMENTARY DATA

Supplemental data to this article can be found at attached appendix.

(See **Supplemental Figure 1**)

(See **Supplemental Table 1**)

(See **Supplemental Table 2**)

REFERENCES

Abe, M., Bonini, N.M., 2013. MicroRNAs and neurodegeneration: role and impact. Trends Cell Biol 23(1), 30-36.

Alieva, A., Filatova, E.V., Karabanov, A.V., Illarioshkin, S.N., Limborska, S.A., Shadrina, M.I., Slominsky, P.A., 2015. miRNA expression is highly sensitive to a drug therapy in Parkinson's disease. Parkinsonism Relat Disord 21(1), 72-74.

Anderegg, A., Lin, H.P., Chen, J.A., Caronia-Brown, G., Cherepanova, N., Yun, B., Joksimovic, M., Rock, J., Harfe, B.D., Johnson, R., Awatramani, R., 2013. An Lmx1b-miR135a2 regulatory circuit modulates Wnt1/Wnt signaling and determines the size of the midbrain dopaminergic progenitor pool. PLoS Genet 9(12), e1003973.

Bartel, D.P., 2009. MicroRNAs: target recognition and regulatory functions. Cell 136(2), 215-233.

Botta-Orfila, T., Tolosa, E., Gelpi, E., Sanchez-Pla, A., Marti, M.J., Valldeoriola, F., Fernandez, M., Carmona, F., Ezquerra, M., 2012. Microarray expression analysis in idiopathic and LRRK2-associated Parkinson's disease. Neurobiol Dis 45(1), 462-468.

Cardo, L.F., Coto, E., Ribacoba, R., Menendez, M., Moris, G., Suarez, E., Alvarez, V., 2014. MiRNA profile in the substantia nigra of Parkinson's disease and healthy subjects. J Mol Neurosci 54(4), 830-836.

Chan, D., Citro, A., Cordy, J.M., Shen, G.C., Wolozin, B., 2011. Rac1 protein rescues neurite retraction caused by G2019S leucine-rich repeat kinase 2 (LRRK2). The Journal of biological chemistry 286(18), 16140-16149.

Chatterjee, P., Bhattacharyya, M., Bandyopadhyay, S., Roy, D., 2014. Studying the system-level involvement of microRNAs in Parkinson's disease. PLoS One 9(4), e93751.

Danborg, P.B., Simonsen, A.H., Waldemar, G., Heegaard, N.H., 2014. The potential of microRNAs as biofluid markers of neurodegenerative diseases--a systematic review. Biomarkers 19(4), 259-268.

Dimmeler, S., Nicotera, P., 2013. MicroRNAs in age-related diseases. EMBO Mol Med 5(2), 180-190.

Dong, H., Wang, C., Lu, S., Yu, C., Huang, L., Feng, W., Xu, H., Chen, X., Zen, K., Yan, Q., Liu, W., Zhang, C., Zhang, C.Y., 2016. A panel of four decreased serum microRNAs as a novel biomarker for early Parkinson's disease. Biomarkers 21(2), 129-137.

Edwards, Y.J., Beecham, G.W., Scott, W.K., Khuri, S., Bademci, G., Tekin, D., Martin, E.R., Jiang, Z., Mash, D.C., ffrench-Mullen, J., Pericak-Vance, M.A., Tsinoremas, N., Vance, J.M., 2011. Identifying consensus disease pathways in Parkinson's disease using an integrative systems biology approach. PLoS One 6(2), e16917.

Fernandez-Santiago, R., Carballo-Carbajal, I., Castellano, G., Torrent, R., Richaud, Y., Sanchez-Danes, A., Vilarrasa-Blasi, R., Sanchez-Pla, A., Mosquera, J.L., Soriano, J., Lopez-Barneo, J., Canals, J.M., Alberch, J., Raya, A., Vila, M., Consiglio, A., Martin-Subero, J.I., Ezquerra, M., Tolosa, E., 2015a. Aberrant epigenome in iPSC-derived dopaminergic neurons from Parkinson's disease patients. EMBO Mol Med 7(12), 1529-1546.

Fernandez-Santiago, R., Iranzo, A., Gaig, C., Serradell, M., Fernandez, M., Tolosa, E., Santamaria, J., Ezquerra, M., 2015b. MicroRNA association with synucleinopathy conversion in rapid eye movement behavior disorder. Annals of neurology 77(5), 895-901.

Flor, I., Spiekermann, M., Loning, T., Dieckmann, K.P., Belge, G., Bullerdiek, J., 2016. Expression of microRNAs of C19MC in Different Histological Types of Testicular Germ Cell Tumour. Cancer Genomics Proteomics 13(4), 281-289.

Fuchs, J., Mueller, J.C., Lichtner, P., Schulte, C., Munz, M., Berg, D., Wullner, U., Illig, T., Sharma, M., Gasser, T., 2009. The transcription factor PITX3 is associated with sporadic Parkinson's disease. Neurobiol Aging 30(5), 731-738.

Gasser, T., 2009. Mendelian forms of Parkinson's disease. Biochimica et biophysica acta 1792(7), 587-596.

Grunblatt, E., Mandel, S., Jacob-Hirsch, J., Zeligson, S., Amariglo, N., Rechavi, G., Li, J., Ravid, R., Roggendorf, W., Riederer, P., Youdim, M.B., 2004. Gene expression profiling of parkinsonian substantia nigra pars compacta; alterations in ubiquitin-proteasome, heat shock protein, iron and oxidative stress regulated proteins, cell adhesion/cellular matrix and vesicle trafficking genes. J Neural Transm (Vienna) 111(12), 1543-1573.

Habig, K., Gellhaar, S., Heim, B., Djuric, V., Giesert, F., Wurst, W., Walter, C., Hentrich, T., Riess, O., Bonin, M., 2013. LRRK2 guides the actin cytoskeleton at growth cones together with ARHGEF7 and Tropomyosin 4. Biochimica et biophysica acta 1832(12), 2352-2367.

Healy, D.G., Falchi, M., O'Sullivan, S.S., Bonifati, V., Durr, A., Bressman, S., Brice, A., Aasly, J., Zabetian, C.P., Goldwurm, S., Ferreira, J.J., Tolosa, E., Kay, D.M., Klein, C., Williams, D.R., Marras, C., Lang, A.E., Wszolek, Z.K., Berciano, J., Schapira, A.H., Lynch, T., Bhatia, K.P., Gasser, T., Lees, A.J., Wood, N.W., International, L.C., 2008. Phenotype, genotype, and worldwide genetic penetrance of LRRK2-associated Parkinson's disease: a case-control study. Lancet Neurol 7(7), 583-590.

Heman-Ackah, S.M., Hallegger, M., Rao, M.S., Wood, M.J., 2013. RISC in PD: the impact of microRNAs in Parkinson's disease cellular and molecular pathogenesis. Front Mol Neurosci 6, 40.

Hesse, M., Arenz, C., 2014. miRNAs as novel therapeutic targets and diagnostic biomarkers for Parkinson's disease: a patent evaluation of WO2014018650. Expert opinion on therapeutic patents 24(11), 1271-1276.

Khoo, S.K., Petillo, D., Kang, U.J., Resau, J.H., Berryhill, B., Linder, J., Forsgren, L., Neuman, L.A., Tan, A.C., 2012. Plasma-based circulating MicroRNA biomarkers for Parkinson's disease. J Parkinsons Dis 2(4), 321-331.

Kim, J., Inoue, K., Ishii, J., Vanti, W.B., Voronov, S.V., Murchison, E., Hannon, G., Abeliovich, A., 2007. A MicroRNA feedback circuit in midbrain dopamine neurons. Science 317(5842), 1220-1224.

Kumar, A., Kopra, J., Varendi, K., Porokuokka, L.L., Panhelainen, A., Kuure, S., Marshall, P., Karalija, N., Harma, M.A., Vilenius, C., Lillevali, K., Tekko, T., Mijatovic, J., Pulkkinen, N., Jakobson, M., Jakobson, M., Ola, R., Palm, E., Lindahl, M., Stromberg, I., Voikar, V., Piepponen, T.P., Saarma, M., Andressoo, J.O., 2015. GDNF Overexpression from the Native Locus Reveals its Role in the Nigrostriatal Dopaminergic System Function. PLoS Genet 11(12), e1005710.

Lang, A.E., Lozano, A.M., 1998a. Parkinson's disease. First of two parts. N Engl J Med 339(15), 1044-1053.

Lang, A.E., Lozano, A.M., 1998b. Parkinson's disease. Second of two parts. N Engl J Med 339(16), 1130-1143.

Liu, C.G., Wang, J.L., Li, L., Xue, L.X., Zhang, Y.Q., Wang, P.C., 2014. MicroRNA-135a and -200b, potential Biomarkers for Alzheimers disease, regulate beta secretase and amyloid precursor protein. Brain Res 1583, 55-64.

Liu, Y., Liao, S., Quan, H., Lin, Y., Li, J., Yang, Q., 2016. Involvement of microRNA-135a-5p in the Protective Effects of Hydrogen Sulfide Against Parkinson's Disease. Cellular physiology and biochemistry : international journal of experimental cellular physiology, biochemistry, and pharmacology 40(1-2), 18-26.

Mandel, S., Grunblatt, E., Riederer, P., Amariglio, N., Jacob-Hirsch, J., Rechavi, G., Youdim, M.B., 2005. Gene expression profiling of sporadic Parkinson's disease substantia nigra pars compacta reveals impairment of ubiquitin-proteasome subunits, SKP1A, aldehyde dehydrogenase, and chaperone HSC-70. Annals of the New York Academy of Sciences 1053, 356-375.

Margis, R., Margis, R., Rieder, C.R., 2011. Identification of blood microRNAs associated to Parkinsonis disease. J Biotechnol 152(3), 96-101.

Marras, C., Alcalay, R.N., Caspell-Garcia, C., Coffey, C., Chan, P., Duda, J.E., Facheris, M.F., Fernandez-Santiago, R., Ruiz-Martinez, J., Mestre, T., Saunders-Pullman, R., Pont-Sunyer, C.,

Tolosa, E., Waro, B., Consortium, L.C., 2016. Motor and nonmotor heterogeneity of LRRK2-related and idiopathic Parkinson's disease. Mov Disord 31(8), 1192-1202.
Martins, M., Rosa, A., Guedes, L.C., Fonseca, B.V., Gotovac, K., Violante, S., Mestre, T., Coelho, M., Rosa, M.M., Martin, E.R., Vance, J.M., Outeiro, T.F., Wang, L., Borovecki, F., Ferreira, J.J., Oliveira, S.A., 2011. Convergence of miRNA expression profiling, alpha-synuclein interacton and GWAS in Parkinson's disease. PLoS One 6(10), e25443.
Mutez, E., Larvor, L., Lepretre, F., Mouroux, V., Hamalek, D., Kerckaert, J.P., Perez-Tur, J., Waucquier, N., Vanbesien-Mailliot, C., Duflot, A., Devos, D., Defebvre, L., Kreisler, A., Frigard, B., Destee, A., Chartier-Harlin, M.C., 2011. Transcriptional profile of Parkinson blood mononuclear cells with LRRK2 mutation. Neurobiol Aging 32(10), 1839-1848.
Reeve, A., Simcox, E., Turnbull, D., 2014. Ageing and Parkinson's disease: why is advancing age the biggest risk factor? Ageing research reviews 14, 19-30.
Ritchie, W., Rajasekhar, M., Flamant, S., Rasko, J.E., 2009. Conserved expression patterns predict microRNA targets. PLoS computational biology 5(9), e1000513.
Romani-Aumedes, J., Canal, M., Martin-Flores, N., Sun, X., Perez-Fernandez, V., Wewering, S., Fernandez-Santiago, R., Ezquerra, M., Pont-Sunyer, C., Lafuente, A., Alberch, J., Luebbert, H., Tolosa, E., Levy, O.A., Greene, L.A., Malagelada, C., 2014. Parkin loss of function contributes to RTP801 elevation and neurodegeneration in Parkinson's disease. Cell death & disease 5, e1364.
Saal, K.A., Galter, D., Roeber, S., Bahr, M., Tonges, L., Lingor, P., 2017. Altered Expression of Growth Associated Protein-43 and Rho Kinase in Human Patients with Parkinson's Disease. Brain Pathol 27(1), 13-25.
Sales, G., Coppe, A., Bisognin, A., Biasiolo, M., Bortoluzzi, S., Romualdi, C., 2010. MAGIA, a web-based tool for miRNA and Genes Integrated Analysis. Nucleic acids research 38(Web Server issue), W352-359.
Sanchez-Danes, A., Consiglio, A., Richaud, Y., Rodriguez-Piza, I., Dehay, B., Edel, M., Bove, J., Memo, M., Vila, M., Raya, A., Izpisua Belmonte, J.C., 2012a. Efficient generation of A9 midbrain dopaminergic neurons by lentiviral delivery of LMX1A in human embryonic stem cells and induced pluripotent stem cells. Hum Gene Ther 23(1), 56-69.
Sanchez-Danes, A., Richaud-Patin, Y., Carballo-Carbajal, I., Jimenez-Delgado, S., Caig, C., Mora, S., Di Guglielmo, C., Ezquerra, M., Patel, B., Giralt, A., Canals, J.M., Memo, M., Alberch, J., Lopez-Barneo, J., Vila, M., Cuervo, A.M., Tolosa, E., Consiglio, A., Raya, A., 2012b. Disease-specific phenotypes in dopamine neurons from human iPS-based models of genetic and sporadic Parkinson's disease. EMBO Mol Med 4(5), 380-395.
Serafin, A., Foco, L., Zanigni, S., Blankenburg, H., Picard, A., Zanon, A., Giannini, G., Pichler, I., Facheris, M.F., Cortelli, P., Pramstaller, P.P., Hicks, A.A., Domingues, F.S., Schwienbacher, C., 2015. Overexpression of blood microRNAs 103a, 30b, and 29a in L-dopa-treated patients with PD. Neurology 84(7), 645-653.
Shannon, P., Markiel, A., Ozier, O., Baliga, N.S., Wang, J.T., Ramage, D., Amin, N., Schwikowski, B., Ideker, T., 2003. Cytoscape: a software environment for integrated models of biomolecular interaction networks. Genome Res 13(11), 2498-2504.
Soreq, L., Salomonis, N., Bronstein, M., Greenberg, D.S., Israel, Z., Bergman, H., Soreq, H., 2013. Small RNA sequencing-microarray analyses in Parkinson leukocytes reveal deep brain stimulation-induced splicing changes that classify brain region transcriptomes. Front Mol Neurosci 6, 10.
Vallelunga, A., Ragusa, M., Di Mauro, S., Iannitti, T., Pilleri, M., Biundo, R., Weis, L., Di Pietro, C., De Iuliis, A., Nicoletti, A., Zappia, M., Purrello, M., Antonini, A., 2014. Identification of circulating microRNAs for the differential diagnosis of Parkinson's disease and Multiple System Atrophy. Front Cell Neurosci 8, 156.

Vandesompele, J., De Preter, K., Pattyn, F., Poppe, B., Van Roy, N., De Paepe, A., Speleman, F., 2002. Accurate normalization of real-time quantitative RT-PCR data by geometric averaging of multiple internal control genes. Genome Biol 3(7), RESEARCH0034.

Vlachos, I.S., Paraskevopoulou, M.D., Karagkouni, D., Georgakilas, G., Vergoulis, T., Kanellos, I., Anastasopoulos, I.L., Maniou, S., Karathanou, K., Kalfakakou, D., Fevgas, A., Dalamagas, T., Hatzigeorgiou, A.G., 2015a. DIANA-TarBase v7.0: indexing more than half a million experimentally supported miRNA:mRNA interactions. Nucleic acids research 43(Database issue), D153-159.

Vlachos, I.S., Zagganas, K., Paraskevopoulou, M.D., Georgakilas, G., Karagkouni, D., Vergoulis, T., Dalamagas, T., Hatzigeorgiou, A.G., 2015b. DIANA-miRPath v3.0: deciphering microRNA function with experimental support. Nucleic acids research 43(W1), W460-466.

Wei, Y., He, R., Wu, Y., Gan, B., Wu, P., Qiu, X., Lan, A., Chen, G., Wang, Q., Lin, X., Chen, Y., Mo, Z., 2016. Comprehensive investigation of aberrant microRNA profiling in bladder cancer tissues. Tumour Biol 37(9), 12555-12569.

Wu, J., Bao, J., Kim, M., Yuan, S., Tang, C., Zheng, H., Mastick, G.S., Xu, C., Yan, W., 2014. Two miRNA clusters, miR-34b/c and miR-449, are essential for normal brain development, motile ciliogenesis, and spermatogenesis. Proceedings of the National Academy of Sciences of the United States of America 111(28), E2851-2857.

Table 1

Clinical details of PD patients and iPSC-derived DAn cell lines characterized by genome-wide miRNA expression analysis

Cell line code	Code previous study*	Subject type	*LRRK2* mutation	Family history of PD	Gender	Age at donation	Age at onset	Initial symptoms	L-DOPA response	Selected iPSC clone	Cell ratio TUJ1+/DAPI+ (neurons)[a]	Cell ratio TH+/TUJ1+ (DA neurons)[b]
C-01	SP-15	Control	No	No	Female	47	-	-	-	15-2	34.7	45.0
C-02	SP-11	Control	No	No	Female	48	-	-	-	11-1	40.0	59.9
C-03	SP-09	Control	No	No	Male	66	-	-	-	9-4	52.2	55.5
C-04	SP-17	Control	No	No	Male	52	-	-	-	17-2	54.0	65.8
PD-01	SP-13	L2PD	G2019S	Yes	Female	68	57	T	Good	13-4	47.0	65.2
PD-04	SP-16	sPD	No	No	Female	51	48	B	N/A	16-2	32.1	55.2
PD-05	SP-06	L2PD	G2019S	Yes	Male	44	33	T	Good	6-2	40.9	61.9
PD-07	SP-12	L2PD	G2019S	Yes	Female	63	49	T	Good	12-3	42.7	60.0
PD-09	SP-01	sPD	No	No	Female	63	58	T and B	N/A	1-1	32.2	44.9
PD-10	SP-08	sPD	No	No	Female	66	60	T	Good	8-1	41.6	67.1

Key: sPD, sporadic PD; L2PD, LRRK2-associated PD; N/A, not assessed; T, tremor; B, bradykinesia; D, foot dystonia; iPSC, induced pluripotent stem cell; DAn, dopaminergic neuron; miRNA, microRNA.

[a] Ratio of neurons / total cells, calculated by immunofluorescence as the ratio of TUJ1 (neuron-specific class III b-Tubulin)-positive cells/ DAPI-positive cells.

[b] Ratio of iPSC-derived DAn / total neurons, calculated by immunofluorescence as the ratio of TH (tyrosine hydroxylase)-positive cells / TUJ1 positive cells.

* Sanchez-Danes, A., et al., 2012b. Disease-specific phenotypes in dopamine neurons from human iPS-based models of genetic and sporadic Parkinson's disease. EMBO Mol Med. 4(5):380-95.

Fernández-Santiago, R., et al., 2015a. Aberrant epigenome in iPSC-derived dopaminergic neurons from Parkinson's disease patients. EMBO Mol Med. 7, 1529-46.

Table 2

Differentially expressed microRNAs (DEmiR) associated with PD ordered by statistical significance

Differencially expressed microRNA (DEmiR)	Assay Commercial Code (ABI)	mean $2^{-\Delta Ct}$ expression levels ± S.D. in PD	mean $2^{-\Delta Ct}$ expression levels ± S.D. in controls	Fold Change (FC)	Expression change	P-value	Multiple testing adj. P-value
hsa-miR-135a-5p	4373140	0.300 ± 0.140	0.011 ± 0.005	26.78	Up-regulated	0.000017	0.004
hsa-miR-135b-5p	4395372	0.313 ± 0.060	0.059 ± 0.013	5.26	Up-regulated	0.0001	0.006
hsa-miR-449a	4373207	0.380 ± 0.250	0.007 ± 0.005	51.76	Up-regulated	0.0001	0.007
hsa-miR-449b-5p	4381011	0.150 ± 0.095	0.003 ± 0.002	40.97	Up-regulated	0.0001	0.007
hsa-miR-199a-5p	4373272	0.329 ± 0.145	0.822 ± 0.414	-3.33	Down-regulated	0.0008	0.035
hsa-miR-299-5p	4373188	0.001 ± 5.5E-5	0.003 ± 0.001	-3.33	Down-regulated	0.0009	0.035
hsa-miR-518e-3p	4395506	0.0026 ± 0.001	0.067 ± 0.060	-24.39	Down-regulated	0.0011	0.035
hsa-miR-9-5p	4373285	2.280 ± 2.130	0.018 ± 0.015	133.06	Up-regulated	0.0012	0.035
hsa-miR-141-3p	4373137	0.009 ± 0.004	0.026 ± 0.007	-2.94	Down-regulated	0.0014	0.035
hsa-miR-519a-3p	4395526	0.003 ± 0.0009	0.054 ± 0.042	-17.00	Down-regulated	0.0016	0.035

Key: S.D, standard deviation.

Table 3

Biological enrichment analysis of DEmiR / DEG pairs from interaction clusters 1 and 2 identified in PD. Key: DEmiR, differentially expressed miRNA; DEG, differentially expressed gene.

Cluster 1 terms (down-regulated DEmiR, up-regulated DEG)	Nr. of genes	Total of genes	*P* Value	Benjamini adj. *P* value
GO:0030182~neuron differentiation	13	63	5.68E-07	4.59E-04
GO:0048858~cell projection morphogenesis	10	63	1.59E-06	6.43E-04
GO:0032990~cell part morphogenesis	10	63	2.29E-06	6.16E-04
GO:0031175~neuron projection development	10	63	2.29E-06	6.16E-04
GO:0048667~cell morphogenesis involved in neuron differentiation	9	63	4.69E-06	9.47E-04
GO:0048812~neuron projection morphogenesis	9	63	5.40E-06	8.72E-04
GO:0030030~cell projection organization	11	63	5.99E-06	8.06E-04
GO:0000904~cell morphogenesis involved in differentiation	9	63	1.46E-05	0.0017
GO:0048666~neuron development	10	63	2.21E-05	0.0022
GO:0007409~axonogenesis	8	63	2.73E-05	0.0025
GO:0000902~cell morphogenesis	10	63	3.24E-05	0.0026
GO:0032989~cellular component morphogenesis	10	63	7.55E-05	0.0055
GO:0060562~epithelial tube morphogenesis	5	63	2.47E-04	0.0165
GO:0021915~neural tube development	5	63	2.62E-04	0.0161
GO:0001843~neural tube closure	4	63	3.41E-04	0.0195
GO:0060606~tube closure	4	63	3.41E-04	0.0195
GO:0014020~primary neural tube formation	4	63	4.53E-04	0.0241
GO:0048598~embryonic morphogenesis	8	63	4.89E-04	0.0244
GO:0001841~neural tube formation	4	63	8.03E-04	0.0374
Cluster 2 terms (up-regulated DEmiR, down-regulated DEG)	**Nr. of genes**	**Total of genes**	***P* Value**	**Benjamini adj. *P* value**
GO:0044057~regulation of system process	9	64	8.80E-05	0.0950
GO:0006790~sulfur metabolic process	6	64	1.93E-04	0.1038
GO:0051094~positive regulation of developmental process	8	64	2.97E-04	0.1063
GO:0045597~positive regulation of cell differentiation	7	64	6.69E-04	0.1730
GO:0032101~regulation of response to external stimulus	6	64	8.55E-04	0.1764
GO:0006898~receptor-mediated endocytosis	4	64	0.0019	0.3035
GO:0019915~lipid storage	3	64	0.0031	0.3968
GO:0048754~branching morphogenesis of a tube	4	64	0.0034	0.3852
GO:0006897~endocytosis	6	64	0.0036	0.3617
GO:0010324~membrane invagination	6	64	0.0036	0.3617
GO:0001569~patterning of blood vessels	3	64	0.0042	0.3822
GO:0006937~regulation of muscle contraction	4	64	0.0046	0.3765
GO:0001763~morphogenesis of a branching structure	4	64	0.0049	0.3735
GO:0051241~negative regulation of multicellular organismal process	5	64	0.0071	0.4641
GO:0016044~membrane organization	7	64	0.0084	0.4970
GO:0048661~positive regulation of smooth muscle cell proliferation	3	64	0.0091	0.4993
GO:0048878~chemical homeostasis	8	64	0.0095	0.4905
GO:0042127~regulation of cell proliferation	10	64	0.0102	0.4970
GO:0006940~regulation of smooth muscle contraction	3	64	0.0135	0.5748

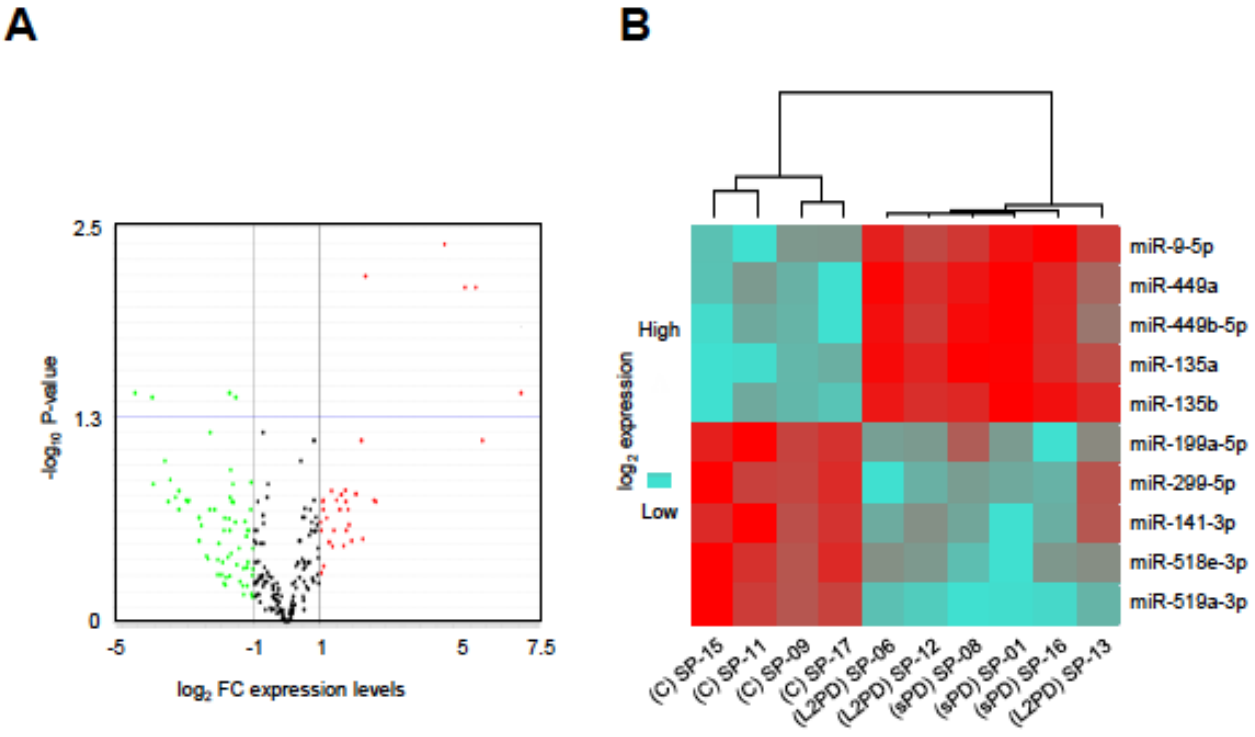

Fig. 1.

Identification of differentially expressed miRNA (DEmiR) in PD. (A) Volcano plot showing up-regulated DEmiR in upper right and down-regulated DEmiR in upper left cuadrants. Horizontal axis represents relative miRNA expression levels between PD and controls whereas vertical axis represents *P*-value. (B) Heatmap showing the ten DEmiR associated with PD and density color code for miRNA expression levels showing discrimination between PD either sPD or L2PD, and healthy controls. Key: DEmiR, differentially expressed miRNA; sPD, sporadic PD; L2PD, LRRK2-associated PD.

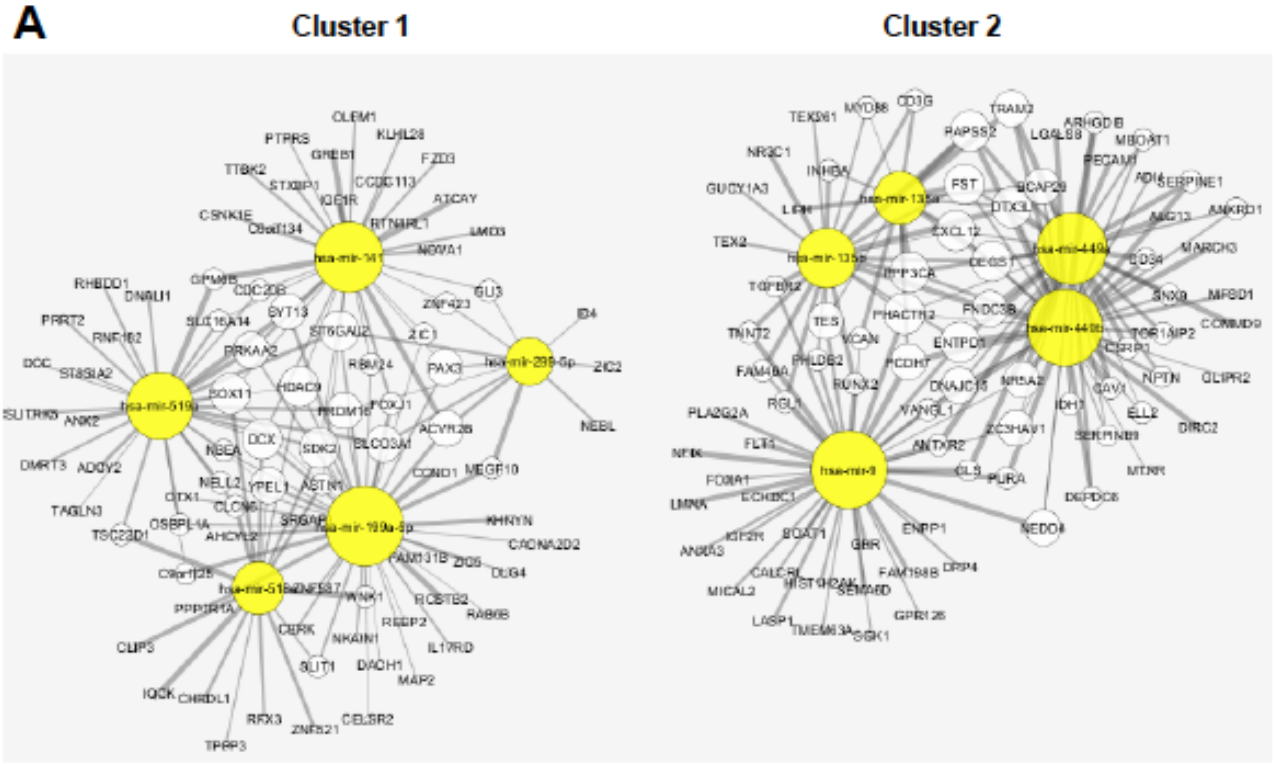

Fig. 2.

Interaction network of differentially expressed miRNA (DEmiR) and differentially expressed genes (DEG) identified in PD showing two interaction clusters which encompass Cluster 1 of PD down-regulated DEmiR, and Cluster 2 of PD up-regulated DEmiR, and their respective interacting DEGs. DEmiR are represented in yellow, and DEG in white. The size of DEmiR / DEG nodes are proportional to the number of direct DEmiR / DEG interactions, and thickness of edges from DEmiR to DEG are proportional to the degree of correlation. Key: DEmiR, differentially expressed miRNA; DEG, differentially expressed gene.